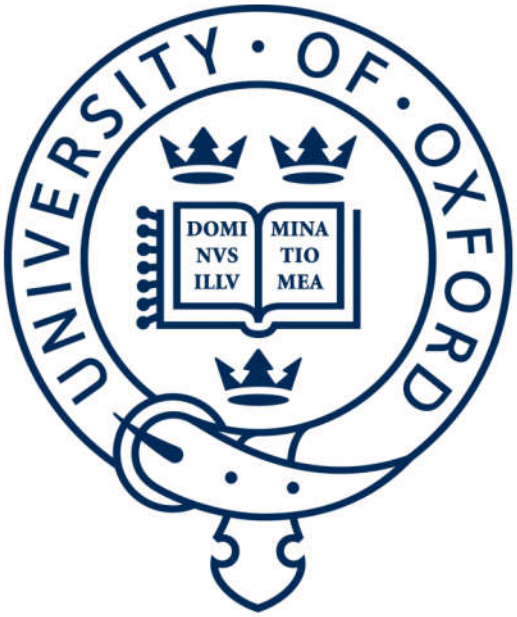
REGULATION AND MODULATION OF THE CREATINE KINASE SYSTEM



Fang Cao

A thesis submitted for the degree of Doctor of Philosophy

Supervisors

Prof. Craig Lygate, Dr Sevasti Zervou, Prof. Stefan Neubauer

Trinity Term 2018

University College

Department of Cardiovascular Medicine

Wellcome Centre for Human Genetics

University of Oxford

Declaration of own work

This D.Phil. thesis is entirely my own work unless otherwise indicated. It has not been submitted, either wholly or substantially, for another degree of this University, or for a degree at any other institution. Any assistance from colleagues or collaborators has been appropriately acknowledged.

Publications

The following publications include data from experiments described in this thesis:

Hannah J Whittington, Philip J Ostrowski, Debra J McAndrew, Fang Cao, Andrew Shaw, Thomas R Eykyn, Hannah A Lake, Jack Tyler, Jurgen E Schneider, Stefan Neubauer, Sevasti Zervou, Craig A Lygate; Over-expression of mitochondrial creatine kinase in the murine heart improves functional recovery and protects against injury following ischaemia–reperfusion. Cardiovascular Research, 2018, P. 858–869

Sevasti Zervou, Hannah J. Whittington, Philip J. Ostrowski, Fang Cao, Jack Tyler, Hannah A. Lake, Stefan Neubauer, Craig A. Lygate; Increasing creatine kinase activity protects against hypoxia / reoxygenation injury but not against anthracycline toxicity *in vitro*. PLOS ONE, 2017, 12(8): e0182994.

Abstract

Substantial evidence indicates that impaired myocardial bioenergetics play a role in the pathogenesis of various cardiovascular disorders. In particular, creatine kinase (CK) system dysfunction has been associated with heart failure, ischemia/reperfusion (I/R) injury, and doxorubicin-induced cardiotoxicity. The goal of the experiments detailed in this thesis was to determine whether cardiac CK upregulation could be of therapeutic potential in these diseases.

The literature suggests that overexpressing mitochondrial creatine kinase (CK-Mt) could adversely affect mitochondria, hence experiments were undertaken to elucidate the bioenergetic phenotype of a mouse model modestly overexpressing cardiac CK-Mt. CK-Mt overexpression was found to be benign in regards to metabolism and mitochondrial respiration. The mitochondrial swelling assay showed that CK-Mt overexpression inhibits opening of the mitochondrial permeability transition pore (mPTP), which may contribute towards protection during I/R.

Subsequently, CK-Mt overexpressing mice were utilized to investigate whether CK-Mt overexpression improved outcomes in an *in vivo* model of pressure-overload chronic heart failure. Based on echocardiography and haemodynamic analysis, CK-Mt augmentation did not significantly improve cardiac function or morphology. Biochemical assays revealed that the transgenic mice had over 90% higher CK-Mt activity and ^{31}P-MRS study confirmed that CK-Mt overexpression was sufficient to restore physiological PCr/ATP ratios during heart failure, suggesting that elevated CK-Mt does not protect against pressure-overload chronic heart failure.

Doxorubicin (DOX) is a potent chemotherapeutic agent whose use is limited by a dose-dependent cardiotoxicity that progresses to heart failure. An *in vitro* model was developed in HL-1 cells to explore whether CK overexpression protected against DOX-induced cardiotoxicity. HL-1 cells were transiently transfected with muscle, brain, and mitochondrial creatine kinase (CK-M, CK-B, and CK-Mt, respectively), and a significant increase in isoenzyme-specific CK activity was confirmed. Transfected cells were challenged with 250 nM DOX for 48 hours with or without creatine, and cell death was measured by flow cytometry. Increased CK overexpression and/or creatine supplementation did not reduce DOX-induced cell death.

As CK augmentation was previously found to be beneficial in various cardiac conditions, an *in vitro* tool was developed in HEK293 cells to investigate the transcriptional regulation of CK-M and CK-Mt. Two HEK293 cell lines stably overexpressing the CK-M and CK-Mt promoter regions and luciferase reporter genes were established and validated. These cell lines were used in preliminary screens to identify potential compounds that could affect CK mRNA transcription. Sixty six compounds were screened and 12 positive hits were found.

In summary, the experiments in this thesis explored the effects of overexpressing CK under physiological and pathophysiological conditions. It was found that modest overexpression of CK-Mt is safe and inhibits mPTP opening, which may attenuate cardiac damage during I/R injury. However, the current level of CK-Mt overexpression does not protect against pressure-overload heart failure nor DOX-induced cardiotoxicity. An *in vitro* screening model system has been developed for exploration of CK transcriptional regulators, and can be used in the future for high-throughput screening of pharmacological CK regulators that could provide potential alternative treatments for heart diseases.

Acknowledgements

I found that this section was by far the most difficult to write. It was challenging to condense all of the mentorship and support that I've received throughout my D. Phil into a few pages, which does not do justice to my gratitude towards my mentors and colleagues – each sentence summarizes dozens, if not hundreds of hours of support so that I can be where I am today.

First and foremost, I want to acknowledge my mentors, Prof. Craig Lygate, Dr Sevasti Zervou and Prof. Stefan Neubauer. I transferred into the D. Phil program only after I arrived at Oxford, hence it was miraculous that they were willing to accept me after the start of the term. Added to this was the complication of the limited time I had as a D. Phil student because I needed to start medical school at Harvard in approximately three years. Therefore, I cannot stress enough my immense gratitude towards my supervisors for making today possible. Since day one, Craig and Sevi have guided me to continuously operate at full capacity – I was able to hit the ground running with two projects, and it has been just as busy ever since. I am extremely fortunate that my supervisors considered my work a top priority, and their door was always open for me to discuss the next endeavour. Even Stefan, who leads CVMed and OCMR, somehow managed to find the time to be with me in person at every critical juncture in my D. Phil. With the unwavering mentorship of my supervisors, I always had a clear sense of direction as to where I was going next, and all of the support that I needed to get there.

Science requires mental resilience, especially given the fair share of unexpected results that I experienced during my time here. After my experiences in college, it was a difficult transition to an environment in which a day's work was often a failed experiment (euphemistically termed "optimization"). I am very grateful to Craig and Sevi for helping me to adjust to the mentality required of a scientist, and to understand that despite the challenge, I was still making forward progress and learning from the experiences. Through their mentorship, I came to realize that scientists change the world because their resilience and unshakable inner resolve allow them to constantly push on the boundaries of what is possible. Craig and Sevi have supported me when the DOX optimization experiments lasted much long time than expected, and when the swelling assay experiments were misbehaving in the face of reviewers' deadlines. Therefore, I am deeply thankful for their guidance beyond science – through these experiences I am far stronger than I was when I first arrived at Oxford.

Equally important to my success have been my colleagues in the lab, who have taught me so much about experimental science. Debra McAndrew has been an instrumental mentor from the beginning, teaching me everything I know about mouse colony management and the various *in vivo* techniques that were critical to my experiments – Debs truly is a master surgeon. That being said, sometimes I wonder if she is an even better baker, as I know her cakes will be one of the things I miss most about Oxford. Hannah Whittington has taught me so much during our time together – I rarely used the same techniques and assays in my experiments, so it was often up to Hannah to continuously teach me. She guided me through many of my cell culture experiments, and was incredibly patient as I slowly figured out how to keep isolated cardiac mitochondria happy for two hours. Hannah has recently departed for Milan, and I know she will enjoy new adventures there. Both Debs and Hannah welcomed their first baby while I was a D. Phil student, and it has been an absolute pleasure to watch Jonathan and Izzy grow into such happy and lovely toddlers.

Hannah Lake, Jack Tyler, and Kuan Cha have provided invaluable advice and support. The multitasking required during a D. Phil could only have been achieved through their management of lab supplies and equipment. For example, I was only able to complete my HPLC experiments on time through Hannah's dedication – she spent months reviving our ailing HPLC machine from what appeared to be an irrecoverable illness. Hannah, Jack, and Kuan have always went out of their way to accommodate my schedule and needs, for which I am extremely thankful.

I have also received substantial support from the Schneider and Channon groups. Dr Mahon Maguire stepped in to offer his expertise with the ^{31}P-MRS experiments, which were far beyond my capacities as a first year D. Phil student. I am so grateful to Mahon for taking the time from his busy schedule to go through experimental theory and results with me. The same goes to Lee-Anne Stork, who managed to find the time to help us to set up the ^{31}P-MRS experiments despite her busy schedule. The Channon group has in many ways acted as a second family during my time at Oxford. Prof. Mark Crabtree was my transfer assessor, and I'm extremely thankful that he went over my first year's work and offered me great advice on how to move forward. Dr Eileen McNeill assisted me throughout my flow cytometry experiments, helping me with an antique piece of software that only ran on Windows XP (which was released when I was in elementary school). Dr Gillian Douglas guided me through mitochondria isolation, providing crucial advice at a time of great need. Dr Andrew Shaw and I became fast friends, and we often ran into each other in lab on weekends, when it was always great to have some company. Jade Bailey was the only other D. Phil student who accompanied me in Lab 3, and I appreciate that she has always been there to offer advice and chat about experiments. Ashley Hale and Victoria Rashbrook were always available when I needed help. Dr Surawee Chuaiphichai encouraged me to try rowing, which became one of my favourite hobbies, and I'll treasure all of the coaching he gave me.

Many other members of CV Med and beyond also supported me throughout my research. Prof. Martin Farrall and Dr Bob Mahoney, my graduate study administrators, have supported and guided me throughout my degree, and were always available on a moment's notice to discuss any issues that arose. Dr James Brown, our lab manager, works tirelessly to ensure that our experiments were feasible – at one point going on an epic journey with Sevi and me to locate the Goldilocks plate reader that would actually work with the mitochondrial swelling assay. After trying five plate readers in various buildings over two months, James joked that we were seeing plate readers in our sleep (which was technically true), and I cannot thank him enough for maintaining good spirits through our adventure. The Watkins group also provided a sanctuary for me to discuss science and life, and they were always available for me, especially at night and on weekends when the labs were quiet. Drew Worth at the Jenner Institute provided invaluable help with flow cytometry, and his expertise is greatly appreciated.

I'd like to thank my various assessors, Prof. Carolyn Carr, Prof. Ellen Aasum, Prof. Katja Gehmlich, and Prof. Lisa Heather. A special thanks to Prof. Carr for bearing the difficulty of my schedule twice – first allowing me to delay my confirmation so that I could complete experiments, and second for accommodating a rigid timeline for my viva voce. Without a doubt, my degree would not be possible without her flexibility and patience. I'd also like to thank Prof. Aasum changing her vacation plans to accommodate my viva schedule. Prof. Carr and Prof. Aasum exemplify the generosity of scientists that have made my journey possible.

My Oxford experience was made possible through the Rhodes Trust, and words cannot describe how much I appreciate the program and its wonderful community. Mary Eaton has always been around to offer me her wisdom and advice on matters large and small. She helped me to find my calling here at Oxford, and architected my late transition to the D. Phil program, offering me one of the greatest opportunities of my life. It has always brought me comfort to know that Mary is available to help me in times of need. It was an honour to be a Rhodes Scholar under Warden Charles Conn, who has substantially improved the future outlook of the Scholarship and expanded the global reach of the program. Charles took me under his wing, and has guided me in mapping out my future career path As a co-founder of the Rhodes Biomedical Association, a special thanks goes out to all of the Rhodes scholars and staff that made the program possible – including hosting the inaugural Rhodes Healthcare Forum. Through my experiences at Rhodes House, I had the good fortune of befriending Gerald Chan and Dr Fred Cohen, titans in pharmaceutical development that have helped me regarding my future career goals. At Rhodes House, I've had the opportunity to truly connect to the current and future leaders of the world, for which I am very thankful. A special acknowledgement also to John Morrison, president of the American Association of Rhodes Scholars for spending a day with me on each of his Oxford trips. I am certain our friendship will only grow stronger with time, and he is truly an inspirational figure for what one can accomplish at Oxford.

Much of my success is also founded on the support of University College. Prof. Peter Jezzard, Director of Graduate Studies, has helped me get through many a rough patch in my D. Phil. Our master, Sir Ivor Crewe, has always kept an eye out for me and ensured that I would have access to any resources that I needed from the college.

Finally, I'd like to thank my friends and family, whom have kept me company throughout my time here at Oxford. The dreary winters of Oxford were tough, and things were always easier after a night with friends in the pub. A special thanks to Billy Rathje, Maya Krishnan, Peter Kalugin, Alex Coccia, and Robert Fisher and the rest of my friends for their kindness and generosity throughout my time at Oxford. Last, but definitely not least, I'd like to thank my parents, whom have gone through the highs and lows with me during my time in Oxford – I have always felt blessed to always know that they are there for me whenever I need them. As I head back to the US, I am amazed by how much my experiences at Oxford have shaped me, and I look forward to new adventures at Harvard and in the years to come.

Table of Contents

1 Introduction 23

1.1 High energy phosphates and the creatine kinase system 23

1.1.1 Adenosine triphosphate 23

1.1.2 ATP hydrolysis and ΔG_{ATP} 23

1.1.3 Creatine kinase reaction 24

1.1.4 Biosynthesis and metabolism of creatine 25

1.1.5 Functions of the creatine kinase system 28

1.1.6 Creatine kinase isoforms 29

1.2 Muscle creatine kinase (CK-M) 32

1.2.1 Genetics and developmental regulation 32

1.2.2 Protein structure 32

1.2.3 Localization and function 33

1.2.4 Post-translational modification (PTM) and Regulation 34

1.3 Mitochondrial creatine kinase (CK-Mt) 36

1.3.1 Genetics and developmental regulation 36

1.3.2 Protein structure 37

1.3.3 Localization and function 38

1.3.4 Post-translational modification and regulation 41

1.4 Brain creatine kinase (CK-B) 43

1.4.1 Gene structure 43

1.4.2 Protein structure 43

1.4.3 Localization and function 44

1.4.4 Post-translational modification and regulation 44

1.5 Cardiac bioenergetics in the healthy heart 45

1.5.1 Substrate utilization and energy production 45

1.5.1.1 Fatty acid metabolism 46

1.5.1.2 Glucose metabolism 46

1.5.1.3 Lactate metabolism 47

1.5.1.4 Randle cycle 48

1.5.1.5 Regulation of mitochondrial energy production 48

1.5.2 Energy utilization 49

1.5.3 Phosphotransfer systems 49

1.5.3.1 Adenylate kinase and AMPK 50

1.5.3.2 Energy transfer and storage 51
1.6 Cardiac bioenergetics and CK system in heart failure 53
1.6.1 Impaired cardiac metabolism 53
1.6.2 Changes in CK system function 55
1.6.2.1 Loss of creatine substrate 55
1.6.2.2 CK dysfunction 56
1.7 Modulation of the cardiac creatine kinase system 58
1.7.1 Pharmacological and genetic modulations of creatine content 58
1.7.1.1 β-GPA studies 58
1.7.1.2 Guanidinoacetate-N-Methyltransferase (GAMT) knockout model 60
1.7.1.3 Arginine:Glycine Amidinotransferase (AGAT) knockout model 62
1.7.1.4 Creatine Transporter (CrT) knockout model 63
1.7.1.5 Creatine Transporter (CrT) overexpression model 64
1.7.2 Pharmacological and genetic modulation of creatine kinase 66
1.7.2.1 Pharmacological models 66
1.7.2.2 CK-M/CK-Mt knockout models 67
1.7.2.3 CK-M overexpression model 74
1.8 Summary and experimental aims 75
2 General materials and methods 77
2.1 Chemical and laboratory supplies 77
2.2 Colony Management 77
2.2.1 Mouse husbandry 77
2.2.2 DNA extraction 78
2.2.3 PCR 78
2.2.4 Agarose gel electrophoresis of PCR products 79
2.2.5 Harvesting of tissue 79
2.3 Biochemical measurements of CK activity/composition 80
2.3.1 Homogenization of heart and cell samples 80
2.3.1.1 Powder heart samples 80
2.3.1.2 Cell culture samples 81
2.3.2 Analysis of CK isoenzyme composition 81
2.3.3 Analysis of CK activity by spectrophotometry 83
2.3.4 Citrate synthase assay 85
2.3.5 Lowry protein assay 86

2.4 Cell culture 87
2.4.1 Cell lines 87
2.4.2 Cell culture conditions 89
2.4.3 Passaging 89
2.4.4 Plating 90
2.4.5 Long-term storage 90
2.4.6 Cell microscopy 90
2.5 Transfection methods 91
2.5.1 Transient transfection 91
2.5.2 Stable transfection 92
2.6 One-step qRT-PCR 93
2.6.1 RNA isolation from cell culture 93
2.6.2 One-step qRT-PCR 93
2.6.3 Quantification and data analysis 94
2.7 Flow cytometry experiments 94
2.8 Statistical analysis 95
3 Mitochondrial and metabolic phenotyping of the CK-Mt overexpression mouse model 96
3.1 Introduction 96
3.1.1 CK-Mt crystal aggregation – the limitations of CK-Mt overexpression 96
3.1.2 Characteristics of the CK-Mt OE transgenic mouse model 97
3.1.3 The mitochondrial permeability transition pore (mPTP) and its relationship to CK-Mt 98
3.1.3.1 mPTP molecular structure 98
3.1.3.2 Regulation and effects of mPTP 100
3.1.3.3 mPTP functions in physiology and pathophysiology 102
3.2 Hypotheses and aims 103
3.3 Methods 105
3.3.1 ^{1}H-NMR analysis of the metabolic profile 105
3.3.2 Mitochondrial isolation and evaluation of mitochondrial function 106
3.3.2.1 Bicinchoninic acid (BCA) protein assay 108
3.3.3 Assessment of the effects of CK-Mt overexpression on mPTP opening through mitochondrial swelling assay and western blotting 109
3.3.3.1 Optimization of mitochondrial swelling assay methodology 109
3.3.3.2 Optimized mitochondrial swelling assay protocol 111

3.3.3.3 Western blotting for cytochrome C 112
3.3.3.4 Assessment of mitochondrial quality through citrate synthase assay..... 114
3.4 Results 115
3.4.1 CK-Mt overexpression does not affect baseline metabolic profile 115
3.4.2 CK-Mt overexpression does not affect mitochondrial respiration 119
3.4.3 CK-Mt overexpression delays mitochondrial swelling..... 121
3.4.4 CK-Mt overexpression reduces cytochrome C release 122
3.4.5 CK-Mt overexpression does not affect mitochondrial integrity 123
3.5 Discussion 124
3.5.1 CK-Mt overexpression does not affect metabolism and mitochondrial respiration 124
3.5.2 Potential mechanisms underlying CK-Mt overexpression in protection against mPTP opening..... 126
3.6 Future work 131
4 Mitochondrial creatine kinase overexpression in an in vivo model of chronic heart failure 135
4.1 Introduction 135
4.1.1 Heart failure and the necessity for novel therapies 135
4.1.2 CK and heart failure 136
4.1.3 Principle of transverse aortic constriction (TAC) 137
4.2 Hypothesis and aims..... 138
4.3 Methods 139
4.3.1 Study design and CK-Mt OE mice 139
4.3.2 TAC protocol 140
4.3.3 *In vivo* characterization of heart failure in CK-Mt OE mice..... 141
4.3.3.1 Echocardiography 141
4.3.3.2 Metrics measured..... 144
4.3.3.3 In vivo LV haemodynamics..... 145
4.3.4 Measurement of lung/heart weights and tibia length 146
4.3.5 ^{31}P-MRS measurement of high energy phosphates..... 147
4.3.6 Analysis of creatine by HPLC..... 148
4.3.7 CK and citrate synthase (CS) activity 149
4.4 Results 150
4.4.1 Protocol n numbers and survival rates 150

4.4.2 Effects of CK-Mt overexpression on cardiac function as assessed by echocardiography 153
4.4.2.1 Correlation between banding severity and cardiac function 158
4.4.3 Effects of CK-Mt overexpression on cardiac function as measured by *in vivo* haemodynamics 160
4.4.3.1 Organ weights and tibia length 162
4.4.4 Characterization of cardiac bioenergetics during heart failure in CK-Mt OE mice 163
4.4.4.1 PCr/ATP ratio as assessed through ^{31}P-MRS 163
4.4.5 LV creatine content 165
4.4.6 Separation of CK isoenzyme and CK activity 166
4.4.6.1 Separation of CK isoenzymes by CK gel electrophoresis 166
4.4.6.2 CK isoenzyme and total CK activity 169
4.4.7 Citrate synthase activity as a measure of mitochondrial volume 171
4.5 Discussion 172
4.5.1 TAC as a model of heart failure and its effect on CK system 172
4.5.2 CK-Mt overexpression does not affect baseline cardiac function 175
4.5.3 CK-Mt overexpression in chronic heart failure and limitations of current study 176
4.5.4 The CK system in heart failure 178
4.6 Future work 180
5 In vitro model of creatine kinase overexpression to investigate doxorubicin cardiotoxicity 182
5.1 Introduction 182
5.1.1 Doxorubicin hydrochloride and cardiotoxicity 182
5.1.1.1 Mechanisms of DOX as an antineoplastic and a cardiotoxic agent 183
5.1.1.2 DOX and reactive oxygen species (ROS) 183
5.1.1.3 DOX-induced ROS interacts with CK-Mt 185
5.1.1.4 DOX impairs bioenergetics and CK function 186
5.1.2 CK system augmentation against DOX cardiotoxicity 187
5.2 Aims and hypothesis 189
5.3 Methods and Results 190
5.3.1 Methods and Results I: DOX in HEK293 cells 190
5.3.1.1 Protocol optimization 190
5.3.1.2 Use of FITC Annexin V stain 192

5.3.1.3 HEK293 cells are not susceptible to DOX 198
5.3.2 Methods and Results II: Experiments in HL-1 cells 202
5.3.2.1 HL-1 cell culture optimization 202
5.3.2.2 Optimization of DOX incubation conditions 205
5.3.2.3 Identifying positive controls 208
5.3.2.4 Confirmation of transient transfection in HL-1 cells with CK overexpression vectors 219
5.3.2.5 Transfection and verification of transfected cells 223
5.3.2.6 Evaluation of protective effects of CK overexpression on DOX cytotoxicity in transfected HL-1 cells 226
5.4 Discussion 230
5.4.1 HEK293 cells and resistance to DOX 230
5.4.1.1 Summary of experiments and conclusions 230
5.4.1.2 DOX cytotoxicity in HEK293 cells 231
5.4.2 CK overexpression does not protect against DOX cardiotoxicity in HL-1 cells 232
5.4.2.1 Summary of findings and conclusions 232
5.4.2.2 DOX cardiotoxicity and impaired bioenergetics 233
5.4.2.3 DOX cardiotoxicity and ROS 235
5.4.2.4 DOX cardiotoxicity and DNA intercalation 236
5.5 Future work 237
6 Development of *in vitro* tools for investigation of CK transcriptional regulators 239
6.1 Introduction 239
6.1.1 The necessity for tools to explore CK transcriptional regulation 239
6.1.2 The firefly luciferase reporter system 240
6.1.3 Principle of luciferase assay 241
6.1.4 Promoter structure and regulation of CK genes 242
6.1.4.1 CK-M 242
6.1.4.2 CK-Mt 244
6.1.5 Putative CK transcriptional regulators 245
6.2 Experimental aims 247
6.3 Methods 247
6.3.1 Luciferase vector structure and reporter system 247
6.3.2 Optimization of puromycin concentration 248

6.3.3 RNA extraction and qRT-PCR verification of mRNA expression 249
6.3.4 Luciferase assay protocol 250
6.3.4.1 Standard Luciferase assay protocol 250
6.3.4.2 Steady-Glo Luciferase and Resazurin Assay 250
6.3.5 Validation of CK-Luc constructs in transiently transfected cells 252
6.3.5.1 Verification of transfection efficiency and luciferase mRNA expression 252
6.3.5.2 Verification of luciferase expression 253
6.3.6 Generation of stably transfected CK-Luc cell lines 254
6.3.6.1 Vector linearization 254
6.3.6.2 Stable transfection 255
6.3.6.3 qRT-PCR analysis of luciferase mRNA 256
6.3.6.4 Luciferase assay 256
6.3.7 Luciferase screening of putative CK transcriptional regulators 257
6.3.7.1 Strategy for compound identification. 257
6.3.7.2 Screening of optimal incubation conditions by luciferase assay 258
6.3.7.3 Evaluation of CK mRNA by qRT-PCR 259
6.3.7.4 Assessment of putative control compounds with Steady-Glo Luciferase/Resazurin assay 259
6.3.8 Luciferase screening of compounds for CK-M-Luc cell line 260
6.3.9 Luciferase screening of compounds for CK-Mt-Luc cell line 261
6.4 Results 262
6.4.1 Puromycin kill curve 262
6.4.2 CK-Luc constructs in transiently transfected cells 263
6.4.2.1 Transfection efficiency and luciferase mRNA expression 263
6.4.2.2 Transiently transfected cells express luciferase 265
6.4.3 Characterization of stably transfected CK-Luc cell lines 266
6.4.3.1 Linearized vector by restriction digest 266
6.4.3.2 Identification and selection of stably transfected colonies 267
6.4.3.3 Detection of luciferase mRNA through qRT-PCR 268
6.4.3.4 Stably transfected cells expressed luciferase 269
6.4.4 Evaluation of putative CK transcriptional regulators 270
6.4.4.1 Effects on luciferase activity in CK-M-Luc cell line by luciferase assay 270
6.4.4.2 Changes in CK-M mRNA transcription as assessed by qRT-PCR 272
6.4.4.3 Effects on luciferase activity in CK-Mt-Luc cell line by luciferase assay 273
6.4.4.4 Changes in CK-Mt mRNA transcription as assessed by qRT-PCR 276

6.4.5 Screening of compounds for the CK-M-Luc and CK-Mt-Luc cell lines with the luciferase assay 277
6.4.5.1 Initial screening results using standard luciferase assay 277
6.4.5.2 Steady-Glo Luciferase, Resazurin, and qRT-PCR Results for CK-M-Luc cell line 280
6.4.5.3 Steady-Glo Luciferase, Resazurin, and qRT-PCR Results for CK-Mt-Luc cell line 283
6.5 Discussion 285
6.5.1 Validation of CK-luciferase constructs 285
6.5.2 Effects of putative CK transcriptional regulators on CK-M and CK-Mt transcription 286
6.5.3 Results from compound screen 289
6.5.3.1 CK-M-Luc results 289
6.5.3.2 CK-Mt results 290
6.5.4 Limitations of the luciferase assay 291
6.6 Future Work 291
7 Summary and future directions 294

Table of Figures

Figure 1-1: Molecular structures of ATP and phosphocreatine 25
Figure 1-2: Creatine synthesis and metabolism 27
Figure 1-3: Schematic of creatine kinase function 29
Figure 1-4: Schematic representation of CK subunit gene structures in different species 30
Figure 1-5: Sarcomeric CK-Mt structure 38
Figure 1-6: Illustration of VDAC-CK-Mt-ANT complex (mitochondrial interactosome) 40
Figure 1-7: Myocardial phosphotransfer network 52
Figure 1-8: Mitochondrial changes in dKO mice: 73
Figure 2-1: SPIFE CK isoenzyme assay 82
Figure 2-2: CK activity assay mechanism 84
Figure 2-3: Citrate synthase assay 86
Figure 3-1: Schematic detailing the activation and outcomes of mPTP opening 101
Figure 3-2: PCA analysis of aqueous and lipid metabolites in WT and Tg mice 118
Figure 3-3: Mitochondrial respiration assay 119
Figure 3-4: Mitochondrial respiration results of CK-Mt OE and WT mice 120
Figure 3-5: CK-Mt overexpression reduces mitochondrial swelling in response to Ca2+ 121
Figure 3-6: Western blot analysis of mitochondrial cytochrome C content after induction of mPTP opening 122
Figure 3-7: Citrate synthase results for samples from mitochondrial swelling assay 123
Figure 4-1: Schematic of experimental design and timeline of parameters analysed 140
Figure 4-2: Parasternal end-diastolic mid-ventricular echocardiography images 142
Figure 4-3: Coronal aortic arch echocardiography images 143
Figure 4-4: Survival curve of TAC and sham mice during chronic heart failure experiment 152
Figure 4-5: Effects of sham operation on echocardiography parameters in CK-Mt OE and WT mice 154
Figure 4-6: Effects of TAC on echocardiography parameters in CK-Mt OE and WT mice during heart failure 155
Figure 4-7: Aortic arch view and aortic arch ratio 159
Figure 4-8: LV haemodynamics in CK-Mt OE and WT mice 161
Figure 4-9: Morphometric data in CK-Mt OE and WT mice at the end of protocol 162
Figure 4-10: Sample ^{31}P-MRS spectra of WT and CK-Mt OE Sham/TAC Mice 163
Figure 4-11: PCr/ATP ratio assessed by phosphate MRS in CK-Mt OE and WT mice 164
Figure 4-12: LV creatine content of CK-Mt OE and WT mice 165
Figure 4-13: Separation of CK isoenzymes isolated from LV by SAS-1 gel electrophoresis 166
Figure 4-14: Relative CK Isoenzyme Composition in the LV tissue of WT and CK-Mt OE sham/TAC mice 168
Figure 4-15: Method for calculating CK isoenzyme activity from band density 169
Figure 4-16: CK activity in the LV tissue of WT and CK-Mt OE sham/TAC mice 170
Figure 4-17: Citrate synthase activity in the LV tissue of WT and CK-Mt OE sham/TAC mice 171
Figure 5-1: DOX redox cycle 185
Figure 5-2: Doxorubicin dose-response curve in HEK293 cells 192
Figure 5-3: Dual stain flow cytometry interpretation 194

Figure 5-4: DOX cytotoxicity in HEK293 cells as measured by PI and Annexin V-FITC... 196
Figure 5-5: Annexin V assay indicates that DOX does not kill HEK293 cells 197
Figure 5-6: DOX and PI emission spectra 197
Figure 5-7: HEK293 cells are not susceptible to DOX..... 200
Figure 5-8: Trypan blue exclusion assay for DOX-treated HEK293 cells 201
Figure 5-9: HL-1 cell proliferation experiments..... 204
Figure 5-10: Comparison of responses to DOX in HEK 293 and HL-1 cells..... 205
Figure 5-11: Optimization of DOX concentrations and treatment times in HL-1 cells..... 208
Figure 5-12: Structures of Trolox and vitamin E..... 210
Figure 5-13: DEX protection in cells treated with 48-hour DOX treatment..... 212
Figure 5-14: Optimized DEX conditions do not protect against DOX toxicity in HL-1 cells214
Figure 5-15: Metformin does not protect against DOX cytotoxicity in HL-1 cells..... 215
Figure 5-16: Visnagin does not protect against DOX cytotoxicity in HL-1 cells..... 216
Figure 5-17: Optimization of Trolox concentrations in HL-1 cells with 48 hour treatment. 218
Figure 5-18: 72-hour Trolox treatment protects against DOX-induced cytotoxicity in HL-1 cells 219
Figure 5-19: CK-Mt OE vector and GFP vector maps 220
Figure 5-20: Confirmation of transfection technique in HL-1 cells 221
Figure 5-21: CK mRNA expression in transfected HL-1 Cells 222
Figure 5-22: Increased total CK and CK isoenzyme activity in CK-transfected HL-1 cells. 225
Figure 5-23: Representative flow cytometry results of DOX in CK OE HL-1 cells 229
Figure 5-24: Lack of protection of CK-isoenzyme overexpression in HL-1 cells treated with DOX 229
Figure 6-1: Firefly luciferase reaction..... 241
Figure 6-2: Schematic illustration of CK-M promoter region 243
Figure 6-3: Schematic illustration of CK-Mt promoter region 245
Figure 6-4: Vector maps of luciferase reporter system..... 248
Figure 6-5: Puromycin causes dose-dependent death HEK293 cells..... 262
Figure 6-6: Puromycin kill curve as assessed by flow cytometry..... 263
Figure 6-7: Expression of luciferase mRNA in transiently transfected HEK293 cells by qRT-PCR. 264
Figure 6-8: Luciferase assay results from HEK293 cells transiently transfected with CK-Mt-Luc or CK-M-Luc 265
Figure 6-9: Restriction digest of CK-Luc vectors..... 266
Figure 6-10: Puromycin selection of CK-M-Luc or CK-Mt-Luc plasmid transfected HEK293 cells 267
Figure 6-11: Confirmation of luciferase mRNA expression in stably transfected HEK293 cells 268
Figure 6-12: Luciferase assay results for stably transfected CK-Luc cells..... 269
Figure 6-13: Effect of putative transcriptional regulators on luciferase activity of CK-M-Luc cells 271
Figure 6-14: Effect of LYS294002 on luciferase activity of CK-M-Luc cells..... 272
Figure 6-15: Effects of putative transcriptional regulators on CK-M mRNA as analysed through qRT-PCR in CK-M-Luc cells..... 273
Figure 6-16: Effect of putative transcriptional regulators on luciferase activity of CK-Mt-Luc cells 274

Figure 6-17: Effect of LYS294002 on luciferase activity of CK-Mt-Luc cells 275
Figure 6-18: Effects of putative transcriptional regulators on CK-Mt mRNA as analysed through qRT-PCR in CK-Mt-Luc cells 276
Figure 6-19: Positive hits from luciferase screening for CK-M-Luc cell line 278
Figure 6-20: Steady-Glo Luciferase and Resazurin results for CK-M-Luc cell line 281
Figure 6-21: Effects of treatments on CK-M mRNA analysed through qRT-PCR 282
Figure 6-22: Steady-Glo Luciferase, Resazurin, and qRT-PCR screening results for CK-Mt-Luc cell line 284

Table of Tables

Table 2-1: Genotyping primers for CK-Mt OE mice. 79
Table 3-1: Metabolomics profile of CK-Mt OE homozygote and WT mice 116
Table 4-1: Causes of death of mice on protocol 151
Table 4-2: Number of mice used in each experimental group 151
Table 4-3: Pulmonary artery and aortic arch echocardiography measurements at 6 weeks on sham protocol mice 156
Table 4-4: Pulmonary artery and aortic arch echocardiography measurements at 6 weeks on TAC protocol mice 157
Table 5-1: Primers for CK transfection experiments in HL-1 cells 222
Table 5-2: Optimized final protocol for investigation of CK or creatine in protection against DOX cytotoxicity in HL-1 cells transfected with CK 226
Table 6-1: CK-M promoter binding elements* 243
Table 6-2: Primers for luciferase transfection experiments 249
Table 6-3: Digestion solutions for vector linearization 254
Table 6-4: Concentrations and solvents for candidate CK transcriptional regulators 258
Table 6-5: All results of luciferase screening for the CK-M-Luc cell line 279

List of Abbreviations

ADP, adenosine diphosphate
AGAT, arginine:glycine amidinotransferase
α-MHC, alpha-myosin heavy chain
AK, adenylate kinase
AMP, adenosine monophosphate
AMPK, AMP-activated protein kinase
ANT, adenine nucleotide translocase
APP, amyloid precursor protein
ASP-9, ankyrin repeat and suppressor of cytokine signalling box protein-9
AT-1 cells, atrial tumor-1 cells
ATP, adenosine triphosphate
BCA, bicinchoninic acid (assay)
β-GPA, beta-guanidinopropionic acid
β-MHC, beta-myosin heavy chain
BSA, bovine serum albumin
cAMP, cyclic adenosine monophosphate
cDNA, complementary DNA
CK, creatine kinase
CK-B, brain creatine kinase
CK-M, muscle creatine kinase
CK-M-Luc, CK-M promoter-driven luciferase vector
CK-Mt, mitochondrial creatine kinase
CK-sMt, sarcomeric mitochondrial creatine kinase
CK-uMt, ubiquitous mitochondrial creatine kinase
CK-Mt-Luc, CK-Mt promoter-driven luciferase vector
CO, cardiac output
CoA, Coenzyme A
CrT, creatine transporter
CS, citrate synthase
CSA, cross-sectional area
CsA, cyclosporin A
CSI, chemical shift imaging
DEX, dexrazoxane
dKO, double knockout
DNA, deoxyribonucleic acid
DMEM, Dulbecco's Modified Eagle's Medium
DMSO, dimethyl sulfoxide
DNFB, fluoro-2,4-dinitrobenzene
dNTP, deoxynucleotide triphosphate

DOX, doxorubicin
DTNB, 5,5'-dithiobis-(2-nitrobenzoic acid)
E-box, enhancer box
ECG, electrocardiogram
EDA, end-diastolic area
EDTA, ethylenediamine tetraacetic acid
EDP, end-diastolic pressure
EDV, end-diastolic volume
EF, ejection fraction
ESA, end-systolic area
ESP, end-systolic pressure
EDV, end-systolic volume
EGTA, ethylene glycol-bis(β-aminoethyl ether)-N,N,N',N'-tetraacetic acid
ETC, electron transport chain
EV, empty vector
FA, fatty acids
FAD, flavin adenine dinucleotide
$FADH_2$, reduced form of FAD
FAO, fatty acid oxidation
FBS, fetal bovine serum
FCCP, carbonyl cyanide-4-(trifluoromethoxy)phenylhydrazone
FDA, US Food and Drug Administration
ΔG_{ATP}, free energy change of ATP hydrolysis
GAA, guanidinoacetate
GAMT, guanidinoacetate-N-methyltransferase
GFP, green fluorescent protein
G6PDH, glucose-6-phosphate dehydrogenase
GLUT, glucose transporter
HEK293, human embryonic kidney 293 (cells)
HEPES, 4-(2-hydroxyethyl)piperazine-1-ethanesulfonic acid
HIV, human immunodeficiency virus
HPLC, high performance liquid chromatography
IGF-1, insulin growth factor-1
I/R, ischemia/reperfusion
IA, iodoacetamide
IMM, inner mitochondrial membrane
K_{ATP} channel, ATP-sensitive K^+ channel
kD, kilodalton
KME, KCl-MOPS-EGTA buffer
KO, knockout
LDH, lactate dehydrogenase

LPL, lipoprotein lipase
LV, left ventricle
LVID, left ventricular internal diameter
NAC, Creatine-kinase-N-acetylcysteine (substrate solution)
MCT-1, monocarboxylate transporter-1
MEF-2, myocyte enhancement factor-2
MI, myocardial infarction
MIB, mitochondrial inclusion bodies
MOPS, 3-(N-morpholino)propanesulfonic acid
mPTP, mitochondrial permeability transition pore
MRI, magnetic resonance imaging
mRNA, messenger RNA
MuRF-1/4, muscle RING-finger protein 1/4
NAD, nicotinamide adenine dinucleotide
NADH, reduced form of NAD
NADP, nicotinamide adenine dinucleotide phosphate
NADPH, reduced form of NADP
NEB, New England Biolabs
O-CK, oxidized CK-M
OE, overexpressing
OMM, outer mitochondrial membrane
PBS, phosphate buffered saline
PCA, principle component analysis
PCR, polymerase chain reaction
PCr, phosphocreatine
PI, propidium iodide
Pi, inorganic phosphate
PKC, protein kinase C
PI3K, phosphatidylinositol 3-kinase
^{31}P-MRS, phosphorus-31 magnetic resonance spectroscopy
Polr2A, RNA polymerase II
PPAR, peroxisome proliferator-activated receptor
PTM, post-translational modification
RAR/RXR, retinoid/retinoic acid receptor
qPCR, quantitative polymerase chain reaction
qRT-PCR, quantitative reverse-transcriptase polymerase chain reaction
R-CK, reduced CK-M
RCR, respiratory control ratio
RIPA, radioimmunoprecipitation assay (buffer)
ROS, reactive oxygen species
ROSA26, reverse orientation splice acceptor 26

RT, room temperature
RV, right ventricle
SDS, sodium dodecyl sulfate
SERCA, sarco-endoplasmic reticulum calcium ATPase
SRF, serum response factor
SV, stroke volume
TAC, transverse aortic constriction
TBE, Tris/borate/EDTA (buffer)
TCA, tricarboxylic acid (cycle)
Tg, transgenic
TMRM, tetramethylrhodamine methyl ester
TMS, tetramethylsilane
TMSP, trimethylsilyl propanoic acid
TNBT, tetra nitro blue tetrazolium
TR, time resolution
TSA, transition-state analogue complex
UTR, untranslated region
UV, ultraviolet
VDAC, voltage dependent anion channel
WCHG, Wellcome Centre for Human Genetics
WT, wild-type

1 Introduction

1.1 High energy phosphates and the creatine kinase system

1.1.1 Adenosine triphosphate

Adenosine triphosphate (ATP) is the universal energy currency for energy-requiring cellular functions, such as cardiac muscle contraction and relaxation. Of all human organs, the heart has the highest demand for ATP (about 6 kg per day), with approximately 70% of cardiac ATP being consumed by myosin ATPase to power the contractile apparatus required to pump blood. Despite this intensive demand for ATP, the left ventricle (LV) contains only enough ATP for approximately 10 seconds of function - ~5 μmoles ATP/g, or ~10 mM ATP [1], with normal cardiac function requiring ~1 mM ATP per second [2]. This ATP pool is primarily generated through oxidative phosphorylation, and buffered by phosphotransferases, particularly creatine kinase (CK), to effectively maintain ATP homeostasis during periods of altering energetic demands.

1.1.2 ATP hydrolysis and ΔG_{ATP}

The hydrolysis of ATP to ADP and phosphate (P_i) (Reaction 1 below) releases energy to power cellular functions, such as cardiomyocyte contraction. Feedback occurs from ADP and P_i, which can stimulate oxidative phosphorylation and subsequent ATP synthesis [3].

Reaction 1: $ATP + H_2O \Leftrightarrow ADP + P_i$

The energy released by the hydrolysis of one mole of ATP is represented by ΔG_{ATP}, which is calculated by Equation 1 below.

$$\text{Equation 1: } \Delta G_{ATP} = \Delta G^0{}_{ATP} - RT \times ln(\frac{[ATP]}{[ADP][P_i]})$$

In the equation above, $\Delta G^0{}_{ATP}$ represents the energy released at standard state (-30.5 kJ/mol), R represents the universal gas constant (8.3 J/mol/K), and T represents temperature in Kelvin. The [ATP]/[ADP][P_i] ratio is termed the "phosphorylation potential", and contains the variables that change significantly in cells to determine cellular ΔG_{ATP} [1]. ΔG_{ATP} will be considered in terms of absolute value ($|\Delta G_{ATP}|$) to minimize confusion regarding comparing negative values.

1.1.3 Creatine kinase reaction

Creatine kinase (CK, EC 2.7.3.2) was first described in 1935 by Karl Lohmann [4] who had previously discovered ATP in 1929. Creatine kinase catalyses the reversible transfer of a phosphoryl residue between ATP and creatine, a β-guanidino phosphate carrier, as shown in Reaction 2.

$$\text{Reaction 2: Creatine + ATP} \Leftrightarrow \text{Phosphocreatine + ADP + } H^+$$

In the forward direction, Reaction 2 produces phosphocreatine (PCr), a high-energy phosphate carrier that is the major short-term energetic buffer of the cell. As shown in Figure 1-1, ATP consists of a nitrogen base, a de-oxy ribose sugar, and three polar phosphate groups (α. β, γ phosphate), whereas PCr consists of creatine and a single phosphate group. PCr provides a spatial, energetic, and temporal buffer for ATP, as discussed in Section 1.1.5.

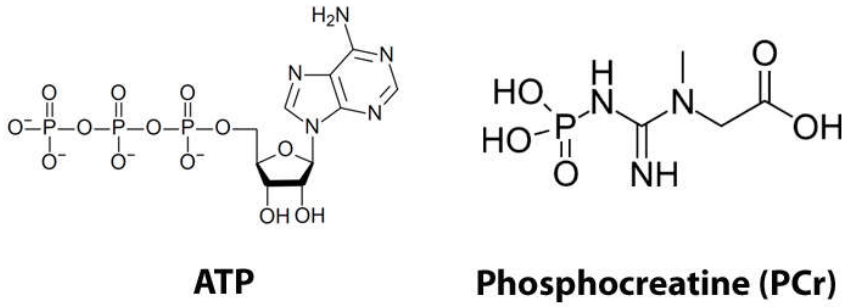


Figure 1-1: Molecular structures of ATP and phosphocreatine

1.1.4 Biosynthesis and metabolism of creatine

Creatine is a β-amino acid that is obtained either through meat in the diet, or through *de novo* synthesis. In mammals, about half of required creatine comes through diet, while the remainder is synthesized as shown in Figure 1-2 [5]. *De novo* creatine synthesis involves a two-step process that occurs in the kidney, liver, and pancreas. The process begins in the kidney, in which arginine-glycine amidinotransferase (AGAT, EC 2.1.4.1) combines glycine and arginine to form the creatine precursor guanidinoacetate (GAA). GAA is carried in the bloodstream to the liver and pancreas, in which guanidinoacetate N-methyl transferase (GAMT, EC 2.1.1.2) catalyses the methylation of GAA to form creatine [6]. It should be noted that both AGAT and GAMT can be found in other organs (*e.g.* skeletal muscle [6]) at much lower concentrations [7]. AGAT and GAMT are not found in the heart, which therefore cannot synthesize creatine [6,8].

After *de novo* synthesis, creatine is transported to target tissues (*e.g.* striated muscle, brain, kidney, and uterus) by the bloodstream. Creatine is actively transported against a 50-fold

concentration gradient into cells by creatine transporter (CrT), a specific chloride and sodium dependent transporter [5,9]. CrT is the only known method by which creatine can enter cardiomyocytes [5]. After entry into cells, creatine is phosphorylated by CK to PCr, and the PCr:creatine ratio in the myocardium is roughly 2:1 [1]. The activity of CrT is regulated by extracellular creatine concentrations, and increased extracellular creatine downregulates CrT activity (discussed further in Section 1.7.1.5) [10,11]. Thus, CrT acts as a major regulator in maintaining constant intracellular creatine content.

Approximately 95% of the human body's creatine (~118g) is stored in skeletal muscle, with most of the remainder found in the heart and brain [5]. Approximately 1.6% of total creatine in humans is lost each day through a non-enzymatic degradation into creatinine [12]. Creatinine is passively diffused across the cell membrane into the bloodstream, and is transported to the kidney where it is excreted in the urine.

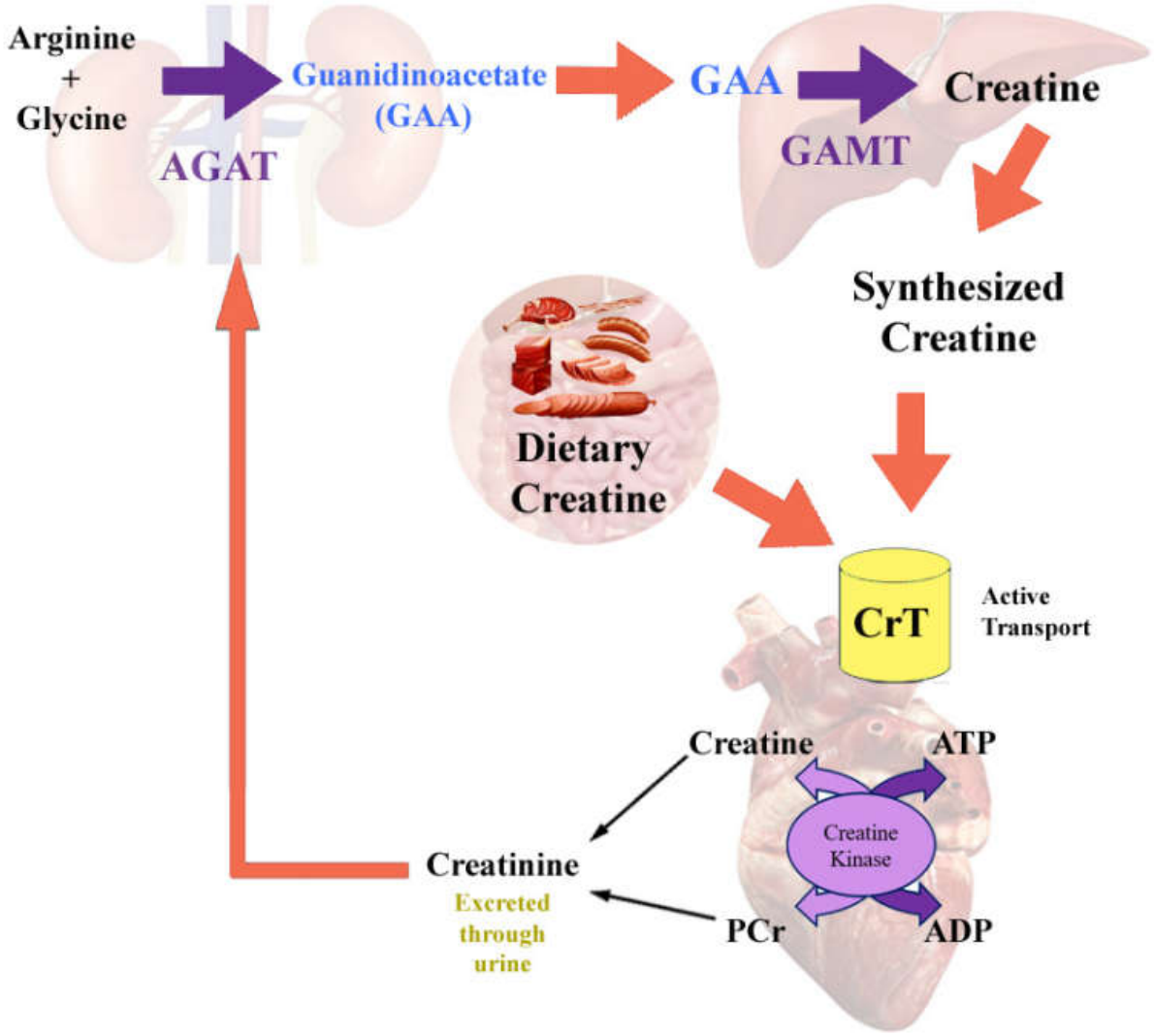


Figure 1-2: Creatine synthesis and metabolism

Creatine is synthesized *de novo* in kidney, liver, and pancreas, or obtained through diet. Creatine enters myocardium (and other cells) via active transportation by creatine transporter (CrT). AGAT: arginine:glycine amidinotransferase, GAMT: guanidinoacetate N-methyl transferase, PCr: Phosphocreatine. Purple arrows: Enzymatic processes; Pink arrows: Transport through the bloodstream. Figure adapted from [13].

1.1.5 Functions of the creatine kinase system

The CK system presents several advantages over using ATP alone to satisfy cardiac energetic demands. First, PCr functions as a transportable high-energy phosphate. As seen in Figure 1-1, PCr is much more diffusible in cytosol as compared to ATP due to its smaller size and lower polarity [14], which allows PCr to rapidly diffuse from the mitochondria to its various sites of utilisation in the cytosol, such as at the contractile apparatus. To facilitate transport, mitochondrial creatine kinase (CK-Mt) is located on the inner mitochondrial membrane, and primarily catalyses the transphosphorylation of ATP to PCr immediately after ATP synthesis in the inner matrix. Conversely, muscle and brain creatine kinase (CK-M and CK-B, respectively) are found in the cytosol, where their main function is to regenerate ATP from PCr at sites of energy utilization, often through functional coupling with ATPases.

Second, the creatine kinase system acts as the largest energy reserve that can be immediately used for ATP synthesis. In the heart, PCr is utilized when energetic demand outstrips the ATP supply provided by oxidative phosphorylation and glycolysis [1]. CK can regenerate ATP from PCr in humans at a rate (3.2 μmol ATP/sec/gram tissue wet weight) ten times higher than the rate of aerobic metabolism (0.3 μmol ATP/sec/gram tissue wet weight) [15], providing a rapid energy supply for sudden increases in metabolic demand. Therefore, the CK system functions as a reserve energy source, as well as a temporal buffer for energy generation.

Third, the creatine kinase system functions as a spatial buffer that improves the efficiency of ATP synthesis and hydrolysis. At mitochondria, ATP synthesized in the inner matrix through oxidative phosphorylation is immediately dephosphorylated back to ADP by CK-Mt while creatine is phosphorylated to PCr. This concentrates ADP at mitochondria, which stimulates further respiration. In the cytosol, CK-M and CK-B minimize local free ADP by using PCr to

phosphorylate ADP to ATP. At sites of ATP use, this increases $|\Delta G_{ATP}|$ and allows the ATP: ADP ratio to be maintained at above 100:1, compared to a cytosolic PCr:creatine ratio of only ~2:1 [9]. Thus, CK acts as a spatial buffer, maximizing the energetic favourability of ATP synthesis at mitochondria, and ATP hydrolysis at sites of ATP utilisation. The functions of CK in mitochondria and cytosol are illustrated in the Figure 1-3 below.

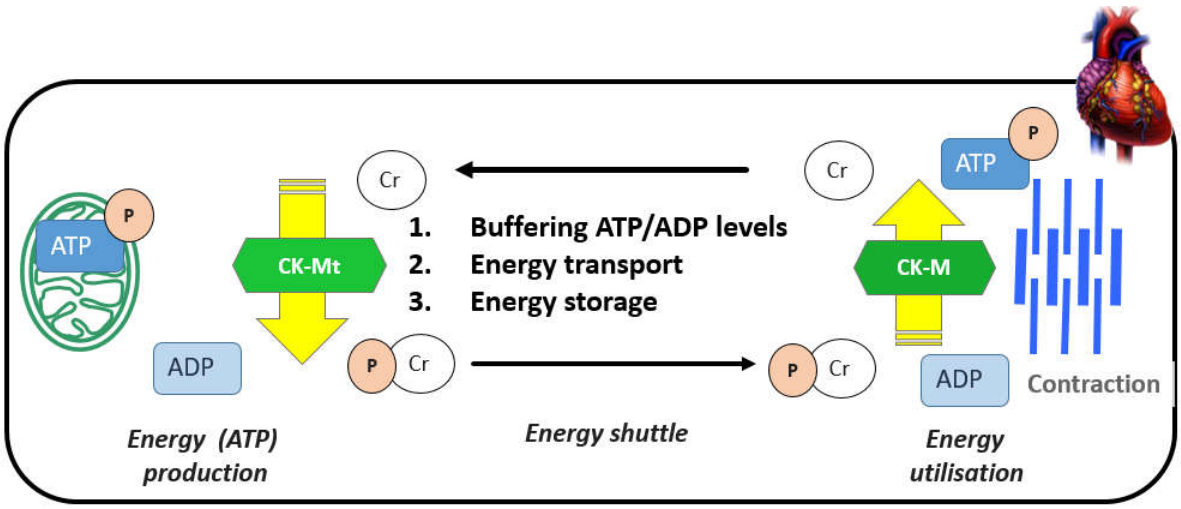


Figure 1-3: Schematic of creatine kinase function

Illustrates the various functions and isoenzymes of creatine kinase. Note the localization of CK-Mt in the mitochondria and CK-M in the cytosol, near sites of ATP use such as at sarcomeres. The major function of CK-Mt is to generate PCr for diffusion, whereas the major role of CK-M is to generate ATP for cellular function. Adapted from [8].

1.1.6 Creatine kinase isoforms

The four subunits of CK (CK-M, CK-B, ubiquitous CK-Mt, and sarcomeric CK-Mt) can form five functional isoenzymes of CK: muscle-muscle (CK-MM), brain-brain (CK-BB), muscle-brain (CK-MB), octameric sarcomeric mitochondrial (CK-sMt), and octameric ubiquitous mitochondrial (CK-uMt). It should be noted that while the primary functional isoform of both

mitochondrial subunits is the homo-octamer, homo-dimers also exist under physiological conditions. Each isoform is discussed in greater detail in subsequent sections.

Each subunit is encoded by a distinct gene, regulated by different elements, and serves unique functions. Nevertheless, there is a high degree of homology between the different subunits and across mammalian species. For example, the cytosolic subunits (CK-M and CK-B) in humans have 80% sequence homology, as do the mitochondrial subunits (CK-sMt and CK-uMt). The homology of CK subunit gene structures between species is illustrated in Figure 1-4 below.

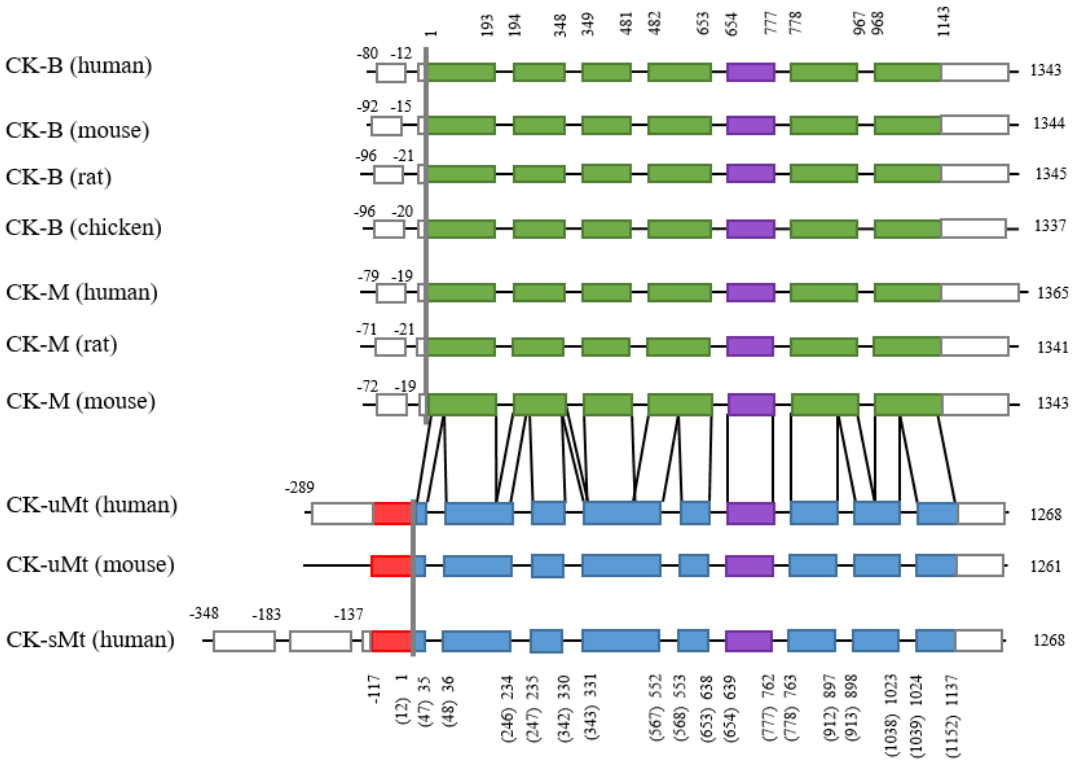


Figure 1-4: Schematic representation of CK subunit gene structures in different species

Human, mouse, rat, and chicken genes of CK subunits are presented. Exons are drawn to scale. The purple bar represents the coding exon that has been conserved throughout all mammalian and avian CK subunits. The green and blue bars represent the other coding exons, which are spliced differently in the cytosolic and mitochondrial CK isoforms. The red bars represent the mitochondrial transit peptide for the mitochondrial isoforms. The white bars represent various non-coding regions. Numbers on the bars represent the corresponding nucleotide sequences within cDNA sequences. Figure adapted from [16].

The expression of CK subunits is developmentally regulated and is tissue specific. For instance, the ratio between CK-M and CK-Mt in a given muscle is correlated with the preferred energy source of the muscle [17]. Cardiac muscle primarily utilizes oxidative phosphorylation to generate ATP, and as a result, CK-Mt accounts for ~25% of total CK activity, since the main role of CK-Mt is to transphosphorylate mitochondrial ATP to PCr, forming more ADP to stimulate further oxidative phosphorylation. The remaining CK activity in cardiac muscle is accounted for by CK-M (~75%) and CK-B (~2%) [17,18]. In contrast, fast-twitch skeletal muscle relies mostly on glycolytic pathways for energy production, and thus CK-Mt only accounts for <5% of total CK activity [17,19]. CK-M is substantially more abundant in fast-twitch muscle (~95%), as it reversibly transphosphorylates PCr to ATP at myofibrils, maximizing immediate utilization of the PCr energy reserve. Slow-twitch skeletal muscle has traits of both cardiac and fast-twitch skeletal muscle with more balanced contributions from glycolysis and oxidative phosphorylation, and thus has a CK-Mt/CK-M activity distribution in between (~7-10% CK-Mt; 90-93% CK-M) [17,19]. The general structures, functions, and locations of these CK isoenzymes are introduced in the following sections. From this point forward, “CK system” will refer to CK enzyme and substrate, whereas “CK” refers specifically to the enzyme.

1.2 Muscle creatine kinase (CK-M)

1.2.1 Genetics and developmental regulation

The CK-M gene is located at 19q13 [20]. In the early stages of myocyte formation, CK-B is the predominant subunit, but CK-M mRNA expression and protein activity overtake that of CK-B gradually in the first several weeks post-partum in rats [21,22]. This transition is most likely caused by the decline in mitogen concentrations in maturing heart and skeletal myoblasts, which occurs concomitantly with increased CK-M mRNA expression and CK-M activity [23]. In the heart, the increase in CK-M activity coincides with the switch in the main energy source of the myocardium from glycolysis during the foetal period to oxidative phosphorylation after birth, to meet the increased energy demand of mature myocardium [23,24]. The genetic regulation of CK-M is discussed in detail in Section 6.1.4.

1.2.2 Protein structure

The structure of CK-M was first identified in 1998 via X-ray diffraction [25]. Specifically, the 85 kD CK-MM dimer from rabbit was analysed because CK-M is unstable as a monomer. The N-terminus domain of CK-M, responsible for dimer formation, was found to be around 100 residues, whereas the C-terminus domain was larger, approximately 250 residues. It was reported that the N-terminus of CK-M differed from that of CK-sMt, which prevents CK-M and CK-sMt subunits from forming hetero-dimers. In total, the CK-M contained 12 α-helices and 10 β-sheets in two main domains. The ATP/ADP binding site, which is conserved in CK-M and CK-sMt, is specified by five highly-conserved arginine residues at positions 130, 132,

236, 292, and 320, and the creatine binding site achieves binding specificity to creatine through residues Ile69 and Val325 [26].

1.2.3 Localization and function

CK-M is found in the cytosol and at the sarcomeres, sarcoplasmic reticulum, and plasma membrane of striated muscle cells. The pattern of CK-M localization appears to match cellular components that have high energy demand.

CK-M directly binds to the I-band and M-line of myofibrils and is functionally coupled to myosin ATPase [27-30]. Functional coupling, or metabolic channelling, describes a relationship in which the product from one enzyme (in this case ATP from CK-M) is prioritized as the substrate for a second enzyme (in this case myosin ATPase) [31]. The rate of ATP regeneration from CK-M is sufficient to supply myosin ATPase at maximum muscle contraction rates [30]. An investigation in isolated cardiac muscle fibre demonstrated that CK-M is essential for optimal myosin ATPase function [28], and the coupling increases in conditions of acidic pH and increased glycolysis, which could occur in response to increased energy demand (*e.g.* exercise) [32].

CK-M also binds to the sarcoplasmic reticulum membrane, and is functionally coupled with sarcoplasmic reticulum Ca^{2+} ATPase (SERCA) [33,34]. This relationship is significant as SERCA has very high $|\Delta G_{ATP}|$ demands (52 kJ/mol) [1], thus the enhancement to energetic efficiency provided by CK-M is especially critical [2,34]. CK-M has been shown to support SERCA function and improve calcium homeostasis in cardiac muscle [35], skeletal muscle [33,34,36], and *in vitro* cultured myotubes [37]. Crucially, CK-M knockout (KO) studies in

mice reported that CK-M deficiency resulted in impaired calcium homeostasis in cardiac muscle [35] and skeletal muscle [34].

Additionally, CK-M is physically associated with cardiac sarcolemmal ATP-sensitive K^+ (K_{ATP}) channels, which belong to a group of intracellular ATP sensors [38]. K_{ATP} channels are activated during the periods of metabolic stress, and couple metabolic status with membrane excitability. It has been suggested that CK-M, when associated to the K_{ATP} channel, will close the channel if there are adequate PCr reserves, which suggest an energy-sufficient environment [38]. In contrast, should the PCr supply be depleted, CK-M activity decreases, resulting in K_{ATP} channel opening, which reduces the myocardial action potential length and subsequently shortens the contraction duration and energy demand [39].

CK-M is also functionally coupled to other sites of ATP utilization, such as the plasma membrane Na^+/K^+ pump [40].

1.2.4 Post-translational modification (PTM) and Regulation

CK-M exists in an oxidized (O-CK) and reduced (R-CK) form. R-CK is the active, stable enzyme and accounts for 85% of CK-M at rest [41]. The O-CK form is enzymatically inactive, structurally unstable, and easily degraded back to monomer subunits. O-CK is generated by an intrachain disulphide bond between Cys74 and Cys146, which prevents CK from interacting with binding partners [41]. It has been reported that O-CK negatively regulates CK function, as the Muscle Ring Finger (MURF-1)/ubiquitin and other degradation pathways only target O-CK [41]. Thus, O-CK may exist as an oxidation-based control mechanism for regulating cellular CK-M content.

CK-M is phosphorylated by protein kinase C (PKC) and AMP-activated protein kinase (AMPK). In diabetic rat hearts, reduced PKC phosphorylation of CK-M at Ser 128 was associated with a 70% increase in synthesis of ATP from PCr as compared to the rate in normal hearts [42]. In other words, under physiological conditions, phosphorylation of CK-M at Ser 128 favours preservation of the PCr energetic reserve, whereas decreased PKC-mediated phosphorylation occurs in pathophysiological situations, such as diabetic hearts, to allow increased ATP synthesis through CK [42]. AMPK phosphorylates different residues on CK-M (Ser136 or Ser199), and results in the opposite effect of PKC phosphorylation. AMPK phosphorylation favours the regeneration of ATP from PCr in rat liver and heart [43,44]. AMPK is activated during situations of decreased energy supply and may occur to maximize ATP synthesis through PCr under increased workload. These findings indicated that phosphorylation of CK-M at different residues by various protein kinases provides a post-translational method of modulating CK activity based on energetic demands.

Emerging research suggests that CK-M is a target of post-translational modification by coenzyme A (CoA), termed "CoAlation" [45]. CoA is a thiol structure that is best known for its role in fatty acid oxidation and the TCA cycle, though it has recently been identified to covalently bind to protein cysteine thiols to form mixed disulphides, which occurs primarily in situations of oxidative and metabolic stress. *In vitro* catalytic assays demonstrated that CoA disulphides completely inhibited CK activity, but that the inhibition was reversible after application of a reducing agent. Further experiments in *ex vivo* rat hearts treated with H_2O_2 revealed that all CK subunits were susceptible to CoAlation. While the underlying mechanism and function of this PTM are unknown, it is hypothesized that CoAlation of CK occurs in acute

oxidative stress conditions, during which reversible CoAlation may protect CK from irreversible oxidative damage [45].

CK-M is also subjected to PTM from carboxypeptidase-N [46], which is the basis of formations of the cytosolic CK dimers (MM/MB/BB) [47]. Carboxypeptidase removes a C-terminus lysine from subunits of CK-M to allow the CK-MM dimer to form [48]. CK-M is also inactivated through acetylation of a cysteine residue in the active site [49,50], which is the mechanism by which iodoacetamide (IA) inactivates CK [49]. IA is a pharmacological inhibitor of CK discussed in Section 1.7.2.1. Finally, CK-M can be inactivated through S-nitrosylation of essential cysteine residues, which has been shown to reduce the functional coupling between CK-M and SERCA, hence affecting calcium homeostasis [51].

1.3 Mitochondrial creatine kinase (CK-Mt)

1.3.1 Genetics and developmental regulation

CK-uMt and CK-sMt are encoded by two genes known as CKMT1 (ubiquitous) and CKMT2 (sarcomeric), respectively. CKMT1 is located at 15q15.1, whereas CKMT2 is located at 5q13.3 [52,53]. CK-sMt shows an expression pattern very similar to CK-M, and is found only in striated muscle. Likewise, CK-uMt is found in tissues that express primarily CK-B, such as neurons, glial cells, placenta, uterine tissue, and spermatozoa [54,55]. As CK-uMt and CK-sMt are not expressed in the same tissues, they do not undergo the developmental subunit-shift that occurs between CK-B and CK-M in striated muscle development [22,55,56]. During the development of rat embryos, CK-uMt mRNA was detected in brain and intestine *in utero*,

whereas CK-sMt was not detected in any tissues until 7 days after birth [55]. Additional experiments in mouse embryos confirmed that CK-sMt is not expressed *in utero* [55,57]. Rather, it has been suggested that the appearance of CK-sMt in cardiomyocytes (between 1 week to 1 month after birth) may coincide with the completion of cardiomyocyte maturation [55]. CK-Mt gene regulation is discussed in detail in the 6.1.4.2.

1.3.2 Protein structure

The chicken CK-sMt octamer protein crystal structure was elucidated by X-ray crystallography in 1994 and was the first CK isoenzyme visualized [58]. The monomer structure of CK-sMt contains a 100-residue N-terminus domain and a larger C-terminus domain. The N-terminus domain consists of five α-helices and C-terminus domain consists of seven α helices and eight antiparallel β-sheets. The N terminus is responsible for both homodimer and homo-octamer formation, prevents binding to cytosolic CK subunits, and contains the signal sequence for mitochondrial transport. The C-terminus domain appears to be a homologous, conserved domain found in all CK isoenzymes, and contains the active site. CK-Mt immediately organizes into dimeric structures upon transport into mitochondrial, and subsequently forms octamers, which are energetically favoured [59].

The octameric structure has overall dimensions of 105 × 105 × 86 Å, and creates a central pore of 20 Å diameter (Figure 1-5) [58]. The four monomers on the hemisphere facing the inner mitochondrial membrane (IMM) utilize negatively charged C-terminal sections (Asp357-Lys380) to bind to positively charged cardiolipin on the outer leaflet of the IMM, which anchors the CK-Mt octamer to the IMM [60]. The height of the CK-Mt octamer allows it to fit tightly

between the inner and outer mitochondrial membranes, suggesting the octameric form may play a role in mitochondrial structural integrity [61].

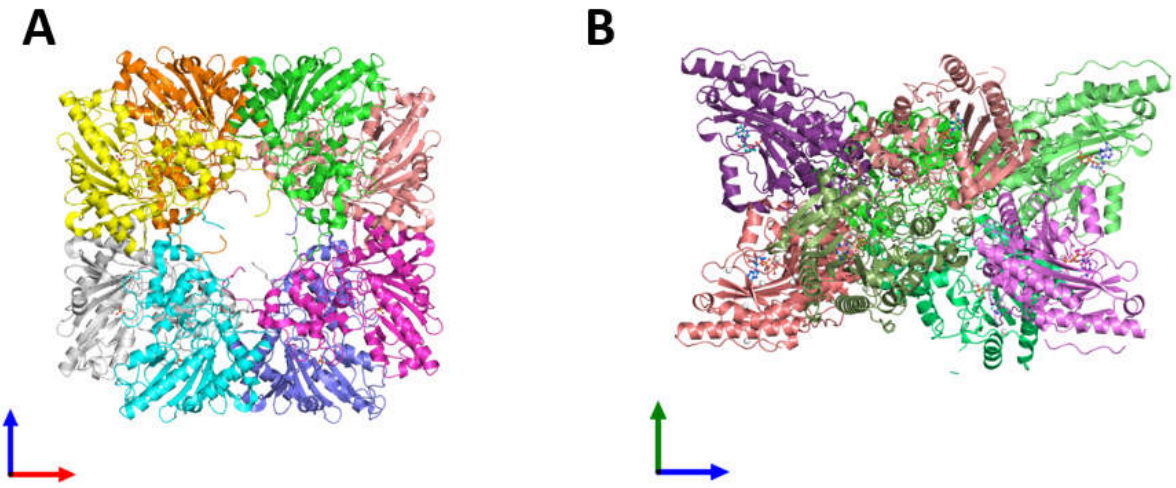


Figure 1-5: Sarcomeric CK-Mt structure

(A) Top, and (B) side views of human sarcomeric mitochondrial creatine kinase octamer (ID: 4Z9M). Structures obtained from the Protein Databank in Europe (www.ebi.ac.uk).

1.3.3 Localization and function

The intracellular localization of both CK-Mt isoforms is identical, and in the following paragraphs, "CK-Mt" refers to both isoforms. CK-Mt is situated in the inter-membrane space and cristae of mitochondria [31]. CK-Mt binds to cardiolipin in the IMM, and is functionally coupled to the adenine nucleotide translocase (ANT) in the cristae [17] and in the IMM [62]. CK-Mt binds to porin, also known as voltage-dependent anion channel (VDAC), on the outer mitochondrial membrane (OMM) [31].

Ultimately, this VDAC-CK-Mt-ANT multi-enzyme complex, termed the "mitochondrial interactosome" [63], allows CK-Mt to facilitate energy transfer between the inner/outer membranes (Figure 1-6). Specifically, ATP generated in the inner matrix through oxidative phosphorylation is shuttled through ANT to CK-Mt, which catalyses the transfer of the high-energy phosphate from ATP to PCr. PCr then exits into cytosol through VDAC, while ADP remains in the mitochondria. Thus, by modulating the local ATP/ADP ratio at mitochondria, CK-Mt plays a regulatory role in oxidative phosphorylation [1,64]. It should be noted that the mitochondrial interactosome requires octameric CK-Mt, as dimeric CK-Mt cannot form the same functional relationship with VDAC and ANT [65]. Therefore, the octamer-dimer transition may regulate CK-Mt function, and is discussed in detail in Section 1.3.4.

In addition to its function in bioenergetics, CK-Mt may also play a role in regulation of mitochondrial membrane transition pore (mPTP) opening, which causes mitochondrial-induced apoptosis and necrosis [66,67]. ANT and VDAC have both been suggested to be involved in regulating mPTP opening [68], and the possibility of mPTP regulation by CK-Mt is described in detail in Chapter 3.

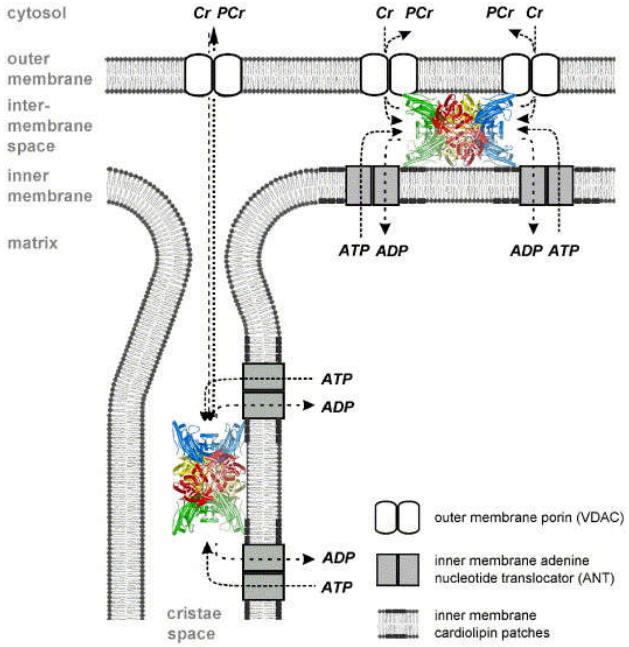


Figure 1-6: Illustration of VDAC-CK-Mt-ANT complex (mitochondrial interactosome)

The triple-protein complex is localized between the IMM and OMM. As seen in the figure, CK-Mt concentrates ADP in the mitochondrial inner matrix, enhancing ADP-stimulated respiration in the mitochondria. Adapted from [31].

CK-sMt is only known to have VDAC as a binding partner, although it is functionally coupled to ANT. CK-uMt has been reported to have several additional binding targets: ankyrin repeat and suppressor of cytokine signalling (SOCS) box protein-9 (ASP9), amyloid precursor protein (APP), and itself (to form macroenzymes). ASB-9 binds CK-uMt [69] and CK-B [70] to initiate destruction of these kinases through the ubiquitin system. It has also been suggested that the decline in CK-uMt function in Alzheimer's disease may be due APP binding and inactivation of CK-uMt [71]. Finally, CK-uMt creates "macroenzymes", large CK-uMt aggregates, which appear to be an epiphenomenon of HIV treatment with anti-retrovirals [72].

1.3.4 Post-translational modification and regulation

CK-sMt exists as dimers and octamers, with ~90% in the octamer form under physiological conditions [58]. The conversion between dimer and octamer forms represents a post-translational regulation mechanism of CK-Mt [73], and the octamer:dimer ratio is affected by pH and free radicals [59]. The following discussion focuses on CK-sMt, but largely apply to CK-uMt as well [59,74]. It should be noted that there are some minor differences between isoforms – for instance CK-uMt octamers are more stable, hence there is reduced octamer dissociation in response to peroxynitrite as compared to CK-sMt [59,74].

Effect of pH on octamer:dimer ratio

CK-sMt dimers will rapidly and spontaneously aggregate to octamers if present at sufficient concentrations in room temperature water, suggesting that the octameric form is more energetically favourable [58]. Dissociating octamers into dimers required a specific mixture of Mg^{2+}, ADP, creatine, and nitrate in alkaline pH, which induces a transition-state analogue complex (TSAC) [75]. As the octameric form is favoured in more acidic pH, this may imply that muscles under increased metabolic demand (↓pH) may generate more mitochondrial interactosomes to enhance energy production at the mitochondria [58].

Effect of free radicals on octamer:dimer ratio

CK-Mt is especially sensitive to oxidation and inactivation by various free radicals (reviewed in [31]), of which the most extensive studies have been done with peroxynitrite (ONO_2^-).

ONO_2^- is a potent oxidant synthesized by cells during its normal metabolism. ONO_2^- can dissociate CK-sMt octamers into dimers in a dose-dependent manner [74,76], and oxidizes residues at the dimer/dimer interface to permanently disable future octamer formation [74]. Additionally, ONO_2^- can directly inhibit CK-Mt enzymatic activity by oxidizing amino acid residues at the active site [74]. This inhibition can be prevented by high-energy phosphates, which competitively bind the same residues. Thus, under physiological conditions, when high-energy phosphates are present, CK-Mt is protected from free radical oxidation. However, under ischemic conditions in which PCr and ATP are depleted and the production of free radical species increases, CK-Mt can be rapidly disabled through oxidative damage. In conclusion, oxidation of CK can inhibit both the enzymatic activity and formation of the mitochondrial interactosome through interference of the CK-Mt octamer [76-78].

As discussed earlier, both CK-M and CK-Mt are subject to PTM by CoA, and it has been suggested that this CoAlation of CK-Mt is a protective mechanism against oxidative stress [45]. This hypothesis is further supported by the fact that CK-sMt can also be reversibly inactivated by S-nitrosylation of Cys278 mediated by glutathione/nitric oxide analogues [45,79], which has been proposed to function as a protective mechanism during conditions of oxidative stress [45,79].

Finally, ubiquitination, another PTM, may occur through CK-uMt binding to ASB9 as previously discussed. A study in dilated cardiomyopathy has shown increased ubiquitination of both CK-M and CK-sMt, though the pathway of this effect was not specified [80].

1.4 Brain creatine kinase (CK-B)

CK-B is present primarily in neurons, glial cells, uterus, sperm, and placenta [17]. The presence and function of CK-B in the brain has been intensively studied due to its potential implication in many neurological diseases. CK-B is also present in striated muscles, though it generally accounts for < 2% of total CK activity in the matured striated muscles [81,82].

1.4.1 Gene structure

The CK-B gene is located at 14q32.3 [83]. The CK-B enhancer region has many similarities to CK-M; for instance, MEF-2 was also found to regulate CK-B [84]. However, additional nuclear factors that regulate CK-B gene likely lead to the different expression patterns of the two cytosolic isoenzymes [85]. So far, unique CK-B gene binding proteins and processes remain largely unidentified [86].

1.4.2 Protein structure

The CK-B protein structure is similar to that of CK-M, with 80% of residues in common, including a common backbone, and the same two domains of α-helices and β-pleated sheets, although the N-terminus is different [87].

1.4.3 Localization and function

In the heart, CK-B mRNA expression and activity are highest *in utero*, and are inversely correlated with the maturation of cardiomyocytes, declining significantly post-partum [22]. After birth, CK-B is continuously expressed at low levels in the myocardium throughout life in the healthy heart, thought the significance of this residual CK-B expression in the myocardial CK system remains to be established.

In the brain, the highest expression of both proteins is in the cerebellum, especially in Purkinjie fibres [17,88]. A recent study reported that CK-B is localised at the endoplasmic reticulum of astrocytes, where it may be associated with energy demanding membrane-based processes such as ER Ca^{2+}-handling through an association with SERCA [89]. CK-B has been identified throughout neurons and/or glial cells (*e.g.* cytoskeleton, nucleus, plasma membrane), hence it may play a diverse role in cellular bioenergetics [89,90] . Unsurprisingly, CK-B has been implicated in a wide range of neurological conditions, including Alzheimer's disease [71,91] and Huntington's disease [92]. CK-B knockout models suggest that it is involved in spatial learning and memory [93,94].

1.4.4 Post-translational modification and regulation

Hydrogen peroxide (H_2O_2) causes irreversible oxidation of the active site cysteine on CK-B [95], which also undergoes other, unspecified oxidation processes. For example, in Alzheimer's disease, there is reduced CK-B activity even though the concentration of CK-B mRNA is unchanged [96]. This has been attributed to high oxidation rates found in these

neurological diseases, although the specific mechanisms of disease remain unknown. CK-B, like CK-M, has been shown to undergo phosphorylation by PKC in chicken brain [97] and by AMPK , in rat [89] and rabbit [98] brains. The specific physiological purpose of these PTMs remains to be conclusively determined, though preliminary research suggests that AMPK phosphorylation of CK-B increases its association with the endoplasmic reticulum surface, which may improve SERCA function [89]. Along with the other CK subunits, CK-B also undergoes CoAlation by coenzyme A [45].

1.5 Cardiac bioenergetics in the healthy heart

To pump over ten tons of blood each day, the heart relies on an intricate network of enzymes and metabolites, which can be broadly divided into three categories: 1) substrate utilization and energy production, 2) energy utilization, and 3) energy transfer and storage through phosphotransfer networks [9]. The CK phosphotransfer system affects all three categories, and its relevance is discussed when appropriate.

1.5.1 Substrate utilization and energy production

The cardiac metabolic network is highly flexible in its ability to utilize various carbon substrates including fatty acids (FA), carbohydrates, lactate, and ketone bodies [99]. The relative contribution of each substrate changes substantially in various conditions. For instance, the foetal heart generates a majority of its ATP through carbohydrate fuel sources, with FA being

the main energy substrate in the fasting adult heart. During exercise, lactate emerges as a major energy source, while ketone bodies are used during fasting/starvation conditions.

1.5.1.1 Fatty acid metabolism

β-oxidation of fatty acids represents the primary energy source of the fasted adult heart, accounting for approximately 70% of synthesized ATP [99]. More than 90% of plasma FA is contained within lipoproteins as triglycerides [100]. Lipoprotein lipase (LPL) on the outer plasma membrane of endothelial cells hydrolyses triglycerides and released fatty acids are transported into cardiomyocytes either by passive diffusion or with the support of transmembrane proteins such as CD36, which has been identified as the rate-limiting step of fatty acid uptake in cardiomyocytes [100]. Long chain fatty acids are esterified into fatty acyl-CoA, which is then transported into mitochondria through the carnitine shuttle to undergo β-oxidation in the mitochondrial inner matrix. The oxidation is accompanied by reduction of electron carriers NAD^+ and $FADH^+$, which in turn drive ATP production through oxidative phosphorylation at the mitochondrial inner matrix. The carbon chain of fatty acyl-CoA is then split into acetyl-CoA, which enters into the tricarboxylic acid (TCA) cycle to generate additional NADH and $FADH_2$ for ATP synthesis.

1.5.1.2 Glucose metabolism

The heart can also metabolize carbohydrates to fuel its function, which account for approximately 30% of the ATP synthesized in the fasted adult heart. Glucose is actively transported against a steep concentration gradient into the cardiomyocyte by glucose

transporter-1 and -4 (GLUT-1 and GLUT-4) on the cell membrane. GLUT-4, which is insulin-dependent, has been identified as the rate-limiting step of cardiac glucose metabolism in the healthy heart. After transport into the cell, glucose can be stored as glycogen, metabolized into pyruvate through glycolysis, or processed to lactate. At rest, less than 5% of myocardial ATP is produced by glycolysis, but glycolysis is of higher importance in the foetal heart and hypoxic conditions such as myocardial infarction (MI). Pyruvate can either be reduced to lactate in anaerobic conditions, or decarboxylated to acetyl-CoA in mitochondria to be used in the TCA cycle for further ATP synthesis through oxidative phosphorylation. It should be noted that creatine supplementation increased glucose oxidation in skeletal muscle [101], though whether such an effect occurs in cardiac muscle remains to be investigated.

1.5.1.3 Lactate metabolism

Lactate is produced from pyruvate by lactate dehydrogenase (LDH), and is generally transported out of the cell through the monocarboxylate transporter-1 (MCT-1) [102,103]. Lactate can also be imported from the bloodstream by MCT-1, oxidized into pyruvate by LDH, and metabolized through the TCA cycle to generate additional ATP at mitochondria through oxidative phosphorylation. Lactate is metabolized at rest but becomes the predominant substrate during exercise, when skeletal muscles release substantial quantities of lactate into the bloodstream, which is imported into cardiomyocytes through MCT-1 to generate energy alongside endogenously produced lactate [103,104].

1.5.1.4 Randle cycle

In the fasted state, cardiac fatty acid oxidation (FAO) competitively inhibits glucose utilization through downregulation of various steps in glucose metabolism, including glucose transport, glycolysis, and glucose oxidation [105]. This mechanism is thought to preserve glucose for organs that cannot metabolize fatty acids, such as the brain. Conversely, glucose can also modulate FAO, such as through malonyl-CoA, a product of glucose metabolism that can regulate FA transport and oxidation. This competitive interaction between FAO and glucose oxidation, termed the Randle cycle, is largely responsible for controlling cardiac substrate utilization at rest [105,106].

Under various stress conditions, substrate utilization is altered and the regulations of the Randle cycle is overruled. For instance, under metabolic or haemodynamic stress (*e.g.* oxygen deprivation, exercise), AMPK activation concurrently upregulates both glucose and FA oxidation, overriding the competitive interaction [105,107]. Similarly, in situations of β-adrenergic stimulation, there is simultaneous increases in both glucose and fatty acid oxidation to power the sudden increase in cardiac function [105].

1.5.1.5 Regulation of mitochondrial energy production

Mitochondrial respiration is essential for energy production in the heart, since mitochondria account for over 30% of the volume of the cardiomyocyte, and generate >95% of myocardial ATP through respiration [99]. Therefore, mitochondrial oxidative phosphorylation is regulated by various factors that participate in energy production and utilization, such as FA [105],

calcium, P_i, ADP, and creatine [3]. Since ADP and creatine are substrates for CK-Mt, it has been found that CK-Mt also modulates mitochondrial respiration and ATP production [31].

1.5.2 Energy utilization

Myocardial ATP utilization can be broadly divided into three categories [108,109]. First, there are mechanical processes that generate contraction, such as cross-bridge cycling. Second, significant energy is utilized form maintaining calcium homeostasis to couple excitation and contraction. Third, energy is consumed to maintain basic cellular processes. The CK system enhances the energetic efficiency of all three categories of ATP consumption. As previously discussed, CK-M is functionally coupled with myosin ATPase, which is the primary ATP consumer in cross-bridge cycling [110]. Similarly, CK-M has been shown to improve local bioenergetic efficiency at SERCAs [36], which are the most energy-intensive pumps required to maintain myocardial calcium homeostasis. Finally, CK-M is known to associate with the Na^+/K^+ plasma membrane pump [40], which is the major ATP-consuming process in basal metabolism [108]. Therefore, CK plays an important role in cardiomyocyte energy utilization.

1.5.3 Phosphotransfer systems

Myocardial energy production and utilization are connected through phosphotransfer systems that facilitate ATP transfer, act as energetic regulators, and function as energy storage. CK, the

primary phosphotransfer system has already been discussed in Section 1.1, and a second phosphotransfer system, adenylate kinase (AK), is detailed below.

1.5.3.1 Adenylate kinase and AMPK

The AK system supports CK function by shuttling high-energy phosphates [111], though ATP flux through AK (E.2.7.4.2) is several-fold lower than that of CK [112]. The main role of the AK system appears to be regulating energy demand, as seen through Reaction 3:

Reaction 3: 2 ADP ⇔ ATP + AMP

By generating ATP from ADP, AK synthesizes additional ATP that would otherwise not be available, while decreasing free ADP, which improves the thermodynamic favourability of $|\Delta G_{ATP}|$ at sites of ATP utilization. AK also generates AMP, which allows regulation of the total adenosine nucleotide pool, as AMP can be further degraded into adenosine via dephosphorylation by 5'-nucleotidase. Adenosine is membrane permeant and can be lost from the cell, which has been found to be cardioprotective during ischemia [113].

AMP is also of critical importance in the cardiomyocyte as the AMP/ATP ratio regulates AMPK activity. AMPK, a serine-threonine kinase, functions as an essential mediator of cellular energy homeostasis. AMPK is activated by energy depletion as reflected by elevated intracellular AMP/ATP ratios, and responds to the increased metabolic demand by activating catabolic pathways and downregulating anabolic pathways [107]. For instance, AMPK upregulates both FA β-oxidation as well as glucose metabolism, while inhibiting protein synthesis [105,107]. As previously discussed, there is also evidence that AMPK modulates CK-M and CK-B activity, affecting energy production and transfer.

1.5.3.2 Energy transfer and storage

ATP is primarily synthesized in the mitochondria whereas it is consumed elsewhere, detailed in Section 1.5.2. ADP and ATP are poorly diffusible, thus from a kinetic perspective, unassisted transfer of adenosine nucleotides would be ineffective given the substantial cardiac ATP demand. Furthermore, cardiomyocytes contain significant intracellular compartmentalization, and it has been suggested that cellular function depends primarily on local $|\Delta G_{ATP}|$ (*e.g.* at mitochondria, sarcoplasmic reticulum) rather than that of the entire cell [114]. In this context, simple diffusion of adenosine nucleotides is thermodynamically inefficient due to accumulation of ATP at mitochondria, and ADP and P_i at sites of ATP use.

As a result, a network of phosphotransfer systems such AK and CK facilitates transport of adenosine nucleotides, accounting for phosphotransfer of ~90% of the ATP generated through oxidative phosphorylation. While it is possible that PCr generated by CK-Mt in the mitochondria can diffuse to sites of ATP use, it has been postulated that there may be near-equilibrium networks of phosphotransfer enzymes that can transfer energy even more rapidly, without the need for major substrate movement, as depicted in Figure 1-7 [115]. It should be noted that in addition to energy transfer, these phosphotransfer networks also serve as energy reserves and spatial energy buffers as described in Section 1.1.5 for CK system.

Evidence suggests that the CK, AK, and glycolytic phosphotransfer systems are able to compensate for each other (glycolytic phosphotransfer systems have also been implicated in the phosphotransfer network depicted in Figure 1-7), indicating an interchangeable and resilient network. For instance, knockout of CK may cause upregulation of AK and glycolytic pathways in the heart [28,81]. Similarly, simultaneous knockout of CK and AK in skeletal muscle was found to result in significantly increased activity of glycolytic pathways [112]. Despite

compensatory mechanisms, both CK and AK knockout models exhibited measurable declines in intracellular energy transport and phosphotransfer communication [81,112], indicating that each component played an appreciable role in energy transfer.

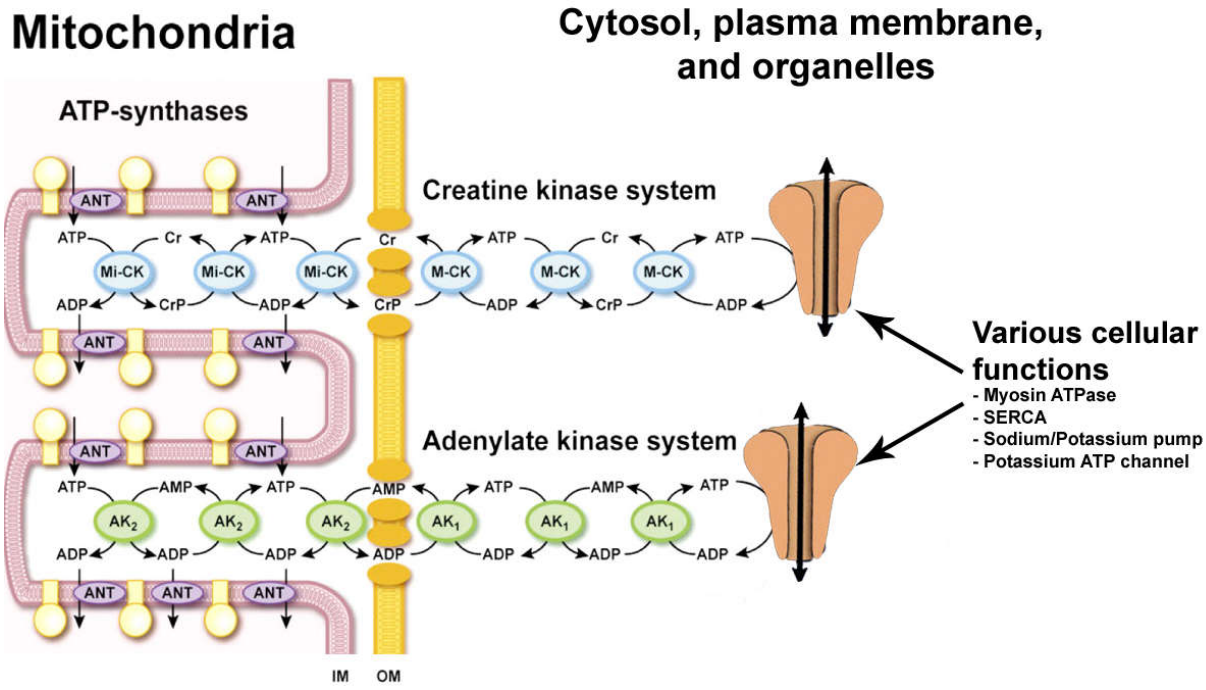


Figure 1-7: Myocardial phosphotransfer network

The postulated pathways for near-equilibrium enzymatic flux transfer networks is presented, with adenylate kinase (AK_1 and AK_2) and creatine kinase (Mi-CK (*i.e.* CK-Mt) and M-CK (*i.e.* CK-M)). In this system, AK and CK are found throughout the cytosol and in intracellular compartments, and catalyse near-equilibrium reactions. Hence the displacement of equilibrium in one compartment (*e.g.* increased ADP at sarcoplasmic reticulum) would be rapidly transmitted by a series of rapid, sequential equilibrating reactions through CK and AK to other connected compartments, such as the mitochondria. Similarly, energy from ATP generated at the mitochondria would be rapidly transmitted to sites of ATP use without the need for substrate movement. Through this method, adenosine nucleotide pools are recycled locally within compartments with minimal leakage between compartments. Figure adapted from [115].

In summary, ATP concentrations are remarkably stable in situations of fluctuating energy demands such as exercise, suggesting that energy production and energy utilization are precisely regulated and highly synchronous [1]. Due to their roles in energy transfer, communication, and storage, phosphotransfer systems are therefore considered as important energetic regulators. For instance, the CK phosphotransfer system has been proposed as an energetic regulator because it can modulate mitochondria respiration through CK-Mt and muscle contraction/calcium homeostasis through the CK-M [1,116]. Furthermore, the CK system acts as energy transport, and PCr serves as an energy reserve. As the CK phosphotransfer system affects many aspects of cardiac bioenergetics, considerable investigation has been conducted to elucidate the role of the CK system and cardiac bioenergetics during heart failure.

1.6 Cardiac bioenergetics and CK system in heart failure

1.6.1 Impaired cardiac metabolism

Pathological hypertrophic heart failure generally develops as a response to mechanical overload (*e.g.* hypertension, valvular disease or post-MI), whereas metabolic cardiomyopathy is primarily due to diabetes and obesity [99]. The metabolic remodelling in the pathological hypertrophic heart failure is different from the metabolic cardiomyopathy [99]. The following discussion focuses on pathological hypertrophic heart failure (*i.e.* induced by MI and pressure overload) since the majority of research into the CK system was conducted regarding these disease conditions [2,15,18,117,118].

The disruption in energy homeostasis that occurs in heart failure affects various aspects of cardiac bioenergetics. First, there is a switch in metabolic substrates that leads to significant changes in energy production. Through the course of heart failure, there is a gradual yet clear decrease in FAO, while glucose metabolism (primarily glycolysis) is substantially upregulated [9,99,119], possibly due to reactivation of foetal genes and/or down-regulation of adult genes involved in FAO and/or glycolysis [9,99,119-121]. It has been hypothesized that this shift to carbohydrate metabolism may be beneficial as carbohydrate oxidation produces more ATP per mole of oxygen than FAO [99,109], but upregulation of glucose metabolism cannot fully compensate for the reduction in FAO in terms of ATP production.

Second, the substrate shift is accompanied by significant mitochondrial pathology and dysfunction. For instance, mitochondria may have reduced size and compromised structural integrity [122], as well as impaired function of electron transport chain (ETC) elements and ATP synthase [123]. Moreover, there is reduced mitochondrial respiratory coupling and elevated in mitochondrial uncoupling proteins during heart failure [124]. Overall, these factors contribute to the decline in ATP production throughout the progression of heart failure [9].

Third, there is evidence of reduced efficiency in energy utilization. For instance, it has been shown that in heart failure, the depression in contractile force is more severe than the decline in energy consumption, suggesting that there is energetic inefficiency in the contractile apparatus [116,125]. Fourth, metabolic sensory systems, such as the cardioprotective K_{ATP} channel, are disrupted in heart failure, which compromises the ability for AK and glycolytic pathways to compensate for bioenergetic dysfunction [126]. Finally, there is a steep decline in high-energy phosphate reserve and energy transfer, which primarily occurs due to CK system dysfunction, as discussed in the next section.

1.6.2 Changes in CK system function

While significant research has focused on various facets of metabolic change during heart failure, the CK system plays a uniquely important role since it impacts many aspects of myocardial bioenergetics. The CK system stimulates respiration at mitochondria, functionally couples with ATPases such as SERCA and myosin ATPase (detailed in Section 1.2.3), serves as a form of energy storage through PCr, and acts as a shuttle for transporting high-energy phosphates. Due to its broad impact, CK system has been described as a regulator of myocardial bioenergetics [25]. Indeed, there are strong correlations between CK system dysfunction and heart failure severity, which is detailed in this section.

1.6.2.1 Loss of creatine substrate

One of the most prominent phenomena of impaired bioenergetics in heart failure is the gradual decline in creatine and PCr that occurs concomitantly with heart failure progression, indicating that the heart cannot adequately maintain its energetic reserve [116,127]. In various animal models of heart failure, LV total creatine decreased by up to 40%, as assessed through high performance liquid chromatography (HPLC) [128]. Similarly, LV PCr was reduced by as much as 48% [15,117,129], as assessed by phosphorus magnetic resonance spectroscopy (^{31}P-MRS). A reduction of total creatine by 50% [130] and PCr by 18% [15] has been reported in the myocardium of heart failure patients. A common trend found in these studies is that the decline in creatine and PCr precedes ATP loss [128,131] and occurs more rapidly [15,117,129]. It is reasonable that CK maintains ATP at the cost of PCr, given that the CK equilibrium constant favours ATP production over PCr production by 100:1 [1,132].

PCr:ATP ratios obtained non-invasively in patients through ^{31}P-MRS can be used as a diagnostic criteria to evaluate disease severity and mortality [133]. This index has been shown to be a sensitive predictor of mortality in heart failure, with similar prognostic capability as the New York Heart Association class [15][20]. It should be noted that PCr/ATP ratios may actually improve in late state heart failure as ATP concentrations eventually fall, hence this pseudo-normalization limits its use as a prognostic method. Overall, it is evident that the loss of myocardial creatine at least correlates with, if not causes, pathophysiology of heart failure.

The decline in total creatine content in heart failure may be caused by downregulation of creatine transporter [134], which is not necessarily pathological. Rather, this may be a beneficial compensatory mechanism, as decreasing creatine content in stress conditions may reduce levels of free ADP, thus, maintaining high $|\Delta G_{ATP}|$ [1]. Indeed, excessive creatine loading can induce heart failure, as CK cannot not adequately phosphorylate the enlarged adenosine pool, resulting in increased free ADP and decreased $|\Delta G_{ATP}|$ [135].

1.6.2.2 CK dysfunction

Across species, there are also significant reductions of CK isoenzymes and activity (except for CK-B) throughout different etiology of heart failure, in humans [15,130] or experimental animal models [18,117,128,136]. The average decrease in total CK activity across species is ~30%, with similar losses in CK-Mt and CK-M activity/protein (~30%). The reduced CK activity and protein were associated with a concomitant 30-40% reduction in high-energy phosphates (creatine, PCr, ATP, ADP) [15,18,117,128,130,136]. In contrast, CK-B protein and activity increased on average 770% and 240% during heart failure, respectively, which may be

a compensatory mechanism and/or a result of foetal gene activation in heart failure [18,128]. For instance, CK-B may be able to utilize PCr more effectively because it has a higher affinity for substrates such as ADP than other CK isoforms [89]. However, as CK-B only accounts for < 2% baseline CK in the heart, upregulation has only a minor effect on overall CK activity.

More recent advances in ^{31}P-MRS have allowed the measurement of *in vivo* rates of ATP turnover through the CK system (also termed "CK flux"). CK flux reflects changes for both enzyme and substrate and avoids the pseudo-normalization that occurs with PCr/ATP during late stage heart failure [132]. Thus, CK flux has been reported to be a more sensitive indicator of heart failure severity than PCr/ATP ratio [131]. For example, it was found that cardiac CK flux falls approximately 50% in patients with mild-moderate heart failure whereas PCr/ATP ratios declined only 18% [15]. Additionally, CK flux, but not PCr/ATP ratio, was a significant predictor of cardiovascular mortality in patients with non-ischemic cardiomyopathy [131]. The fall in CK flux in heart failure patients appears to be particularly severe since the ratio of CK flux to oxidative phosphorylation falls from 5-7 in patients without heart failure to 2-3 in chronic heart failure patients, indicating substantially compromised phosphotransfer in heart failure patients [15]. However, CK flux measurements are technically challenging and require long scan times, limiting sample sizes. Additionally, the technology does not differentiate between intracellular compartments and cannot measure unidirectional flow; therefore the measurement only represents an average of all CK reactions in the acquisition area [132].

Taken together, these impairments in the myocardial CK system have multifaceted consequences in heart failure. The most immediate effect is compromised energy transfer and storage, as the CK system is one of the primary facilitators of phosphotransfer and acts as a prominent energetic reserve. Additionally, there is evidence that the CK system stimulates both

glycolytic pathways [101] and mitochondrial respiration [64], hence impairments in the system may affect energy production. Reduced CK system function may contribute to the energetic inefficiency observed in the contractile apparatus in heart failure [116,125] due to the functional coupling between CK-M and myosin ATPase [137,138]. Finally, as CK-M is functionally coupled to cardiac K_{ATP} channels, deterioration of CK system function may contribute to the compromised metabolic signalling observed in heart failure [114].

1.7 Modulation of the cardiac creatine kinase system

A considerable body of research has been conducted on pharmacological and genetic modulations of the CK system in health and disease states, especially pertaining to heart failure. The collective findings from each model system is discussed in detail, and is summarized in a disease-specific manner in their respective Chapters (Chapter 3 for ischemia/reperfusion (I/R) injury and Chapter 4 for heart failure).

1.7.1 Pharmacological and genetic modulations of creatine content

1.7.1.1 β-GPA studies

Early investigations of creatine depletion relied on the use of pharmacological inhibitors, especially β-guanidinopropionic acid (β-GPA) [139]. β-GPA is a competitive antagonist for the creatine transporter and reliably reduces intracellular creatine and PCr in rodent striated muscle [140]. In the rat heart, β-GPA treatment resulted in an average 62% and 82% reduction of creatine and PCr, respectively [141], but is dependent on treatment length since the myocardial creatine loss is gradual.

β-GPA inhibition of creatine has been associated with cardiac pathology in various model systems. Isolated cardiac muscle fibres of β-GPA fed rats demonstrated decreased cross-bridge cycling and alterations in myosin subtype ratios [142]. Furthermore, rats pre-fed with β-GPA for 2 - 4 weeks could not survive acute MI, with 92-100% mortality within 24 hours after MI, compared to 40-50% mortality in wild type (WT) controls [143,144]. This increased mortality may have occurred because PCr depletion reduced the ability of residual intact myocardium to compensate for increased haemodynamic stress, indicating that a functional CK system was required to survive MI in the acute setting [143]. To explore the effects of β-GPA on MI-induced chronic heart failure, rats were first infarcted and then fed with or without β-GPA for 8 weeks. β-GPA fed rats showed no further difference in impaired cardiac functions, indicating that creatine depletion did not affect the post-MI cardiac dysfunction [143]. This was remarkable as the hearts of these rats exhibited a 94% decrease in CK flux and 70% lower creatine content [143].

There are significant limitations of β-GPA studies that must be considered when interpreting study results. These include: 1) β-GPA elimination of intracellular creatine is usually incomplete [141,143,144], 2) β-GPA can inhibit glycolytic enzymes [141,145,146], and 3) β-GPA can be a substrate for CK-M [144,147]. Indeed, ^{31}P-MRS studies have detected phosphorylated β-GPA, which can be utilized in tissue as a high-energy phosphate carrier (albeit with low reaction velocity) [147]. Thus, interpretation of β-GPA results is difficult as the results may be not exclusively caused by creatine depletion. Additionally, as β-GPA studies were conducted exclusively on rats, it remained unclear whether the results were species specific.

These confounding factors provided justification for the development of knockout mouse models of creatine deficiency. Specifically, creatine synthesis enzymes Guanidinoacetate-N-Methyltransferase (GAMT) and Arginine:Glycine Amidinotransferase (AGAT) were eliminated to investigate the effects of total creatine deficiency.

1.7.1.2 Guanidinoacetate-N-Methyltransferase (GAMT) knockout model

The first creatine deficient mouse was generated in 2004 by Schmidt *et al.*, resulting in whole-body constitutive knockout of GAMT [148]. This model resulted in loss of creatine in all relevant organs, including striated muscle, brain, uterus, spermatozoa, and other organs and tissues. As a result, various abnormalities were detected, including muscle hypotonia, increased neonatal mortality, decreased male fertility, and decreased body weight due to reduced fat reserves. Nevertheless, results from the initial study were inconclusive because GAMT KO hearts had 27% of WT creatine concentrations, which was attributed to intake of creatine through coprophagia from WT littermates [148].

Our group investigated the cardiac function of GAMT KO mice in more detail [149]. It was confirmed that GAMT KO mice had reduced body weight (~30%), increased relative LV weight [148,149], and almost normal baseline cardiac function at up to one year of age, with only a small but significant decline in LV systolic pressure (8%) [148-150]. The increased relative LV weight did not appear to be pathological since expression of hypertrophy markers such as atrial natriuretic factor and β-myosin heavy chain (β-MHC) was unchanged, and myocyte cross-sectional area was not significantly higher than that of WT mice [149]. However, *in vivo* haemodynamics analysis showed that GAMT KO mice had decreased

contractile reserve, as the hearts generated significantly less LV pressure and preload-recruitable stroke work under β-adrenergic challenge [149,151].

GAMT KO mice were also studied after acute MI and chronic heart failure secondary to MI. GAMT KO mice were found to survive similarly to WT mice after acute MI [151], which was remarkable given that β-GPA fed rats had ~90% mortality rates [143,144]. To explore whether this was attributable to an off-target effect of β-GPA, WT and GAMT KO mice were fed β-GPA prior and after MI. The death rates of both WT and GAMT KO mice were unaffected by β-GPA feeding, suggesting that the effects of β-GPA on cardiac function during MI in rats may be species specific [143,144]. In the chronic setting, mice were followed for six weeks after MI, during which survival was not significantly different between GAMT KO and WT mice. Both groups of mice developed similar degrees of post-MI heart failure which closely recapitulated β-GPA studies [143], suggesting that loss of PCr is not a driving force of pathophysiology in chronic heart failure.

In various GAMT KO studies, it was observed that the creatine precursor GAA accumulated inside cardiomyocytes of GAMT KO mice at millimolar concentrations [148,149,151,152]. It was found that GAA could be used as a high-energy phosphate carrier, though only at 1% of the CK reaction velocity for creatine [147,148]. It is possible that GAA phosphotransfer may have provided sufficient compensation for creatine deficiency at baseline [153], hence GAMT KO mice were tested in the context of I/R injury, a situation of significant energy depletion. In this context, GAA proved inferior to creatine, likely due to the reduced reaction kinetics. During ischemia, GAMT KO mice exhibited an increased preponderance to undergo ischemic contracture, and recovery was prolonged during reperfusion [149].

Other compensatory mechanisms may have attenuated the effect of creatine depletion, although mitochondria localization/function and AK activity were not significantly different from that of WT controls, and general protein expression patterns were unchanged [151,152]. In conclusion, it appears that creatine deficiency does not substantially impair cardiac function at rest or during MI, but was more detrimental during I/R injury.

1.7.1.3 Arginine:Glycine Amidinotransferase (AGAT) knockout model

Due to the complications of GAA, the AGAT knockout mouse model was generated, which lacked a functional CK phosphotransfer system due to a complete deficiency of AGAT, GAA, and creatine [154]. Initial investigation of AGAT KO skeletal muscle demonstrated significant dysfunctions, including decreased grip strength, gastrocnemius muscle volume, and ATP content [155]. Creatine supplementation reversed all impairments, providing compelling evidence that creatine is necessary for optimal skeletal muscle function [155].

A subsequent study investigating the AGAT KO cardiac phenotype found that AGAT KO mice appeared to exhibit increased LV weight, but did not have consistent increases in LV hypertrophy markers and myocyte cross-sectional area [156], which supported GAMT KO findings [149] that creatine deficiency does not spontaneously cause pathological LV hypertrophy. However, creatine-naïve AGAT KO mice did exhibit significant contractile dysfunction, including impaired contractile parameters (dP/dt_{max} and dP/dt_{min}), reduced inotropic reserve, and lower LV systolic pressure [156,157]. When myocardial creatine content was normalized by creatine supplementation, there was no recovery in contractility and ionotropic reserve, suggesting a creatine-independent cause of dysfunction [156,157].

Aside from creatine, AGAT also synthesizes homoarginine, and as such, AGAT KO mice had reduced homoarginine levels [156]. Supplementation of homoarginine in AGAT KO mice eliminated all contractile dysfunction both *in vivo* and in Langendorff perfused hearts (*i.e.* isolated perfused hearts), demonstrating that depletion of homoarginine, rather than creatine, was responsible for the AGAT KO cardiac phenotype [156-158]. Homoarginine, an L-arginine homologue [159], is correlated with outcomes in cardiovascular disease [160] and stroke [161], though its exact function remains unknown. Thus, overall, AGAT KO studies indicated that creatine was not essential for cardiac function at rest, but interpretation was complicated by concomitant homoarginine deficiency.

1.7.1.4 Creatine Transporter (CrT) knockout model

A CrT knockout mouse model (Cincinnati, USA) has also been generated to study the effects of eliminating intracellular creatine, though there is currently no conclusive information on the cardiac phenotype of these mice because residual creatine (0-21% of WT control value) was detected in myocardium, possibly due to sensitivity of the methodology used to measure creatine content [162,163]. Unpublished data from a different CrT knockout model (Hamburg, Germany) shows myocardial creatine content at 4 ± 1 nmol/mg protein, as compared to 64 ± 7 nmol/mg protein in WT controls (Professor Craig Lygate, *personal communication*). As 4 nmol creatine/mg protein is at the limits of detection of high performance liquid chromatography (HPLC), it appears that further investigation on the effects of cardiac creatine depletion can be conducted with the Hamburg CrT KO model.

1.7.1.5 Creatine Transporter (CrT) overexpression model

There is a strong correlation between cardiac creatine deficiency and heart failure in animal models [117,118,128] and patients [15] (reviewed in detail in Section 1.6.2), along with some causative evidence that creatine depletion reduces cardiac function during I/R and β-adrenergic stress. The most practical approach to counteract this creatine loss would be to increase myocardial creatine via oral or parenteral administration. Unfortunately, feeding creatine did not increase intracellular creatine concentrations in rat heart, hence there was no protective effect in chronic heart failure [11]. It was subsequently discovered that this was because the number and affinity of active creatine transporters in rat cardiomyocytes were precisely regulated in order to maintain a constant intracellular creatine concentration [10]. For instance, β-GPA administration resulted in a five-fold increase in active CrT on the plasma membrane, whereas creatine supplementation resulted in a 35% decrease in active CrT due to receptor sequestration. This CrT regulation mechanism allowed cardiomyocytes to maintain physiological creatine levels despite creatine loading or depletion, hence an alternate approach was required to elevate myocardial creatine concentrations [10].

Our group developed the first genetically modified mouse that overexpressed the creatine transporter exclusively in the heart [164]. Unexpectedly, it was found that mice with more than 2-fold higher myocardial creatine showed symptoms of heart failure, including 24% increased heart weight, LV dilation, and impaired LV ejection fraction. The severity of dysfunction was strongly correlated with intracellular creatine concentrations. Further investigation revealed that the spontaneous heart failure occurred because there was insufficient CK to adequately phosphorylate the enlarged creatine pool – for instance, CrT overexpressing (OE) mice with three-fold or higher creatine had a PCr:creatine ratio of less than 1:1, compared to a

physiological ratio of 2:1. The inability to adequately phosphorylate creatine increased free ADP two-fold and caused $|\Delta G_{ATP}|$ to decrease to 57.7 kJ/mol, as compared to 59.6 kJ/mol in WT mice. An increase in free ADP and decrease in $|\Delta G_{ATP}|$ closely mimic the impaired bioenergetics noted in models of heart failure [164-166]. These findings demonstrated the important role that CrT played in maintaining balanced bioenergetics in myocardial cells.

A follow-up study in CrT OE mice showed that creatine loading appeared to downregulate glycolysis by reducing enolase protein and activity [135]. As decreased enolase was also identified in cardiomyopathy [167,168] and hypertrophy [169] models, it is possible that the LV dysfunction caused by excessive creatine loading could be in part due to knock-on effects on cardiac metabolism.

In the previous studies [135,164], it was observed that CrT OE mice with moderate (20%-100%) increases in myocardial creatine showed no signs of cardiac dysfunction up to 18 months of age [2]. To test whether moderate creatine loading had any beneficial effects, these mice were then challenged with acute MI, heart failure, and I/R injury [2]. In response to *in vivo* infarction, mice with moderate creatine elevation exhibited 27% less myocardial necrosis with infarct area inversely correlated with intracellular creatine content. In *ex vivo* I/R, CrT OE mice maintained a significantly higher rate pressure product (RPP) during ischemia and recovered faster during reperfusion, with a shorter period of hypercontractility compared to control. ^{31}P-MRS revealed that CrT OE mice had on average 49% higher PCr content than WT mice before onset of ischemia, and that $|\Delta G_{ATP}|$ was higher in CrT OE mice at baseline and during ischemia. Thus, creatine loading may have a protective benefit during ischemia by improving energetic efficiency. Additionally, it was found that creatine loading could delay opening of the mitochondrial permeability transition pore, which is a seminal event in I/R injury [170], and a

follow-up study demonstrated that creatine loading protected against I/R injury even in the context of co-morbidities such as old age and LV hypertrophy [171]. Unfortunately, moderate creatine elevation had no protective effect on MI-induced heart failure, further supporting the hypothesis that creatine primarily plays a role in the acute setting.

1.7.2 Pharmacological and genetic modulation of creatine kinase

1.7.2.1 Pharmacological models

To date, there are no known CK-specific inhibitors, though iodoacetamide (IA) is the most commonly used non-specific inhibitor of CK. IA is a sulfhydryl group reactant that inhibits CK by inactivating critical cysteine residues [172,173]. IA inhibition of CK in Langendorff perfused rat hearts did not produce any contractile dysfunctions at baseline, suggesting CK may not be required for cardiac function under physiological conditions [172]. However, these hearts did exhibit ~50% lower contractile reserve under hypercalcemic, β-adrenergic, and hypoxic conditions, indicating the CK phosphotransfer system may play a more significant role in stress response. Unfortunately, as IA inhibits other metabolic proteins such as glyceraldehyde-3-phosphate dehydrogenase [172,174], the results from these studies may not necessarily be specific to CK loss. It should be noted that CK can also be irreversibly inactivated by 1-Fluoro-2,4-dinitrobenzene (DNFB), though utility is limited to cell culture studies [114,175,176].

1.7.2.2 CK-M/CK-Mt knockout models

To elucidate the specific roles of CK in striated muscle bioenergetics, creatine kinase knockout models were developed in mice. CK-M, CK-Mt, and CK-M/CK-Mt double knockouts (dKO) were consecutively generated and often explored simultaneously, thus the effects of CK knockout on cardiac functions in these models will be discussed together. From this point onward, for simplicity, CK-Mt refers to CK-sMt in all studies done on cardiac and striated muscle.

The initial cardiac study of CK-M KO mice was conducted on isolated ventricular muscle fibres to test for effects on contractile function [177]. It was found that CK-M KO caused decreased cross-bridge cycling rate without altered myosin isoform patterns, which could be related to the loss of functional coupling between CK-M and myosin ATPase [137,177]. However, the initial maximal twitch force and calcium sensitivity of CK-M KO cardiac muscle were not significantly different from those of WT controls, and there was no visible myofibril remodelling as a result of CK-M loss. These results were recapitulated in CK-M KO skeletal muscle [178], in which CK flux was reduced 20-fold and baseline free ADP was increased two-fold, though unexpectedly, resting concentrations of PCr, ATP, total creatine, and total adenosine nucleotide were maintained at physiological levels despite the CK-M ablation [178]. These parameters were not analysed for cardiac muscle of CK-M KO mice, but did suggest CK-M KO only altered some aspects of the resting bioenergetic profile.

1.7.2.2.1 Ex vivo cardiac studies of CK knockout

In the intact heart, the cardiac characterization of CK-M and dKO was initially conducted with Langendorff preparation [35,179,180]. Unexpectedly, there were no detectable signs of contractile dysfunction nor impaired bioenergetics in the CK-M KO mouse heart, both at rest and under hypercalcemia-induced inotropic stress [179]. dKO mice similarly exhibited no outright cardiac dysfunction, though imbalances in high-energy phosphates were detected, such as 24% lower PCr and 42% higher ADP at rest. Under hypercalcemia-induced stress, two-fold higher ADP and significant lower $|\Delta G_{ATP}|$ were reported in dKO mice hearts. Thus, Saupe *et al.* concluded that dKO mice may display measurable cardiac dysfunction under more severe stress conditions, such as I/R [149,179,181]. A follow-up study reported that during I/R, dKO mice had earlier onset and longer durations of LV ischemic contracture, as well as impaired diastolic and systolic performance during reperfusion [35]. Using a calcium-activated photoprotein, Spindler *et al.* were able to demonstrate that the contractile dysfunction during I/R in dKO mice was caused by impaired calcium homeostasis [35]. Since CK-M is functionally coupled to SERCA, it is possible that the loss of CK-M contributed to substantially lower local $|\Delta G_{ATP}|$ at SERCA (which has a high $|\Delta G_{ATP}|$ requirement), thus impairing its ability to maintain calcium homeostasis [2,35,36,179].

The cardiac function of CK-Mt KO mice was also investigated in Langendorff preparations, and no signs of cardiac dysfunction were detected at rest and under hypercalcemia-induced stress [180]. CK-Mt loss resulted in an impaired high-energy phosphate profile similar to that of dKO mice [179], such as 35% lower PCr and over two-fold higher ADP at baseline [180]. Overall, *ex vivo* studies demonstrated that CK knockout resulted in a mild phenotype with no measurable cardiac dysfunction at baseline, but impaired cardiac performance during I/R.

1.7.2.2.2 In vivo cardiac studies of CK knockout

The effects of CK deficiency on *in vivo* cardiac function were first explored in two studies utilizing magnetic resonance imaging (MRI) [82,182]. At baseline, CK-M KO, CK-Mt KO, and dKO models exhibited 33%, 64% and 73% higher LV weight than WT controls, respectively, a difference that reached statistical significance with the latter two models [82]. The higher LV weight in CK-Mt KO and dKO mice was associated with significantly elevated β-MHC expression and increased myocyte cross-sectional area, suggesting pathological LV remodelling. This hypertrophy was accompanied by LV dilation, with ~30% higher LV end-diastolic volume in dKO and CK-Mt KO hearts. While previous findings have also reported increased LV weight in CK KO mice [28,183], this was the first confirmed finding of significant pathological LV remodelling.

To investigate the functional effects of CK-KO induced LV hypertrophy in heart failure, dKO and WT mice were subject to MI and subsequently followed as heart failure developed. At 4 weeks after MI, LV weights in WT infarcted mice increased ~60% due to pathological LV hypertrophy [82]. However, in dKO mice, MI did not produce any additional LV remodelling beyond the LV hypertrophy that had occurred prior to MI. In line with this result, functional parameters such as ejection fraction and end-diastolic volume were similar between dKO and WT infarcted mice. Subsequently, Nahrendorf *et al.* demonstrated that dKO hearts did exhibit some subtle functional differences as compared to WT hearts, including decreased myocardial perfusion at baseline and decreased maximum contractile velocity at baseline and after MI, which may have been a consequence of the larger heart size [182]. However, it was confirmed that there was no significant difference between dKO and WT hearts in gross functional metrics such as EF and CO, at baseline and after MI. Ultimately, these *in vivo* results recapitulated *ex*

vivo findings indicating that CK deficiency did not cause substantial cardiac dysfunction at baseline and during heart failure.

While most studies concurred that CK knockout does not cause overt cardiac dysfunction, whether it causes LV hypertrophy remained controversial. For instance, while several studies reported up to 72% increased LV weight in dKO and CK-Mt KO mice [28,182-184], others reported no visible hypertrophy in either group [35,179,180]. Age and sex may have played a crucial role since LV hypertrophy appeared to occur in older or male mice [182-184]. Likewise, genetic drift may also have been a confounding factor. The transgenic mice were created on an unfixed, mixed C57BL/6 x 129Sv background, yet were always compared to unrelated C57BL/6 controls. C57BL/6 mice may not have been the appropriate control, as 129Sv mice naturally have larger hearts [185]. Thus, our group undertook a study to elucidate what impact these factors had on the development of LV morphological changes in CK-deficient mice [186]. By back-crossing CK-Mt KO mice with the C57BL/6 strain for over 8 generations, our group generated fixed-background CK-Mt KO mice that were >99.99% genetically identical to C57BL/6 controls, allowing more appropriate comparison to WT C57BL/6 littermate controls. In these fixed-background male/female CK-Mt KO mice, there were no signs of cardiac dysfunction at baseline and under β-adrenergic induced stress, and LV hypertrophy was not detected at up to 57 weeks of age. Given the existing results [82], these findings demonstrated how genetic background could affect the phenotype of CK deficient mice.

The findings in the fixed-background CK-Mt KO mice did not necessarily prove that CK-Mt deficiency was inconsequential to the heart, as compensatory mechanisms were found, including a 20% increase in CK-M activity. Consequently, a follow-up study was undertaken to characterize fixed-background dKO mice [187]. Similarly to the fixed-background CK-Mt

KO mice, fixed-background male/female dKO mice demonstrated no signs of LV hypertrophy, and *in vivo* haemodynamics revealed no significant functional differences as compared to C57BL/6 littermates. To conclusively demonstrate the impact of genetic background, mixed-background dKO mice were assessed alongside fixed-background mice. The previously reported LV hypertrophy in the mixed-background mice were recapitulated at 58 weeks of age, compared either to 129Sv or C57/BL6 controls [182,184]. This compensated LV hypertrophy progressed to congestive heart failure (*e.g.* pulmonary oedema and decline in dP/dt_{max} in dKO hearts) in male mice. Taken together, the results from both studies [186,187] suggested that the effects of CK KO on cardiac function were strain dependent, and that there may be cardioprotective genetic factors in the C57BL/6 background. Furthermore, it demonstrated that CK deficiency could conceivably cause spontaneous heart failure in certain situations.

1.7.2.2.3 Compensation in CK knockout models

While results between studies were variable, a common trend throughout CK knockout studies was the surprisingly mild phenotypes - the loss of creatine kinase yields no major contractile dysfunction outside of severe energetic challenges, such as skinned fibre experiments and I/R. However, the true effects of CK loss may be masked by various compensatory mechanisms, which demonstrate the remarkable redundancy and resilience of cardiac bioenergetics. They include 1) upregulation of alternate metabolic pathways, 2) mitochondrial adaptations, and 3) compensation from other CK isoforms.

Glycolytic compensation for CK loss has been detected in various model systems. In isolated ventricular muscle fibres of dKO mice, it was shown that glycolysis could provide energy for calcium homeostasis regulation in the absence of CK [28]. Increased glycolysis was also

observed in Langendorff preparations of both CK-M KO and dKO mouse hearts [81], though not in CK-Mt KO hearts [180]. AK is the most important energy shuttle besides CK, thus it was logical to suspect upregulation of AK in CK KO mice. Indeed, there is some evidence of AK upregulation in the heart [81,186], though findings are not consistent [183,187,188], and it currently remains unclear exactly when compensation from AK occurs. Dzeja *et al.* postulated that the near-complete ablation of CK in dKO mice was sufficient [81], yet increased AK activity was not found in the hearts of dKO mice on a fixed-genetic background [187]. Additionally, upregulation of guanine nucleotide transferases was observed in Langendorff preparations [81]. In summary, various bioenergetics pathways can compensate for loss of CK, which may be able to maintain sufficient phosphotransfer in CK deficient mice [37,81,189].

The muscle mitochondria of CK KO mice have also exhibited various compensatory adaptations. Increased mitochondrial volume has been reported, as assessed by measurement of citrate synthase activity in cardiac muscle [186], and by staining for succinate dehydrogenase [178] in skeletal muscle, though mitochondrial volume was unchanged in several other studies [180,187,189]. Mitochondria localization may also be different in dKO mice – specifically, rather than an organized linear arrangement in muscle fibres, mitochondria in dKO hearts form bulky aggregates near myofibrils and sarcoplasmic reticulum (Figure 1-8) [183]. It has been postulated that this arrangement allows mitochondria to directly supply ATP to SERCA and myosin ATPases, thus bypassing the need for the CK shuttle [183]. Indeed, SERCA and myosin ATPases were found to have nearly identical affinity for mitochondria-generated ATP and CK-generated ATP [183], indicating mitochondria can compensate for the loss of the primary phosphotransfer network. It should be noted that the cardiac mitochondria of GAMT KO

(creatine deficient) mice did not show any changes in intracellular positioning, hence altered mitochondria localization may not a universal compensation for CK system dysfunction [152].

Other adaptive mechanisms to compensate for CK ablation have been suggested, such as increased activity of remaining isoforms [81,186,188], and increased myocyte size [82]. In summary, the mild phenotypes of cardiac dysfunction seen in CK KO models should be interpreted with caution, as cardiac energy homeostasis is maintained by a network of interchangeable phosphotransfer pathways. It is possible that compensatory mechanisms are sufficient to maintain relatively normal cardiac function in genetically modified mice since they can gradually adapt to the loss of CK from embryonic development until adulthood. However, heart failure patients may present with relatively rapid CK system impairment, which could cause a more severe phenotype, as there is far less time for adaptive measures.

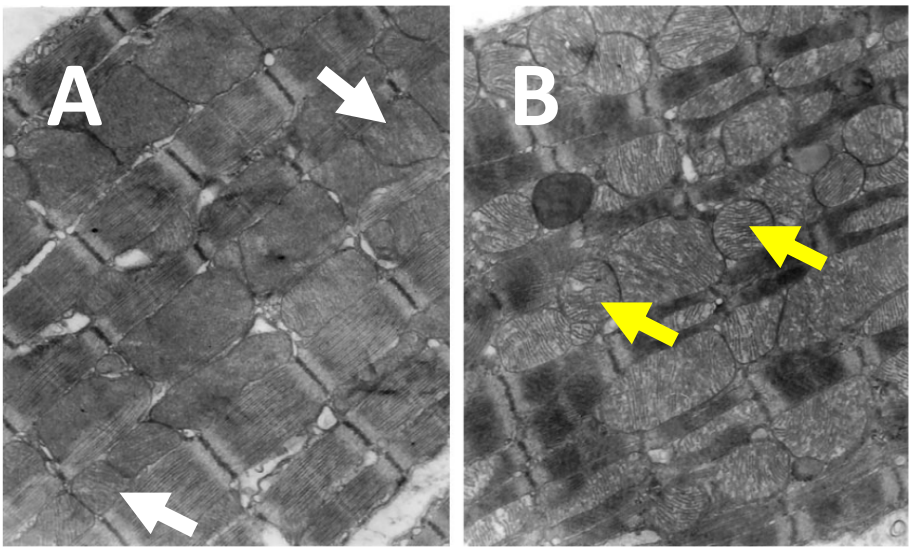


Figure 1-8: Mitochondrial changes in dKO mice:

Mitochondria of dKO mice had distinctly different morphologies in the cardiomyocyte ultrastructure. (A): Ultrastructure of wild type cardiomyocytes demonstrating mitochondria (white arrows) arranged longitudinally in well-organized myofibrils. (B) Abundant round mitochondria (yellow arrows) interspersed between myofibril bands with minimal organization. Magnification x 12,000. Figure and details were adapted from [183]

Overall, results from knockout models and studies with pharmacological agents broadly suggest that the CK system is not required for baseline cardiac function, but contributes significantly in stress situations such as in I/R and MI. Thus, animal models overexpressing various components of the creatine kinase system were established to investigate the therapeutic potential of CK system augmentation. CrT overexpression was previously discussed in Section 1.7.1.5, and CK-M overexpression is discussed on the next page.

1.7.2.3 CK-M overexpression model

CK-M OE mice were generated to investigate whether augmentation of creatine kinase is therapeutic in chronic heart failure [190], ischemic/reperfusion [191], and doxorubicin-induced cardiotoxicity [192] (doxorubicin is an anti-neoplastic agent with cardiotoxicity as a side effect). The CK-M OE mouse model for these experiments generated 70%-200% higher total CK activity, which was maintained during all three pathophysiological conditions [190-192]. *In vivo* MRI studies demonstrated that this magnitude of overexpression, at baseline, did not alter cardiac function, PCr/ATP ratios, intracellular creatine content, or other metabolic pathways such as AK [190,191]. CK-M overexpression did increase CK flux by 40%, although ATP concentrations remained at physiological levels [190]. CK-M overexpression was found to substantially improve cardiac function during pressure-overload heart failure [190]. Over the 8 week study, pressure-overload heart failure caused a ~30% reduction of total CK activity in WT mice (~6 IU/mg protein), whereas CK-M OE mice had total CK activity that were two-fold higher (~13 IU/mg protein). During heart failure, the transgenic mice attenuated the deficiency in high energy phosphates by restoring PCr/ATP ratios and ATP concentrations to

physiological levels. Probably as a result of improved CK function, CK-M OE mice exhibited significantly better contractile function (*e.g.* CO, EF, and SV) and nearly two-fold higher survival rates than WT mice during heart failure[190]. Furthermore, a significant decline in cardiac function was noted in CK-M OE mice if the overexpression was repressed at week 4 of heart failure, indicating that continuously increased CK activity was essential for the protective benefit. Thus, this study presented the first evidence that upregulation of the creatine kinase enzyme could produce a measurable protective effect during chronic heart failure.

CK-M overexpression also improved cardiac performance during *ex vivo* I/R challenges as indicated by more rapid recovery of RPP during reperfusion [191]. While ATP concentrations were not significantly different between CK-M OE mice and WT mice during I/R, PCr levels recovered more rapidly in CK-M OE mice, indicating CK-M overexpression improved the CK phosphotransfer system kinetics. Additionally, as the CK reaction consumes protons, increased CK-M expression mitigated ischemic acidosis. In mice subject to chronic doxorubicin administration, CK-M overexpression also increased survival and attenuated the decline in myocardial high-energy phosphates and contractile function [192].

Taken together, these findings present CK augmentation as a strategy with translational potential for treating patients with various cardiac pathophysiologies.

1.8 Summary and experimental aims

In summary, the existing research provides a preponderance of evidence that impaired CK system function correlates with cardiac pathophysiology in heart failure and ischemic heart disease, albeit it is less clear whether CK dysfunction has a causative effect. Nevertheless,

investigations that enhance CK system components (CrT, CK-M) have delivered promising findings, suggesting that CK system augmentation can improve cardiac function in chronic heart failure, I/R injury, and doxorubicin-induced cardiotoxicity. Therefore, experiments in the following chapters detail *in vivo* and *in vitro* studies conducted on CK-OE mouse and cell culture models, particularly in regards CK-Mt overexpression, which has not been addressed in the literature. Ultimately, these studies aim to further elucidate the therapeutic potential of CK system augmentation in the context of various cardiac pathophysiologies.

2 General materials and methods

2.1 Chemical and laboratory supplies

Reagents and chemicals are from Sigma-Aldrich (Dorset, UK) unless otherwise stated. Appendix A.4 provides detailed information on essential solutions.

2.2 Colony Management

2.2.1 Mouse husbandry

Mice were maintained by the Functional Genomics Facility in the Wellcome Centre for Human Genetics (WCHG). The unit operates on a standard 12 hour night/day cycle with controlled temperature (~ 21^{o}C) and humidity, and contains individually ventilated cages (Techniplast). Mice were weaned three weeks after birth, provided Global Diet 2916 (Envigo, Huntingdon, UK) and water *ad libitum*, and housed in specific-pathogen-free conditions with littermates whenever possible. All animal experiments were approved by the Committee for Animal Care and Ethical Review at the University of Oxford, and comply with Home Office Regulations incorporating the Animals (Scientific Procedures) Act of 1986 and Directive 2010/63/EU of the European Parliament.

Transgenic CK-Mt OE mice (described in detail in Section 3.1.2) that were previously created on a mixed background (C57BL/6J x Sv129) were back-crossed with C57BL/6J mice (Envigo) for >8 generations to generate a genetic background >99.9% congenic with C57/BL6J. This transgenic line was maintained through heterozygote x heterozygote breeding, and occasional

homozygote and wild-type crosses to increase availability for experiments. The line was regularly crossed with C57BL/6J from Envigo to prevent genetic drift. WT controls used in experiments were non-transgenic littermates bred in our establishment.

2.2.2 DNA extraction

All mice were ear-notched and genotyped to ensure genetic integrity, with additional genotype verification conducted as necessary on small tail-snips preserved from sacrificed mice. Ear notch discs were digested overnight at 55°C, in 500 µL of lysis buffer (100 mM ethylenediamine tetraacetic acid (EDTA), 50 mM Tris-HCl (pH 8.0), 1% SDS, and 200 mM NaCl) supplemented with 60 µg/mL proteinase K. After gently vortexing the digested sample, 600 µl of isopropanol was added to the sample, which was mixed and centrifuged for 10 minutes at 13,000 rpm. After discarding the supernatant, the precipitate was washed with 500 µL 70% ethanol followed by centrifugation for 5 minutes at 13,000 rpm. The supernatant was discarded, and the purified DNA pellet was then air dried for 30 minutes at 55°C and subsequently re-suspended in 300 µL T0.1E (1 M Tris-Cl, 0.5 M EDTA) overnight at room temperature (RT).

2.2.3 PCR

PCR for genomic DNA was performed using the Immolase DNA polymerase (Bioline, UK). Table 2-1 lists the genotyping primers for CK-Mt OE mice.

Table 2-1: Genotyping primers for CK-Mt OE mice.

Transgenic mouse line	Primer names	Primer Sequences
CK-Mt OE	Ckmt2_ex9-10_F	5'-TCGGCAGATCAGAGGTTGAG-3'
	HA_R	5'-TGCGTAATCTGGAACATCGT-3'
	Rosa26_F	5'-ATACCTTTCTGGGAGTTCTCTGCTGC-3'
	Rosa26_R	5'-GGAGCGGGAGAAATGGATATG -3'

2.2.4 Agarose gel electrophoresis of PCR products

1% agarose gels were made with powder agarose in 1x Tris/Borate/EDTA (TBE) buffer (89 mM Tris, 89 mM boric acid, 2 mM EDTA), with 0.5 µg/mL ethidium bromide. PCR products were prepared for loading by mixing with blue gel loading dye (ThermoScientific) at a 1:3 ratio. 15 µL of sample was loaded into the agarose gel, and electrophoresis was performed in 10% TBE buffer with 0.5 µg/mL ethidium bromide. An appropriate DNA ladder was run alongside each experiment. The gel was run for ~45 minutes at 100V to separate bands, which were visualized under UV light using a Biorad Chemi Doc MP imaging system and processed using Image Lab 5.0 (Bio-Rad Laboratories).

2.2.5 Harvesting of tissue

Biochemical assays were conducted on hearts from WT and transgenic mice. To extract fresh hearts, mice were sacrificed by cervical dislocation. Incisions were made under the rib cage to expose the chest cavity, and hearts were excised and quickly washed in a dish of ice-cold

heparinized saline (125 U/ml heparin sodium in 0.9% sodium chloride). Hearts were blotted on tissue, and the left ventricle was dissected and snap frozen in liquid nitrogen with Wollenberger tongs for storage at -80^{o}C until further use. Frozen tissue was crushed into powder using a metal tissue pulveriser on dry ice prior to further experiments described below.

2.3 Biochemical measurements of CK activity/composition

2.3.1 Homogenization of heart and cell samples

Frozen powdered heart tissue and lysed HL-1 cells were subjected to isoenzyme composition analysis and CK activity.

2.3.1.1 Powder heart samples

Crushed powdered heart tissue (5-10 mg) was reconstituted in a droplet of ice-cold homogenizing buffer (0.08 M K_2HPO_4, 0.02 M KH_2PO_4, 1 mM β-mercaptoethanol, and 1 mM EGTA, pH 7.4), blotted on weighing paper, and weighed. The sample was then placed in a glass homogenising vessel containing additional ice-cold homogenisation buffer, with buffer volume adjusted to create a tissue concentration in buffer of 5 mg/mL for each sample. The sample was then fully homogenised using an IKA Eurostar digital stirrer at 1300 rpm for 15 seconds (IKA, North Carolina, USA).

200 µL of the homogenate was immediately aliquoted and mixed with 200 µL of 4% NaOH to create a solution for the Lowry assay (detailed in 2.3.5), and the mixed solution was heated in a water bath at 60^{o}C for a minimum of 2 hours before being stored at 4^{o}C. The remaining

homogenate was then incubated for 30 minutes at 4ºC with 0.1% Triton-X 100 to permeabilize plasma and other lipid membranes, and the supernatant was used for subsequent experiments.

2.3.1.2 Cell culture samples

HL-1 cells seeded at 80,000 cells/cm^2 in a 24-well plate were grown to full confluency prior to CK activity analysis. Twenty four hours after seeding, HL-1 cells were transfected with appropriate CK-OE vectors and incubated in transfection media for an additional 24 hours. Cells were then washed with Dulbecco's Phosphate Buffered Saline (PBS), detached using 0.05% Trypsin (Gibco), and pelleted by centrifugation at 1000 rpm for 5 minutes, before being re-suspended in ice-cold homogenization buffer. Triplicate wells for each experimental condition were then pooled into a single homogenizer and homogenized as described above. Triton X 100 (0.1%) was then added as previously described to permeabilize plasma and lipid membranes.

2.3.2 Analysis of CK isoenzyme composition

Analysis of CK isoenzyme composition (CK-M, CK-B and CK-Mt) was conducted using the SAS-1+ automated compact electrophoresis analyser (Helena Biosciences), which separates isoenzymes based on their electrophoretic mobility by agarose electrophoresis. The gel was then incubated with chromogen to allow visualization of the separated CK isoenzyme bands, and the relative concentration of bands was quantified by densitometry. The principle of this method is described in Figure 2-1.

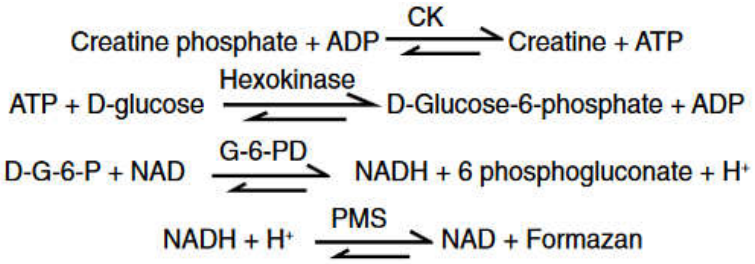


Figure 2-1: SPIFE CK isoenzyme assay

CK drives formation of ATP from the ADP and creatine phosphate (PCr) available in the SPIFE CK Isoenzyme reagent. ATP generates NADH and H^+, when incubated with D-glucose, hexokinase, NAD, and glucose-6-pyruvate dehydrogenase (all part of the SPIFE CK Isoenzyme Reagent). NADH and H^+ then reduce Tetranitro Blue Tetrazolium (TNBT) to produce formazan in the presence of phenazine methosulfate (PMS). Formazan is chromogenic, and produces a dark band that can be visualized and quantified.

The supernatant from Section 2.3.1.1 was diluted 1:20 (5 µL sample in 95 µL ice-cold homogenization buffer) for this assay, and incubated with SPIFE CK Activator (114 mM β-mercaptoethanol in Tris base) for 10 minutes. Mixed samples were then loaded onto an agarose gel for electrophoresis by the SAS-1+ machine, followed by an additional 20-minute incubation with CK Chromogen (Helena Biosciences) and CK Isoenzyme Reagent (Helena Biosciences). The gel was then washed for 10 minutes with 10% citric acid to destain excess TNBT, and dried at 60°C for one hour before being visualized. Photos of samples were taken using a ChemiDoc MP Imager (Bio-Rad), and analysis was conducted in Image Lab. Relative concentrations of isoenzymes were assumed to be equal to the relative saturation of the bands in each sample, which was measured by automated scanning fluorometry. A marker specifically identifying CK-MM, CK-MB, and CK-BB protein in the gel was run with each assay. A molecular marker for CK-Mt was not available commercially, but our group has previously verified the electrophoresis pattern of all isoenzymes, and confirmed that the top band of each gel contained CK-Mt (see Section 4.4.6.1 for sample gel) [176].

CK Chromogen contains Tetra Nitro Blue Tetrazolium (TNBT) at a concentration of 0.023 g/ml in dimethyl-formamide. CK isoenzyme reagent contains 12 mM ADP, 90 mM creatine phosphate, 15 mM AMP, 60 mM magnesium acetate, 0.1 mM diadenosine pentaphosphate, 10 mM NAD, 60 mM D-glucose, 7,500 IU/L G6PD, 9,000 IU/L hexokinase, 0.15 mM phenazine methosulfate, and 4.5 g/L bovine serum albumin (BSA).

2.3.3 Analysis of CK activity by spectrophotometry

Total CK activity was measured using spectrophotometry, as described in Figure 2-2. The methodology is described in Figure 2-2, and was first established by Oliver [193], and later modified by Rosalki [194] and Szasz [195]. The reagents for the reactions were obtained as CK-N-acetylcysteine (NAC) Reagent (Thermo Scientific, UK). The absorbance at 340 nm (A_{340}) was measured by spectrophotometry using an Ultraspec 2100 Pro Spectrophotometer (Amersham Biosciences, UK), with analysis conducted using Swift II Kinetics software (Swift Analytical, Ltd, York UK).

20 µL of supernatant was diluted 1:5 in ice-cold homogenization buffer and placed in a cuvette. 1 mL of CK-NAC reagent, incubated at 30^{o}C, was subsequently added and the resulting solution was incubated for five minutes at room temperature. Total CK activity was then determined by measuring A_{340} in two-minute intervals over the course of ten minutes. A_{340} increased steadily over this interval due to generation of NADH, which was recorded as a measure of total CK activity, expressed as IU/mg protein. Triplicate runs were conducted for each LV sample. Total

CK activity was then normalized to total protein level for each sample, which was measured by Lowry protein assay as discussed in Section 2.3.5.

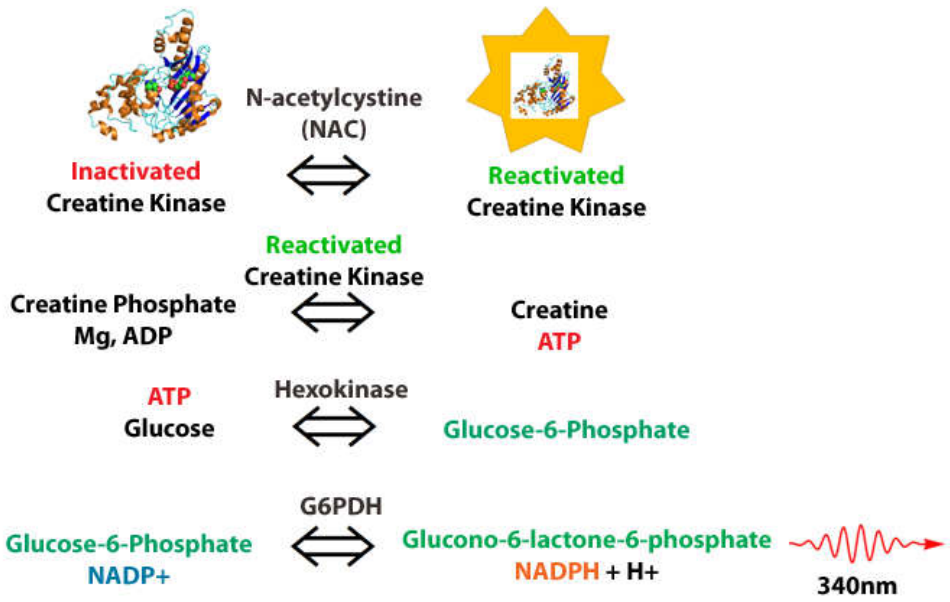


Figure 2-2: CK activity assay mechanism

Out of tissue, CK is rapidly inactivated by oxidation of sulfhydryl groups at the active site. To restore CK activity, N-acetyl cysteine is incubated with the reconstituted sample for five minute, which reduces oxidized sulfhydryl groups. Once CK is re-activated, it catalyses conversion of creatine phosphate and ADP in the reagent mixture to ATP and creatine. Hexokinase utilizes ATP to transphosphorylate glucose to glucose-6-phosphate. Glucose-6-phosphate is utilized by G6PDH (glucose-6-phosphate dehydrogenase) to reduce $NADP^+$ to NADPH. NADPH production rate can be measured by spectrophotometry via monitoring the rate of change in absorbance at 340 nm.

After determining total CK activity, isoenzyme-specific CK activity was then calculated. The isoenzymes have similar reaction velocity [196], and thus relative activities could be considered to be proportional to the relative isoenzyme concentrations as determined in Section 2.3.2. For instance, if CK-Mt accounted for 30% of the total lane saturation in the chromogen gel in Section 2.3.2, then CK-Mt activity was calculated to be 30% of total CK activity.

The complete reagent composition of the CK-NAC reagent includes 100 mmol/L Bis/Tris Buffer, 31.5 mmol/L creatine phosphate, 5.3 mmol/L AMP, 2.2 mmol/L NADP, 2.1 mmol/L EDTA, 10.3 µmol/L AP5A, 10.5 mmol/L Mg^{2+}, 2.7 mmol/L ADP, 21 mmol/L D-Glucose, 21 mmol/L N-acetyl-l-cysteine, >3000U/L Hexokinase (yeast), and >2,000U/L G-6-PDH. The reagent mix contains AP5A (P^1P^5-Di(adenosine-5'-) pentaphosphate pentasodium) and AMP for the purpose of blocking the activity of AK. This prevents AK from interfering with the ADP → ATP conversion by creatine kinase.

2.3.4 Citrate synthase assay

Citrate synthase is an enzyme present in the mitochondrial inner matrix [197], and its activity is correlated with mitochondrial volume [198]. Thus, citrate synthase activity was measured as an indicator of mitochondrial volume, as described in Figure 2-3.

50 µL of the supernatant of the LV homogenate or 50ul of isolated mitochondria (at 1 µg/µL) was placed in a cuvette, and incubated with 850 µL of reagent (0.35 mM Acetyl-CoA, 0.12 mM DNTB) for three minutes at RT. 100 µL of 1 mM oxaloacetate was then added, and absorbance was measured at 412 nm over a 1-minute interval. Two runs were conducted for each

experimental sample, and mean activity was reported in IU/mg protein. Protein concentrations were measured separately using Lowry assay, as detailed in Section 2.3.5.

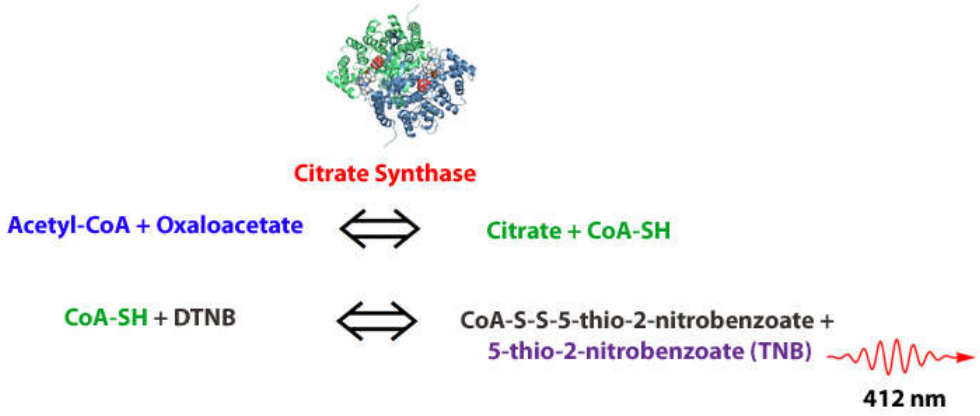


Figure 2-3: Citrate synthase assay

Citrate synthase catalyses the conversion of acetyl-CoA and oxaloacetate to citrate and CoA-SH. CoA-SH interacts with dinitrothiocyanobenzene (DTNB) to create 5-thio-2-nitrobenzoate (TNB), which is measured by spectrophotometry at 412 nm.

2.3.5 Lowry protein assay

Protein concentrations were measured for samples used in the CK and citrate synthase activity assays, as well as for high performance liquid chromatography (HPLC) samples. An aliquot of homogenised samples was mixed with 4% NaOH, incubated for two hours at 60°C in a water bath, and stored at 4°C until the assay. On the day of the assay, triplicates of Lowry samples were diluted in H_2O (1:10 for CK and citrate synthase assay samples, 1:50 for HPLC samples). Simultaneously, duplicate control samples were made using known concentrations of BSA between 0-80 µg/mL to generate a standard curve. Samples and standards were then mixed

with 1mL of Lowry reagent, after which all samples were vortexed and incubated at RT for 20 minutes. Then, 500 µL of Folin and Ciocalteu's Pheno Reagent Working Solution was added, and samples were vortexed and incubated at RT for 30 minutes. Samples were then filtered through a 0.45 µM filter into cuvettes, and protein concentration was quantified by measuring absorbance at 650 nm with the Ultraspec 2100 Pro spectrophotometer. Sample protein concentrations were extrapolated from the standard curve generated from BSA standards.

2.4 Cell culture

2.4.1 Cell lines

For the *in vitro* assay, two cell lines, HEK293 and HL-1, were utilized. The HEK293 cell line was originally derived from human embryonic kidney cells transformed by incorporating human adenovirus type 5 (Ad5) DNA, and is widely used for gene manipulation in mammalian cells [199]. HEK293 is an excellent cell line for transfection experiments due to its high transfection efficiency, which makes it especially useful for generating stably transfected cell lines [199]. Furthermore, HEK293 is ideal for optimizing experimental conditions due to its ease of culturing and handling. The cell line used in current experiments was obtained from Sigma-Aldrich (85120602 Sigma) through a collaboration with the European Collection of Authenticated Cell Cultures, and experiments were conducted on cells passage number 58 or later. The cell line was used in preliminary screening and validation of experiments detailed in Chapter 5 and 6.

HL-1 cells are derived from the AT-1 mouse right atrial tumour lineage, and are the most commonly utilized cell line that has a cardiac phenotype [200]. HL-1 cells express many cardiac proteins, such as K_{ATP} channels, Na^+/Ca^{2+} exchangers, desmin, α-MHC heavy chain, and α-cardiac actin [200,201]. Furthermore, the gene expression profile of HL-1 cells closely resembles that of an adult mouse cardiomyocytes [200]. It should be noted that the energetic profile of HL-1 cells differs significantly from adult cardiomyocytes – specifically, HL-1 cells rely substantially more on glycolysis and have lower respiratory activity compared to primary cardiomyocytes [202]. HL-1 cells were kindly donated by Prof. William Claycomb (Louisiana State University Health Science Center, New Orleans, USA) and were utilized at passage #38 or later.

HL-1 cells can be repeatedly passaged while maintaining the ability to contract and retaining differentiated cardiomyocyte morphology [200]. To contract, HL-1 cells require norepinephrine. In the current experiment, it was found that norepinephrine in the preferred ascorbic acid solvent produced crystals in cell culture that inhibited HL-1 cell growth. Therefore, norepinephrine was excluded from the current experiment, and the experiments described in this thesis utilized non-beating HL-1 cells. The literature suggests that the energetic profile between beating and non-beating HL-1 cells is nearly identical, thus this factor should not make a significant difference for the current experimental aims. For instance, total CK activity is not significantly different, and both phenotypes rely primarily on glycolytic pathways for energy generation [203]. In the current study, HL-1 cells were utilized for the model of doxorubicin cardiotoxicity.

2.4.2 Cell culture conditions

HEK293 cells were cultured in Dulbecco's Modified Eagle Medium (DMEM) (Sigma) with 10% foetal bovine serum (FBS), 100 U/ml of penicillin, 100 µl/ml of streptomycin, and 2 nM L-glutamine. Generally, cells were cultured in media in a 75 cm^2 flask, at 37°C in a humidified incubator with 5% CO_2/95% O_2, and incubated for ~48 hours or until 90-100% confluence at which time they were then harvested, passaged, or frozen as appropriate.

HL-1 cells were incubated in Claycomb Media (Sigma) with 10% HL-1-specific FBS (F24420, Sigma, UK), 100 U/ml of penicillin, 100 µl/ml of streptomycin, and 2 nM L-glutamine in a flask pre-coated with a 0.02% gelatin and fibronectin solution (5 µg/ml) for a minimum of 1 hour (Gelatin: Sigma; Fibronectin: Cambridge Bioscience). Cells were incubated at the same condition as HEK293 cells, for 72 hr or until 90-100% confluent before harvesting, passaging, and freezing.

2.4.3 Passaging

Once confluent, HEK293 cells were washed with PBS, trypsinized with 0.05% trypsin-0.02% EDTA solution (T3924, Sigma) for 5 minutes, pelleted at 1000 rpm for 5 minutes in a centrifuge, and then transferred into fresh flasks at a 1:3 dilution.

Pilot studies in HL-1 cells demonstrated that 0.05% trypsin solution (Sigma) was not a strong enough reagent to dissociate HL-1 cells from the fibronectin/gelatin matrix. Thus, 0.05% trypsin-0.02% EDTA solution (Gibco; Life Technologies) was used to dissociated cells, which were washed with PBS, re-suspended, and incubated in a new flask using the same procedures

as for HEK293 cells as described above. Cells were re-suspended at a 1:3 dilution in fresh flasks that were pre-coated with gelatin/fibronectin solution for at least 1 hour.

2.4.4 Plating

Cells were pelleted, and re-suspended in appropriate media, with a 20 µL aliquot taken for cell density measurement using a Nexcelom Cellometer Auto2000 cell-counting machine (Nexcelom Biosciences). Plating densities were optimized and discussed in Chapter 5 and 6.

2.4.5 Long-term storage

HEK293 and HL-1 cells were kept in liquid nitrogen for long-term storage. Fully confluent flasks were trypsinized and cells were re-suspended in 95% FBS with 5% DMSO freezing medium, and cooled at -80°C before long-term storage in liquid nitrogen. Cells were revived by warming frozen samples in a water bath (37°C) for a maximum of two minutes. HL-1 cells were then spun down at 1000 rpm for five minutes in culture media before re-suspension and incubation, whereas HEK293 cells were re-suspended immediately.

2.4.6 Cell microscopy

Green fluorescent protein (GFP) expressing cells were visualized using a Nikon TE2000U epifluorescence microscope with GFP filter. Fiji software was used to take images and apply image bars, and image processing was conducted using Image J.

2.5 Transfection methods

2.5.1 Transient transfection

HL-1 cells were seeded at 8 x 10^4 cells/cm^2 in a 24 well plate, and incubated for 24 hours prior to transfection. HEK293 cells were seeded at 2 x 10^4 cells/cm^2 in a 96 well plate for 24 hours prior to transfection. Cells were approximately 60% confluent prior to transfection.

Vectors used in the doxorubicin assay were previously generated and verified by restriction digest and direct sequencing by Dr Philip Ostrowski, a former D. Phil student. Vectors used in luciferase assay were custom-made by gene synthesis and the sequence was verified by Genewiz (London, UK). Cells were transfected using FuGENE HD (Promega), a non-liposomal cationic lipid transfection reagent. Transfection solution consisted of a 1 μg vector: 3 μL FuGENE HD mixture, which was placed in serum-free OptiMEM (Invitrogen) transfection medium. The transfection solution was incubated at room temperature for 30 minutes before being added to fresh medium. Cells were then incubated in this fresh transfection medium for 24 hours before further experimentation. Transfection success and efficiency were verified via quantitative reverse transcriptase polymerase chain reaction (qRT-PCR) analysis of transgene mRNA expression, visualization of the cells co-transfected with GFP, and counting GFP/total cell numbers using the Nexcelom Cellometer cell counter. The protocol for Fugene was previously optimized by our group for transfection in HEK293 (based on manufacturer's protocols and databases) and HL-1 cells.

2.5.2 Stable transfection

Previous results from our laboratory demonstrated that HL-1 cells could not be stably transfected to express CK vectors due to high death rates during the antibiotic selection process. Thus, HL-1 cells were only used in transient transfection experiments.

HEK293 cells were assessed for antibiotic (puromycin) sensitivity through kill curve experiments, which suggested 1 μg/mL puromycin was the most appropriate concentration. Density studies demonstrated that a concentration of 8 x 10^4 cells/cm^2 in a 24 well plate was the most optimal concentration for stable selection.

While existing circular vectors were utilized for transient transfection, the vectors had to be linearized for stable transfection by genomic integration to generate stable luciferase-expressing cell lines as described in Section 6.3.6.1. Vectors were linearized via restriction digest using appropriate restriction enzymes (New England Biolabs, Hitchen, UK). The linearized product was confirmed by gel electrophoresis and then added to a 1:3 mixture of FuGENE HD transfection reagent, mixed in OptiMEM, and subsequently incubated for 30 minutes before being added to fresh medium. This transfection medium was added to cells 24 hours after plating, and incubated with the cells for 24 hours. Transfected cells were subsequently cultured in fresh medium containing a lethal dose of puromycin (1 μg/μL), until the appearance of antibiotic resistant colonies. Vector expression in the stably transfected cells was verified via qRT-PCR.

2.6 One-step qRT-PCR

2.6.1 RNA isolation from cell culture

RNA was extracted from various cell lines using the RNeasy Mini Kit (Qiagen). Cells were lysed from 24 well plates using 300 µL Buffer RLT with 3.3 µL (1%) β-mercaptoethanol, and RNA was extracted from lysed samples as per manufacturer's instructions. RNA quality and quantity were measured spectrophotometrically (Nano-Drop N-1000 Spectrophotometer, UK), and a 1 ng/µL mixture was prepared for use in qRT-PCR.

2.6.2 One-step qRT-PCR

PCR for plasmid DNA was conducted using the iScript 1-step SYBR Green RT PCR Kit (Qiagen), which allowed cDNA synthesis and PCR amplification to be conducted in continuous reactions. This was carried out in 96-well hard-shell PCR plates (Bio-Rad), in duplicates of 10 µL reaction mixture per sample. The 10 µL reaction mixture typically contained:

2 µL RNA at 1 ng/ µL
0.06 µL each of forward/reverse primers at 50 µM
5 µL 2x iTaq Universal SYBR mix
0.2 µL iScript reverse transcriptase
2.68 µL H_2O

In addition to samples, standards were created by pooling RNA extracts and creating a serial dilution to generate a standard curve for each assay. Specifically, the pooled standards were

generated from 0.01 ng/µL to 100 ng/µL, and 2 µL of RNA from each standard was used to generate the master mix listed above.

Utilized primers are depicted in Chapters 5 and 6. The qRT-PCR protocol can be found in Appendix A.2. A single peak on melt curve analysis confirmed a single amplified targeted DNA product, and a lack of any non-specific products (*e.g.* secondary structures, primer dimers).

2.6.3 Quantification and data analysis

Analysis of qRT-PCR data was performed on Bio-Rad CFX manager (Bio-Rad). Relative Florescence Units (RFU) were measured per cycle, and data was analysed using the published $2^{-\Delta\Delta Ct}$ method [204,205]. The value compared between samples was the cycling threshold (C_q; 'quantification cycle'), which was the cycle number at which the fluorescence of the sample exceeded a fluorescence benchmark as determined by the manufacturer.

The relative fluorescence of each sample was normalized to the mRNA expression of the reference gene RNA polymerase II (Polr2A). For every assay, each cell line had duplicate samples tested for Polr2A mRNA, which served as a quantitative reference for normalizing transgene qRT-PCR data [206].

2.7 Flow cytometry experiments

HEK293 and HL-1 cells were plated in 24 well and 96 well plates at varying density and incubated overnight before experimental procedures as detailed in Chapters 5 and 6. At the end

of treatment protocols, cells were subject to five minutes of trypsinization by 500 µL 0.05% Trypsin (Sigma) for HEK293 cells or 0.05% Trypsin (Gibco) for HL-1 cells. After adding an equal volume of trypsin-neutralizing medium, cells were pelleted by centrifugation at 1000 rpm for five minutes. Pelleted cells were washed twice with PBS, and then re-suspended in flow cytometry tubes with 300 µL PBS and 1% propidium iodide (Biolegend, UK), or with 300 µL Annexin V binding buffer containing Annexin V (Biolegend) and Thermo Live/Dead Dye (Thermo Scientific). Samples were then processed using a Beckman Coulter CyAn ADP LX High Performance Flow Cytometer using the 405 nm and 488 nm lasers for excitation. Appropriate laser modifications, such as signal compensation, were made with the assistance of Mr Andrew Worth (Flow Cytometry Facility, Jenner Institute, University of Oxford) and Dr Eileen McNeill (Division of Cardiovascular Medicine, WCHG). Data was collected and analysed in Summit v.4.3 software.

2.8 Statistical analysis

All results are expressed as mean ± SEM, and statistical significance was established when $p < 0.05$ between analysed groups. Experiments with two groups were analysed using two-tailed Student's t-test assuming equal variance. Experiments with more than two independent groups and one independent variable were analysed using one-way ANOVA with either Bonferroni's or Tukey's post hoc adjustment as specified. Experiments with two independent variables were measured with two-way ANOVA with appropriate post-hoc tests for comparisons between groups. Statistical analysis was conducted using Graphpad Prism v. 5 and v. 7, Microsoft Excel, and IBM SPSS, and Minitab. All measurements and statistical analysis were performed blind to genotype wherever applicable.

3 Mitochondrial and metabolic phenotyping of the CK-Mt overexpression mouse model

3.1 Introduction

As detailed in Section 1.6 and 1.7, the results of various studies suggest that CK system deterioration is a prominent phenomenon of various cardiac pathophysiologies, and that enhanced CK system function shows promise in improving cardiac function and outcomes of disease states. For example, our group demonstrated that moderate elevation of myocardial creatine content protected against ischemic insult [2], and CK-M overexpression improved outcomes during chronic heart failure and in post-ischemic myocardium [190,191]. However, there is no published data regarding whether CK-Mt augmentation could provide therapeutic benefit, hence our group generated a CK-Mt OE mouse model to address this gap in the literature.

3.1.1 CK-Mt crystal aggregation – the limitations of CK-Mt overexpression

In contrast to CK-M overexpression, CK-Mt overexpression has the limitation that functional CK-Mt is localized in the limited space of the mitochondrial intermembrane space and cristae. As a result, excessive overexpression can disrupt mitochondrial morphology and may produce a detrimental effect because of the formation of aggregates of CK-Mt crystals. It was reported that creatine depletion in adult rat cardiomyocytes was associated with increased sarcomeric CK-Mt expression, resulting in crystalline aggregations in mitochondria known as

mitochondrial inclusion bodies (MIB). These MIB are large rod-like structures that forced mitochondria into bloated, disfigured configurations termed “giant mitochondria” [207], which have been found to lack creatine-stimulated mitochondrial respiration [208]. The morphological changes associated with excessive CK-Mt overexpression were recapitulated in a study genetically expressing ubiquitous CK-Mt in the liver, in which ubiquitous CK-Mt similarly was observed to form crystal aggregates [209]. Of clinical relevance, giant mitochondria have been observed in mitochondrial cardiomyopathy [210], and it has been reported that sarcomeric CK-Mt crystal aggregates are found in the skeletal muscle mitochondria of patients with mitochondrial myopathy conditions [211]. In summary, caution was required when generating a CK-Mt overexpressing transgenic model to minimize the risk of altering mitochondrial structure and function.

3.1.2 Characteristics of the CK-Mt OE transgenic mouse model

The CK-Mt OE vector and mouse model were generated and characterized by Dr Philip Ostrowski, and details are available regarding this model [212].

In summary, the transgenic vector consisting of murine CKMT2, driven by an α-myosin heavy chain (α-MHC) promoter, was microinjected into mouse blastocysts through a targeted insertion at the ROSA26 (reverse orientation splice acceptor 26) locus located on chromosome 6 in *mus musculus*. The ΦC31 integrase-mediated cassette exchange system was used to ensure that only a single copy of the transgene was inserted at the ROSA26 site. The ROSA26 locus and the ΦC31 were purposefully selected to moderate CK-Mt augmentation, to avoid the aforementioned problems with excessive CK-Mt overexpression.

Whittington *et al.* conducted *in vivo* LV haemodynamic assessment in mice 12 weeks of age to examine cardiac function of heterozygote and homozygote mice as compared to WT controls [212]. There were no significant difference, both at rest and under dobutamine-stimulated adrenergic stress. Likewise, *in vivo* cine-MRI studies revealed no significant functional and morphometric differences at baseline [212]. Taken together, these studies indicated that there was no structural and functional consequence of CK-Mt overexpression in the resting heart.

Furthermore, transgenic CK-Mt localization to cardiac mitochondria was confirmed by electron microscopy and immunogold staining [212]. Moreover, quantification of electron microscopy images revealed that transgene expression did not alter mitochondrial cell density, and citrate synthase activity was not significantly different, suggesting that there was no major change in mitochondrial volume. In summary, it appears that CK-Mt overexpression did not significantly alter mitochondrial phenotype

3.1.3 The mitochondrial permeability transition pore (mPTP) and its relationship to CK-Mt

3.1.3.1 mPTP molecular structure

As previously described, the mPTP is a structure that can form in mitochondria under stress conditions, and may contribute to I/R injury. The specific molecular components that comprise the mPTP have yet to be conclusively identified. The initial breakthrough in understanding mPTP structure occurred when Crompton *et al.* demonstrated that cyclosporine A (CsA) could

increase the amount of calcium required to induce mPTP opening [213]. Tanveer *et al.* subsequently demonstrated that CsA bound to cyclophilin D to inhibit mPTP opening, which was the first evidence that cyclophilin D may be an mPTP component [214]. While the complete mechanism of action remains unknown, the most acceptable hypothesis is that CsA inactivates cyclophilin D, preventing cyclophilin D from interacting with either ANT [215] or the F_0/F_1 ATP synthase [216], hence inhibiting mPTP formation, as discussed below. ANT was initially suggested as an mPTP structural component because bongkrekic acid, an ANT inhibitor, was able to delay mPTP opening [217]. In addition, Hunter *et al*. had demonstrated that ADP, an ANT ligand, was able to delay permeability transition [218]. VDAC has been implicated in the mPTP structure as it forms a large pore with ANT that produces current patterns similar to those seen with mPTP opening [219]. Furthermore, chemical inhibition of VDAC was found to decrease mPTP opening in isolated rat liver mitochondria [220]. Knockout mouse models were subsequently generated for all three proteins to elucidate their specific roles in mPTP opening. VDAC knockout mice (Vdac1/2/3$^{-/-}$) were found to have no significant differences in mPTP function as compared to wild type controls [221]. In contrast, cardiac mitochondria from ANT knockout mice resisted mPTP opening, as elevated [Ca^{2+}] were required to induce pore formation [222]. Similarly, cyclophilin D knockout mice were shown to have increased calcium thresholds for mitochondrial swelling and mPTP opening [223]. It appeared that ANT and cyclophilin D both had regulatory roles in mPTP opening, but as pore opening could still occur in the absence of either protein, neither could be considered essential structural components.

A role for CK-Mt in mPTP opening was initially proposed due to the interaction between CK-Mt and ANT/VDAC in the formation of the mitochondrial interactosome [224]. It has been

reported that CK-Mt may protect against mPTP opening in isolated mouse liver mitochondria and in cell culture [224,225]. Additionally, studies have concluded that creatine may reduce mPTP opening through a mechanism that likely requires functional CK-Mt [2,64]. However, the effects of CK-Mt knockout on mPTP opening have not been assessed.

As results from studies on VDAC, ANT, and cyclophilin D were inconclusive, further attempts have been made to identify mPTP structural elements, and more recently the F_0/F_1 ATP synthase [216,226,227], phosphate carrier [213], and pro-apoptotic Bcl-2 elements (Bax and Bak) have been proposed as candidates [228]. The F_0/F_1 ATP synthase has emerged as the most promising candidate, but because viable F_0/F_1 ATP synthase knockout mouse models cannot be easily generated, a conclusive result remains elusive. Thus far, no specific mPTP structural components have been unequivocally confirmed.

3.1.3.2 Regulation and effects of mPTP

Mitochondria are responsive to cytosolic calcium concentrations as feedback to increase energy production, since calcium stimulates mitochondrial dehydrogenases [229]. Specifically, it was first reported in 1978 by Hunter and Haworth that isolated mitochondria could buffer calcium until IMM calcium reached approximately 60 nmol of Ca^{2+} per mg protein [230,231]. However, if excessive calcium is added (>50 μM) to isolated mitochondria [232], the inner mitochondrial membrane rapidly permeabilizes. This leads to an expulsion of all solutes with molecular weights of less than 1.5 kD and induces a measurable change in membrane potential due to the loss of the proton gradient [230,231]. The abrupt permeabilization of the inner mitochondrial

membrane, likely through formation of large pore structures, is defined as mPTP opening. The activators, inhibitors, and outcomes of mPTP opening are summarized in Figure 3-1 below.

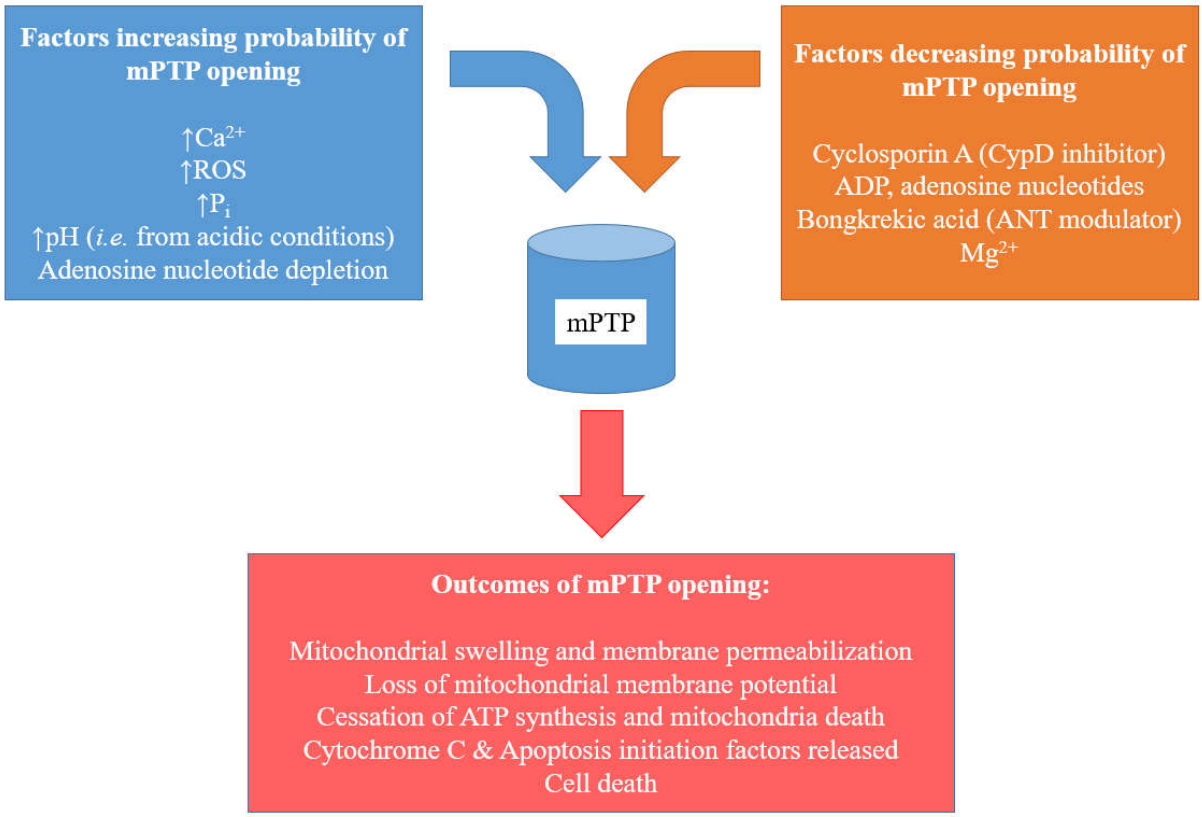


Figure 3-1: Schematic detailing the activation and outcomes of mPTP opening

Signals of increased intracellular stress (elevated cytosolic calcium concentration, reactive oxygen species production, and free P_i) are activating factors of mPTP opening. Inhibitors of mPTP opening generally modulate potential mPTP components, as detailed in Section 3.1.3.1. After mPTP opening, the membrane permeabilization also allows influx of extra-mitochondrial solutes, which results in significant mitochondrial swelling. Furthermore, there is a rapid loss of the mitochondrial membrane potential, which prevents oxidative phosphorylation and a cessation of mitochondrial ATP synthesis. These disturbances lead to a cascade of events resulting in mitochondria destruction, as well as potential cell death through rupture of the OMM and release of cytochrome C and apoptosis initiation factor into the cytosol [216,218,224]. Information presented in the figure is derived from [215,216,218,233].

3.1.3.3 mPTP functions in physiology and pathophysiology

The physiological function of the mPTP remains to be elucidated, though more is known about its role in pathophysiology, especially in the context of I/R injury. Physiologically, the mPTP transiently opens, during which the IMM is briefly permeable to calcium. These ephemeral exchanges are thought to balance calcium in the mitochondrial inner matrix [234]. It has also been postulated that the mPTP could in theory regulate mitochondrial metabolism (ATP synthesis) by modulating mitochondrial calcium [218]. Overall, the physiological function of mPTP in the heart may not be essential, as several studies of cyclophilin-D knockout mice have failed to detect any signs of cardiac dysfunction at baseline [233].

mPTP opening has been extensively studied in I/R injury as there is elevated cytosolic calcium following ischemia, and increased reactive oxygen species (ROS) synthesis and recovery of pH during reperfusion (reviewed in [215]). These changes induce simultaneous mPTP opening in mitochondria, which in turn leads to substantial cell death [215] - possibly responsible for up to 50% of final infarct size [170]. Indeed, studies have shown that inhibiting mPTP opening can significantly reduce infarct size [235], an effect that has been proven clinically. For instance, MI patients given IV CsA, an mPTP inhibitor, showed less cardiac necrosis and exhibited improvement in LV ejection fraction after MI [236,237]. While the results from CsA studies in patients have been inconsistent [238,239], inhibition of the mPTP represents a promising avenue of ongoing investigation as a pharmacological target. In addition to I/R injury, mPTP opening has also been observed in heart failure, possibly due to poor calcium homeostasis, though the research in this area remains limited [215,240].

In conclusion, there is a substantial body of evidence that links CK-Mt to the mPTP and to I/R injury. In regards to CK-Mt and the mPTP, it has been shown that transgenic CK-Mt can inhibit mPTP opening in rat liver, which may be related to the functional coupling between CK-Mt and ANT, a known mPTP modulator [64,208]. The literature suggests CK-Mt may play a causative role in I/R injury. For instance, CK-Mt/CK-M double KO mice exhibited impaired calcium homeostasis and increased susceptibility to I/R injury [35]. Furthermore, our group has reported that CK-Mt overexpression protects against hypoxia / reoxygenation induced cell death *in vitro* [176]. Most importantly, our group has recently demonstrated that CK-Mt overexpression protects against *in vivo* and *ex vivo* I/R injury, improving cardiac function and reducing necrotic area. Yet despite this preponderance of evidence, there is only limited evidence that CK-Mt in the heart protects against mPTP opening [212]. The CK-Mt OE mouse model generated by our group provided a unique opportunity to investigate whether increased CK-Mt expression could inhibit mPTP opening, which could inform on mechanisms by which CK-Mt protects against I/R injury.

3.2 Hypotheses and aims

There is limited information regarding what, if any, effect CK-Mt overexpression has on metabolism and mitochondrial function. Our group had previously demonstrated that excessive CrT overexpression led to widespread metabolic perturbations in the mouse heart, including changes suggestive of impaired glycolysis and FAO such as decreased enolase content/activity and TCA cycle intermediates (*e.g.* fumarate, succinate) [135,241]. CK-Mt is required for creatine-stimulated mitochondrial respiration and creatine-mediated inhibition of mitochondria

permeability transition [64,242,243]. Moreover, PCr and creatine modulate ADP-stimulated mitochondrial respiration [64,242,243] and glucose oxidation [101]. Therefore, it is plausible that CK-Mt overexpression could affect various aspects of cardiac metabolism by altering PCr:creatine ratios and/or mitochondrial respiration. The first aim of this study was therefore to investigate the metabolomics profile and the mitochondrial function of CK-Mt OE mice.

The first approach involved a non-biased metabolomics methodology to determine whether CK-Mt overexpression resulted in any unexpected knock-on effect on whole cell metabolism (*e.g.* glucose metabolism, FAO, and the TCA cycle) by exploring the same set of aqueous and lipid metabolites previously analysed for CrT OE mice [241].

The second approach was to utilize the mitochondrial respiration assay to investigate whether CK-Mt overexpression affected the function of isolated cardiac mitochondria. This would clarify whether the moderate overexpression strategy caused any detrimental effect on mitochondrial function (*e.g.* due to crystal aggregate formation), while concurrently evaluating whether CK-Mt overexpression enhanced any aspects of mitochondrial respiration.

As discussed in the Section 3.1, there was evidence that CK-Mt may play a role in mPTP opening, hence it was hypothesized that elevated CK-Mt would delay mPTP opening, which would manifest as reduced mitochondrial swelling and cytochrome C release. Therefore, the second aim was to use the mitochondrial swelling assay to explore whether CK-Mt overexpression affected mPTP opening.

3.3 Methods

3.3.1 ^{1}H-NMR analysis of the metabolic profile

A collaboration with Dr Tom Eykyn of King's College, London, was undertaken to develop a baseline metabolomics profile with ^{1}H-NMR in CK-Mt OE and WT mice. Homozygous (n = 6) CK-Mt OE and WT (n = 6) female mice on average 14 weeks old were sacrificed, and cardiac tissue was prepared for analysis by ^{1}H-NMR. Mice were sacrificed through cervical dislocation, and confirmation of death was performed with heart excision. Hearts were washed in 4^{o}C PBS before being snap frozen in liquid nitrogen and stored at -80^{o} C. Frozen hearts were weighed and crushed into a fine powder, and 5-10 mg of tissue was suspended in ice-cold methanol, chloroform, and ddH_2O. The samples were then centrifuged at 3600 rpm for an hour at 4^{o}C, which allowed separation of samples to aqueous, protein, and lipid fractions. The aqueous fraction was extracted and purified of metals with 20-30 mg Chelex 100 (Bio-Rad), a chelating resin, for 5 minutes at 3600 rpm at 4^{o}C. The supernatant was extracted and mixed with 15 µL of universal pH indicator solution (Sigma) and stored at -80^{o}C. The lipid layer was then extracted and aliquoted into in a glass scintillation vial, which was incubated for three hours in a fume cupboard under ambient conditions to evaporate the chloroform, after which the dried lipid fraction was then stored at -80^{o}C.

Freeze-dried aqueous extracts were re-dissolved in 600 µL deuterated water (D_2O) containing 1.15 g/L Na_2HPO_4, 0.2 g/L KH_2PO_4, 8 g/L NaCl, 0.2 g/L KCl, and 0.0075% w/v deuterated trimethylsilyl propanoic acid (TMSP). TMSP is commonly used as an internal standard for calibration and normalization of the chemical shift in in aqueous solvent NMR spectroscopy. The pH of aqueous samples was then adjusted to 7 using 1 M HCl and 1M NaOH before being

analysed. Dried lipid samples were re-suspended in 600 µL deuterated chloroform ($CDCl_3$) with 0.05% tetramethylsilane (TMS). TMS is an organosilicon compound used as an internal standard for calibrating chemical shift in organic solvent NMR spectroscopy.

Aqueous and lipid samples were then analysed on a Bruker 9.4T (400 MHz) spectrometer with a Broadband Observe probe at 25°C. Aqueous samples were analysed using a NOESY 1D-pulse sequence with 64 scans and 4 dummy scans over the course of 550 seconds. A 20.5-ppm sweep width, 4s pre-scan delay, and 90° flip angle were used for the experiment. For lipid samples, a ZG30 pulse sequence was used with 64 scans and 4 dummy scans, 16.1 ppm sweep width, 5s-pre-scan delay, and 30° flip angle. Each lipid sample was analysed for 690 seconds. Raw data was processed using TopSpin software (version 2.1) and further processing was conducted in Excel, Matlab, and Graphpad Prism. Metabolites were matched to peaks based on previously obtained in-house data, and confirmed by chemical shifts. Peak areas were then standardized by comparing to the TMSP peak area in the aqueous fraction and the TMS peak in the lipid fraction. Normalized peak areas were corrected for the weight of tissue, and final results were expressed in µmol/gram tissue. Sample preparation was conducted by the author, and NMR samples were run and analysed by Dr Tom Eykyn with support from the author.

3.3.2 Mitochondrial isolation and evaluation of mitochondrial function

For the mitochondrial respiration assay, isolated mitochondria were extracted from male CK-Mt OE homozygote (n = 8) and WT control mice (n = 9) on average 13 weeks old.

Mice were culled via cervical dislocation, and hearts were immediately extracted and washed in ice-cold PBS. Following removal of non-myocardial tissue, hearts were quickly dried and

weighed. Hearts were then minced in a Petri dish of ice-cold KCl-based Chappell-Perry Buffer-1 (100 mM KCl, 50 mM MOPS, 1mM ATP, and 0.5 mM EGTA, pH 7.4) ("CP-1 buffer") and stored in an ice-cold glass Potter-Elvehjem homogenizer (Glass-Col, USA). Approximately 1 mL of fresh ice-cold CP-1 buffer was added to the homogenizer, and the tissue was manually homogenized with a tapered bottom PTFE Teflon pestle (Glass-Col). Approximately 100 µL of ice-cold 10% trypsin solution (2.5 mg trypsin/mL) was added to trypsinize the homogenate through a 10-minute incubation step on ice. Post-incubation, 1 mL/ 100 mg tissue of ice-cold CP-1 buffer with 2 mg/ mL fatty acid free BSA ("CP-2 buffer") was added to the trypsinized homogenate to neutralize the trypsin, and the mixture was further homogenized using the PTFE Teflon pestle. Mitochondria were then isolated by two-step centrifugation. First, a 10-minute 900g centrifugation was performed at 4°C to remove myofibrillar components. Afterwards, the supernatant was transferred to a new Eppendorf tube for an 10-minute 5200g centrifugation at 4°C, which pelleted mitochondria. The pelleted mitochondria were washed with CP-2 buffer and re-pelleted through an additional 10-minute 5200g centrifugation at 4°C. Mitochondria were then re-suspended in 200 µL iced KME solution (100 mM KCl, 50 mM MOPS, and 0.5 mM EGTA, pH 7.4), and kept on ice until the start of the respiration assay. Mitochondria concentration was determined via the bicinchonic acid (BCA) assay with the Pierce BCA Protein Assay kit (Thermoscientific, UK), as described in Section 3.3.2.1. Mitochondrial respiration assay was conducted within two hours after mitochondrial isolation.

Respiration was measured using a Mitocell S200A Micro-Respiration System (Strathkelvin Instruments, North Lanarkshire, UK) and data was analysed using the Strathkelvin 782 System Data Analysis Module 2010 v. 4.0.1.15. First, respiration medium warmed at 25°C (0.5 mM EGTA, 3 mM $MgCl_26H_2O$, 60 mM K-lactobionate, 20 mM taurine, 10 mM KH_2PO_4, 20 mM

HEPES, 110 mM sucrose and 1mg/ml fatty acid free BSA, pH 7.4) was added into the system chamber for a five-minute incubation step. 250-300 µg of ice-cold mitochondria, as measured by the BCA assay, was then added to the system chamber, bringing the total chamber concentration to 300 µL. The chamber was then sealed to prevent exogenous oxygen entry, and after an additional five-minute incubation step, respiration measurements were started. Basal respiration was defined as respiration after addition of 5 mM glutamate, 2.5 mM malate and 5 mM sodium pyruvate. ADP-derived respiration (State 3) was assessed after addition of 150 µM ADP, and proton leak (State 4) was measured by inhibiting respiration through addition of 2 µM oligomycin. Uncoupled respiration was measured as the maximum rate achieved after 2-6 additions of 60 – 100 nM carbonyl cyanide-4-(trifluoromethoxy)phenylhydrazone (FCCP), an uncoupling agent. Finally, non-mitochondrial respiration was assessed through addition of antimycin A (0.25 µg/ml) into the chamber. Quality control was conducted on mitochondria by including only samples with a respiratory control ratio (RCR) ≥ 3 in the experiment. RCR is the ratio between State 3 and State 4, and is commonly used to assess mitochondrial quality [244]. A high RCR indicates that the mitochondria have low proton leak and have a robust response to ADP-stimulated respiration [244]. Therefore, samples with RCR < 3 were excluded from the final results.

3.3.2.1 Bicinchoninic acid (BCA) protein assay

The BCA protein assay (Pierce BCA Protein Assay Kit) was utilized to determine protein concentration in isolated mitochondria experiments. An aliquot of protein was mixed with 200 µL BCA assay working solution in triplicate wells of a 96 well plate. The plate was then incubated at 37^{o}C for 30 minutes, and the absorbance at 562 nm was measured by a

spectrophotometer (VMax plate reader; Molecular Devices, USA). The protein concentrations of samples were extrapolated from a BSA standard curve (0-2000 µg/ml), as per manufacturer's instructions.

3.3.3 Assessment of the effects of CK-Mt overexpression on mPTP opening through mitochondrial swelling assay and western blotting

The mitochondrial swelling assay was selected to measure mPTP opening. In the mitochondrial swelling assay, mPTP opening is induced by the addition of a trigger, in this case calcium. mPTP opening causes mitochondrial swelling, which resulted in a corresponding reduction in absorption at 540 nm (A_{540}). This decline in A_{540} over 20 minutes was measured through spectrophotometry, and was used as a measure of mPTP opening, a method widely adopted in the literature [245-247].

3.3.3.1 Optimization of mitochondrial swelling assay methodology

The experimental protocol for the mitochondrial swelling assay was derived from Hall *et al.* [246], and various conditions were optimized.

Optimization experiments were performed on pooled hearts from two 6 month old ex-breeder C57BL/6 females (Envigo), which yielded ~700 µg mitochondria. In each experiment, the isolated mitochondria were partitioned into one of three groups for the swelling assay (200 µg/group): 1) mitochondria with no calcium, 2) mitochondria with calcium, and 3) mitochondria with calcium and CsA. The first group acted as a time control to benchmark how

A_{540} changed over the 20-minute measurement interval with no calcium added. The second group was the test group, and the decline in A_{540} after calcium addition was used as the measurement of mPTP opening and mitochondrial swelling. The third group utilized CsA to inhibit mPTP opening induced by calcium, and thus served as a positive control that was expected to have less decline in A_{540} signal as compared to the calcium-only group.

CsA was selected as a positive control to prevent calcium-induced mitochondrial swelling, as it is commonly used to confirm that mitochondrial swelling induced by agents (in this case calcium) is specifically mediated by mPTP opening [232,248]. The consensus in the literature suggests that 1 μM CsA would protect against mPTP opening in isolated mouse cardiac mitochondria [232,248,249], which was tested with success in the current assay, hence no further optimization was required.

The second factor to be optimized was concentration of mitochondria used in each well. The literature suggested concentrations ranging from 200 ng - 1 μg mitochondria per 1 μL of swelling buffer [232,246,247]. Initial pilot experiments revealed that insufficient mitochondria (*i.e.* <0.5 μg/μL) produced inconsistent A_{540} readings due to low baseline optical density values. Conversely, high mitochondrial concentrations (*i.e.* >1 μg/μL) were found to result in sedimentation of mitochondria (despite plate shaking between reads), which likewise generated inconsistent A_{540} signals. Optimization experiments revealed that the A_{540} signal was most stable at 1 μg/μL concentration of mitochondria with the Vmax plate reader, thus this was the concentration selected for subsequent assays. Two pooled hearts were found to yield ~700 μg of mitochondria, which at 1 μg/μl, would yield approximately 600 μL of mitochondria solution for the swelling assay (the remaining mitochondria were needed for BCA and citrate synthase assay, as discussed in Section 3.3.2.1 and 3.3.3.4, respectively). The 600 μL of mitochondria

solution was subsequently aliquoted into 3 wells (200 µL of mitochondria/well), with 1 well being assigned to each of the three experimental groups as previously described: control, calcium added, and calcium/CsA added.

Calcium concentrations to induce swelling were also optimized. Initial experiments required very high Ca^{2+} concentrations to induce mPTP opening (~2.4 mM), which were far greater than the concentrations tested in the literature (~600 µM or less) [232,246,247]. It was subsequently found that this was due to the high EGTA concentrations in the resuspension buffer - swelling could only be induced at more appropriate calcium concentrations (600 µM) by using EGTA-free resuspension buffer.

3.3.3.2 Optimized mitochondrial swelling assay protocol

The final optimized protocol used to acquire the experimental data is as follows. Two hearts were extracted in parallel and homogenized/isolated in isolation buffer (250 mM sucrose, 10 mM Na-HEPES, 1 mM EGTA, pH 7.4) using the protocol described in Section 3.3.2.

The two hearts were kept separate during the isolation process until the final resuspension step, during which they were pooled together. For the final resuspension step, the mitochondria pellet was gently re-suspended in 200 µL EGTA-free isolation buffer at concentration of 3-4 µg/µL at 4°C. An aliquot (12.5 µL) of this solution was then diluted 1:4 in EGTA-free isolation buffer and immediately frozen at -80°C for the citrate synthase assay (Section 3.3.3.4). An additional 15 µL aliquot was incubated on ice for the BCA assay to quantify protein concentration. Approximately 140 µL of the remaining solution was added to 500 µL of RT swelling buffer (200 mM sucrose, 10 mM HEPES, 5 mM KH_2PO_4, 10 µM EGTA, pH 7.3) to

generate a final mitochondrial swelling solution at a concentration of approximately 1 µg/µL. This solution was then mixed and pipetted into a clear-bottom Greiner 96-well plate at 200 µL/well in three wells. The plate was inserted into a VMax plate reader at RT, and 1 µM CsA in 0.5 µL DMSO was added to the "CsA + calcium" positive control group, and an identical volume of DMSO was added to the control and calcium wells.

After five minutes incubation at RT, 600 µM calcium chloride was added to the experimental groups to initiate mPTP opening, after which A_{540} was measured every minute after shaking, to characterize the development of mitochondrial swelling over twenty minutes.

At the end of the assay, samples were collected in Eppendorf tubes, and centrifuged at 4°C at 5200 g for 10 minutes. The supernatant was discarded, and the pellet was re-suspended in 50 µL of ice-cold RIPA buffer (Sigma) and immediately frozen at -80°C for cytochrome C quantification.

3.3.3.3 Western blotting for cytochrome C

Mitochondria were re-suspended in ice-cold RIPA buffer (Sigma) supplemented with protease and phosphatase inhibitors (Roche), and stored at -80°C for analysis of cytochrome C by western blotting. The concentration of mitochondrial protein in the re-suspended sample was determined by BCA assay.

Based on the protein concentrations, a 10 µg aliquot of protein was mixed with 12.5 µL 4x NuPAGE loading buffer (Invitrogen) and 5 µL of 10 x NuPAGE reducing buffer (Invitrogen). The final sample volume was adjusted to 50 µL with additional RIPA buffer, and then incubated at 95°C for 5 minutes to denature protein. Samples (2 µg of protein in 10 µL solution) were

loaded in duplicates into 12% SDS polyacrylamide gel (Mini-PROTEAN TGX Stain-Free pre-cast 12% polyacrylamide gel, Bio-Rad). Proteins were separated by gel electrophoresis with 1x Tris/Glycine/SDS running buffer at 120V for 30-45 minutes using the Bio-Rad Mini-Protean gel electrophoresis system. Protein was subsequently transferred onto a nitrocellulose membrane (BioRad) over 10 minutes at RT using the Transblot Turbo Transfer System (BioRad).

After transfer, the membrane was blocked in 5% dry skimmed milk powder with 0.1% Tween 20 in PBS (Tween-PBS) for 1 hour at 21°C. Blocking solution was removed through 5 x 5 minute Tween-PBS wash steps. Samples were then incubated with a 1:2,000 dilution of cytochrome C primary antibody (mouse monoclonal [37BA11], Abcam #ab110325) overnight at 4°C, in 5% dry milk powder dissolved in Tween-PBS. After overnight incubation, any unbound primary antibody was removed through 5 x 5 minute Tween-PBS wash. The membrane was then incubated with 1:20,000 diluted anti-mouse IgG horseradish peroxidase-linked secondary antibody (Promega W4021) for 1 hour at 21°C. Any unbound secondary antibody was then removed from the membrane through 5 x 5 minute Tween-PBS wash. The membrane was incubated for 5 minutes with the ECL Prime chemi-luminescence substrate (GE Healthcare), and then cytochrome C was visualized using the Biorad Chemi Doc MP imaging system, and concentration was quantified using Image Lab v. 5.0 software.

Since VDAC was utilized to normalize cytochrome C protein content, membranes were washed in Tween-PBS and stripped after quantification of cytochrome C. Washed membranes were incubated with stripping buffer (2.5% SDS, 100 mM β-mercaptoethanol, 62.5 mM Tris-HCl, pH 6.8) for 30 minutes at 55°C. Stripping buffer was rinsed from the membranes through 2 x 10 minute Tween-PBS wash steps, and primary antibody for VDAC (rabbit polyclonal, Abcam

#15895) was added at 1:2,000 dilution for re-probing, followed by incubation with 1:20,000 diluted anti-rabbit IgG horseradish peroxidase-linked secondary antibody (Santa Cruz sc-2030).

3.3.3.4 Assessment of mitochondrial quality through citrate synthase assay

The citrate synthase assay described in Section 2.3.4 was modified to allow analysis of citrate synthase in isolated mitochondria samples (*i.e.* as opposed to tissue samples). First, mitochondria were frozen and thawed before the assay, which disrupted the mitochondrial membrane to allow release of citrate synthase, primarily located in the mitochondrial inner matrix [250]. Hence, aliquots of isolated mitochondria were frozen at -80ºC for at least 24 hours and thawed on ice prior to the citrate synthase assay. Second, Triton-X, a detergent used to lyse lipid membranes, is required to permeabilize the mitochondrial membrane [250]. Thus, the protocol in Section 2.3.4 was modified to include 0.25% Triton X in the citrate synthase reagent (0.35 mM Acetyl-CoA, 0.12 mM DNTB, 0.25% Triton X). Other parameters, such as mitochondria concentrations, were also optimized for the assay.

The final protocol used to obtain the experimental data is as follows. After mitochondria isolation with sucrose buffer, an aliquot (12.5 µL with ~50 µg) of mitochondria was taken from the same samples used for the mitochondrial swelling assay. This aliquot was re-suspended in 37.5 µL of EGTA-free isolation buffer to make a 50 µL solution at ~1 µg/µL mitochondria. Samples were immediately frozen at -80ºC for 7 days, were then thawed on ice for 10 minutes, and duplicates of each sample were run for citrate synthase using Triton-X supplemented citrate synthase reagent, according to the protocol detailed in Section 2.3.4.

3.4 Results

3.4.1 CK-Mt overexpression does not affect baseline metabolic profile

The results for 23 aqueous and 24 lipid metabolites are presented in Table 3-1. While 6 samples were prepared for each group, ultimately data was not obtained from one Tg aqueous sample (damaged during sample transport from Oxford to London) and one WT lipid sample (damaged NMR tube).

Student's t-tests were used to compare between genotypes, and suggested that CK-Mt overexpression had a negligible impact on metabolism. Of the aqueous metabolites analysed, only acetylcarnitine showed a significant difference between the WT and Tg groups (45% higher in the Tg group). No lipid metabolites analysed were significantly different between WT and Tg groups.

Student's t-tests were not ideal for analysis of the metabolomics results, as with 23 aqueous and 24 lipid metabolites, there was a distinct possibility of a false positive with $p < 0.05$. Thus, a different statistical test, the principle component analysis (PCA), was carried out to determine whether there were holistic differences in the metabolic profiles of WT and Tg mice. The PCA profile (Figure 3-2), conducted with Minitab 18 software, supported the conclusion that CK-Mt overexpression did not significantly affect the metabolomics profile, as there was no clear separation between WT and Tg groups for either aqueous or lipid metabolites.

Table 3-1: Metabolomics profile of CK-Mt OE homozygote and WT mice

Aqueous metabolites detected and quantitated by ^{1}H-NMR					
	WT (n=6)#	SEM	Tg (n=5)#	SEM	p*
NAD	0.407	0.021	0.416	0.042	0.87
Formate	0.222	0.023	0.241	0.025	0.62
NAD+NADH	0.418	0.017	0.448	0.043	0.54
ATP + ADP	1.20	0.124	1.31	0.253	0.70
Fumarate	0.012	0.004	0.015	0.005	0.67
Alpha-glucose	0.191	0.056	0.177	0.042	0.86
Creatine (CH_2)	3.95	0.226	4.35	0.336	0.38
Glycine	0.279	0.023	0.327	0.024	0.24
Taurine	16.3	0.921	20.4	1.93	0.11
Carnitine	0.334	0.034	0.380	0.045	0.47
Phosphocholine	0.173	0.019	0.183	0.017	0.72
Choline	0.073	0.008	0.077	0.009	0.76
Acetyl carnitine	**0.187**	**0.015**	**0.272**	**0.031**	**0.04**
Creatine (CH_3)	6.17	0.342	6.75	0.542	0.42
Aspartate	1.41	0.203	1.78	0.319	0.38
Glutamine	3.341	0.349	3.04	0.252	0.56
Succinate	0.390	0.046	0.412	0.038	0.75
Glutamate	2.70	0.218	2.91	0.209	0.55
Acetate	0.463	0.029	0.475	0.016	0.76
Alanine	1.15	0.099	1.15	0.066	0.98
Lactate	4.35	0.733	4.15	0.238	0.84
Valine	0.058	0.010	0.056	0.003	0.87
Isoleucine	0.074	0.011	0.073	0.003	0.94

#: Values are given in µmol/gram wet weight.

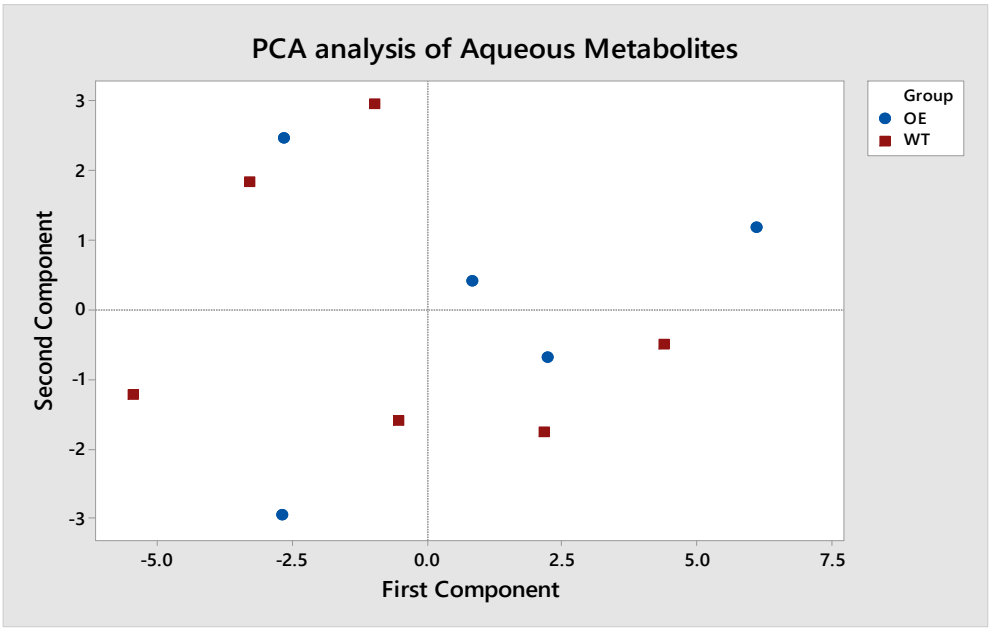
*: Data from WT and Tg mice were analysed using student's t-Test (p values reported here).

Lipid Metabolites detected and quantitated by ^{1}H-NMR

	WT (n=5)[#]	SEM	Tg (n=6)[#]	SEM	p*
Sphingolipid	8.69	1.30	8.30	1.04	0.84
Fatty acid residues (−CH=CH-)	794	153	914	73.8	0.52
Triglycerides(C2H of glycerol)	45.1	14.7	63.0	13.3	0.43
Total phospholipids (Glycerol (C2H2))	66.6	9.78	69.1	4.75	0.84
Total phospholipids (Glycerol (C3H2))	156	23.9	158	8.63	0.95
Triglycerides (C1H and C3H of glycerol)	33.1	13.9	53.3	11.4	0.33
Triglycerides (C1H and C3H of glycerol)	31.1	17.6	56.3	16.4	0.37
Triglycerides (C1H and C3H of glycerol)	143	41.9	189	30.9	0.43
Total phospholipids (Glycerol (C3H2))	206	29.5	214	12.2	0.81
Total phospholipids (Glycerol (C3H2))	84.5	13.5	88.3	5.42	0.81
Phosphatidylcholine (−CH2-N-(CH3)3)	411	66.6	420	25.0	0.90
Phosphatidylethanolamine (−CH2-NH2)	68.5	8.45	76.5	3.71	0.43
FA, PUFA (CH=CH-CH2-(CH=CH-CH2)n, n>1)	473	73.3	505	24.5	0.69
Fatty acid residues (−CH=CH-CH2-CH=CH-of linoleic acid)	121	26.4	141	15.5	0.58
Monoglycerides(FA, RH -CH2-CO-O-C2)	469	129	609	88.9	0.43
Fatty acid residues (CH2-CH=)	801	154	1010	97.6	0.31
Fatty acid residues (COCH2-CH2)	1100	193	1060	83.6	0.86
Fatty acid residues ((CH2-)n)	6120	1230	7590	763	0.37
Free Cholesterol (C19H3)	46.9	7.11	48.7	2.29	0.82
Fatty acid residues (ω-CH3 of DHA+EPA+linolenic)	32.0	4.55	34.5	1.24	0.62
Fatty acid residues (ω-CH3 of DHA+EPA+linolenic)	50.0	7.57	53.9	1.96	0.64
Fatty acid residues (ω-CH3 of DHA+EPA+linolenic)	28.6	4.16	30.7	1.19	0.64
Fatty acid residues (ω-CH3)	1130	205	1370	159	0.42
Total Cholesterol (C18H3)	32.2	5.50	32.6	2.13	0.95

#: Values are given in µmol/gram wet weight.

*: Data from WT and Tg mice were analysed using student's t-Test (p values reported here).



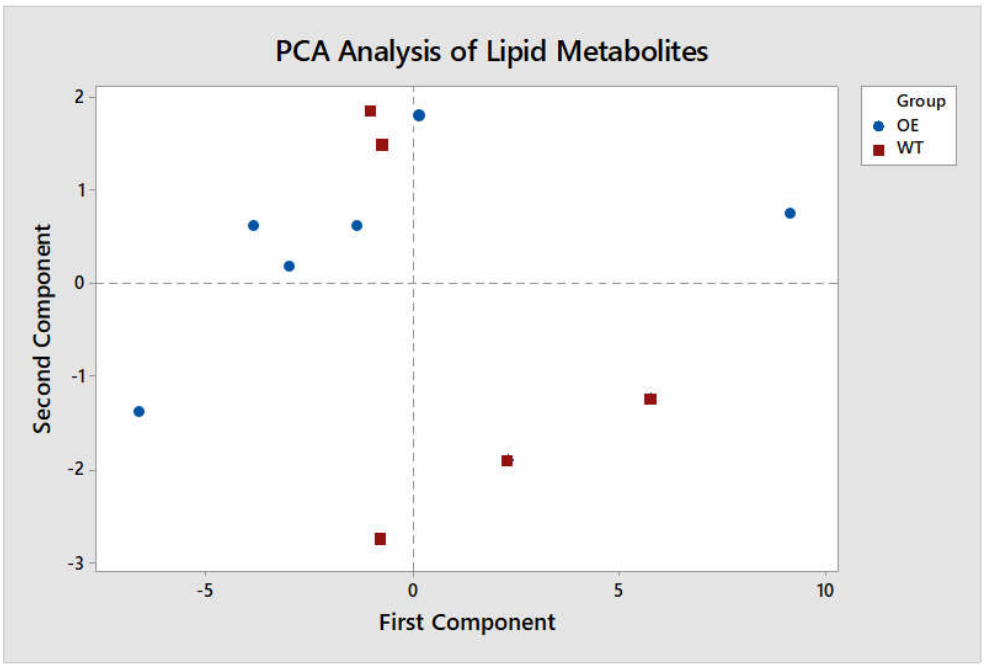


Figure 3-2: PCA analysis of aqueous and lipid metabolites in WT and Tg mice

Aqueous phase: n = 6 WT, and 5 Tg. Lipid phase: n = 5 WT, and 6 Tg.

3.4.2 CK-Mt overexpression does not affect mitochondrial respiration

Mitochondrial respiration was assessed by measuring the change in oxygen consumption in the chamber during the timeframe compound addition as described in Section 3.3.2. Respiration was measured after the rate of oxygen consumption had become constant for each State, as demonstrated by a constant slope in Figure 3-3, which is representative of a typical respiration assay curve.

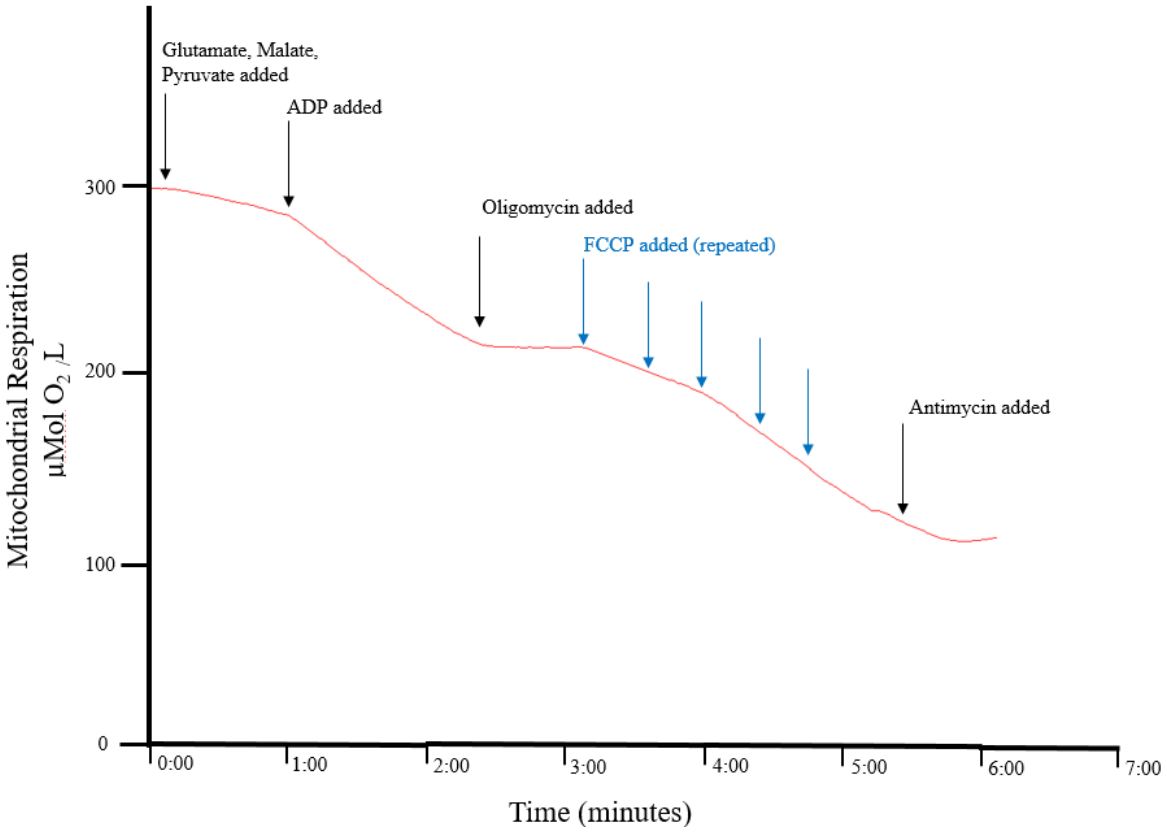


Figure 3-3: Mitochondrial respiration assay

The graph is a representative sample of the mitochondrial respiration assay, with time-points of compound addition labelled.

Mitochondrial respiration assay results strongly suggested that CK-Mt OE did not alter the respiratory function of isolated mitochondria (Figure 3-4). Both basal respiration and ADP stimulated respiration were not significantly different in CK-Mt OE mice as compared to WT controls (Basal respiration: WT 7.0 ± 1.9 nmol O_2/min/mg mitochondria; Tg 8.9 ± 2.1 nmol O_2/min/mg mitochondria; $p > 0.05$; ADP-stimulated respiration: WT 27.6 ± 5.1 nmol O_2/min/mg mitochondria; Tg 29.7 ± 6.5 nmol O_2/min/mg mitochondria; $p > 0.05$). Proton leakage, uncoupled respiration, and non-mitochondrial respiration were also not significantly different between the two groups (Figure 3-4). There were four WT and five Tg sets of mitochondria that were excluded due to low RCR values (*i.e.* unhealthy), hence data exclusion did not appear to be affected by CK-Mt overexpression.

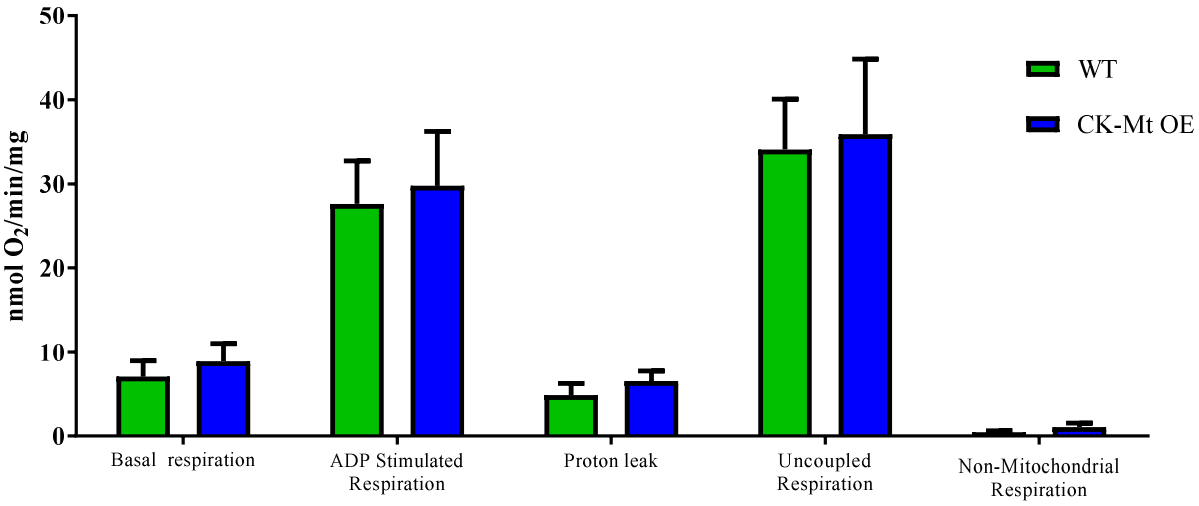


Figure 3-4: Mitochondrial respiration results of CK-Mt OE and WT mice

Results were analysed through student's t-test between groups for each parameter ($p > 0.05$). n = 9 WT, and 8 Tg.

3.4.3 CK-Mt overexpression delays mitochondrial swelling

The swelling assay was conducted on 10 Tg and 12 WT C57BL/6J male mice with average 24.7 and 28.4 weeks of age, respectively. As 2 hearts were pooled to generate one sample, this ultimately resulted in n = 5 Tg and 6 WT samples. Results of the assay are shown in Figure 3-5 below. The results suggest that CK-Mt overexpression protected mitochondria from calcium-induced mitochondrial swelling, and that the protection was as effective as 1 µM CsA. There was a slight additive protective benefit of CsA in Tg mitochondria, however, this effect was not significant at any time point. There was a significant difference between the WT calcium group and the WT CsA + calcium group, suggesting that the swelling was a result of mPTP opening, as CsA successfully reduced mitochondrial swelling.

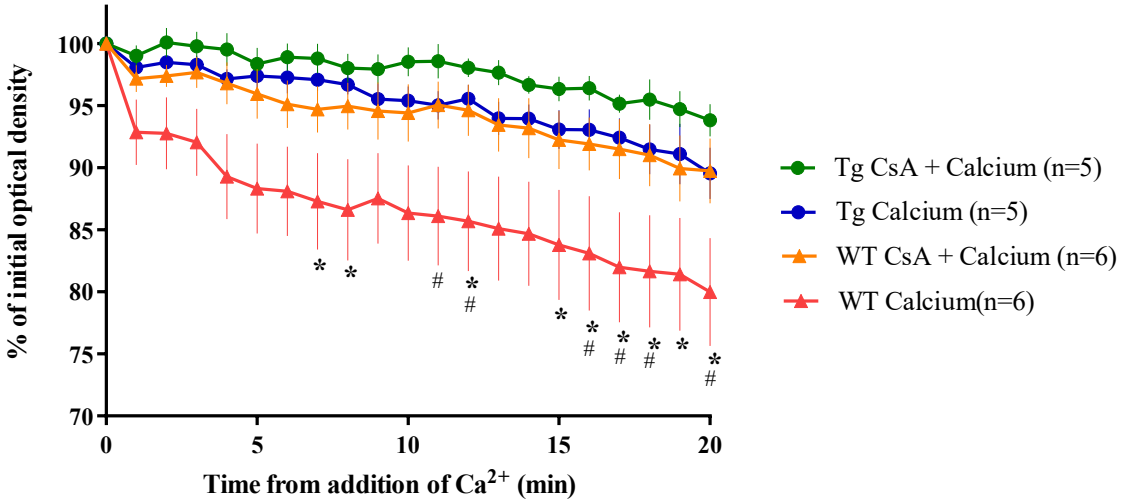


Figure 3-5: CK-Mt overexpression reduces mitochondrial swelling in response to Ca2+

Increased calcium-induced swelling was observed in the WT group (red line) as compared to the Tg group (blue line). A_{540}, measured every one minute, was used as an indicator of swelling. A_{540} is a measure of the light scattering properties of mitochondria; mitochondria absorb less light at 540 nm as they swell. Results are displayed as: % of initial optic density = (A_{540} at timepoint/initial A_{540} at time = 0) x 100%. Two-way ANOVA with Tukey's post-hoc test was conducted separately at each minute of the assay. * = $p < 0.05$ between WT calcium group and Tg calcium group. # = $p < 0.05$ between WT calcium group and WT CsA + calcium group.

3.4.4 CK-Mt overexpression reduces cytochrome C release

mPTP opening is accompanied by cytochrome C release from swollen/ruptured mitochondria [251]. Therefore, the isolated mitochondria were collected after the swelling assay for cytochrome C measurement to confirm results from the mitochondrial swelling assay.

The Tg calcium group retained significantly more cytochrome C compared to the WT calcium group, suggesting that cytochrome C release was lower (Figure 3-6). This, combined with the results of the swelling assay, was evidence that CK-Mt overexpression protected against mPTP opening.

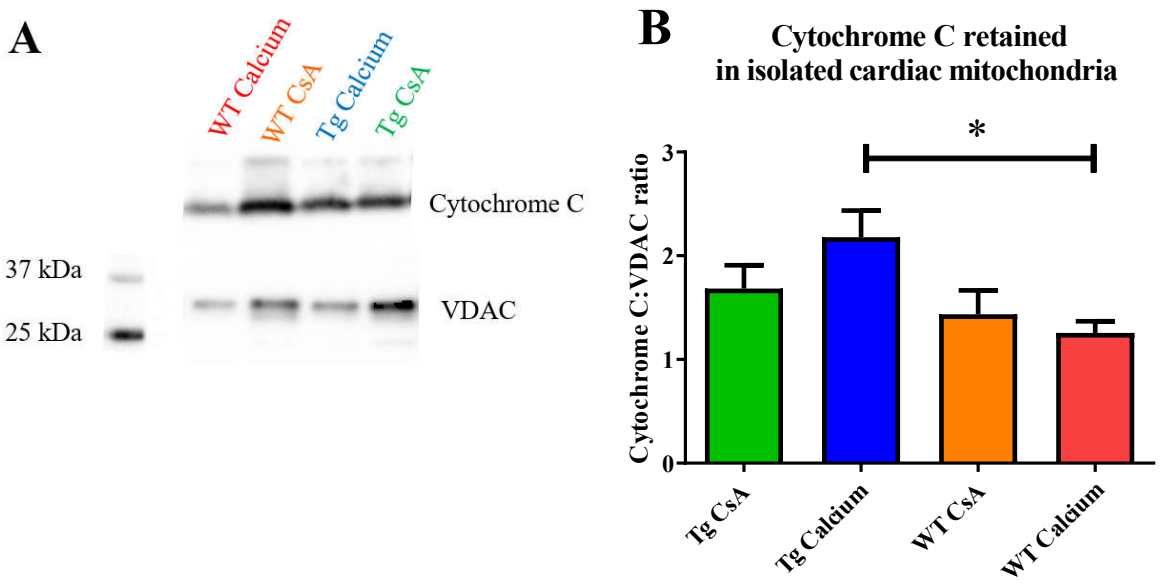


Figure 3-6: Western blot analysis of mitochondrial cytochrome C content after induction of mPTP opening

(A) Representative western blots of the mitochondrial cytochrome C and VDAC (which was used for protein content normalization). (B) Mitochondrial cytochrome C retained for each of the four groups, normalized for VDAC content (n = 5 samples per group). Results were analysed by one-way ANOVA with Bonferroni's post-hoc test (* = $p < 0.05$).

3.4.5 CK-Mt overexpression does not affect mitochondrial integrity

The citrate synthase activity assay demonstrated robust responses for all mitochondrial samples used for the swelling assay, thus verifying the enzyme integrity of the samples. Results were normalized to mitochondrial protein as measured by the BCA assay. There was no significant difference in citrate synthase activity between WT and Tg groups (Figure 3-7).

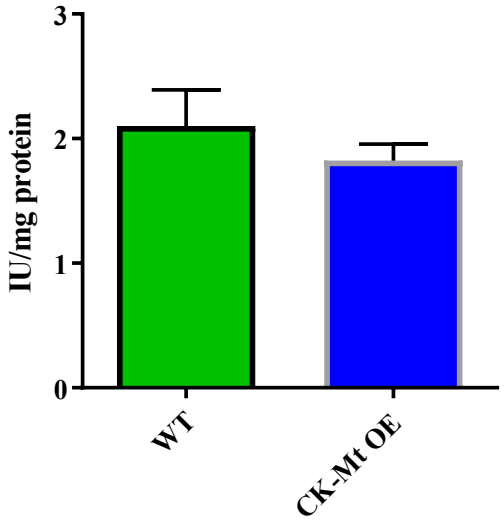


Figure 3-7: Citrate synthase results for samples from mitochondrial swelling assay

Citrate synthase results for samples from the mitochondrial swelling assay suggested no significant difference in citrate synthase activity between WT and Tg mitochondria. Results were analysed by student's t-test.

3.5 Discussion

In this chapter, three assays were undertaken to characterize the CK-Mt OE mouse line. ^{1}H-NMR metabolomics and mitochondrial respiration experiments suggested that CK-Mt overexpression appeared to metabolically benign at baseline. The mitochondrial swelling assay and western blots demonstrated that CK-Mt overexpression delayed mPTP opening. The results from these studies were recently published in Cardiovascular Research [212].

3.5.1 CK-Mt overexpression does not affect metabolism and mitochondrial respiration

A baseline metabolomics profile including 23 aqueous and 24 lipid metabolites was evaluated for CK-Mt OE mice. The only parameter that was significantly different from that of control mice was increased acetylcarnitine, which was elevated 45% in CK-Mt OE mice. Acetylcarnitine is generally synthesized as a result of excess acetyl-CoA, which suggests an energy rich environment, likely from increased lipid metabolism due to elevated fatty acid supply [252]. However, an increased fatty acid supply was not evident in the lipid metabolite results, for which Tg mice did not exhibit any significant deviations as compared to control mice. Thus, the increased acetylcarnitine result should be interpreted with caution. Further multivariate analysis with PCA did not reveal any differences between the metabolic profiles of Tg mice and controls, which suggests that CK-Mt overexpression did not result in any knock-on effects on glucose and fatty acid metabolism, TCA cycle function, and oxidative phosphorylation. These results are supported by the findings that there were no differences in

the baseline cardiac function and phenotype of CK-Mt OE mice, as assessed by *in vivo* haemodynamics and cine-MRI studies [212].

While the metabolomics result support other findings that CK-Mt overexpression was benign, there are limitations of ^{1}H-NMR that must be considered. The most crucial limitation of ^{1}H-NMR is the relative insensitivity (*i.e.* compared to mass spectrometry) [253]. As a result, the number of metabolites tested was limited to those with relatively high concentrations. Subtle alterations in metabolite concentrations, especially those with low starting concentrations or metabolic intermediates, may not have been detected.

Second, ^{1}H-NMR as currently applied, only describes the metabolite concentration of powdered heart tissue and does not necessarily inform regarding to the *in vivo* situation. Recent advances have allowed real-time measurement of key metabolites through the use of hyper-polarized substrates, such as ^{13}C pyruvate in the beating heart [254]. Third, ^{1}H-NMR only measures metabolite concentrations, and does not describe any changes in metabolic flux. This is a particularly important limitation in the current model, as overexpression of an enzyme could significantly affect various flux and activity rates, yet these changes would be undetected if they did not substantially alter metabolite concentrations. To resolve this issue would require proteomics and supporting methods to measure (*e.g.* biochemical analysis of enzyme activity or the use of hyper-polarized substrates such as ^{13}C pyruvate) [241]. Ultimately, had the ^{1}H-NMR results revealed significant differences, further investigation would have been conducted in these avenues.

The respiration assay results on isolated mitochondria indicate that the current level of CK-Mt overexpression did not significantly affect any of the respiration states measured. This shows that the current level of CK-Mt overexpression was well-tolerated, and did not affect the

function of respiratory proteins in the mitochondrial intermembrane space. A limitation of the current respiration assay was that there was no measurement of creatine-stimulated respiration, which may have been enhanced due to CK-Mt overexpression. As noted by Dolder *et al.*, creatine was suggested to be required for CK-Mt-induced protection of mPTP opening in the liver, where CK-Mt is not naturally expressed [64]. As cardiac mitochondria naturally express CK-Mt and contain creatine to facilitate Cr/PCr exchange in the intermembrane space and cristae, exogenous creatine addition was not required [31]. Overall, the results of mitochondrial respiration and metabolomics, combined with the protective effects mediated by current level of CK overexpression in I/R injury [212], establish a therapeutic level of CK overexpression.

3.5.2 Potential mechanisms underlying CK-Mt overexpression in protection against mPTP opening

The results of the mitochondrial swelling assay demonstrate that CK-Mt overexpression delays CsA-inhibited mitochondrial swelling, which indicates that CK-Mt prevents mPTP opening. This was supported by significantly more retained cytochrome C in Tg mitochondria as measured by Western blot. Citrate synthase activity was used to confirm the integrity of the isolated mitochondria.

There were two notable limitations of the current approach. First, the cytochrome C measured by Western blot was the protein retained in the mitochondria not released from mitochondria during the mitochondria assay. Thus, the assumption was made that total quantity of cytochrome C in mitochondria (normalized to VDAC) was the same in the four groups before adding calcium. Second, mitochondria quality was verified using the citrate synthase assay

rather than mitochondrial respiration assay. While the citrate synthase has been utilized for mitochondria validation [250], mitochondrial integrity would have been more thoroughly verified through the mitochondrial respiration assay, which evaluates membrane integrity, respiratory function, and enzyme activity. However, the mitochondrial respiration assay required approximately five-fold more mitochondria than the citrate synthase assay, which was selected due to limitations in available mitochondria.

The current experiment recapitulates results of another study conducted by our group, in which CK-Mt OE primary cardiomyocytes were found to delay mPTP opening stimulated by ROS as measured through the tetramethylrhodamine methyl ester (TMRM) assay [212]. Taken together, these results demonstrate that CK-Mt overexpression inhibits mPTP opening with two different stimuli (elevated Ca^{2+} and ROS) and experimental models (isolated mitochondria and primary cardiomyocytes). While neither study was conducted in the energy-depleted environment of I/R, elevated Ca^{2+} and ROS are widely considered to be the most important stimulants of mPTP opening during I/R [215,233], thus these results provide compelling evidence that CK-Mt may modulate mPTP opening during I/R. The exact mechanism by which CK-Mt inhibits mPTP opening remains unclear. However, it can be inferred that since the inhibition mediated by CK-Mt occurs with both elevated Ca^{2+} and ROS, the mechanism is stimulus independent. For instance, while CK-Mt was shown to reduce mitochondrial ROS production [255], the fact that CK-Mt protects against calcium-induced mPTP opening suggests that reduced ROS is unlikely to be the exclusive mechanism. Likewise, the fact that prevention of mPTP opening was observed in isolated mitochondria and cardiomyocytes without energy deficit suggests it is less probable that CK-Mt induced improvement of cellular bioenergetics

is the sole mechanism. Therefore, several possible mechanisms that may be involved in the CK-Mt mediated inhibition of mPTP opening, as discussed below.

The hypothesis that CK-Mt is a modulator in opening of mPTP was first derived from studies conducted in mouse livers that expressed transgenic CK-uMt [64,224]. It was found that transgenic CK-uMt significantly inhibited mPTP opening induced by calcium overload [64]. It should be noted that hepatocytes do not normally express CK-uMt, thus CK-uMt expression may have produced an exaggerated effect on mPTP opening. Furthermore, the protection only occurred when octameric CK-uMt was localized in the mitochondrial intermembrane space in the presence of creatine [64,224]. These requirements led to a hypothesis that CK-Mt, in the presence of creatine substrate, may exert mPTP protection by modulating ATP/ADP cycling through ANT. Specifically, through cycling ADP/ATP by phosphorylation of creatine to PCr, CK-Mt stabilizes the ANT m-conformation, which reduces the likelihood of mPTP opening (*i.e.* compared to the ANT c-conformation, which is stabilized by atractyloside, a known ANT inhibitor and mPTP inducer) [64]. This proposed mechanism is supported by the fact that increased ADP availability to ANT delays mPTP opening [215,256]. Creatine is present in cardiac mitochondria, and experiments by our group have confirmed that the transgenic CK-Mt of the current mouse model is expressed in the octameric form in the mitochondrial intermembrane space [212], thus the protection observed in this study could in theory involve a similar mechanism.

Second, an interaction between CK-Mt and other mitochondrial proteins could also play a role in the delayed mPTP opening. While the interaction between CK-Mt and ANT is well-studied, CK-Mt may interact with one or more of the other mitochondrial proteins that have been implicated in mPTP opening, such as the F_0/F_1 ATP synthase [226], or Bcl2 family (Bax and

Bak) [228]. While research has not identified any specific relationships, there are many opportunities for interactions given their similar functions and subcellular localizations.

Third, CK-Mt is highly sensitive to inactivation by ROS, which are especially prevalent during reperfusion [74]. For instance, ROS are also known to promote transition of CK-Mt from octamer to dimer [76], which is particularly important as CK-Mt inhibition of mPTP opening may require the octameric structure [64]. Therefore, it is possible that ROS-induced impairment of CK-Mt function and structure may cause opening of mPTP during I/R injury, hence CK-Mt overexpression may help simply by increasing CK-Mt availability during I/R injury [212]. Additionally, CK-Mt has been reported to reduce mitochondrial ROS synthesis by improving the efficiency of oxidative phosphorylation [255]. Hence, it is also plausible that overexpression of CK-Mt could delay mPTP opening by reducing mitochondrial ROS production. This hypothesis is supported by the results of the TMRM study, which demonstrated that CK-Mt overexpression mitigated ROS-induced mPTP opening [212].

A final possible mechanism is related to the role of CK-Mt in the formation and maintenance of mitochondrial inner and outer membrane contact sites. As previously discussed, CK-Mt forms a complex with ANT and VDAC, which has been reported to improve the mechanical stability of mitochondria by forming contact sites that bridge the inner and outer mitochondrial membranes [61,257]. In the aforementioned studies regarding transgenic CK-uMt in the liver, it was shown that the number of mitochondrial contact sites increased significantly in CK-uMt OE mouse livers [64,209]. The increased contact sites were reported to stabilize and strengthen mitochondrial membrane integrity by improving resistance to detergent-induced membrane rupture [258]. These contact sites have also been postulated to help prevent mPTP opening and may be of physiological significance during I/R [259]. For instance, mitochondrial-bound

hexokinase 2 is involved in stabilizing the contact sites via interaction with ANT and VDAC, and increased dissociation of mitochondrial-bound hexokinase 2 from these contact sites during I/R contributes to increased mitochondrial outer membrane permeability [260]. Therefore, to determine whether the current CK-Mt OE mouse model had increased contact sites, isolated mitochondria were subject to challenge with Triton-X detergent [212]. There was no measurable difference between the responses of Tg and WT mitochondria, which was not unexpected as the heart has high baseline CK-Mt expression, hence contribution from increased contact sites by modest CK-Mt overexpression in current CK-OE model is likely to be difficult to detect.

While it is highly plausible that the effect of CK-Mt overexpression on mPTP opening contributed towards the protection observed during I/R injury [212], there are other mechanisms by which CK-Mt overexpression could be beneficial. For example, a major mechanism meriting consideration relates to improved bioenergetics [212], such as the role of the CK system in maintaining high $|\Delta G_{ATP}|$. Studies demonstrated that overexpression models of CK system components (CK-M OE and CrT OE) had more rapid regeneration of PCr during reperfusion as assessed through ^{31}P-MRS, indicating a more robust CK system [2,191]. For instance, in CrT OE mice, there was rapid correction of $|\Delta G_{ATP}|$ to physiological levels (~57kJ/mol) during reperfusion, which could result in better recovery of vital ATPases such as SERCA. Enhanced SERCA function would improve calcium homeostasis, which may have contributed to the shorter period of hypercontractility upon reperfusion that was observed in CrT OE mice [2]. It is possible that CK-Mt overexpression, like CrT overexpression, improved $|\Delta G_{ATP}|$ during ischemia/reperfusion. This would require measurement of high-energy

phosphates by ^{31}P-MRS, which was not conducted and represents a major limitation of the I/R injury study [212].

In conclusion, the current results are significant in that they represent the first studies in which CK-Mt protected against mPTP opening in isolated heart mitochondria and cardiomyocytes. They also represent the first studies conducted with the sarcomeric CK-Mt subunit - existing studies have only demonstrated protection against mPTP opening with CK-uMt in the liver [64,208]. The results of the TMRM and mitochondrial swelling experiments indicate that inhibition of mPTP opening likely represent an important mechanism by which CK-Mt overexpression protects against I/R injury [212]. However, further investigation is required to conclusively understand the exact mechanisms by which CK-Mt overexpression protects against mPTP opening and I/R injury.

3.6 Future work

There are three major directions for additional research: 1) identifying the mechanism by which CK-Mt protects against mPTP opening, 2) translating these results to the intact beating heart, and 3) investigating effects of CK-Mt overexpression in co-morbidity conditions.

Several experiments can be conducted to elucidate what aspects of CK-Mt overexpression are responsible for protection from mPTP opening. Isolated cardiac mitochondria from CK-Mt OE mice can be treated with IA or DNFB, known CK inhibitors [114,261], before testing for mitochondrial swelling and cytochrome C release. If the inhibition of mPTP opening was dependent on CK activity, addition of CK inhibitors should mitigate the inhibition of CK-Mt on the mPTP opening as reflected by increased rates of mitochondrial swelling and cytochrome

C release. Exogenous creatine could also be added to isolated mitochondria to explore whether increased substrate produces a synergistic effect on delayed mPTP opening mediated by CK-Mt, which would bolster the hypothesis that the protective effect depends on CK-Mt enzymatic activity.

Experiments can also be conducted to test whether CK-Mt localization in the intermembrane space is required for a protective effect. If the localization is required, it would suggest that the coupling to ANT and influencing contact sites would be more likely mechanisms. To test this, purified CK-Mt protein can be added to WT isolated mitochondria in conditions that either promote or inhibit binding to the outer mitochondrial membrane, which have been previously optimized [64], and the effect on mitochondrial swelling can then be measured.

The results of the TMRM assay [255] suggest that the CK-Mt overexpression could protect against ROS-induced mPTP opening because CK-Mt may reduce mitochondrial ROS production. The ROS production by isolated mitochondria could be measured through established mitochondrial ROS measurement methods, such as a technique using horseradish peroxidase to trap H_2O_2 emitted from mitochondria, which is then bound to a fluorescent probe for detection through spectrophotometry [262].

Improved bioenergetics by CK-Mt overexpression is also a mechanism that could contribute to the protective effect of CK-Mt in I/R injury. As previously discussed, ^{31}P-MRS and CK flux measurements would provide a better understanding of the effects of CK-Mt overexpression on bioenergetics during I/R.

CK-Mt induced inhibition of mPTP opening has yet to be confirmed in the intact beating heart. To assess this, mPTP opening can be measured in Langendorff perfused hearts using

radiolabeled 2-deoxy-glucose, which will only enter mitochondria after mPTP opening [263]. This approach would represent the current gold standard in confirming the effect of CK-Mt overexpression on mPTP opening, and recent findings suggest that this method may be able to detect mPTP opening *in vivo* [264].

To date, there are no known chemical agents that specifically increase CK-Mt, thus the potential therapeutic benefit cannot be validated using a pharmacological approach. Considering the promising results obtained with CsA treatment in patients with cardiac ischemia [236,237], the current findings provide substantial rationale for investigating potential pharmacological activators of CK-Mt. Thus, initial experiments were conducted to identify such compounds as discussed in Chapter 6.

It would be worthwhile to investigate whether the protection of CK-Mt overexpression during I/R injury is retained if co-morbidities are present, such as old age, LV hypertrophy, or cardioplegia. Clinically, there are much lower prevalence rates of myocardial infarct in the young and healthy population compared to the aged population and patients with chronic diseases. In contrast, the majority of basic research, including the current experiment, is conducted on young and healthy animals, which may account for why many effective bench-side treatments do not translate in patients. Furthermore, many cardioprotective agents, such as forskolin and sevoflurante are known to lose efficacy under these common co-morbidities [265]. Our group has previously demonstrated that elevated myocardial creatine protects against I/R injury in the context of the co-morbidities described above [171], hence there is rationale to investigate whether the same protective effect of CK-Mt overexpression will be observed in the co-morbidity conditions.

As discussed earlier, there is some evidence indicating that mPTP opening may also be involved in congestive heart failure [215]. This finding, along with a body of evidence from other studies [18,117], suggests that CK-Mt overexpression could have a protective effect in the context of chronic heart failure. Thus, this avenue of investigation was pursued, and the results are detailed in the following chapter.

4 Mitochondrial creatine kinase overexpression in an in vivo model of chronic heart failure

4.1 Introduction

4.1.1 Heart failure and the necessity for novel therapies

Heart failure encompasses a broad range of clinical conditions, and is officially defined by the American Heart Association as "a complex clinical syndrome that can result from any structural or functional cardiac disorder that impairs the ability of the ventricle to fill with or eject blood" [266]. Heart failure is an end-stage symptom of many diseases, most commonly hypertensive and ischemic heart disease, but also including coronary artery disease, diabetes, obesity, and valvular conditions.

Heart failure is a prevalent condition affecting over 500,000 people in the UK [267], and at least 25 million people worldwide [268]. In the UK, its related costs consume 1–2% of the National Health Service annual budget [269], and over 30% of diagnosed patients are expected to die within a year of diagnosis [270]. Thus, novel treatments can significantly improve patient outcomes as well as reduce healthcare costs.

The pharmacological treatment options for chronic heart failure have been relatively unchanged for decades, and are not able to prevent the potentially dire consequences, as they are generally symptomatic treatments that are not curative. A commonality of current pharmacological treatments for chronic heart failure is that they often focus on reducing cardiac bioenergetic demand, blood pressure, and/or heart rate by neuro-hormonal antagonism (*e.g.* β-adrenergic

antagonists, angiotensin converting enzyme, calcium channel blockers, and diuretics). In contrast, drugs that increase energy demand (*e.g.* dobutamine, a beta adrenergic receptor agonists) are often restricted to treatment of acute decompensated heart failure [131,271].

However, the development of additional drugs that further reduce myocardial energetic demand is difficult due to the risk of bradycardia and hypotension [271]. Thus, novel therapies for heart failure should aim to improve myocardial energetic supply. As impaired bioenergetics has been proposed as a unifying causative mechanism of heart failure [1,9,272], improving energy supply and efficiency may offer much promise for novel therapies that could potentially have curative potential. Therefore, the study described in this chapter investigated whether improving bioenergetics through CK-Mt overexpression could be beneficial in heart failure.

4.1.2 CK and heart failure

While there is a preponderance of research indicating that CK dysfunction correlates with heart failure (as discussed in Section 1.6.2), it is less clear from CK system knockout studies (detailed in Section 1.7) whether impairments in the CK system can directly cause heart failure. For instance, GAMT KO mice showed no increases in heart failure severity and death rates after chronic myocardial infarction, despite having undetectable creatine and PCr levels [151]. Likewise, genetic and pharmacological ablation of CK similarly did not appear to alter cardiac phenotypes in heart failure [82,273]. In contrast, our group demonstrated that CK dKO mice could develop LV hypertrophy and heart failure, albeit this was heavily dependent on genetic background, sex, and age [151].

The findings regarding whether CK system augmentation can be therapeutic in heart failure are similarly mixed. As discussed in Section 1.7.1.5, our group showed that excessive myocardial creatine elevation could cause heart failure [135,164], and that moderate creatine elevation was neither protective nor detrimental during post-MI heart failure [2]. In contrast, it has been reported that CK-M overexpression significantly improved cardiac function and survival rates in pressure-overload heart failure [190]. There has been no published research on how heart failure progression is affected by overexpression of the last major myocardial CK component – CK-Mt. Therefore, the experiments in this chapter investigate the cardiac function of CK-Mt OE transgenic mice in the context of pressure-overload chronic heart failure.

4.1.3 Principle of transverse aortic constriction (TAC)

To investigate the effects of elevated CK-Mt on heart failure, CK-Mt OE and WT mice were subject to transverse aortic constriction (TAC), which is a well-established model for LV hypertrophy and pressure-overload heart failure [274,275]. The TAC procedure involves tying a suture around the transverse aorta to create a stenosis that increases afterload. This pressure overload initially induces compensated cardiac hypertrophy, which over time progresses to LV dilation and heart failure. In mouse, changes in cardiac morphology and function post-TAC follow a predictable timeline. Concentric hypertrophy begins within three days to generate additional pressure required to overcome the stenosis. In the initial two weeks, normal systolic function is maintained – thus the first post-operational echocardiograph was scheduled at week 3, when function initially declines [190]. Between 6-10 weeks after TAC surgery, LV mass may double, and the heart gradually progresses from compensated hypertrophy to

decompensated chronic heart failure with dilated cardiomyopathy [18,274]. Thus, a second post-operational echocardiograph was scheduled at week 6, when hearts are expected to progress to chronic heart failure [18].

The TAC protocol was selected in the current study for several reasons. First, it is a widely accepted model of pressure-overload heart failure with high reproducibility rates [274]. Second, the TAC procedure is a reliable method with low mortality (~5-10%) from surgery and high success rate (> 70%) [275,276]. Thus, TAC required far fewer mice than other methods such as coronary artery ligation (CAL), in which 25%-60% of male mice would be expected to die within 7 days due to cardiac rupture, before the LV remodelling process begins [276]. Third, the TAC experiment had previously been utilized by our group to demonstrate CK system impairment in heart failure [18], in the CK-M OE heart failure study by Gupta *et al.* [190], and in other studies [275,277].

4.2 Hypothesis and aims

The experimental hypothesis is that myocardial CK-Mt overexpression would significantly improve cardiac functional and structural parameters during chronic heart failure, such as ejection fraction, myocardial cross sectional area (CSA), and maximal systolic pressure.

The objectives of the experiments in this Chapter were to investigate the effects of increased CK-Mt activity in myocardium during chronic heart failure in an *in vivo* transgenic mouse model. Specifically, the goals were to 1) induce chronic heart failure in mice by TAC, 2) investigate effects of CK-Mt overexpression on heart failure *in vivo*, and 3) characterize the effects of CK-Mt overexpression through biochemical assays.

4.3 Methods

4.3.1 Study design and CK-Mt OE mice

In the first cohort of mice (14 weeks of age), homozygote CK-Mt overexpression (Tg) and WT littermates were randomly assigned to one of the four experimental groups for surgery (n= 12, 12, 22, 22 for WT Sham, Tg Sham, WT TAC, and Tg TAC, respectively). These numbers were chosen based on a previous TAC study by our group, which suggested that these mouse numbers would be sufficient to produce meaningful results while minimizing mouse requirements [18]. These animals received *in vivo* echocardiography, *in vivo* LV haemodynamics, and biochemical assays to evaluate LV CK activity and creatine content (Figure 4-1).

In the second cohort of mice, Tg and WT animals received TAC or sham surgery and were subject to ^{31}P-MRS for analysis of *in vivo* PCr: ATP ratio (n= 6, 7, 12, 9 for WT sham, Tg sham, WT TAC, and Tg TAC, respectively). ^{31}P-MRS was unable to be conducted on the first cohort of animals, as the ^{31}P-MRS study made use of a novel MRS technique that was not ready until late phase of the initial experiment. The first cohort was used for experiments in all subsequent sections except Sections 4.3.5 and 4.4.4.1, which describes the experiments involving the second cohort. The author and other lab members were blinded to genotype for all procedures (*e.g.* TAC surgery, echocardiography, haemodynamics, biochemical assays) and for data analysis whenever possible.

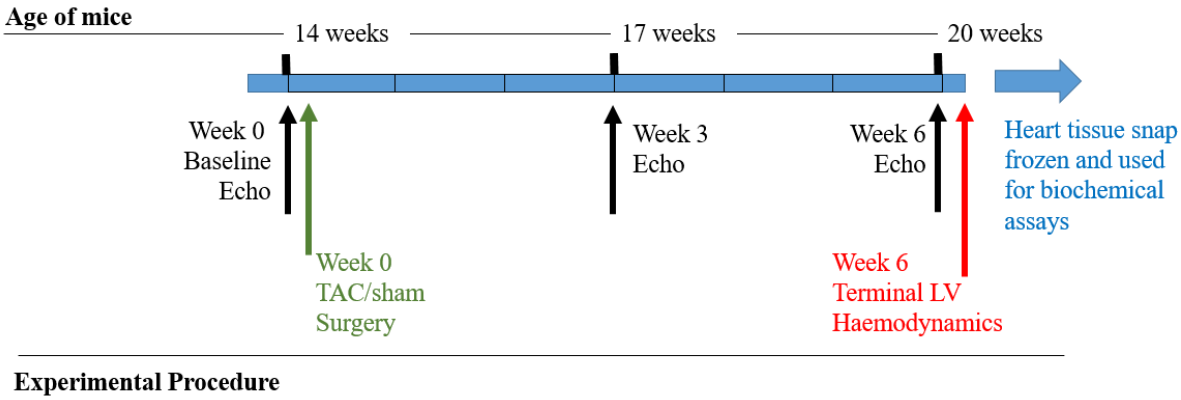


Figure 4-1: Schematic of experimental design and timeline of parameters analysed

CK-Mt OE mice and WT littermate controls were subject to protocol at 14 weeks of age with a baseline echocardiography session. Sham and TAC surgery were then conducted within the same week of the baseline echocardiography. At weeks 3 and 6, echocardiography was conducted to monitor the development of LV hypertrophy and chronic heart failure. At week 6, terminal LV haemodynamics measurements were performed within one week of the 6-week echocardiography session. Organs were then weighed, and hearts were snap-frozen in liquid nitrogen for biochemical assays.

4.3.2 TAC protocol

Surgery was performed by Ms Debra McAndrew with assistance from the author, using a protocol derived by Rockman *et al.* and optimized by our group [275,276]. Surgical instruments for the TAC protocol were autoclaved using a bench-top autoclave (Prestige Medical-Model: 2100 Classic, UK). Anesthesia was induced with 4% isoflurane, and maintained at 2% isoflurane with 0.5 L/mL 100% O_2 through the duration of the procedure. At the time of anesthesia induction, all mice received 0.8 mg/kg buprenorphine subcutaneously to reduce post-surgical pain. The mouse was then placed supine on a homeothermic surgical pad. The chest was shaved, and the surgical field was disinfected. Endotracheal intubation was performed, and mice were ventilated with a tidal volume of 250 µL at a respiratory rate of 150/min using a volume-cycled ventilator (Hugo-Sachs MiniVent type 845, Harvard

Apparatus). To expose the transverse aorta, a trans-sternal thoracotomy was performed, and the sternum retracted. The two lobes of thymus and connective tissues were dissected from the aortic arch. A constriction band was placed on the transverse aorta, between the right subclavian and the left carotid arteries. Aortic ligation was achieved by tying a double knot using 7-0 monofilament (Ethicon, W8725) suture around the aorta and an accompanying 27-gauge blunt needle, which served as a spacer to standardize the degree of constriction. The aorta was allowed to expand within the constricting band after the needle was removed from the suture loop. In the current experiment, the transverse aorta is constricted 55%, as measured by a reduction in cross sectional area. Sham group mice received all above procedures except for the aortic arch ligation. The sternum was then closed with a non-dissolvable interrupted suture. Post-operation, mice received subcutaneous injections of saline if there was significant blood loss (*e.g.* due to damage to the internal mammary artery). Mice were then given softened chow, monitored for post-operational complications, and kept in a heated chamber overnight.

4.3.3 *In vivo* characterization of heart failure in CK-Mt OE mice

4.3.3.1 Echocardiography

Three echocardiographs were conducted for each mouse at 0, 3, and 6 weeks of the TAC protocol as described in Figure 4-1. Mice were initially anesthetized with 4% isoflurane, and anesthesia was maintained with 1-2% isoflurane in O_2. Mice were secured on a 39^{o}C-heated platform, and eye gel (Viscotears, 2% Carbomer polyacrylic acid) was applied to prevent corneal dehydration. The thorax was shaved and covered with ultrasound gel (Skintact).

Echocardiography was performed with the Vevo2100 ultrasound imaging system using a 22 MHz - 55 MHz cardiovascular transducer (VisualSonics, MicroScans MS 550D). The procedure platform contained electrodes to provide real time electrocardiogram data. All echocardiography images and videos were obtained at heart rates >450 beats per minute after anesthesia-induced bradycardia had passed. Examples of echocardiography images of TAC and sham operated mice are shown in Figure 4-2 and Figure 4-3.

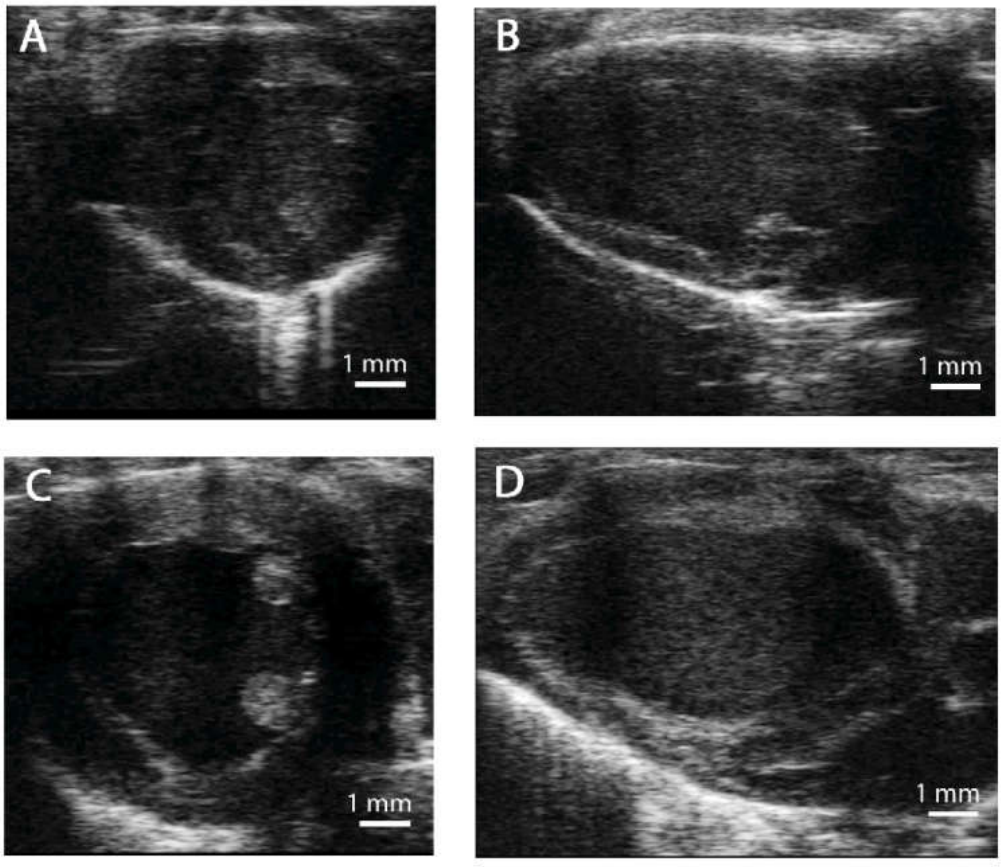


Figure 4-2: Parasternal end-diastolic mid-ventricular echocardiography images

(A) and (B) are representative parasternal, end-diastolic mid-ventricular short axis and long axis images of WT sham-operated LV at 6 weeks after surgery. (C) and (D) are the same views for a WT TAC-operated LV at 6 weeks after surgery. Note the significant LV hypertrophy and dilation seen in the TAC-operated heart.

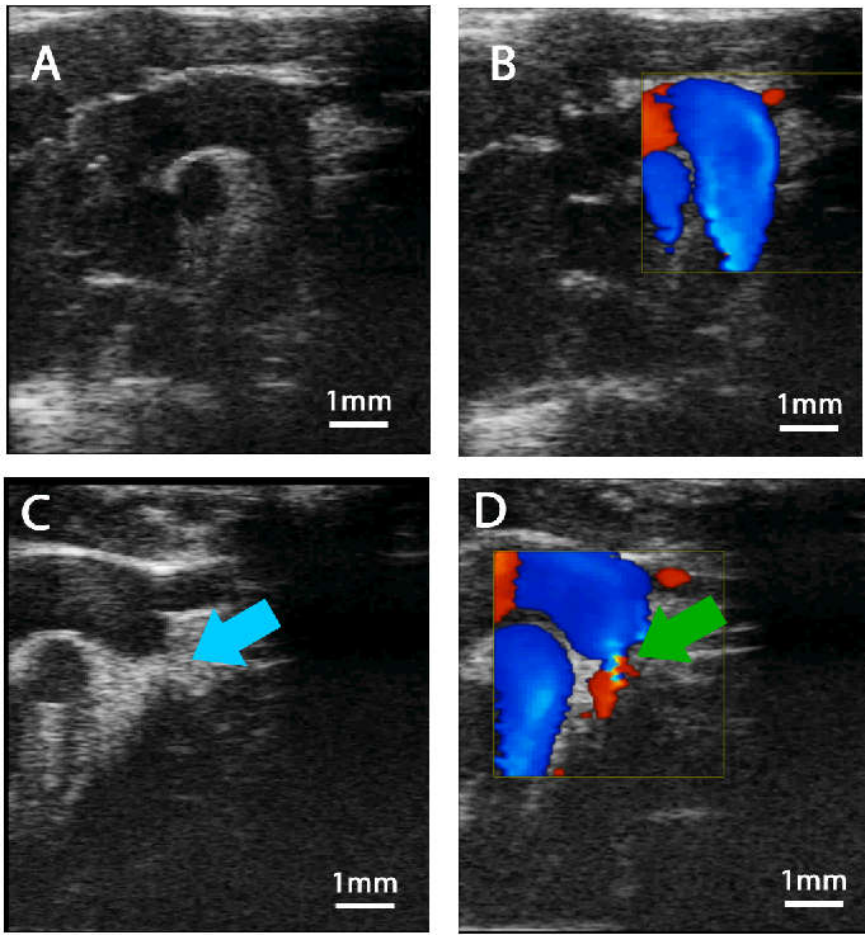


Figure 4-3: Coronal aortic arch echocardiography images

Representative aortic arch view (A) with blood flow by pulse-wave colour Doppler (B) of WT Sham mouse. Same views (C), (D), respectively of WT TAC mouse. Note the stenosis (blue arrow) visible in (C), and the decreased blood flow rate caused by stenosis (D) as indicated by green arrow.

4.3.3.2 Metrics measured

Four views of the heart and surrounding vessels were recorded: 1) short axis of the heart, 2) long axis of heart, 3) pulmonary artery view, and 4) aortic arch view. To our knowledge, the aortic arch view has not previously been presented in the literature, therefore the veracity of the flow and length measurements obtained from this view is unclear. Triplicate measurements were taken for each metric.

For the pulmonary (not shown) and aortic arch imaging (Figure 4-3) views, pulse-wave Doppler allowed measuring of blood flow rate, peak acceleration time, and ejection time through these vessels. The mid-papillary short axis view (Figure 4-2 A/C) provided measurements for LV cavity endocardial systolic area and endocardial diastolic area (ESA; EDA). Additionally, epicardial diastolic area was measured for calculation of the myocardial cross sectional area (CSA), which was defined as epicardial diastolic area – EDA.

The long-axis view (Figure 4-2 B/D) provided parameters to calculate the end systolic volume and end diastolic volume (ESV; EDV) using the area-length method. Specifically, the Tiecholz formula for the area-length method was used, with correction for the spherical volume (LV volume = $[7/(2.4 + LVID)] * LVID^3$), where the LVID represents the LV internal diameter during diastole and systole for calculation of EDV and ESV, respectively [278]. Stroke volume (SV) was calculated as EDV – ESV. Cardiac output (CO) was then calculated as SV × heart rate, with heart rates being obtained from the real-time electrocardiogram (ECG) measurements. Ejection fraction was calculated as ((EDV-ESV)/EDV) * 100%. Many additional parameters were automatically calculated by the software system.

Data analysis was performed using Vevo Lab, Edition 1.7.1 (Visualsonic, USA). The author was blind to genotype while analysing data. To validate measurements (for training purposes),

metrics from five practice samples were cross-referenced with results from an experienced analyst, with <10% differences in calculated results.

Only mice that survived for all 3 echocardiography sessions were used in the final analysis (n = 10, 12, 16, 20 for WT sham, Tg sham, WT TAC, Tg TAC, respectively), as this allowed for appropriate longitudinal analysis. The data from 0, 3, and 6 week measurements for each mouse were considered as repeated measures. Results for each group (WT Sham, WT TAC, Tg Sham, Tg TAC) were first analysed through repeated measures two-way ANOVA with Bonferroni's post-hoc test to evaluate change over time. Then, two-way ANOVA with Bonferroni's post-hoc test was used to compare the two sham groups, and the two TAC groups.

4.3.3.3 In vivo LV haemodynamics

Measurement of left ventricular haemodynamics was conducted by Ms Debra McAndrew. The author provided assistance in the haemodynamic studies and conducted data analysis.

At six weeks post-TAC, mice were prepared for haemodynamics with 4% isoflurane to induce anesthesia, which was maintained with 2% isoflurane in 100% medical oxygen delivered via a nose cone. Mice were weighed and placed on a thermal blanket at 37^{o}C in a supine position. An incision was made at the neck to expose the right carotid artery for catheterization. The artery was cleared of subcutaneous and connective tissue, and kept moist with 0.9% saline solution. Blood flow to the artery was then reduced by occluding the artery proximally with an untied suture, and ligating the artery distally with a tied suture. A 1.4F pressure-volume catheter (Millar Instruments, SPR-839) was then inserted into the artery between the two sutures, and moved retrograde through the aorta into the left ventricle. Echocardiography (Agilent Sonos

5500) was used to guide the catheter into the correct location. After positioning the catheter, the suture proximal to the catheter insertion site was tied, as well as an additional suture tied directly over the insertion site. A second catheter, made of flame-stretch polyethylene tubing (Portex 0.96mm OD, 800/100/200, Smiths Medical, UK), was inserted into the right internal jugular vein for dobutamine HCl infusion (Hameln Pharmaceuticals Ltd, Gloucester, UK) to assess response to β-adrenergic stress. A fifteen-minute baseline recording was obtained after the heart was given ten minutes to adjust to the ventricular catheter insertion. During this recording period, isoflurane concentration was reduced from 2% to 1.5% to reduce anaesthetic-induced cardiovascular depression. After completing the baseline measurement, dobutamine (16 ng/g body weight/minute) was administered intravenously using a timed syringe driver (Graseby MS16A, Smiths Medical Ltd, UK). If there was no response to dobutamine, mice were sacrificed by pentobarbitone infusion, administered through the IV line to confirm its patency. After equilibration, five minutes of additional recordings were obtained to characterize adrenergic stress response. Haemodynamics data was logged using Powerlab 4SP, and visualized using Chart 3.8.6 (AD Instruments). Further statistical analysis was conducted in Excel and Graphpad Prism v. 5 and v.7.

4.3.4 Measurement of lung/heart weights and tibia length

After completion of the haemodynamic measurements, the heart and lungs were removed and weighed, and the LV was snap frozen in liquid nitrogen and stored at -80^{o}C for subsequent biochemical assays. The tibia was excised and its length was measured using digital callipers (Mitutoyo UK, Ltd).

4.3.5 ^{31}P-MRS measurement of high energy phosphates

PCr/ATP ratios were obtained through *in vivo* ^{31}P-magnetic resonance spectroscopy (MRS) on n= 6, 6, 8, and 7 mice for WT Sham, Tg Sham, WT TAC, and Tg TAC groups, respectively. All ^{31}P-MRS data collection was conducted by Dr Mahon Maguire with support from Ms Lee-Anne Stork. All ^{31}P-MRS data were acquired utilizing a horizontal 9.4 T magnetic resonance system equipped with a Direct Drive2 console and 120 mm i.d., 0.6 T/m, shielded gradient set (Agilent Technologies, USA) operating at 400 MHz frequency for ^{1}H and 168 MHz for ^{31}P measurements. Images were acquired using a linear double-tuned, actively decoupled, ^{1}H/^{31}P 39 mm birdcage resonator (i.d. 39 mm) and a 14 mm actively decoupled quadrature surface coil array for ^{31}P signal reception (Rapid Biomedical, Germany). Anatomical images were acquired using the ^{1}H channel of the birdcage resonator for both transmit and receive.

The imaging protocol used was adapted from methodology previously published by our group [279]. Induction of anaesthesia was achieved using 4% isoflurane in 100% oxygen, and maintained at 1.5-2.0% isoflurane in 2 L/min oxygen flow throughout the imaging session. Mice were placed prone in a dedicated animal cradle with the heart directly over the surface coil array. Mouse ECG was recorded using two subcutaneous needle electrodes placed in the forelimbs of the animal, and respiration recorded using a pneumatic pressure balloon connected to a piezoelectric pressure transducer. Cardiac and respiratory signals were monitored throughout the experiment using an in-house developed ECG and respiratory gating device.

^{1}H-MRI was used to acquire scout images necessary to localize the short axis of the heart [279]. Two dimensional, density weighted, ^{31}P chemical shift imaging (2D-CSI) was used in short axis orientation to acquire spectroscopic measurements *in vivo* (FOV 30 x 30 mm^2, 16 x 16 PE

steps, 5 mm slice thickness, 3-fold under-sampled, 2600 FIDs, 60° flip angle, cardiac triggered, TR ≈ 250 ms [*i.e.* two cardiac cycles], total acquisition time ~25 min); the resulting spatial resolution was approximately 1.9 x 1.9 x 5.0 mm (voxel volume of 17.6 μL). Prior to Fourier transform, the data were zero-filled to 64 x 64 PE steps in order to improve the apparent spatial resolution of the images, and a line broadening of 60 Hz was applied in order to improve the SNR of the resulting spectra. Following CSI data acquisition, corresponding short axis high-resolution 2D multi-slice ^{1}H scout images covering the entire FOV of the CSI experiment were acquired to determine the anatomy within each voxel of the CSI data set.

The data were reconstructed using IDL 8.2 (Harris Geospatial Solutions, USA) and spectra corresponding to voxels placed in the myocardium and blood were fitted in the time domain using in-house software [279]. Correction for myocardial signal contamination from blood, and T_1 saturation effects, was carried out in Excel 2014 (Microsoft Corporation, USA); T_1 values for PCr and ATP in the mouse myocardium at 9.4 T were taken from the literature [280]. Initial data analysis was conducted by Dr Mahon Maguire, with further processing conducted by the author in Graphpad Prism.

4.3.6 Analysis of creatine by HPLC

Intracellular creatine content in LV tissue was measured by high-performance liquid chromatography (HPLC), using a Jasco PU-2089 Plus pump, a Jasco UV-2075 Plus UV detector (205 nm detection), and a Supelcosil LC-18-T reverse phase column (5 μM pore size, 25 cm x 4.5 mm), with a method derived from Teerlink *et al.* [281]. Crushed powdered LV tissue (~5 mg) was reconstituted in 350-375 μl of 0.4 M ice-cold perchloric acid in a Dounce

homogenizer. The sample was then homogenized at 1100 rpm for 30 seconds using a mechanical homogenization device. An aliquot of the homogenized sample was then taken for protein quantification through Lowry assay (as detailed in Section 2.3.5). The remainder of the sample was neutralized with 1 M potassium hydroxide, and centrifuged at 4°C for 5 minutes at 5,500 rpm. The supernatant was then filtered through an ice-cold 3 mL syringe with a 0.45 μM PVDF filter, and the filtrate (~100 μL) was loaded into the HPLC column. A set of standards with known creatine concentrations were run at the beginning and end of the experiment. The resulting peak areas of the standards were used to create a standard curve, which allowed calculation of the relative creatine content of samples. Relative creatine contents were then normalized to protein concentrations obtained from the Lowry assay. The purpose of the experiment was to determine the total creatine content, therefore the creatine and PCr content values were combined.

4.3.7 CK and citrate synthase (CS) activity

The detailed methods for the following assays are found in Section 2.3. Briefly, homogenized LV was subjected to the following biochemical assays: SAS gel electrophoresis, creatine kinase activity assay, Lowry assay, and citrate synthase assay. The numbers of heart samples included in these experiments were 10, 13, 12, and 19 for WT Sham, Tg Sham, WT TAC, and Tg TAC groups, respectively. SAS-1 gel electrophoresis was conducted to separate CK isoenzymes (CK-Mt, CK-MM, CK-MB, CK-BB) and determine relative isoform concentrations. The protein concentrations in the LV homogenates were measured by Lowry assay, and were used to normalize values obtained for CK activity and citrate synthase activity.

4.4 Results

4.4.1 Protocol n numbers and survival rates

Of the mice utilized in first cohort, five WT TAC, one Tg TAC, and one Tg Sham mice died after the surgical procedure because of excessive blood loss. Three WT TAC mice and two Tg TAC mice were lost due to reasons detailed in Table 4-1. In addition, the stress of the haemodynamic study resulted in the death of two WT TAC mice and four Tg TAC mice. The causes of death are summarized in Table 4-1. Therefore, a total of 13 WT TAC mice and 15 Tg TAC mice that received dobutamine administration produced valid haemodynamics data. The number of animals used in the evaluation of echocardiography and haemodynamics at pre-determined time points is summarized in Table 4-2. One WT TAC mouse was excluded from the analysis because there was clear signs of aortic internalization of the band, which mitigated the severity of stenosis [282]. The survival curve of the mice on protocol is presented in Figure 4-4.

Table 4-1: Causes of death of mice on protocol

Groups	Causes of death
WT Sham	Culled sick; nonprocedural
WT Sham	Culled in error
WT TAC	Culled due to >15% loss in body weight
WT TAC	Found dead (not heart failure)
WT TAC (n = 3)	Died during surgical recovery
WT TAC (n = 2)	Died during haemodynamics
Tg TAC	Culled because ears were burned due to faulty temperature probe during haemodynamics measurement
Tg TAC	Died due to heart failure
Tg TAC (n = 4)	Died during haemodynamics

Table 4-2: Number of mice used in each experimental group

Groups	Evaluated Parameters					
	Echocardiography			Haemodynamic data		Biochemical Assays
	week 0	week 3	week 6	Baseline	Dobutamine treatment	
WT Sham	12	10	10	10	10	9
Tg Sham	12	12	12	12	12	10
WT TAC	21	18	16	15	13	16
Tg TAC	22	21	20	19	15	19

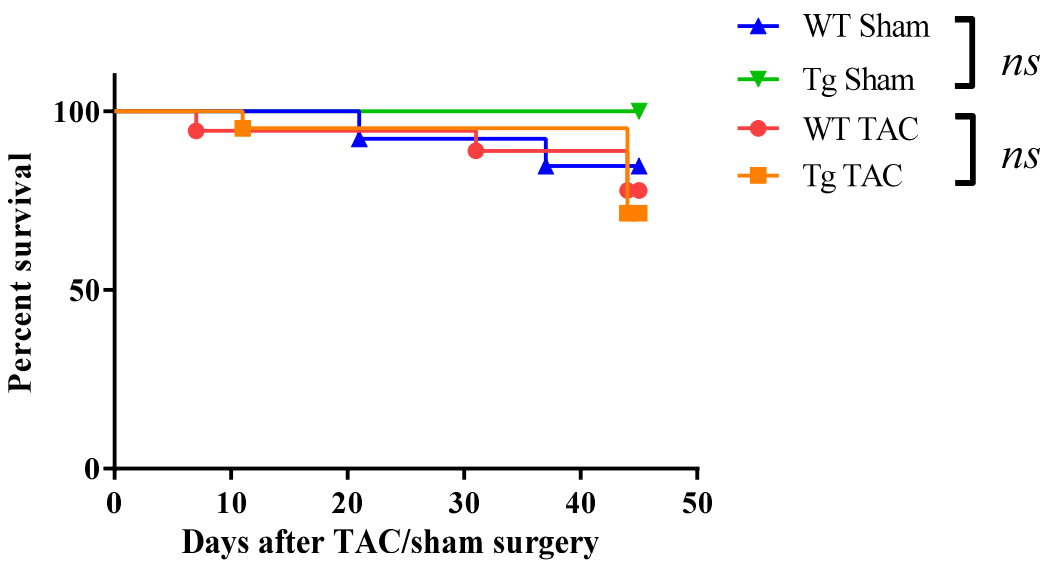


Figure 4-4: Survival curve of TAC and sham mice during chronic heart failure experiment

Log-rank (Mantel-Cox) test revealed no significant differences between the four groups over the course of the 6-week protocol. The decreased survival rate at day 42 in the TAC group was due to deaths that occurred during haemodynamics measurements. Note that only one TAC mouse (Tg) was confirmed to have died of heart failure during the experimental protocol, as based on increased lung weight (an indicator of pulmonary congestion). Note that the survival curve does not include mice that died during surgical recovery. ns: no significant difference between WT and Tg sham mice, and between WT and Tg TAC mice.

Of the mice in the second cohort, three WT TAC, two Tg TAC, and one Tg sham mice were culled due to poor recovery after surgery. One WT TAC mouse was found dead one week after surgery, possibly due to aortic aneurysm as there was a small tear in the aorta directly prior to the band. Therefore, n = 6, 6, 7, 7 mice were ultimately subject to ^{31}P-MRS of which data was successfully obtained for n = 6, 4, 5, 7 for WT sham, Tg sham, WT TAC, and Tg TAC groups, respectively.

4.4.2 Effects of CK-Mt overexpression on cardiac function as assessed by echocardiography

As shown in Figure 4-5, there were no significant differences between WT and Tg sham mice in morphometric (myocardial CSA, EDA, ESA) and functional (EF, CO, and SV) parameters. Similarly, over the 6-week protocol (*i.e.* comparing week 0, 3, and 6 data), sham surgery did not cause any significant differences in structural and functional parameters in either WT or Tg sham groups.

The results between WT TAC and Tg TAC mice are shown in Figure 4-6**.** The only statistically significant difference between WT TAC and Tg TAC mice was myocardial CSA, which was lower in the Tg TAC mice as compared to WT TAC mice at 3 and 6 weeks, by approximately 15% ($p < 0.01$). Tg TAC mice exhibited no other morphometric or functional changes as compared to WT TAC mice at any time points. In both the WT and Tg TAC groups, there were clear signs of progression towards heart failure, including LV hypertrophy and a decline in cardiac function (*e.g.* ejection fraction) over 6 weeks after TAC. For both groups, myocardial CSA increased significantly between 0 to 6 weeks, which suggests LV hypertrophy. There was also a significant increase in EDA and ESA from 0 to 6 weeks, which is indicative of LV dilation due to pressure-overload. However, stroke volume and cardiac output did not significantly decline.

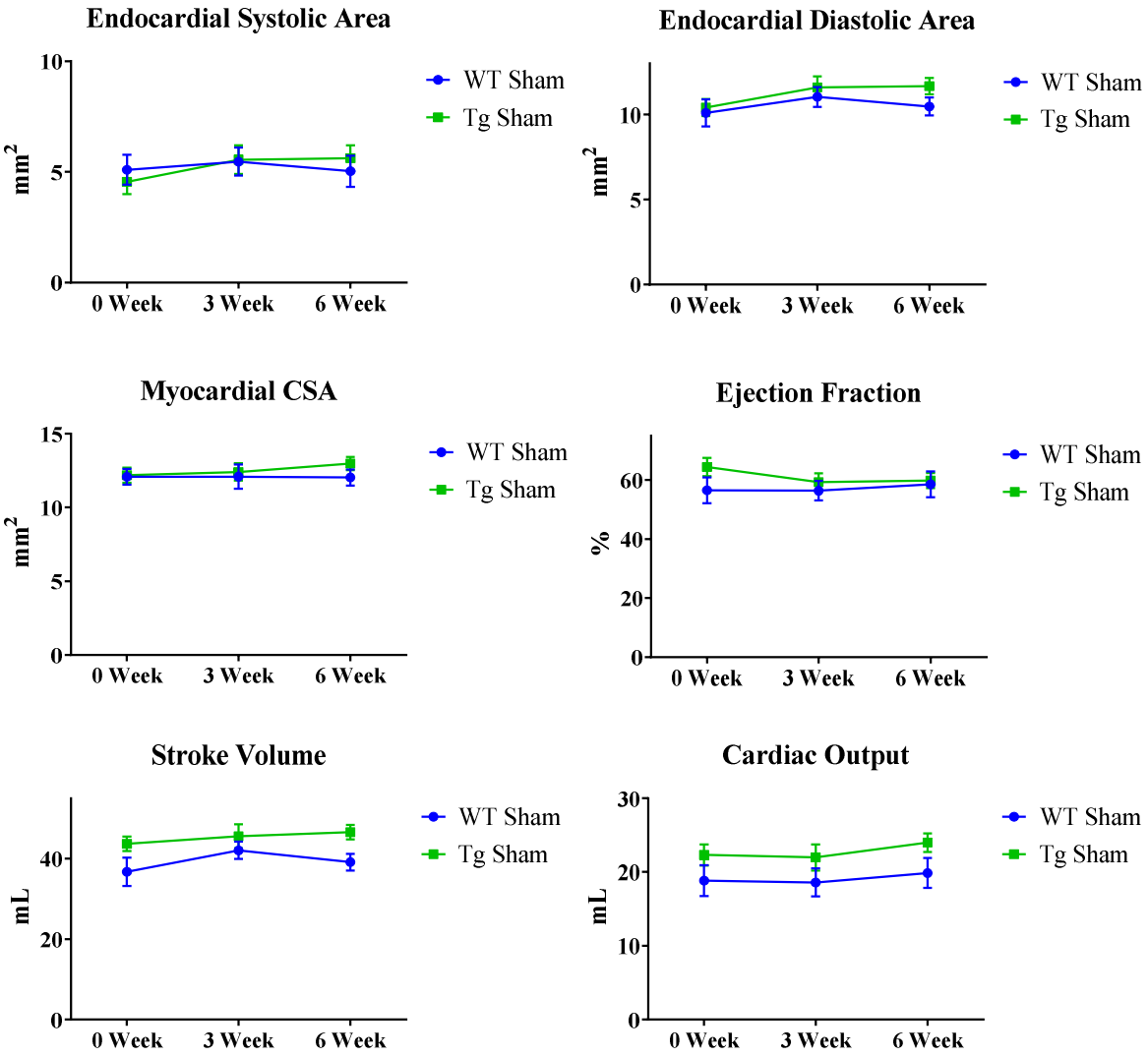


Figure 4-5: Effects of sham operation on echocardiography parameters in CK-Mt OE and WT mice

Cardiac parameters from echocardiography on WT and Tg mice at 0-, 3-, and 6-week time-points. Values were taken prior to sham surgery (0 week), at 3 and 6 weeks after surgery. n numbers varied over time; see Table 4-2. Two-way repeated-measure ANOVA with Bonferroni's post-hoc test was used for analysis, with details in Section 4.3.3.2.

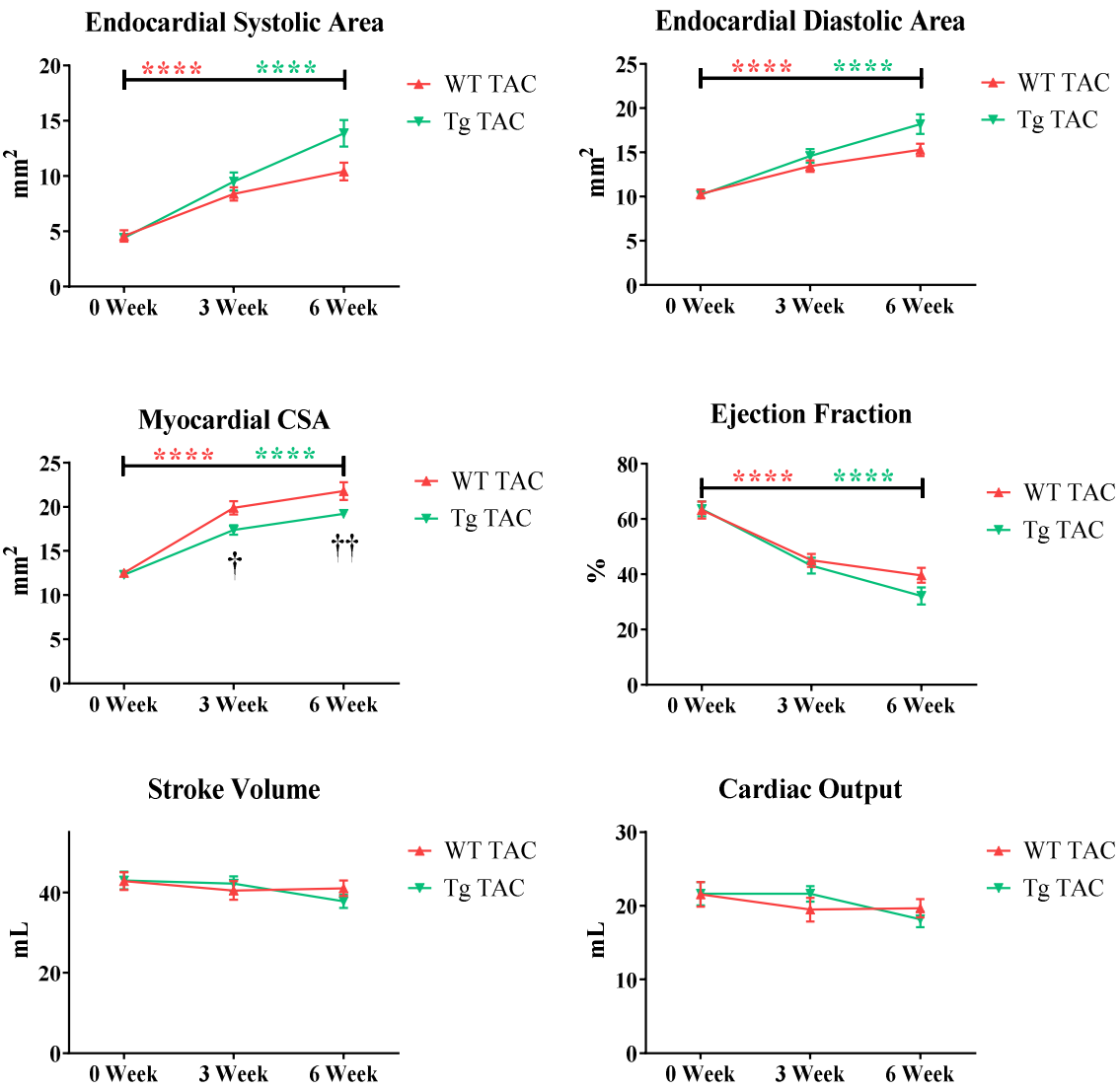


Figure 4-6: Effects of TAC on echocardiography parameters in CK-Mt OE and WT mice during heart failure

Cardiac parameters from echocardiography on WT and Tg TAC mice at 0-, 3-, and 6-week time-points. Values were taken prior to TAC surgery (0 week), at 3 and 6 weeks after surgery. n numbers varied over time; see Table 4-2. Two-way repeated-measure ANOVA with Bonferroni's post-hoc test was used for analysis, with details in Section 4.3.3.2. (*** = $p < 0.001$; **** = $p < 0.0001$ between 0 and 6 weeks. † = $p < 0.05$; †† = $p < 0.01$ between WT TAC and Tg TAC at that time point)

Table 4-3 and Table 4-4 below presents additional echocardiography parameters that were taken through the course of the experiment. The parameters describe the velocity and pressure characteristics of blood flow through the pulmonary artery and the aortic arch, which supplement results from LV measurements. For instance, aortic arch VTI has been found to be closely correlated to cardiac output [283]. There were no statistically significant differences between the two sham groups and the two TAC groups at the 0, 3, and 6 week time points for the metrics detailed below, suggesting that CK overexpression did not impact blood flow through the pulmonary artery and aortic arch (data taken at 0 and 3 weeks is not shown).

Table 4-3: Pulmonary artery and aortic arch echocardiography measurements at 6 weeks on sham protocol mice

Pulmonary Artery Flow						
		WT Sham			**Tg Sham**	
Parameters	**Units**	**Mean**	**SEM**		**Mean**	**SEM**
Velocity time integral (VTI)	mm	25.4	1.7		25.6	1.1
Mean Velocity	mm/s	399.8	26.4		400.0	16.8
Mean Gradient	mmHg	0.67	0.1		0.66	0.1
Peak Velocity	mm/s	687.1	45.1		674.5	30.0
Peak Gradient	mmHg	1.99	0.2		1.87	0.2
Acceleration Time	ms	15.6	0.9		16.0	1.0
Ejection Time	ms	56.9	3.0		56.6	2.0
Aortic Arch Flow						
Parameters	**Units**	**Mean**	**SEM**		**Mean**	**SEM**
VTI	mm	23.6	1.8		27.9	1.6
Mean Velocity	mm/s	360.1	29.0		392.7	19.1
Mean Gradient	mmHg	0.55	0.1		0.63	0.1
Peak Velocity	mm/s	610.6	50.9		662.3	34.9
Peak Gradient	mmHg	1.58	0.3		1.81	0.2
Acceleration Time	ms	16.2	1.2		17.3	0.9
Ejection Time	ms	57.9	2.4		60.7	2.7
Aortic Arch Lengths †						
Parameters	**Units**	**Mean**	**SEM**		**Mean**	**SEM**
Descending aortic arch length	mm	1.11	0.04		1.23	0.04
Transverse aortic arch length	mm	1.45	0.03		1.44	0.05

Footnote: Averages for each group is shown. n = 10 and 12 for WT sham and Tg sham, respectively. All results were analysed using two-way ANOVA with Bonferroni's post-hoc test.
†Arch length measurements are defined and assessed on the following page

Table 4-4: Pulmonary artery and aortic arch echocardiography measurements at 6 weeks on TAC protocol mice

Pulmonary Artery Flow						
		WT TAC			Tg TAC	
Parameters	**Units**	**Mean**	**SEM**		**Mean**	**SEM**
Velocity time integral (VTI)	mm	20.2	1.1		21.3	1.5
Mean Velocity	mm/s	270.7	21.2		269.8	16.2
Mean Gradient	mmHg	0.32	0.1		0.32	0.0
Peak Velocity	mm/s	445.8	37.5		445.8	29.0
Peak Gradient	mmHg	0.89	0.2		0.88	0.1
Acceleration Time	ms	21.7	1.9		22.9	1.4
Ejection Time	ms	73.6	4.4		77.3	2.8
Aortic Arch Flow						
Parameters	**Units**	**Mean**	**SEM**		**Mean**	**SEM**
VTI	mm	25.1	2.1		19.6	1.0
Mean Velocity	mm/s	397.1	26.4		327.0	16.7
Mean Gradient	mmHg	0.68	0.1		0.45	0.0
Peak Velocity	mm/s	678.5	46.6		556.8	29.3
Peak Gradient	mmHg	2.00	0.2		1.31	0.1
Acceleration Time	ms	17.5	0.9		17.3	0.6
Ejection Time	ms	59.5	3.1		56.0	1.5
Aortic Arch Lengths †						
Parameters	**Units**	**Mean**	**SEM**		**Mean**	**SEM**
Descending aortic arch length	mm	0.79	0.03		0.76	0.02
Transverse aortic arch length	mm	1.69	0.02		1.70	0.02

Footnote: Averages for each group is shown. n = 16 and 20 for WT TAC and Tg TAC, respectively. All results were analysed using two-way ANOVA with Bonferroni's post-hoc test.
†Arch length measurements are defined and assessed on the following page

4.4.2.1 Correlation between banding severity and cardiac function

The severity of cardiac dysfunction resulting from TAC can range from compensated LV hypertrophy to full-blown congestive heart failure. While the stenosis is standardized by tying the suture around a 27-guage needle, there is a possibility of the aorta growing through the suture or the knot loosening, which are common occurrences [282,284]. Thus, there is rationale for developing a method to quantify the severity of the stenosis. After the TAC stenosis has been generated, there is generally significant aortic dilation prior to the stenosis, at the transverse aorta. Simultaneously, there is some degree of shrinkage of the aorta distal to the stenosis due to decreased blood flow. Therefore, the diameters of the transverse and descending aorta were measured in the aortic arch view prior to surgery and at 3 and 6 weeks post-surgery as shown in Figure 4-7. This aortic arch ratio (the transverse aorta diameter:descending aorta diameter) in sham-operated WT mice was 1:1, whereas this ratio increased to ~2:1 in the TAC groups, representative of the pre-stenotic dilation. Analysis was conducted to investigate whether there was correlation between this aortic diameter ratio metric and the severity of cardiac dysfunction in the TAC mice. However, no correlation was found between the ratio and functional/structural parameters such as CO, EF, EDA, and ESA, at the 3 and 6 week time-points (data not shown). The lack of significance is likely because the arch measurements are very concentrated in a small range. Therefore, while the ratio is a reasonable indicator of a successful TAC-induced stenosis, it was not adequately precise to predict the severity of cardiac functions induced by the stenosis.

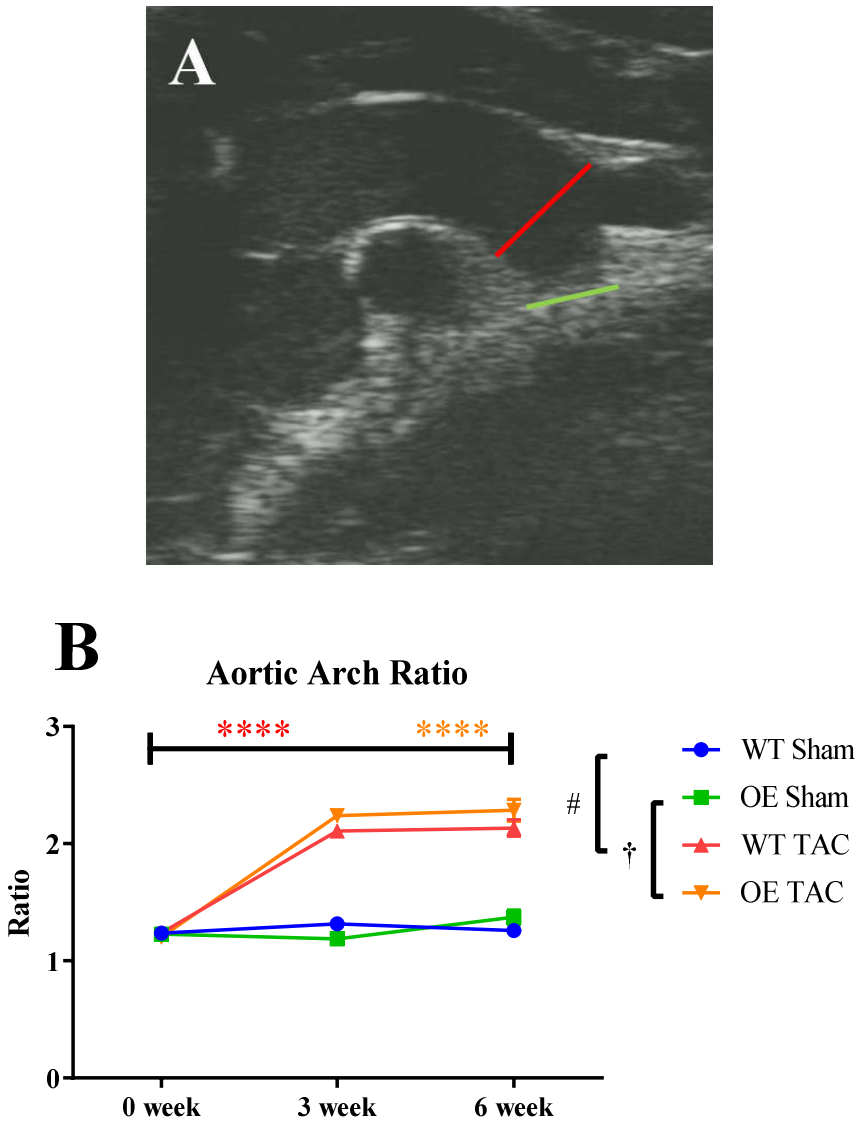


Figure 4-7: Aortic arch view and aortic arch ratio

(A) Aortic arch view. Red line represents diameter of transverse aorta measured, proximal to the TAC-induced stenosis. Green line represents the diameter of the descending aorta measured distal to the TAC-induced stenosis. (B) Aortic arch ratio = Transverse aortic diameter / Descending aortic diameter. n numbers variable; see Table 4-2. ****$p < 0.001$ between TAC groups at 0 weeks and TAC groups at 6 weeks. # = $p < 0.0001$ between WT TAC and WT sham groups; † = $p < 0.0001$ between Tg TAC and Tg sham groups.

4.4.3 Effects of CK-Mt overexpression on cardiac function as measured by *in vivo* haemodynamics

The haemodynamics results (Figure 4-8) demonstrate that there were no significant differences in cardiac function between WT sham and Tg sham groups. This was true both at baseline and after dobutamine stimulation, for which both groups showed a strong contractile response. While Tg TAC mice had lower end systolic pressure (ESP) than WT TAC mice ($p = 0.05$), there were no significant differences in heart rate, end diastolic pressure (EDP), and contractility measures such as dP/dt_{max}, dP/dt_{min}, and tau at baseline and after dobutamine (Figure 4-8), hence overall cardiac function did not appear to be affected by CK-Mt overexpression. The TAC groups demonstrated appropriate response to TAC-induced pressure overload stress. For instance, there was elevated LV systolic pressure in both TAC groups compared to their respective sham groups ($p < 0.0001$ for WT; $p < 0.01$ for Tg), which indicates that hearts were generating additional pressure to overcome the aortic stenosis (Figure 4-8A). Elevated end diastolic pressure (Figure 4-8B), a key hallmark of heart failure, was also observed in the TAC groups compared to their respective sham groups ($p = 0.05$ for WT; $p < 0.001$ for Tg). The relaxation parameters, tau and minimum dP/dt, both suggested that TAC groups had impaired contractile function as compared to their respective sham groups, though neither measure was significantly different. Finally, the TAC groups demonstrated significantly impaired contractile reserve, which is also indicative of heart failure. Contractile reserve represents the increased contractility in response to stress, which in this case was β-dobutamine stimulation. The key measure of contractile reserve, max dP/dt following dobutamine challenge, was significantly decreased in the TAC groups as compared to their respective sham groups ($p < 0.001$ for WT; $p < 0.0001$ for Tg). Indeed, the maximum dP/dt values in the TAC

groups before/after dobutamine were not significantly different, indicating the TAC hearts essentially had no measurable contractile reserve.

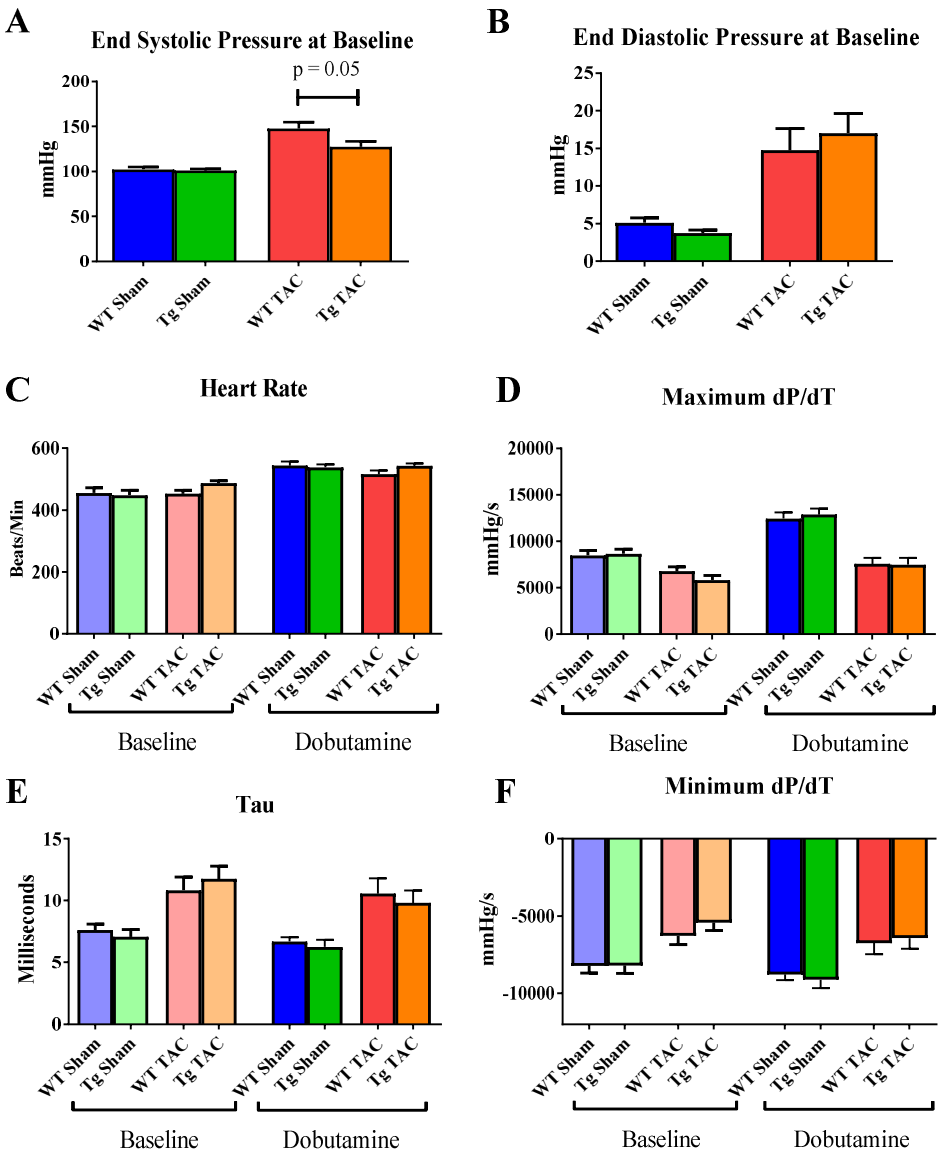


Figure 4-8: LV haemodynamics in CK-Mt OE and WT mice

Haemodynamics were measured at baseline and after administration of 16 ng/g/min dobutamine. CK-Mt OE had no significant effects on HR, EDP, max/min dP/dt and tau. There were also no significant differences between the two TAC groups and the two sham groups. Results were analysed with one-way ANOVA with Bonferroni's post-hoc test at baseline, and after dobutamine infusion. n numbers variable; see Table 4-2.

4.4.3.1 Organ weights and tibia length

Morphometric data were obtained after the haemodynamic studies. The LV, RV, and lungs weights were not significantly different between WT and Tg mice, before or after normalization to body weights (Figure 4-9). Body weight and tibia length were not significantly different amongst the four groups. TAC groups demonstrated significant cardiac hypertrophy as indicated by increased LV and RV weights, as well as pulmonary edema as reflected by increased lung weights (Figure 4-9).

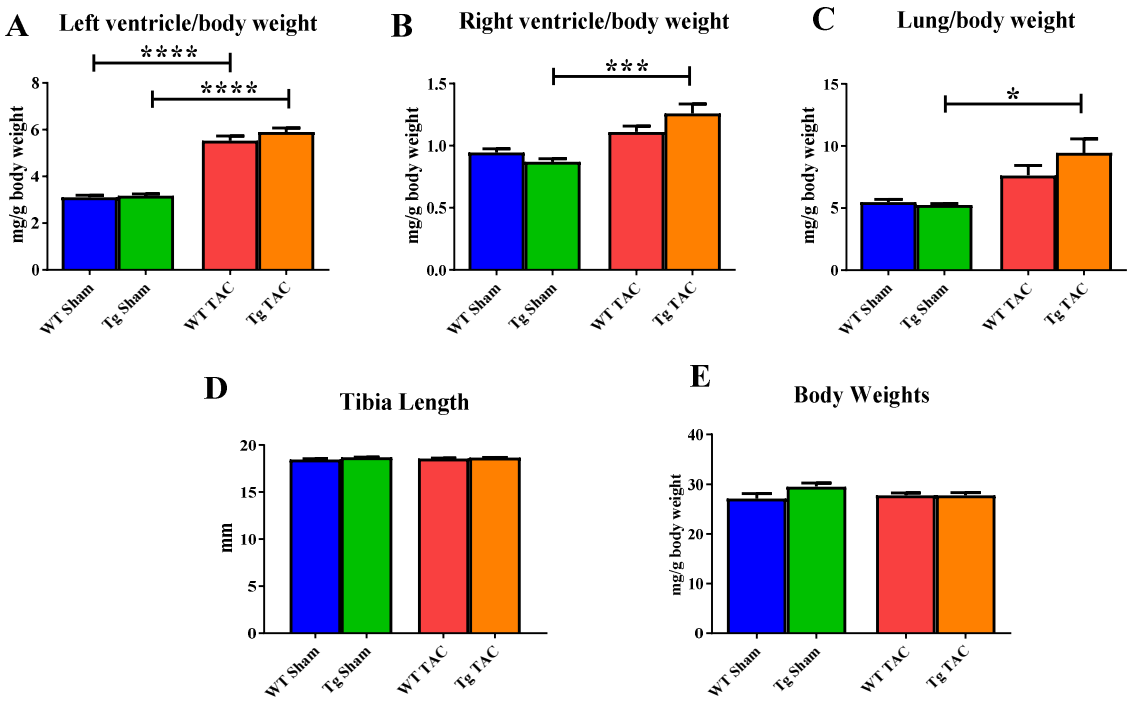


Figure 4-9: Morphometric data in CK-Mt OE and WT mice at the end of protocol

(A),(B),(C) LV/RV/lung weights normalized to body weight. (D) Tibia length. (E) Body weights at the end of protocol used to normalize LV/RV/lung weights. (n = 10, 12, 17, 20 for WT Sham, Tg Sham, WT TAC, and Tg TAC groups, respectively). Results were analysed with one-way ANOVA with Bonferroni's post-hoc test, with comparison amongst all groups.

4.4.4 Characterization of cardiac bioenergetics during heart failure in CK-Mt OE mice

4.4.4.1 PCr/ATP ratio as assessed through ^{31}P-MRS

In vivo PCr/ATP ratios were obtained through ^{31}P-MRS analysis. Sample spectra from the septum of the myocardium of mice are presented in Figure 4-10 with relevant peaks labelled.

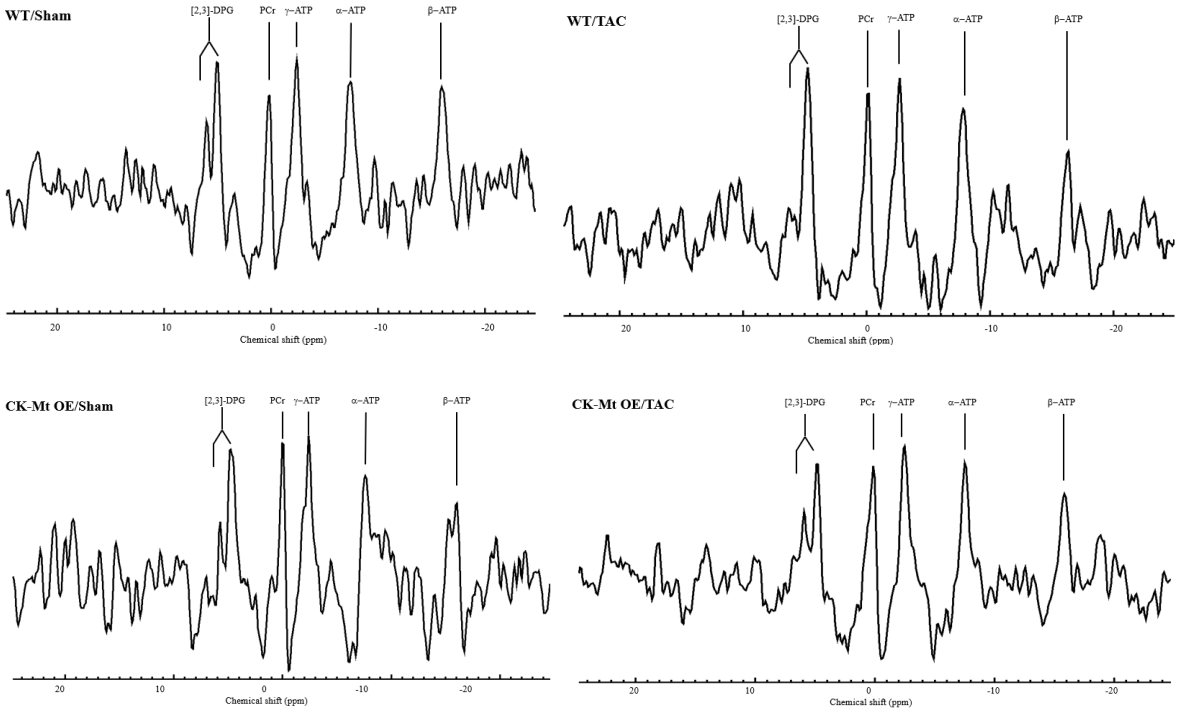


Figure 4-10: Sample ^{31}P-MRS spectra of WT and CK-Mt OE Sham/TAC Mice

Relevant peaks, such as PCr and γ-ATP are labelled. Correction for the ATP peaks due to blood contamination (as indicated by the [2,3]-DPG peak) was conducted using separate voxels/spectrums only containing blood.

The PCr/ATP ratios are shown in Figure 4-11. CK-Mt overexpression had no effect on PCr/ATP ratio in sham hearts, but allowed hearts to maintain a physiological PCr/ATP ratio during TAC-induced heart failure. PCr/ATP ratio decreased significantly in WT TAC mice as compared to WT sham, which is indicative of successful heart failure induction in the WT TAC group.

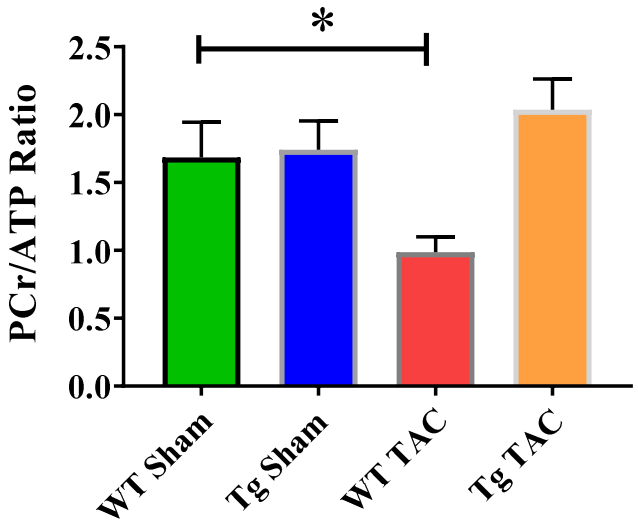


Figure 4-11: PCr/ATP ratio assessed by phosphate MRS in CK-Mt OE and WT mice

PCr/ATP ratios were obtained from 2-D chemical shift imaging (CSI) ^{31}P-MRS. Results were analysed by one-way ANOVA with Bonferroni's post-hoc test, comparing between all groups (*: $p < 0.05$). n = 6, 4, 5, 7 for WT sham, Tg sham, WT TAC, and Tg TAC, respectively.

4.4.5 LV creatine content

The results shown in Figure 4-12 demonstrate that there were no significant differences in total LV creatine content between WT and Tg sham groups, and between the two TAC groups. This suggested that Tg and/or TAC had no effects on LV creatine content.

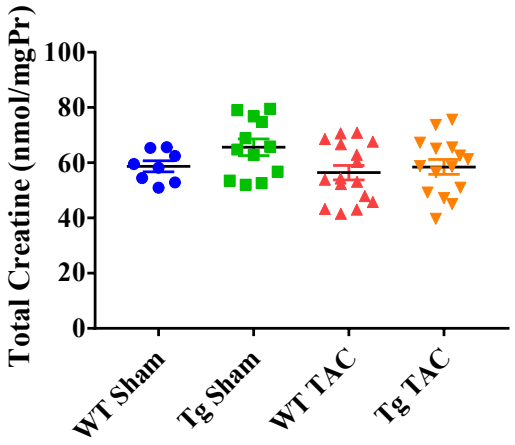


Figure 4-12: LV creatine content of CK-Mt OE and WT mice

LV creatine content as measured by HPLC. Results were analysed by one-way ANOVA with Bonferroni's post-hoc test. n = 8, 12, 16, 15 for WT sham, Tg sham, WT TAC, and Tg TAC, respectively.

4.4.6 Separation of CK isoenzyme and CK activity

4.4.6.1 Separation of CK isoenzymes by CK gel electrophoresis

As shown in Figure 4-13, CK-Mt (blue arrow), CK-MM (green arrow), CK-MB (red arrow), and CK-BB (orange arrow) were separated based on their molecular weights by gel electrophoresis. The cytosolic isoforms are identified based on their molecular weights as indicated by the protein marker (Lane 1) (Helena Biosciences). There is no available protein marker for CK-Mt isoform, but the fraction has been previously validated as the mitochondrial isoenzyme by our group [176]. The gel was photographed using a ChemiDoc MP imager, and relative isoenzyme concentrations were then calculated based on the density of each band, as determined by Image Lab software.

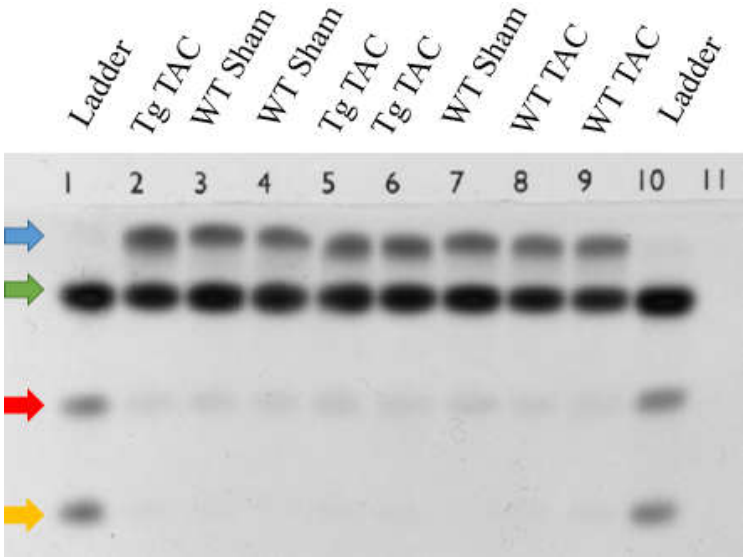


Figure 4-13: Separation of CK isoenzymes isolated from LV by SAS-1 gel electrophoresis

Lanes 1 and 10: protein marker for CK isoenzymes. Lanes 2 to 9: LV samples from different study groups as indicated. The separated CK isoenzymes were indicated by different colour arrows. Blue arrow: CK-Mt. Green arrow: CK-MM. Red arrow: CK-MB. Orange arrow: CK-BB. Ladder was specifically comprised of the three cytosolic CK isoforms (CK-MM, CK-MB, CK-BB). Our group previously verified the top band in samples is CK-Mt [212].

As described in Section 2.3.2, the gel-separated CK isoenzymes reacted with chromogen in the SAS-1 kit to produce visible, distinct band of each isoenzyme as shown in Figure 4-13. The bands represent the composition of CK isoenzyme in each sample [285]. The density of each band was measured and its relative density (to total density of each sample) represented the relative composition of each isoenzyme as shown in Figure 4-14, and as described below. The band density/relative composition was subsequently used to calculate the CK isoenzyme activity presented in Figure 4-16. The detailed method of using the band density to calculate CK isoenzyme activity is presented in Figure 4-15

The relative band density/isoenzyme compositions for each of the four CK isoenzymes were quantified as presented in Figure 4-14. The relative composition of CK-Mt trended higher in both the Tg sham and Tg TAC groups, as compared to their respective WT counterparts, though this was not significant. The relative composition of CK-MM trended lower in the Tg sham compared to the WT sham group and was significantly lower in the Tg TAC group as compared to the WT TAC group ($p < 0.05$). The increased relative CK-Mt proportion and decreased relative CK-MM proportion are indicative of the effects of CK-Mt overexpression. There were no significant differences between the four experimental groups in terms of the relative composition of CK-MB and CK-BB.

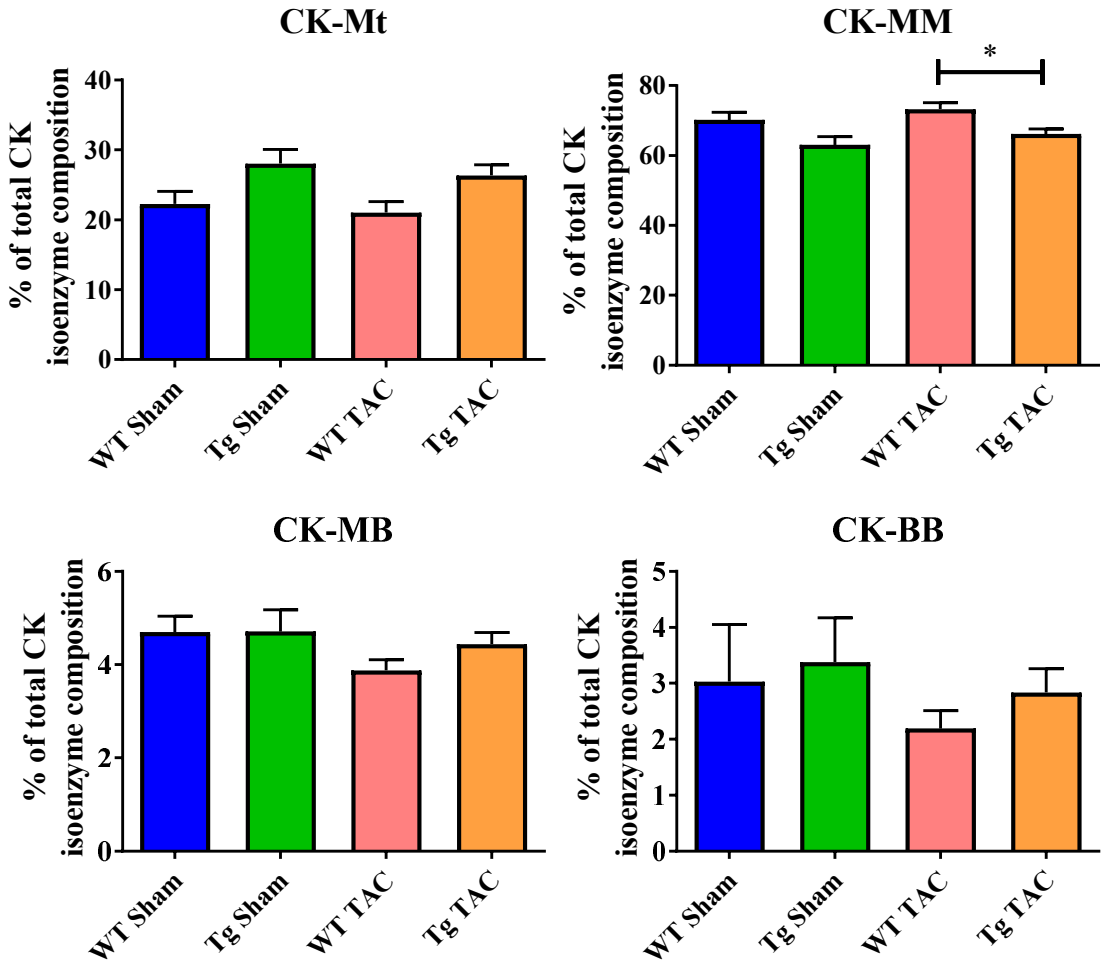
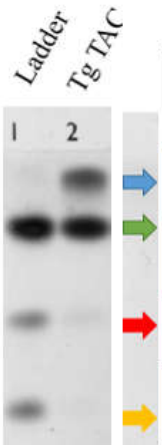


Figure 4-14: Relative CK Isoenzyme Composition in the LV tissue of WT and CK-Mt OE sham/TAC mice

The relative CK isoenzyme composition as determined by SAS-1 gel electrophoresis is described above. The percentage of total CK composition was assumed to be directly proportional to the relative band density of the bands depicted in Figure 4-13. Analysis was done by one-way ANOVA with Bonferroni's post-hoc test. * = $p < 0.05$. n = 10, 11, 17, and 20 for the groups, respectively.



Band identity	Relative band density to total band density	Total CK activity as identified by spectrophotometry	Calculated CK isoenzyme activity
CK-Mt	30.4%	6.6 IU/mg protein	30.4% * 6.6 IU/mg protein = **2.0 IU/mg protein for CK-Mt activity**
CK-MM	63.6%		63.6% * 6.6 IU/mg protein = **4.2 IU/mg protein for CK-MM activity**
CK-MB	4.8%		4.8% * 6.6 IU/mg protein = **0.31 IU/mg protein for CK-MB activity**
CK-BB	1.2%		1.2% * 6.6 IU/mg protein = **0.07 IU/mg protein for CK-BB activity**

Figure 4-15: Method for calculating CK isoenzyme activity from band density

The method of calculating the CK-isoenzyme activities presented in Figure 4-16, from the gel bands in Figure 4-13 is shown above with a CK-Mt OE TAC sample.

4.4.6.2 CK isoenzyme and total CK activity

Total and isoenzyme-specific CK activities are shown in Figure 4-16. Tg sham mice had 92% higher CK-Mt activity than WT sham mice, whereas Tg TAC mice was 47% higher CK-Mt activity than in WT TAC mice. CK-MM, CK-MB, and CK-BB activities were not significantly different between groups. Compared to WT sham mice, Tg sham mice had 38% higher total CK activity. However, a significant increase in total CK activity was not observed in the Tg TAC mice compared to the WT TAC mice – Tg TAC mice trended 18% higher total CK activity (WT TAC mice: 6.1 ± 0.3 IU/mg protein; Tg TAC mice: 7.0 ± 0.3 IU/mg protein). Total CK activity significantly declined during heart failure in the Tg TAC group by 22% ($p < 0.05$), as compared to the Tg sham group. There was no significant difference in total CK activity and CK-Mt activity between the WT sham and the WT TAC groups.

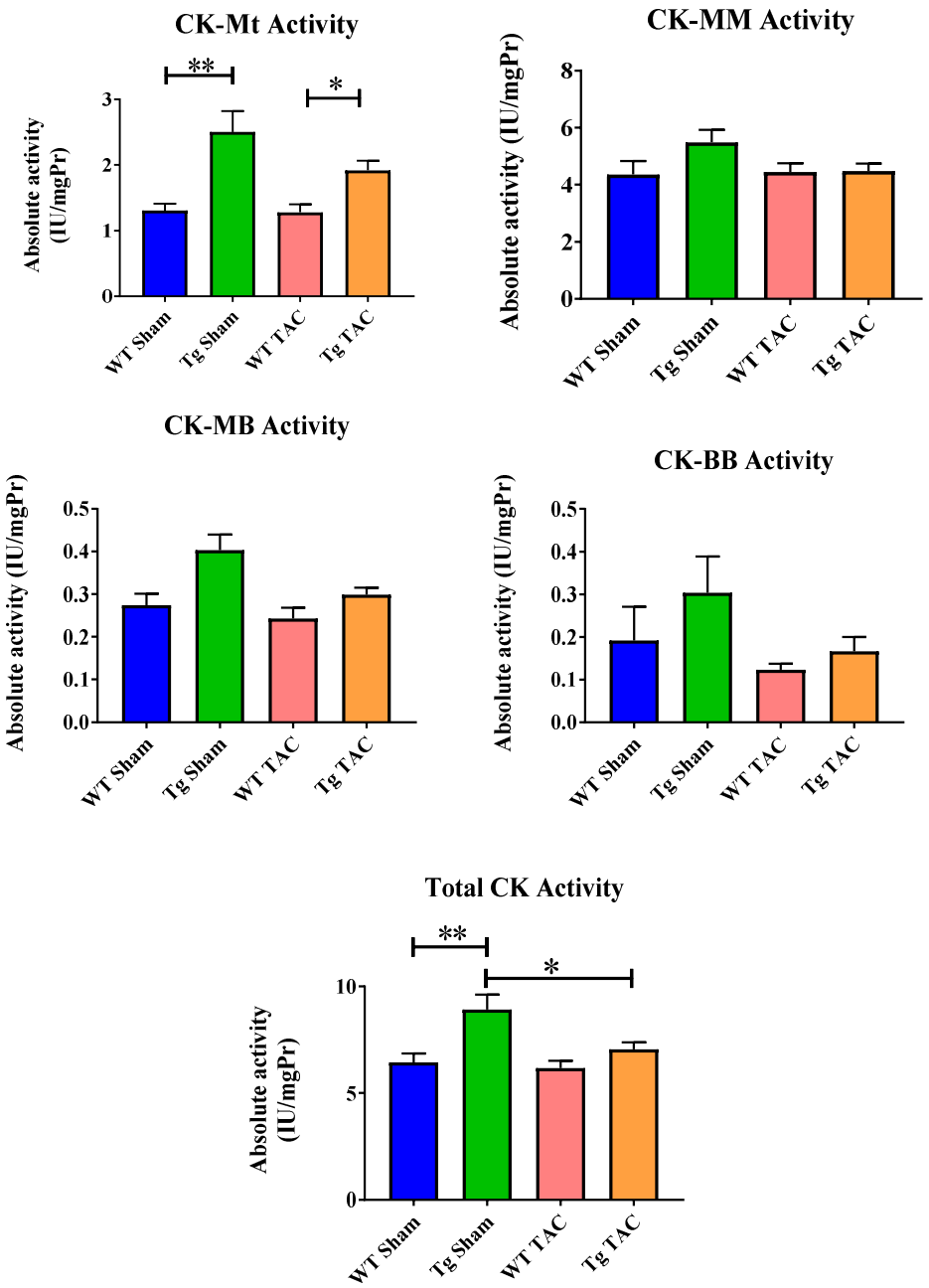


Figure 4-16: CK activity in the LV tissue of WT and CK-Mt OE sham/TAC mice

Isoenzyme-specific and total CK activity were assessed by gel electrophoresis and CK activity assays, and data was normalized for total protein concentration as determined by Lowry assay. Analysis was conducted by one-way ANOVA with Bonferroni's post hoc test (* = $p < 0.05$; ** = $p < 0.01$). n = 10, 12, 16, 20 for WT sham, Tg sham, WT TAC, and Tg TAC, respectively.

4.4.7 Citrate synthase activity as a measure of mitochondrial volume

There were no significant differences in LV citrate synthase activity between the two sham groups, and between the two TAC groups (Figure 4-17). This suggests that CK-Mt overexpression did not induce any changes in myocardial mitochondria content. Citrate synthase activity also did not change significantly between sham and TAC groups.

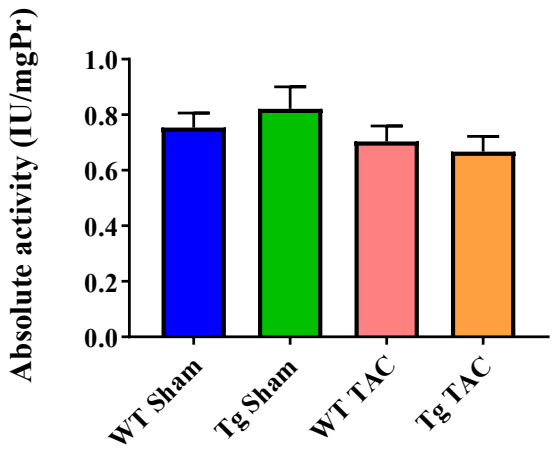


Figure 4-17: Citrate synthase activity in the LV tissue of WT and CK-Mt OE sham/TAC mice

CS activity was not significantly different between sham and TAC groups as analysed by one-way ANOVA with Bonferroni's post-hoc test. n = 10, 12, 16, 20 for WT sham, Tg sham, WT TAC, and Tg TAC, respectively.

4.5 Discussion

The overall results of the experiments in this chapter demonstrate that while the current level of CK-Mt overexpression is safe, it did not protect against TAC-induced chronic heart failure as assessed by morphometric, echocardiography and haemodynamics analysis.

4.5.1 TAC as a model of heart failure and its effect on CK system

One consideration that should be addressed is whether the TAC protocol successfully induced heart failure, as TAC is known to produce a spectrum of cardiac dysfunctions ranging from compensated LV hypertrophy to congestive heart failure [18].

Many morphometric measures indicated that mice in the TAC groups exhibited heart failure. Compared to that of their respective sham groups, both TAC groups showed elevated LV weights and myocardial CSA after 6 weeks on protocol, indicating onset of pathological myocardial remodelling and LV hypertrophy. TAC mice also had significantly increased EDA and lung weights, suggesting LV dilation and pulmonary edema, respectively, which are hallmarks of decompensated heart failure. The morphometric changes corresponded with impaired functional parameters such as significant declines in EF and contractile reserve in the TAC mice. Furthermore, *in vivo* PCr/ATP ratio, a clinically proven metric of heart failure [133], was decreased in WT TAC mice. Therefore, the results indicate that TAC successfully caused heart failure in the current experiment.

However, significantly declined *in vivo* PCr/ATP ratios in WT TAC mice was not accompanied by significant decreases in CK activity and LV creatine as measured through biochemical

assays. *In vivo* measurements are more physiological relevant, though PCr/ATP ratio is not a direct measure of CK activity. The findings represent a highly unusual situation since published studies demonstrated that loss of CK and creatine should occur concomitantly with progression of heart failure [117,128,129,286]. Syrian hamsters that were genetically predisposed to dilated cardiomyopathy demonstrated approximately 50% and 67% losses in creatine and total CK activity, respectively, with a strong relationship between CK dysfunction and heart failure severity [117]. Similarly, mice overexpressing β_1 adrenergic receptor had CK system dysfunction that occurred before/alongside onset of contractile dysfunction [286]. However, the current findings regarding CK activity and LV creatine are consistent with the results from a previous study conducted by our group that investigated the effects of TAC on CK system impairment in WT C57BL/6 mice [18]. TAC-operated mice have a heterogeneous response, and our group previously found that WT TAC mice as a whole did not show a significant decrease in total CK activity nor creatine, as measured through the same techniques used in the current study [18]. Instead, only after stratification for disease severity could a significant decline in CK system function be observed. There were no significant changes in total CK activity or creatine for mice with only LV hypertrophy or early-moderate stages of heart failure. Only mice with clear signs of congestive heart failure (*e.g.* lung weights > 2 SD of normal value) demonstrated significant CK system impairment, with ~30% reduced total CK activity and ~10% reduced creatine. An attempt was made to stratify the current data based on previously established guidelines [18], however, the current sample sizes were too small for proper subset analysis.

It is plausible that impaired CK function could be detected through CK flux measurements, as reduced CK flux occurs substantially earlier than the decline in PCr/ATP ratio in heart failure

[15]. The CK flux measurements would also provide direct evidence as to whether CK function is enhanced in Tg TAC hearts *in vivo*. Unfortunately, CK flux was not conducted because of several technical issues with the novel MRS technique, hence its lack represents a limitation of the current study.

As TAC induces a gradual development of cardiac dysfunction, more severe heart failure could occur on a longer protocol. In the current experiment, animals were sacrificed at 6 weeks after the TAC procedure, whereas mice in the CK-M overexpressing TAC study were followed for 9 weeks after TAC [190]. At 9 weeks in the CK-M TAC study, CK activity in the WT TAC mice declined 30% as measured through biochemical assays. Of particular interest was that survival in the WT TAC group of the CK-M study sharply declined 40% - 50% at approximately 5 - 6 weeks post-TAC [190]. In contrast, 88% mice in the WT TAC group of the current study survived after 6 weeks, with no confirmed deaths from heart failure**.** The current 6-week protocol was adapted as our group had previously found that TAC-induced congestive heart failure should have occurred by this time point (Professor Craig Lygate, *personal communications*). The protocol was not extended further for animal welfare purposes, as this study was not designed to assess survival. The evidence from the CK-M overexpression study [190] and our previous study [18] suggests that higher death rates and more severe cardiac pathophysiology should have been observed for the current 6-week TAC protocol. The reason for the unexpected outcomes in the current study may be attributed to the inherent variation of the TAC protocol (*e.g.* difference in consistency and extent of constriction on the aorta) [276,282]**,** which our group has previously noted is a significant limitation of the procedure. Nevertheless, a longer observation period may produce a more severe phenotype with more

substantial CK system impairment. It remains possible that CK-Mt overexpression could have been protective in this scenario, when there would be more pronounced CK dysfunction.

4.5.2 CK-Mt overexpression does not affect baseline cardiac function

The results of the CK activity assay suggest that the transgenic model was successful, with 92% higher CK-Mt activity and 38% higher total CK activity as compared to WT controls. This elevation of creatine kinase appeared to be benign in physiological conditions, as there were no significant alterations in any baseline cardiac parameters in the Tg sham group. Morphometric measures such as myocardial CSA and LV weight in Tg sham mice were not significantly different from WT shams, nor were contractile parameters at baseline (EF, ESP, EDP) and under adrenergic stress (Max dP/dt, tau). PCr/ATP ratio was nearly identical between the two groups, suggesting that the CK-Mt overexpression did not affect substrate concentrations, which were already at equilibrium in WT sham mice. Additionally, citrate synthase activity was not significantly different between WT and Tg sham mice, indicating that myocardial mitochondrial volume was not affected by CK-Mt overexpression.

These results represent the first *in vivo* functional characterization of CK-Mt OE mice that are on a pure C57BL/6J background, and are in agreement with the published characterization on a mixed C57BL/6J x 129Sv background [212]. Previous studies have shown that excessive CK-Mt expression can result in significant mitochondrial pathology due to formation of large CK-Mt crystal aggregates, as discussed in Section 3.1.1, hence it was important to confirm that the current level of overexpression did not result in any significant pathophysiology.

4.5.3 CK-Mt overexpression in chronic heart failure and limitations of current study

The main objective of the current study was to elucidate whether CK-Mt overexpression in the heart provides a protective effect in heart failure. Despite successful CK-Mt overexpression, Tg TAC mice did not demonstrate improvements in functional and morphometric parameters, as assessed through echocardiography, LV haemodynamics, and organ weights. The only significant difference between WT and Tg TAC mice was a slight reduction (< 15%) in myocardial CSA of the Tg TAC mice as measured through echocardiography. However, this was not supported by a reduction in Tg TAC LV weight. Overall, the results suggest that the current level of CK-Mt overexpression was not protective during chronic heart failure in the TAC pressure-overload model.

The lack of protective effect stands in contrast to a similar study conducted with CK-M OE mice, in which Gupta *et al*. reported that CK-M OE mice had significantly increased survival and improved cardiac function during TAC-induced heart failure (*e.g.* higher CO and enhanced response to adrenergic stress) [190]. The two studies share many similarities, including animal system, heart failure model (TAC), and transgene promoter (α-MHC). Thus, why overexpression of two CK subunits produced such different results merits discussion, especially regarding possible limitations of the current study.

The most obvious explanation for the discrepancy in the results was that the current level of CK-Mt overexpression was insufficient to produce a measurable improvement in cardiac function. In the CK-M study, Gupta *et al.* significantly elevated total CK activity in the Tg TAC mice over two-fold during heart failure as compared to WT TAC controls [287], in

contrast to the 13% increase in the current study. This is partially because CK-M is about three-fold more abundant in myocardium than CK-Mt, thus CK-M overexpression produces significantly more impact on total CK activity. However, it is also partially a result of the intentional moderation of CK-Mt overexpression in the current study. Technically, higher levels of CK-Mt overexpression could have been achieved using a more powerful promoter, or a random integration strategy.

In both studies, PCr/ATP ratios, as assessed by ^{31}P-MRS, were restored to physiological levels by CK overexpression during TAC induced heart failure, but a cardioprotective effect was only measured with CK-M overexpression. The lack of protection of CK-Mt overexpression supports several existing studies that suggest declined PCr/ATP ratio is not always indicative of heart failure severity. For example, our group previously found that GAMT$^{-/-}$ KO mice, which had no cellular creatine (hence a PCr/ATP ratio of ~0), fared no worse than WT mice during heart failure following chronic myocardial infarct [151]. Likewise, it was recently reported that cardiac dysfunction in TAC mice substantially preceded a decline in PCr/ATP ratios [277,288]. Taken together, these findings indicate that there are instances in which PCr/ATP ratio is not closely associated with cardiac function. Therefore, it appears unlikely that CK-M overexpression improved function and survival during heart failure exclusively because of restoration of physiological PCr/ATP ratios.

There are two limitations with the current ^{31}P-MRS results that should be noted. First, PCr/ATP ratios and the other measures (*e.g.* echocardiography, haemodynamics, and biochemical assays) were obtained from two separate cohorts of mice for methodological reasons. Second, as discussed earlier, CK flux measurements would have provided more direct evidence of altered CK function *in vivo* beyond the relative metabolite concentrations offered by the PCr/ATP ratio.

In conclusion, it is highly plausible that the protection of CK-M overexpression during heart failure was primarily due to two-fold elevation of total CK activity, which was not reached with the current CK overexpression model. However, given that the current model restored physiological PCr/ATP ratios during heart failure, it is also possible that CK-M may have protection potential during heart failure because of a specific function that CK-Mt overexpression cannot compensate for, which is discussed in the next section.

4.5.4 The CK system in heart failure

Our group had previously demonstrated that moderate elevation of intracellular creatine similarly did not protect in chronic heart failure [2], thus taken together with the current findings, it appears that CK-M may be the limiting component of CK function during heart failure. This raises the question as to why CK-M is uniquely important in chronic heart failure.

In the CK-M overexpression study, Gupta *et al.* postulated a bioenergetics explanation, citing that CK-M OE mice showed improved PCr/ATP ratios and CK flux during heart failure [190]. Thus, it was proposed that CK-M overexpression improved the decreased energy reserve in heart failure by facilitating energy transfer and improving ATP availability through increased CK activity. While CK flux measurements were not available for the current study, the ^{31}P-MRS results suggest that this hypothesis alone cannot explain the protective benefit of CK-M overexpression.

One possible explanation is related to the different primary functions of CK-M and CK-Mt. CK-M primarily catalyses ATP synthesis at sites of ATP consumption, whereas CK-Mt utilizes ATP to generate PCr at mitochondria. More specifically, CK-M regulates muscle functions

through its two major binding partners: 1) functional coupling to SERCA to regulate calcium homoeostasis [34], and 2) functional coupling to myosin ATPase to influence muscle contraction [27]. These functional coupling relationships may be of critical importance during heart failure as ATPase require high cellular $|\Delta G_{ATP}|$ to function. The typical $|\Delta G_{ATP}|$ in rodent heart is approximately 57 kJ/mol, which declines significantly in heart failure [1]. SERCA and myosin ATPase require 52 kJ/mol and 46 kJ/mol, respectively, for proper function [1,2]. While both CK-M and CK-Mt have been shown to regulate cellular $|\Delta G_{ATP}|$ in mice [179,180], only CK-M play a substantial role in maintaining the local $|\Delta G_{ATP}|$ of the SERCA and myosin ATPase [183]. Therefore, it is plausible that the protective benefit of CK-M overexpression in heart failure may be mediated by this mechanism. However, Gupta *et al.* have tested this hypothesis by conducting *in vitro* experiments on cardiomyocytes isolated from CK-M OE mouse hearts. The results suggest that CK-M overexpression did not affect sarcomere shortening nor calcium transient amplitudes, though further study is required to understand the mechanism *in vivo* [190].

Therefore, the underlying mechanism by which CK-M overexpression protected against TAC-induced heart failure remains unclear, and further investigation is warranted. The current results suggest that the therapeutic effect of CK-M overexpression may not have been solely due to a normalization of PCr and ATP concentrations, as restoring PCr/ATP ratio to physiological levels alone appears to be insufficient to produce protective effect.

4.6 Future work

In conclusion, the current study demonstrates that while moderate CK-Mt overexpression is not detrimental to the heart, it does not produce a protective effect in pressure-overload heart failure in the murine model. Future experiments mostly focus on two categories: 1) how to improve upon the current experiment, and 2) how to generate additional heart failure animal models to investigate the protective potential of the CK system.

The most immediate improvement on the current experiment that could be conducted would be to test whether a longer TAC protocol could potentially reveal any protective effects of CK-Mt at later stages of heart failure. Alternatively, a new model could be generated using a random chromosomal integration-based approach to further elevate CK-Mt overexpression by choosing a line with multiple transgene copies. This approach has its own risks, such as interference with endogenous gene expression and the need to test multiple transgenic lines. Nonetheless, unlike with CrT overexpression [135], the maximum safe level of CK-Mt overexpression was not reached with the current model. If overall CK activity in the CK-Mt OE model could be elevated to two-fold above baseline as seen in the CK-M OE model [190], then it would clarify whether the protective effect of the CK-M model is due to increased total CK activity or a specific role of CK-M.

The effect of CK overexpression on other cardiac pathologies and models could be explored, especially as our group has demonstrated CK-Mt is protective in I/R injury [212]. Another model that our group has previously explored is the use of coronary artery ligation to induce heart failure through chronic MI [2,18]. It is reasonable to explore whether CK-Mt overexpression could have a protective effect on other heart failure models or on other ischemic cardiac conditions such as angina.

While CK-Mt overexpression alone does not improve cardiac function in heart failure, it remains to be seen whether a double transgenic could provide protection. The most logical step would be to cross with the existing CrT OE model, to investigate the effects of simultaneous substrate and enzyme augmentation on heart failure. Overexpressing CK-Mt in conjunction with increased CrT may produce a larger pool of adequately phosphorylated high-energy metabolites. This has been postulated to be a critical factor in improvement of energetics in heart failure by an *in silico* model [289].

The double CK-Mt/CK-M OE mouse has yet to be generated, and represents another avenue of further investigation to elucidate whether simultaneous overexpression of both enzymes could enhance cardiac function by improving kinetics of both major isoforms of CK.

5 In vitro model of creatine kinase overexpression to investigate doxorubicin cardiotoxicity

5.1 Introduction

5.1.1 Doxorubicin hydrochloride and cardiotoxicity

Doxorubicin hydrochloride (DOX) is an antineoplastic drug that is primarily limited in its use by cardiotoxicity, which is the most serious adverse effect in clinical practice. DOX, also referred to as Adriamycin, is a cytotoxic anthracycline isolated from *Streptomyces peucetius var. caesius* in 1969 [290]. DOX is highly potent and widely used in the treatment of a variety of malignant tumours [291,292]. DOX-induced cardiotoxicity is dose-dependent [291], with the onset of cardiac abnormalities occurring in patients at an accumulated dose of 250 mg/m^2 DOX and the incidence of heart failure sharply increasing once the accumulated dose exceeds 550 mg/m^2 [292,293].

Two types (acute and chronic) of DOX-induced cardiotoxicity are described based on the time of onset of cardiac injury and the clinical manifestations. Acute injury is the less common form of cardiotoxicity that usually occurs within a few weeks following the treatment. The clinical manifestations include arrhythmias, pericarditis, or acute left ventricular failure [294]. Chronic cardiotoxicity is the more common and detrimental form of cardiotoxicity, usually presenting within a year of completing DOX treatment, though it may occur years to decades later [294,295]. This delayed cardiotoxicity may evolve into chronic, progressive cardiac damage resulting in irreversible cardiomyopathy. The clinical manifestations include reduced

contractility and ejection fraction, increased afterload, arrhythmias, and ultimately, heart failure [294]. The potential risk is so severe that it is now widely accepted that there is no absolutely safe dose of DOX for the heart; the risk of developing heart failure in patients treated with DOX is a lifelong threat.

5.1.1.1 Mechanisms of DOX as an antineoplastic and a cardiotoxic agent

The underlying mechanisms of DOX antitumor activity have been intensively investigated, but remain controversial. The current literature proposes the following mechanisms: 1) DNA intercalation and alkylation; 2) formation of ROS; 3) initiation of DNA damage via inhibition of topoisomerase II and helicase; and 4) induction of apoptotic pathways [293]. Overall, the primary mechanism appears to be DNA intercalation and Topoisomerase II impairment, which significantly reduces nucleic acid and protein synthesis in rapidly-reproducing cells [296].

Several mechanisims of DOX antitumor activity as described above are also considered to be the mechanisms of DOX-induced cardiotoxicity, which include ROS formation [297,298], DNA intercalation, inhibition of RNA, DNA, and protein synthesis [299,300], alteration of myocardial mitochondrial Ca^{2+} homeostasis [294,301] and initiation of apoptosis [302,303].

5.1.1.2 DOX and reactive oxygen species (ROS)

Although the molecular pathogenesis of DOX-induced cardiotoxicity is multifactorial, it is widely accepted that DOX-induced oxidative stress causes substantial injury to cardiomyocytes and cardiac tissue. Indeed, ROS generated from the DOX oxidation cycle is believed to act as a major trigger of apoptotic and necrotic cell death [295,304,305].

DOX contains a quinone moiety that can accept one electron from NAD(P)H to form a semiquinone (Figure 5-1). In the heart, this reaction commonly occurs in the mitochondria through catalysis by mitochondrial NADPH dehydrogenase. The unpaired electron can then be transferred to O_2 to form superoxide anion radical ($\bullet O_2^-$), which is reduced by superoxide dismutase into H_2O_2. The production of $\bullet O_2^-$ and H_2O_2 is particularly toxic in the presence of iron ions, which cause $\bullet O_2^-$ and H_2O_2 to generate the highly reactive hydroxyl radical (•OH) through the Haber-Weiss and Fenton reactions respectively [306]. •OH, $\bullet O_2^-$ and H_2O_2 all cause widespread cellular damage through peroxidation of lipids and oxidative damage to proteins and nucleic acids. Indeed, the only FDA-approved treatment for doxorubicin-induced cardiotoxicity is dexrazoxane, which is an iron chelator [307,308]. Mitochondrial proteins have been shown to be extremely susceptible to DOX-induced ROS damage, with established effects on ATPases [309], ETC complexes [310], proteolipid complexes such as VDAC, ANT [311], and CK-Mt [312]. In particular, CK-Mt has been suggested to be even more sensitive to oxidative damage as compared to other ETC elements [297,313].

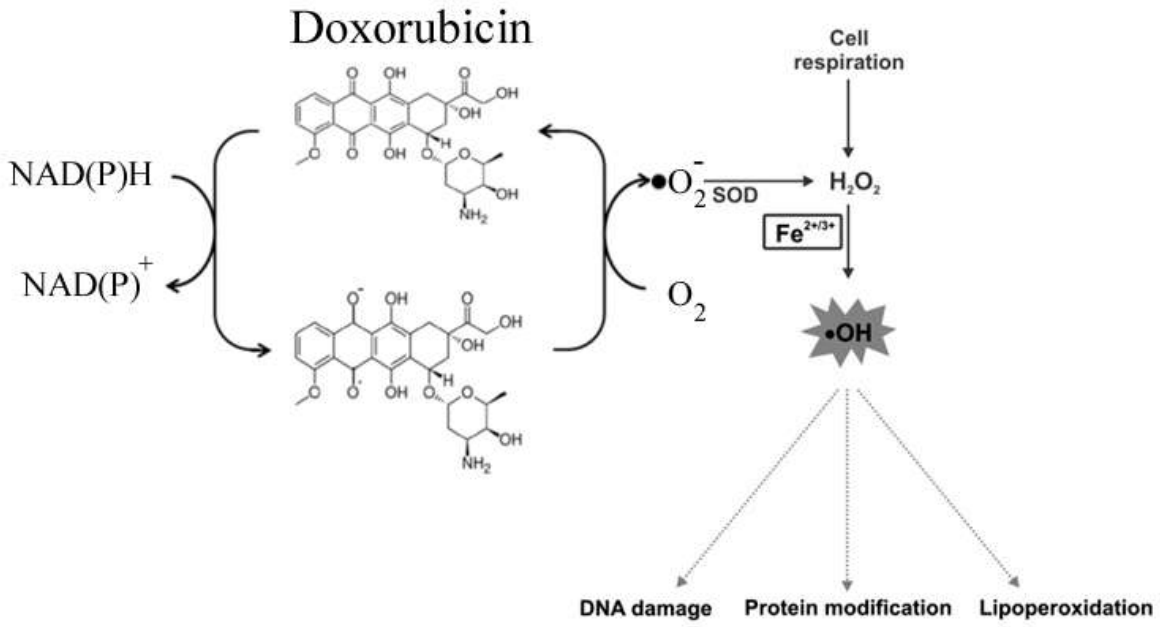


Figure 5-1: DOX redox cycle

DOX generates free radicals by cycling through its quinone and semi-quinone moiety. Most commonly, O_2 accepts the free electron, generating superoxide. This process is especially likely to occur at mitochondria due to its physiological role in ROS generation and presence of NADPH dehydrogenase. Resulting cellular damage is especially likely in the presence of iron due to formation of hydroxyl free radicals, resulting in cell damage. SOD = superoxide dismutase. Adapted from [314].

5.1.1.3 DOX-induced ROS interacts with CK-Mt

DOX-induced ROS inactivates CK-Mt through three major mechanisms. First, ROS directly inactivated CK-Mt via oxidation of the thiol group of the active site cysteine (Cys278), a process that occurs at even low levels of oxidative stress [297,315]. Second, ROS modifies residues responsible for CK-Mt octamer formation (such as oxidation of Met267), thus preventing octamer formation [74]. As a result, ROS also impairs CK-Mt formation of mitochondrial interactosomes with VDAC and ANT, which can only occur with octameric CK-Mt [31,316]. The inability to form the mitochondrial interactosome undermines CK-Mt

functions, namely facilitation of energy transfer, regulation of mPTP function, and maintenance of mitochondrial structural integrity [64]. Indeed, DOX treatment has been shown to induce mitochondrial swelling and increase mPTP opening [317]. Third, DOX-induced ROS destabilizes CK-Mt in the mitochondrial intermembrane space [62] through peroxidation of cardiolipin [318,319], which anchors CK-Mt to the inner membrane. Additionally, DOX also directly competes with CK-Mt for cardiolipin binding sites, as shown in perfused rat heart and in isolated rat and bovine cardiac mitochondria [242,320,321]. Through these mechanisms, ROS damage represents the main pathway by which CK-Mt is impaired during DOX-induced cardiotoxicity.

5.1.1.4 DOX impairs bioenergetics and CK function

DOX also causes impaired myocardial bioenergetics. This decline is in part caused by DOX-induced ROS species and their effect at the mitochondria, though many other factors may also contribute. Regardless of mechanism, *in vitro* [322,323] and *in vivo* [324] studies have demonstrated that ATP production in DOX-treated cardiac tissue can decrease 30%-90%. Similarly, cardiac PCr reserves decrease 30%-73% [322,325], and PCr/ATP ratios have been found to decrease in human patients with DOX-induced cardiomyopathy [326].

The overall consequences of DOX-induced CK system impairment have been well documented, including effects on both CK activity and creatine transport. DOX has been shown to directly reduce CK-M and CK-Mt activity in cultured cardiomyocytes and H9C2 neonatal rat heart myoblasts [298], as well as perfused rat heart [321]. Of particular interest was a study conducted in H9C2 cells, which suggested CK activity may correlate with survival from DOX

toxicity [298]. It was found that healthy DOX-treated H9C2 cells (attached to plate) had 40% higher CK activity than untreated cells, whereas unhealthy cells (viable but detached from plate) had 67% lower CK activity than untreated cells [298].

5.1.2 CK system augmentation against DOX cardiotoxicity

Using ^{14}C-creatine, Darrabie *et al.* demonstrated that even sub-therapeutic DOX concentrations (50-100 nM) significantly impairs creatine uptake in HL-1 cells [327]. It was found that the decline in creatine uptake significantly preceded cell death. For instance, a reduction in intracellular creatine uptake could be seen at 4 hours after initiation of DOX treatment, whereas cell death was not apparent until 24 hours. The fact that intracellular creatine transport was affected substantially earlier than cell death suggested creatine loss could play a causative role in DOX cardiotoxicity. To investigate whether creatine supplementation could reduce cell death, Santacruz *et al.* optimized an *in vitro* model of creatine supplementation in the context of DOX-induced cytotoxicity, and found that 5 mM creatine supplementation reduced DOX-induced HL-1 cell death from 36% to 18% [328]. Thus, it appeared that impaired myocardial bioenergetics due to creatine loss may play a causative role in DOX-induced cardiotoxicity. However, our group could not translate these *in vitro* findings to intact beating hearts. Using Langendorff perfused hearts, our group demonstrated that there were no significant differences in cardiac function and apoptosis rates amongst creatine-deficient (GAMT KO), wild type, and creatine-elevated (CrT OE) mouse hearts treated with 100 minutes of 15 μM DOX perfusion [329]. These results suggested that modulations of myocardial creatine content did not protect hearts from DOX-induced cardiotoxicity in *ex vivo* hearts.

To investigate whether enhanced CK activity reduced DOX-induced cardiotoxicity, Gupta *et al.* generated a CK-M OE mouse line, and assessed *in vivo* function after exposure to 5 mg/kg DOX weekly for five weeks, equivalent to a therapeutic DOX dosage [192]. Mice were followed throughout the treatment period and for an additional three weeks. At eight weeks, CK-M OE mice exhibited physiological contractile function, and had 80% survival, significantly higher than the 56% survival in DOX-treated WT mice [192]. This improved survival and contractile function may be attributed to the bioenergetic improvement afforded by CK overexpression. Transgenic DOX-treated mice exhibited two-fold higher *in vivo* CK flux compared to WT DOX-treated mice, and had physiological PCr/ATP ratios [192]. Taken together, these findings provided the first evidence that CK augmentation has a protective effect in DOX-induced heart failure.

While the roles of both CrT and CK-M have been investigated in DOX-induced cardiotoxicity, there have been no studies conducted to evaluate the protective potential of CK-Mt augmentation. There is a convincing body of evidence for exploring whether CK-Mt overexpression protected against DOX-induced cardiotoxicity. First, CK-Mt is one of the most susceptible targets of DOX-induced ROS damage. Second, CK-Mt maintains PCr/ATP ratio, which declines in DOX-induced cardiotoxicity. Third, *in vivo* CK-M augmentation has provided therapeutic benefit. Fourth, as mitochondria is a specific target of DOX, CK-Mt overexpression might be more protective than CK-M augmentation. Finally, CK-Mt supplementation could potentially prevent the onset of DOX-induced cardiotoxicity, in contrast with current symptomatic treatments such as β-blockers.

Thus, experiments were undertaken to develop an *in vitro* assay in HL-1 and HEK293 cells that could demonstrate whether CK augmentation could reduce DOX-induced cardiotoxicity. As

our group had previously generated similar CK-M, CK-Mt, and CK-B transgenic vectors, the optimized assay was tested with all three vectors. Thus, the optimized assay allowed comparison between subunits and identification of the most promising CK subunit suitable for overexpression experiments *in vivo*.

5.2 Aims and hypothesis

The goals of the experiments in this chapter were to generate and optimize an *in vitro* model of DOX cytotoxicity, and explore whether CK overexpression protected against DOX-induced cardiotoxicity. The first aim was to generate a functional model of DOX-induced cytotoxicity in HEK293 and HL-1 cell lines. The second aim was to transfect HEK293 and HL-1 cells with CK overexpression transgenes and to verify whether the transfected cells had increased CK activity. The final aim was to apply this model to determine whether CK overexpression exerted a protective effect against DOX-induced cytotoxicity in an *in vitro* setting.

The experimental hypothesis was that CK overexpression would exert a protective effect against DOX-induced cytotoxicity by improving cell survival rates. The results of HEK293 and HL-1 experiments are discussed individually as they were distinct experiments.

5.3 Methods and Results

5.3.1 Methods and Results I: DOX in HEK293 cells

Experiments were conducted in HEK293 cells first, and then in HL-1 cells. The objective of this study was to optimize experimental conditions in which HEK293 cells were treated with a lethal dose of DOX, with cell viability measured by flow cytometry.

5.3.1.1 Protocol optimization

5.3.1.1.1 HEK293 cell culture

HEK293 cells were maintained and passaged as discussed in Section 2.4. Initially, HEK293 cells were plated at $1.5x10^5$ cells/cm^2 in 24-well plates, and allowed to proliferate for 24 hours. Triplicate wells were used as biological replicates for each assay. After the 24-hour incubation, cells were incubated with 100-500 nM DOX for 3 hours to generate a kill curve. The concentration of DOX selected was based on the steady state plasma concentrations of doxorubicin in patients, which is approximately 250 nM [293,327]. DOX was solubilized in water, thus there was no vehicle control necessary. Cells were then trypsinized and washed with PBS, pelleted by 10-minute centrifugation at 1,000 rpm, and stained with 300 µL of 1% propidium iodide (PI) in PBS for 15 minutes at RT before being analysed by flow cytometry.

5.3.1.1.2 Quantification of cell viability

Cell viability was assessed by staining dead cells with PI and measuring cellular PI fluorescence through flow cytometry (as described in Section 2.8), which allowed for high-throughput

analysis. PI is a fluorescent DNA intercalating agent that cannot cross the plasma membrane of intact cells, and will only enter cells that have compromised membranes due to apoptosis and necrosis. PI can only be used to identify dead cells because of this mechanism of action, and cannot be used to distinguish between different types of cell death. PI absorbs light at 488 nm and emits at 617 nm. Cell death was quantified using a Beckman Coulter Cyan ADP flow cytometer, with 10,000 cells analysed per sample. Gates were set to exclude non-cellular hits and multi-cellular aggregates, which were minimalized by vortexing each sample before quantification. For each run, a positive control for cell death was created by preparing a heat-shocked sample through a 2-minute incubation at 70ºC before addition of PI. Cell death was counted by assuming untreated, control group cells had 5% cell death, which was accomplished by setting the width of the death gate to include the top 5% of PI stained cells in the control groups, as seen in Figure 5-2A of the control sample. Results are shown in Figure 5-2B.

Results of the initial DOX kill curve were unusual in that they were different from that of heat shock samples (Figure 5-2A). In previous experiments, samples with cytotoxic conditions (*e.g.* heat shock, hypoxia) resulted in clear populations of live and dead cells that manifested as a bimodal graph, with the dead-population peak within the death gate (R3), and the live-population peak outside the death gate as shown in the heat shock sample of Figure 5-2A. In contrast, there was only a single population of cells in DOX-treated groups, which shifted partially into the death gate with increasing DOX concentrations. As shown in Figure 5-2B, DOX appeared to produce a dose-dependent cytotoxicity between 100 – 500 nM, as more of the unimodal population moved within the death gate at higher DOX concentrations.

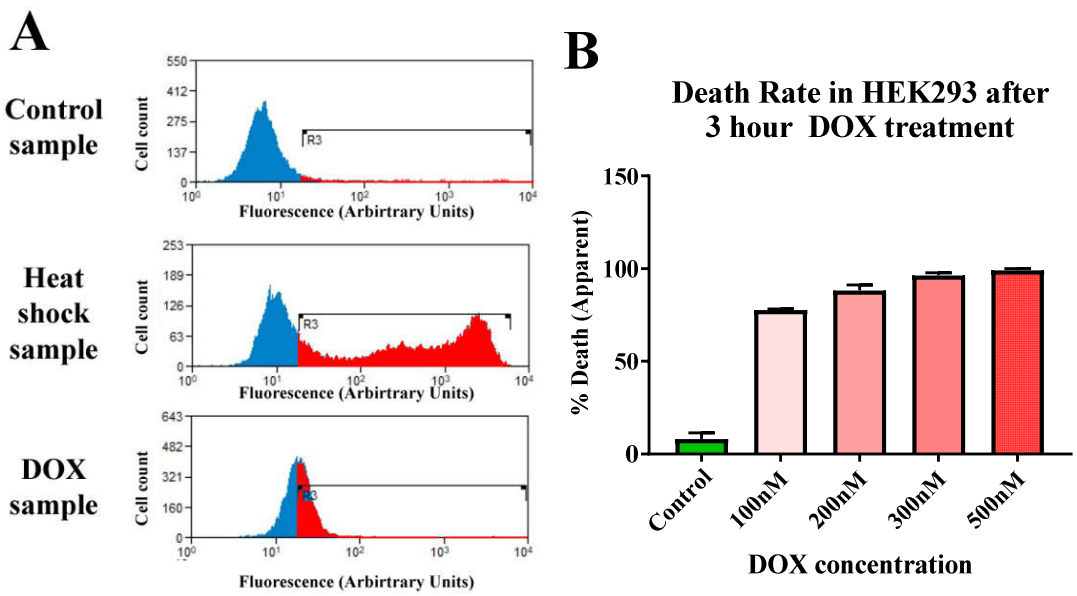


Figure 5-2: Doxorubicin dose-response curve in HEK293 cells

(A) Flow cytometry results for control, heat shock, and 100 nM DOX samples. The curve represents the PI fluorescence distribution of the cell population. Cells in the blue fraction are considered alive. Cells in the red fraction are considered dead. The R3 gate was determined by assuming 5% of cells in the control sample were dead (due to natural death/handling), and the same gate was used for all subsequent samples. (B) Kill curve for HEK293 cells when exposed to different concentrations of DOX, as measured by uptake of PI in flow cytometry. n = 2 trials (4-7 wells) per group.

5.3.1.2 Use of FITC Annexin V stain

Due to the unusual PI staining pattern in flow cytometry, a second dye, Annexin V-FITC, was used to co-stain samples. Annexin V is a Ca^{2+}-dependent phospholipid-binding protein with a high affinity for phospholipid phosphatidylserine, a component of the inner plasma membrane that is flipped onto the outer membrane in early apoptosis. Therefore, Annexin V can stain cells that are in early, reversible stages of apoptosis [330]. While Annexin V is a marker of early apoptosis, irreversibly damaged necrotic cells will also be stained by Annexin V. FITC is an attached fluorophore that amplified the sensitivity of Annexin V.

To accommodate the additional stain, the flow cytometry protocol was slightly modified. Experimental steps were identical with the PI-only experiment until cells had been pelleted and washed with PBS. Rather than re-suspending in 300 µL PBS, samples were re-suspended in 500 µL Annexin V binding buffer containing 1% PI and 5% FITC-Annexin V fluorochrome. The sample was then wrapped in foil to shield from light and incubated for 30 minutes at RT before being run through the flow cytometer. Various DOX incubation strategies were tested, including 18 and 24-hour incubation times, as well as 300 nM-100 µM DOX concentrations. The DOX incubation time had been increased from 3 hours to 18 or 24 hours as the longer time periods were more commonly used in the literature [328,331]. High concentrations of DOX were tested to evaluate whether increased concentration of DOX was required to separate live/dead cells by flow cytometry, as seen in the heat-shock group of Figure 5-2A.

5.3.1.2.1 Gating Optimization

The fluorescent compensation was optimized on the flow cytometer to allow simultaneous measurement of PI and Annexin V-FITC. Gating adjustments were made to allow interpretation of the two stains (Figure 5-3).

With a single stain (PI), the death gate had been set based on the assumption that 5% of untreated cells were dead. However, this assumption proved invalid when simultaneously staining cells with PI and Annexin V, as the rates of cell death were higher and more variable. This was likely a result of Annexin V being more sensitive to cellular damage, and the 30-minute incubation time required by Annexin V before flow cytometry analysis. Thus, the gating was changed to accommodate for this situation. The new plot generated from two dyes

generally contained a population of clearly live cells (Figure 5-4A), and death gates were set to exclude this population (Figure 5-3).

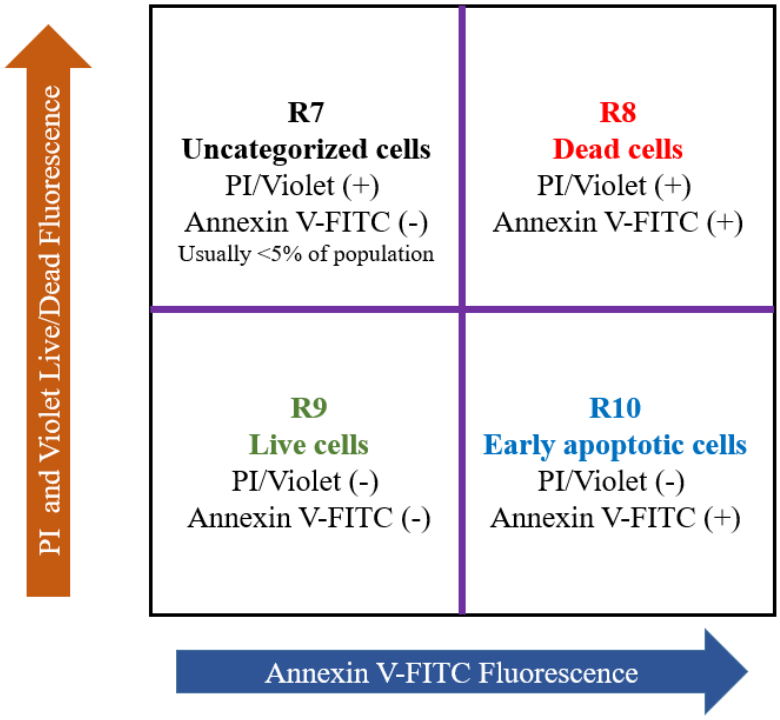


Figure 5-3: Dual stain flow cytometry interpretation

The above figure describes how cells were categorized as live, apoptotic, and dead cells in subsequent experiments with two flow cytometry fluorophores. In each experiment, there was generally a population that was clearly alive (R9), and the gates (purple lines) were moved based on the location of this population.

5.3.1.2.2 PI/Annexin V Experimental Results

The results of the Annexin V/PI flow cytometry experiment described in Section 5.3.1.2 are shown in Figure 5-4 and Figure 5-5. As seen in Figure 5-4 D, E, F, there was a dose-dependent increase in the PI fluorescence signal with increasing DOX concentrations at 18 hours incubation time, recapitulating results seen in Figure 5-2. However, the number of Annexin V-stained cells in quadrants R8 and R10 did not increase significantly in the 18-hour DOX

treatment group as compared to control, even though the DOX concentrations used (100 μM) were up to 100-fold the concentrations normally utilized in cell culture experiments (Figure 5-5). Prolonged DOX treatment also did not increase cell death as indicated by Annexin V staining (Figure 5-4 G, H, Figure 5-5). Two controls for cell death (heat shock and hypoxia) were included to ensure that Annexin V could detect apoptosis and cell death. The hypoxia cell samples were kindly provided by Dr Hannah Whittington and assessed through flow cytometry by the author. Both groups (1% O_2 hypoxia for 18 and 24 hours) showed increased apoptosis and death compared to control as measured by Annexin V staining (Figure 5-4 B, C, I, Figure 5-5), suggesting that Annexin V is a sensitive and effective marker of cell death.

During the experiment, it was observed that 100 μM DOX-treated cells had a red pellet. Thus, the possibility of DOX fluorescent interference with PI was considered, as PI solution also had a red colour. Literature research (discussed in Section 5.3.1) revealed that DOX was weakly auto-fluorescent with a spectrum similar to that of PI (Figure 5-6). This was important since PI fluorescence was elevated with increasing DOX concentrations in a dose-dependent manner (Figure 5-4 D, E, F), whereas Annexin V staining did not change. Furthermore, the result showed a large amount of cells in quadrant R7 (Figure 5-4 E, F), whereas the quadrant is expected to be empty as cells should not stain with PI without initially staining Annexin V. This unusual result was evidence that the PI signal could not be interpreted as it appeared, despite several studies that have used PI to evaluate DOX-induced cytotoxicity [331,332].

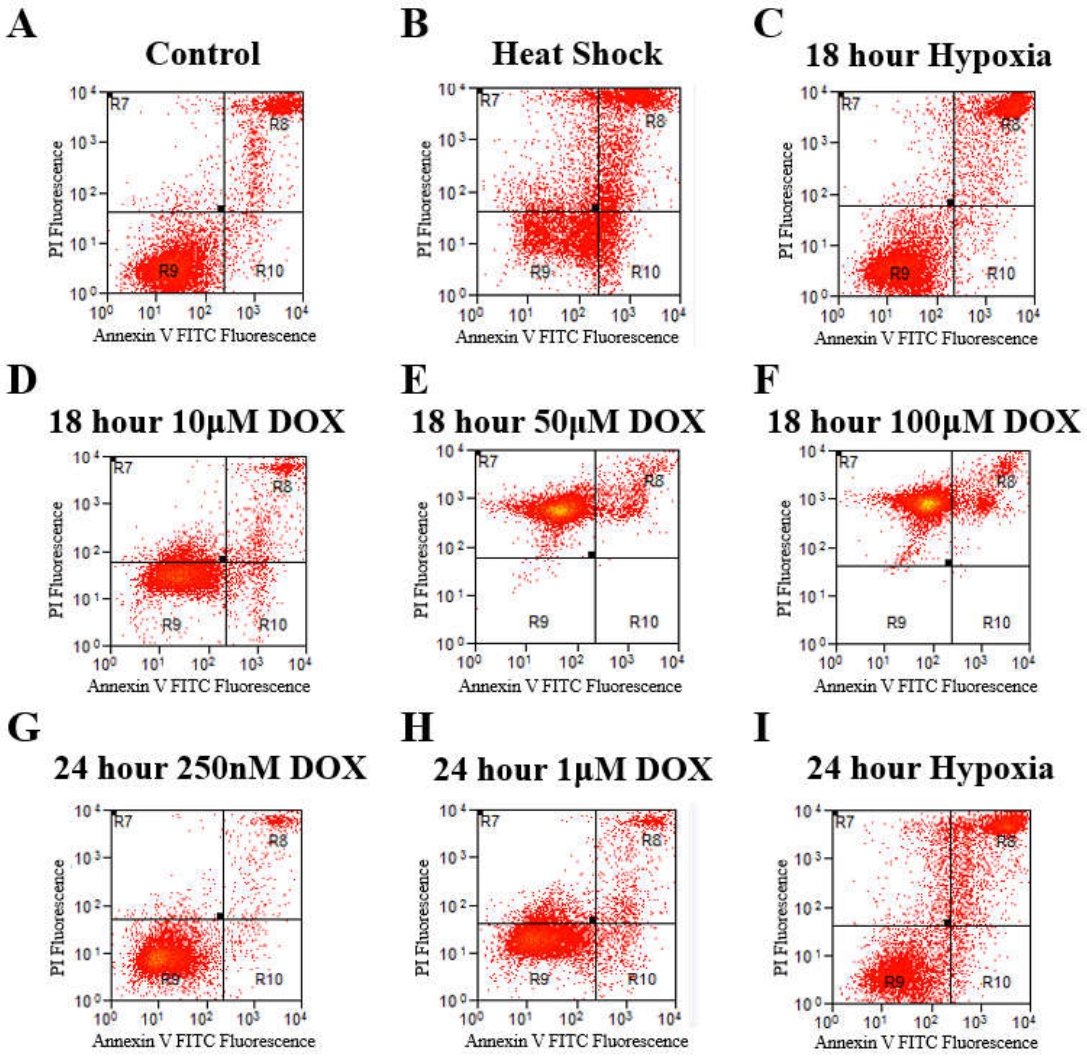


Figure 5-4: DOX cytotoxicity in HEK293 cells as measured by PI and Annexin V-FITC

Representative results from DOX-induced cytotoxicity experiment with co-incubation of cell death marker PI and reversible cell apoptosis marker Annexin V-FITC. (A) Control HEK293 cells and (B) Heat shock control, exhibiting both cell apoptosis and death. (C) 18 hour hypoxia showing increased cell death. (D), (E), and (F) Demonstrate increasing PI/DOX fluorescence with increasing DOX concentration, but a lack of increased cell death compared to control (Cells in R8). (G) and (H) 24 hour DOX incubation still did not show any increased cell death compared to control. In contrast (I) 24 hour hypoxia with notably increased cell death. Note that while the R7 quadrant is usually empty (A, B, C, I), it contains more cells in high DOX concentration samples (D, E, F).

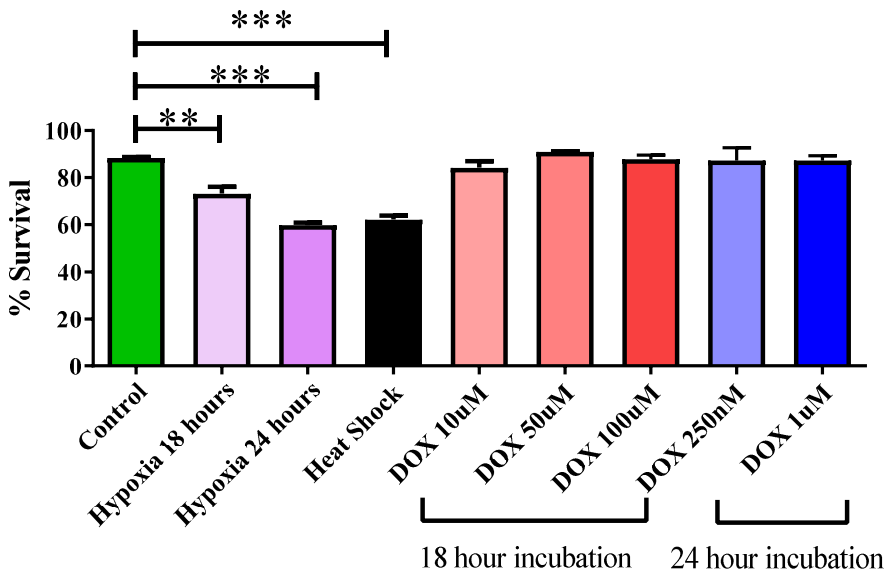


Figure 5-5: Annexin V assay indicates that DOX does not kill HEK293 cells

The above graph depicts the percentage of cells stained with Annexin V, an apoptotic marker, in the experiment described in Figure 5-4. The results suggest that DOX-treated HEK293 cells do not stain Annexin V, whereas HEK293 cells treated with other cellular stresses such as heat-shock and hypoxia do stain Annexin V, and thus are not viable. Annexin V staining was calculated by counting all cells in quadrants R8 and R10 in the figures in Figure 5-4. Results were analysed with one-way ANOVA with Bonferroni's post-hoc test, with all experimental groups compared to control (** = $p < 0.01$; *** = $p < 0.001$). n = 2-4 samples per group.

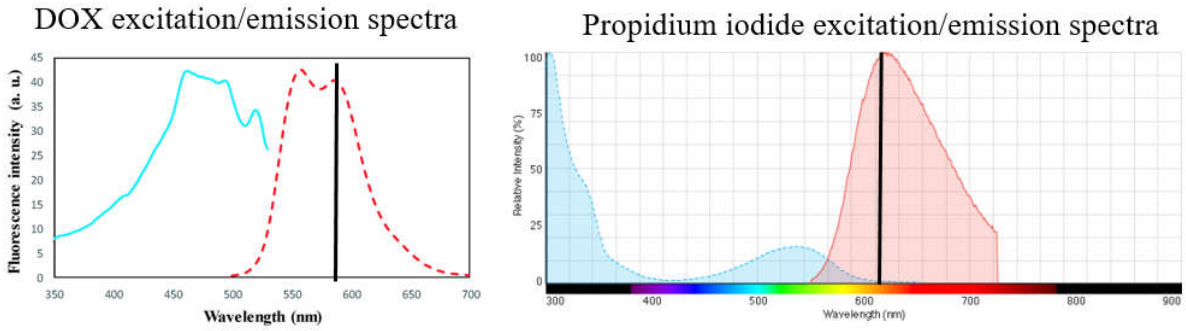


Figure 5-6: DOX and PI emission spectra

Above are the emission spectra of DOX (left) and PI (right). There is significant overlap between the two emission spectra around 600 nm light. DOX emits the maximum light at 580 nm, while PI fluorescence is highest at 610 nm. Images were obtained from [333,334].

5.3.1.3 HEK293 cells are not susceptible to DOX

5.3.1.3.1 Confirmation of HEK293 not susceptible to DOX by flow cytometry assay

Considering that DOX was auto-fluorescent, an experiment was devised to assess the relative contributions of PI and DOX to the fluorescence measured at 610 nm. Cells were treated with 1 μM and 100 μM DOX for 24 hours and pelleted as previously described. However, after being pelleted, cells were re-suspended in 300 μL PBS *without* PI (Annexin V was not used for this experiment to avoid confounding factors). Approximately 100 μL of samples (10,000 cells), including heat shock samples, were run through the flow cytometer without PI addition as a "baseline" measurement. Then, PI was subsequently added at 1% to the remainder of each sample (~200 μL of the initial 300 μL). Samples were incubated at room temperature to mimic normal PI addition protocol, and then vortexed and re-run through the flow cytometer. The rationale behind this experiment was that the first run would show how much fluorescence was being generated by DOX auto-fluorescence, while the shift in the second run would represent the contribution made by PI.

As seen in Figure 5-7, the heat shock control behaved as expected. Before PI was added, there was minimal fluorescence noted in the sample (Figure 5-7A). However, after PI was added, fluorescence at 610 nm increased substantially (Figure 5-7B), showing that the fluorescence at 610 nm from the heat shock sample was entirely due to PI addition. Thus, the top panel of the heat shock group provided a baseline measurement for HEK293 fluorescence at 610 nm when there were no fluorescent components added. Two concentrations of DOX were tested for 24 hours for this experiment – 1 μM was a concentration commonly used in cell culture, whereas 100 μM was used due to the visible red cell pellet at this DOX concentration. Figure 5-7C represents 1 μM DOX-treated cells without PI addition. As compared to Figure 5-7A, a clear

right-shift occurs, which should technically be interpreted as cell death. However, as PI has not yet been added, the only cause for this right-shift was auto-fluorescence from DOX. The shift is about one order of magnitude, with mean fluorescence shifting from ~3AU to ~30AU with 1 μM DOX addition. Figure 5-7D shows the same sample after 1% PI addition. Unlike the heat shock sample, the PI addition failed to cause any right-shift of the curve in Figure 5-7D. This provided evidence that there was actually no cytotoxicity, thus suggesting that DOX does not cause cell death in HEK293 cells. *Before* PI addition, 100 μM DOX, which produced a red cell pellet, resulted in surprisingly similar levels of fluorescence (~1,000 AU) to the heat shock group *after* PI addition (Figure 5-7E). Again, had the results been interpreted according to the initially established gating, it would be interpreted as nearly complete cell death in the sample. However, since PI has not yet been added, the conclusion must be made that the entirety of the signal can be attributed to DOX auto-fluorescence. As seen in Figure 5-7F, PI addition again does not change the location of fluorescence curve, replicating the 1 μM DOX result and strongly suggesting DOX is not cytotoxic to HEK293 cells.

Ultimately, it appears that interference between DOX auto-fluorescence and the PI signal occurs at low concentrations of DOX (~1 μM), and increases in a dose-dependent manner. This interference from DOX may cause misinterpretation of data in fluorescence assays. The emission spectra of DOX and PI, shown in Figure 5-6, demonstrate clear overlap. It should be noted that the current experimental conditions may cause a particularly large amount of fluorescent interference between DOX and PI. This is because the excitation laser used in this experiment was 488 nm, which occurs near the peak of the DOX excitation spectrum (Figure 5-6). The 488 nm laser was chosen in the current experiment since it was the most appropriate

laser available on the utilized flow cytometer to excite PI. However, this choice of laser may have amplified the extent of DOX autofluorescence.

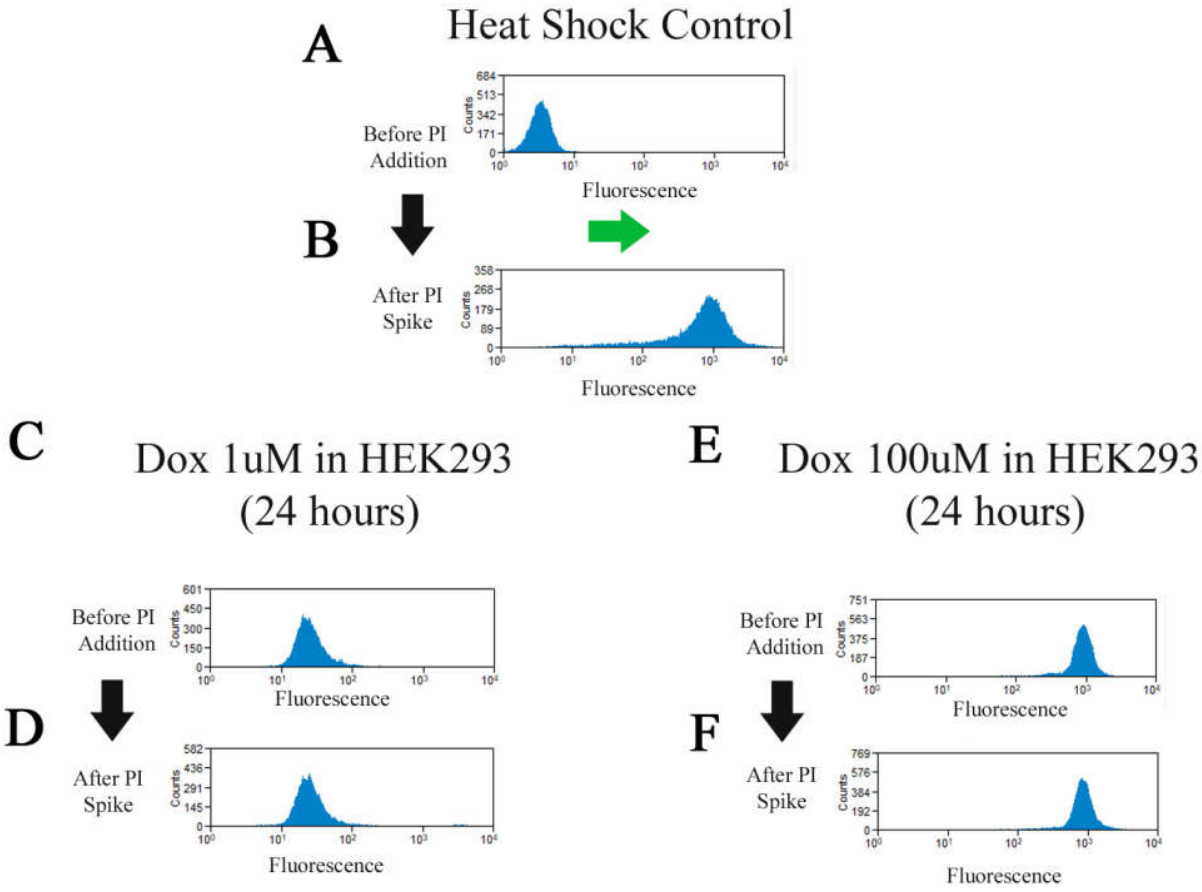


Figure 5-7: HEK293 cells are not susceptible to DOX

Flow cytometry was conducted in DOX-incubated and heat shock samples before and after addition of PI. (A), (C), and (E) represent fluorescence before addition of PI. As seen in (C) and (E), significant DOX auto-fluorescence occurs as compared to heat shock control. The heat shock sample has significantly increased fluorescence after adding PI, indicating uptake of PI (B, green arrow). In contrast, DOX-incubated HEK293 cells show no change in fluorescence after addition of PI (D, F), suggesting impermeable cell membranes and cell survival.

5.3.1.3.2 Confirmation that HEK293 not susceptible to DOX by Trypan Blue exclusion assay

A trypan blue exclusion assay was then undertaken to confirm the lack of cell death in DOX-treated HEK293 cells. Trypan blue is an azo dye that is utilized as a marker of late apoptosis and necrosis [308]. HEK293 cells were seeded at 1.5 x 10^5 cells/cm^2 in a 24 well plate and allowed to proliferate for 24 hours before DOX treatment. Duplicate wells were treated with DOX for 18 hours before being trypsinized, pelleted, and re-suspended in 100 µL media. 20 µL of 0.4% Trypan Blue solution (Sigma) was added to each sample. Percentage survival was assessed automatically using the Trypan Blue protocol of a Nexcelom Cellometer. Results, as shown in Figure 5-8, confirmed that there was no significant difference in survival rates between control cells and cells treated with various concentrations of DOX for 18 hours.

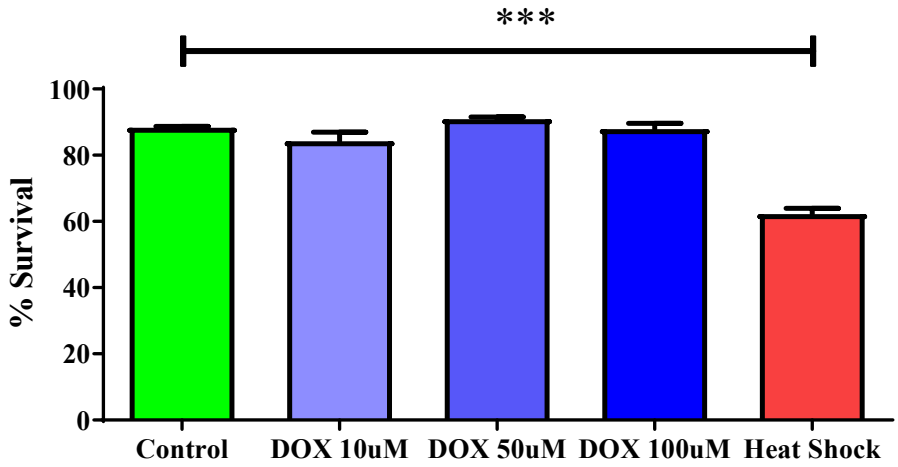


Figure 5-8: Trypan blue exclusion assay for DOX-treated HEK293 cells

HEK293 cells were treated with 10 µM, 50 µM and 100 µM DOX for 18 hours and subject to Trypan Blue staining to assess whether DOX treatment increased cell death. A heat shock sample was prepared by incubating cells at 95°C for 2 minutes, as a control for cell death. Results were analysed with one-way ANOVA with Bonferroni's post-hoc test, with all experimental groups compared to control. n = 4 for each group. (*** = $p < 0.001$).

Overall, the findings from the flow cytometry and the trypan blue assay demonstrated that DOX is not cytotoxic to HEK293 cells under the conditions tested. Thus, HL-1 cells, a cardiac muscle cell line, which maintained many functional and metabolic characteristics of adult cardiomyocytes, were used in the following experiments. Many studies have used the HL-1 cell line as a model to investigate DOX-induced cardiotoxicity [327,328].

5.3.2 Methods and Results II: Experiments in HL-1 cells

This section details experiments conducted to investigate whether overexpression of CK isoenzymes would protect against DOX cytotoxicity in HL-1 cells. First, experiments were conducted to optimize conditions in which DOX is moderately toxic to HL-1 cells. Second, chemicals were tested to identify a positive control that could rescue HL-1 cells from DOX cytotoxicity. Third, HL-1 cells were transiently transfected with CK isoenzyme vectors and transgene function was confirmed through qRT-PCR and CK activity assay. Finally, transfected HL-1 cells were tested for protection against DOX cytotoxicity.

5.3.2.1 HL-1 cell culture optimization

General cell culture techniques for HL-1 cells were discussed in Section 2.4. A search of the literature revealed only a single study utilizing stably transfected HL-1 cells [335], and previous experiments conducted by our group suggested that the HL-1 cell line could not integrate vectors in its genome. Thus, cells would need to be incubated with fresh vector during each experiment. In transfection experiments, cells were exposed to vectors 24 hours after seeding,

and incubated with the vector for an additional 24 hours for vector uptake before DOX treatment. Cells were then incubated with DOX for 48 hours before analysis by flow cytometry.

5.3.2.1.1 Confluency experiments

HL-1 cells were seeded at different densities to determine the appropriate cell density for subsequent experiments. Images were taken at 72 hours after seeding using a Nikon TE2000U microscope (Figure 5-9A). Cells were then washed with PBS, trypsinized, and re-suspended in 1% PI and Annexin V in 300 µL Annexin V binding buffer. After a 30-minute incubation period, cell viability was assessed with flow cytometry.

The cell density of 8 x 10^4 cells/cm^2 was used for experiments that had an overall incubation timeframe of 48-hours, as this density demonstrated the highest cell viability at 48 hours, of the conditions tested (Figure 5-9B). The density selected for 72-hour and 96- hour experiments (*i.e.* the finalized protocol (Section 5.3.2.6)) was 5 x 10^4 cells/cm^2.

The death gates were set using a similar strategy to HEK293 cell experiments: gates were set based on the population that was clearly healthy and alive. It should be noted that while death rates in the control group of HEK293 cell experiments were generally 5-10%, the death rates in the control group of HL-1 cell experiments were significantly higher (10-20%) and more variable. This could be attributed to (1) the longer incubation times used in HL-1 cell experiments, (2) the more delicate nature of HL-1 cells compared to HEK293 cells, and (3) additional mechanical force (*e.g.* scraping with pipette tip) required to detach HL-1 cells from well bottoms due to their attachment to the fibronectin/gelatin matrix during trypsinization.

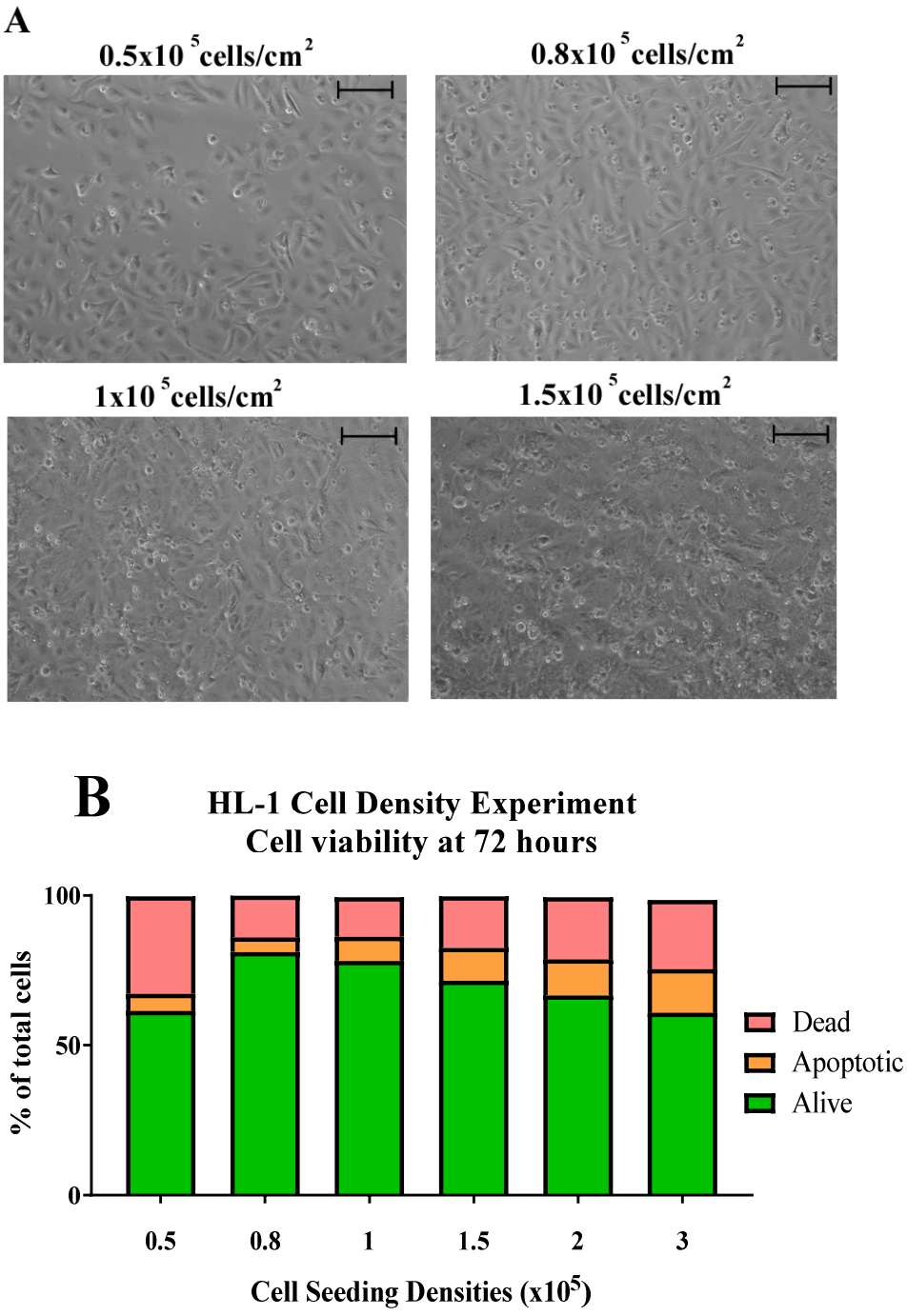


Figure 5-9: HL-1 cell proliferation experiments

Experiments to identify the optimal seeding density of HL-1 cells in 24 wells at 72 hours. (A) HL-1 cells were visualized by brightfield microscopy 72 hours after seeding, with results suggesting 0.8 x 10^5 cells/cm^2 was the optimal cell density. Scale bar: 100 µm. (B) Increased cell death at higher seeding densities, as determined by cell staining of Annexin V only (Apoptotic) and PI + Annexin V (Dead). n = 3 wells per group.

5.3.2.2 Optimization of DOX incubation conditions

5.3.2.2.1 PI and Annexin V

Experiments in HEK293 cells had demonstrated that DOX and PI had interference from overlapping emission spectrums, and thus an alternative marker for cell death was needed. While assessing alternative markers, a pilot experiment was conducted in HL-1 cells using PI and Annexin V to measure DOX cytotoxicity.

As shown in Figure 5-10, 24 hours of DOX treatment at 250 nM and 1 µM produced a distinct population of HL-1 cells that had high Annexin V and low PI staining (R10), suggesting an early stage of apoptosis. This distinct population was absent in a similar experiment conducted in HEK293 cells (Figure 5-10A, B). This result indicated that DOX was likely cytotoxic to HL-1 cells.

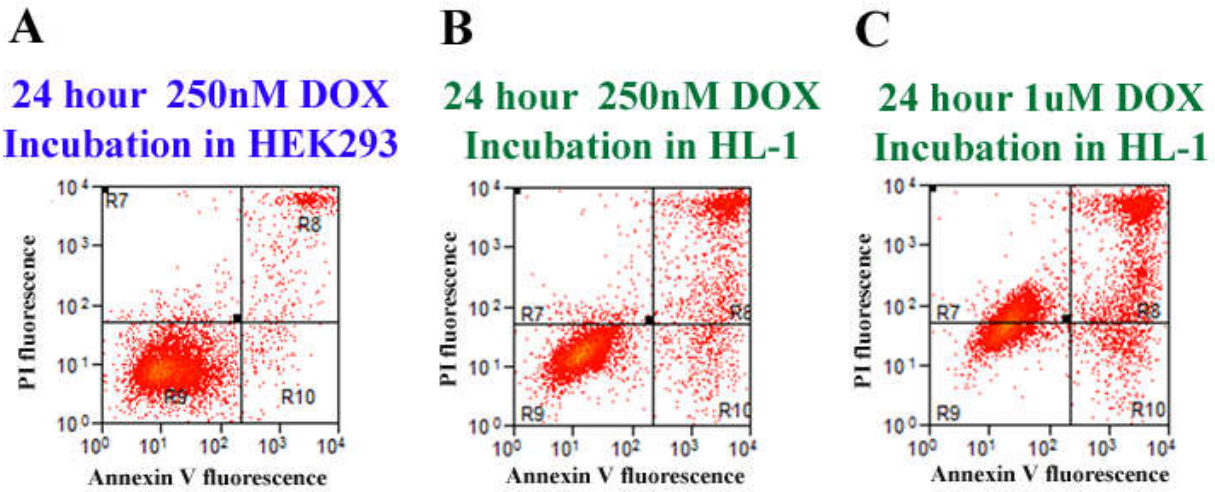


Figure 5-10: Comparison of responses to DOX in HEK 293 and HL-1 cells

(A) Experiments in HEK293 cells treated with DOX failed to produce an apoptotic cell population (R10). (B, C) Experiments in HL-1 cells treated with DOX exhibited an apoptotic cell population as seen in R10.

5.3.2.2.2 Use of Violet Live/Dead stain for measuring cell death

An alternative live/dead marker was needed to measure true cell death, as Annexin V cannot differentiate between early, reversible apoptosis and outright cell death. Violet Live/Dead Dye (Thermo Scientific) was selected for subsequent experiments as it absorbs light at 416 nm, and emits at 451 nm, and thus would not interfere with DOX auto-fluorescent emission at 580 nm [333,336]. This also did not interfere with Annexin V, which excites at 488 nm and emits at 525 nm [330]. Violet Live/Dead dye was used to measure irreversible cellular damage and cell death, and consists of a proprietary compound that reacts with free amines. With live cells, the dye stains weakly as it only reacts with plasma membrane amines; however, the permeable membrane of irreversibly damaged cells allows the dye to react with intracellular amines, thus staining with over 100-fold higher intensity and signifying cell death [334]. Another advantage of the dye was that it did not require a separate binding buffer as experiments showed it could be added to Annexin V binding buffer without interference. A serial dilution experiment was then conducted to optimize the concentration for Violet Live/Dead, which was ultimately diluted 50-fold compared to manufacturer's instructions. As Annexin V and the Violet Live/Dead dye had minimally overlapping emission spectra, only minimal fluorescent compensation was required.

5.3.2.2.3 Optimizing DOX concentrations and incubation times

DOX treatment needed to be optimized for concentration and duration. Existing studies reported that 100 nM DOX reduced intracellular creatine transport into HL-1 cells following 24 hours treatment [327]. DOX cytotoxicity in HL-1 cells at 24 hours occurred between 0.5 μM [337] and 1.5 μM [328]. Further experiments with 48-hour incubation periods produced

significant cytotoxicity between 0.6 μM and 2.5 μM DOX [338]. It should be noted that the maximum plasma concentration achieved in patients is 1-2 μM DOX, which rapidly falls to ~250 nM within 1-2 hours [293]. It has also been suggested that DOX experiments in cell culture should not exceed 1-2 μM as these concentrations were the maximum levels that would be achieved physiologically [291,293]. Therefore, based on these findings, initial optimization experiments tested 250 nM and 1 μM DOX at 24- and 48-hour incubation times.

Cells were seeded at 0.8 x 10^5 cells/cm^2 (24-hour DOX treatment) or 0.5 x 10^5 cells/cm^2 (48-hour DOX treatment) in a 24-well plate for 24 hours. Triplicate wells were then treated with 250 nM and 1 μM DOX, or 175 nM Staurosporine. Staurosporine was utilized as a control for cell death until DOX incubation conditions had been optimized. Cells were then washed, trypsinized, and re-suspended in 500 μL Annexin V binding buffer with 5% Annexin V and 1% 50x diluted Violet Live/Dead dye, and cell viability was analysed by flow cytometry.

As shown in Figure 5-11, DOX produced concentration-, and duration-dependent cell death. At 250 nM, DOX resulted in 15% and 42% cell death following 24- or 48-hour treatment, respectively, which increased to 20% and 70% with 1 μM DOX treatment for 24 and 48 hours, respectively. The low death rates at DOX concentrations of 250 nM or 1 μM at 24 hours treatment provided a too narrow window to discern any protective effect of overexpression of CK in future experiments. Of the four death rates available (15%, 20%, 42%, and 70%), the 42% option (250 nM DOX for 48 hours) was chosen, because it was a moderate toxicity that offered potential for rescue by CK overexpression. This incubation strategy was used in subsequent experiments.

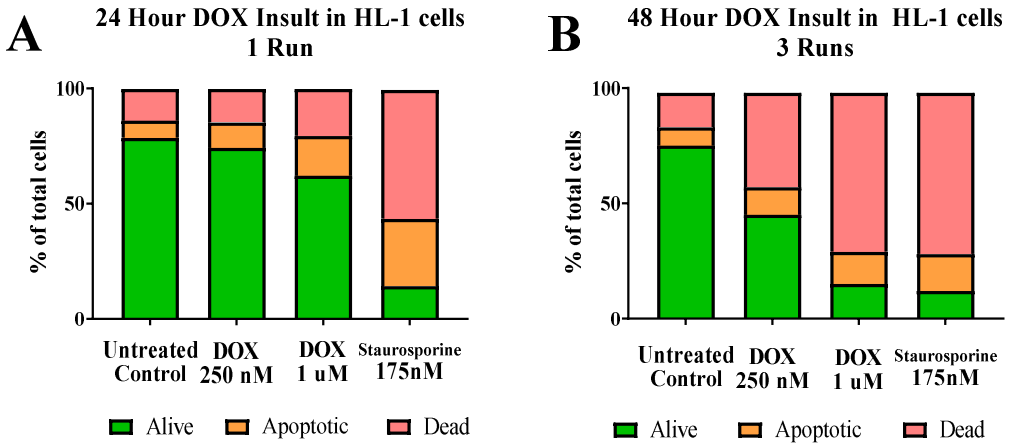


Figure 5-11: Optimization of DOX concentrations and treatment times in HL-1 cells

Cell viability in HL-1 cell treated with 250 nM or 1 μM of DOX or 175 nM of staurosporine for 24 or 48 hours. (A) Cell viability in HL-1 cells treated for 24 hours (1 run; n = 3 wells/run). (B) Cell viability in HL-1 cells treated for 48 hours (3 runs; n = 3 wells/run). Staurosporine is a chemical that is cytotoxic to HL-1 cells, and was included as a control for cell death.

5.3.2.3 Identifying positive controls

After optimizing the aforementioned conditions, a positive control that could rescue from DOX induced cytotoxicity was identified. Four candidates were considered as potential positive controls: Trolox, Dexrazoxane, Metformin, and Visnagin. Of these compounds, dexrazoxane is the only drug approved for clinical use.

5.3.2.3.1 Introduction to tested compounds

Dexrazoxane

Dexrazoxane (DEX) is an EDTA derivative and an iron chelator that binds free iron in cells. DEX is able to reduce DOX-induced ROS generation by scavenging free cellular iron, preventing formation of hydroxyl free radicals. Its protective value against DOX cardiotoxicity has been demonstrated in cell culture [339], *in vitro* rat models [340], and patients

[307,341,342]. DEX was a particularly compelling positive control candidate because of its clinical application and specific protection of mitochondria. For instance, in rats, DEX rescued DOX toxicity by reducing ROS damage at mitochondria and protected against the loss of mitochondrial DNA [340]. Indeed, it has been suggested that DEX is uniquely successful at protecting against DOX because of its ability to chelate mitochondrial free iron [308]. In contrast, other iron chelators (*e.g.* desferoxamine) have failed as they only target cytosolic free iron. DEX also decreases DOX-induced lipid peroxidation at the mitochondrial membrane [340].

Metformin and Visnagin

Metformin, a biguanide agent, is used to treat Type 2 diabetes. Metformin reduces DOX-induced cardiotoxicity, possibly by reducing cellular ROS generation through AMPK pathway activation and increased gene expression of the ferritin heavy chain [343-345]. In HL-1 cells, 24-hour pre-treatment with 4 mM metformin produced ~40% reduction in cell death in cells treated with 5 μM DOX for 24 hours [346].

Visnagin is an organic compound derived from the *ammi visnaga* plant, and has been used to relieve pain associated with urinary tract infections and kidney stones [347]. A high-throughput screening model demonstrated that Visnagin rescued cardiac function from DOX toxicity in a zebrafish model [348]. Visnagin protected against DOX-induced cytotoxicity in HL-1 cells in a dose-dependent manner. The death rate of HL-1 cells treated with 1 μM DOX was reduced by ~50% at 10 μM Visnagin and 70% at 50 μM Visnagin [348].

Trolox

Trolox (6-hydroxy-2,5,7,8-tetramethylchroman-2-carboxylic acid) is a water-soluble analogue of Vitamin E (Figure 5-12), and similarly to Vitamin E, acts as an antioxidant to reduce cellular toxicity from ROS. Vitamin E has been previously suggested to have a protective role in doxorubicin toxicity *in vivo* in mice [349] and rabbit [350]. Trolox has stronger antioxidant capacity than Vitamin E [351,352], and has been shown to reduce ROS-induced cell death *in vitro*, including in cardiomyocytes [353,354]. Furthermore, it protects against oxidative damage and improves contractile recovery during ischemia/reperfusion injury in *ex vivo* and *in vitro* rat models [355,356], possibly by decreasing lipid peroxidation [356]. As an antioxidant, Trolox can prevent the Fenton reaction and subsequent ROS generation, thus inhibiting a key pathway associated with DOX-induced cardiotoxicity. Our group and others had also demonstrated that Trolox protected against oxidative stress in HL-1 cells [2,357], suggesting it could protect against DOX-induced cardiotoxicity in the current experiment.

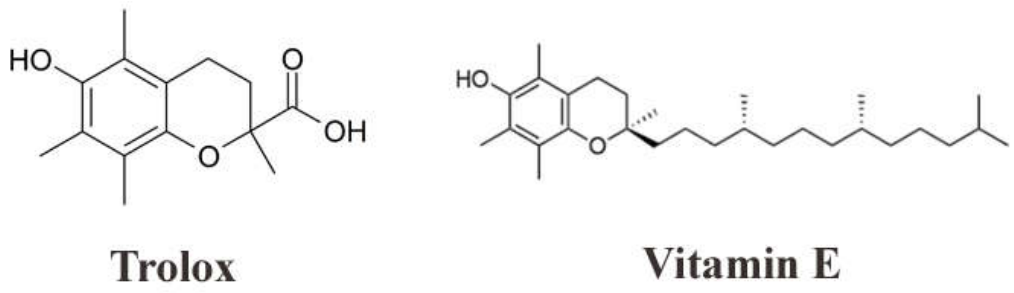


Figure 5-12: Structures of Trolox and vitamin E

5.3.2.3.2 Dexrazoxane does not rescue HL-1 cells from DOX-induced cytotoxicity

A prototype experiment was conducted to test appropriate concentrations of DEX for rescuing from DOX toxicity. Published data suggested that 50 μM DEX shows a protective effect when HL-1 cells were incubated with 500 nM -1 μM DOX for 24 hours [337]. Dexrazoxane HCl (Sigma) was dissolved in DMSO to make a 20 mM stock solution. HL-1 cells were seeded at 0.5 x 10^5 cells/cm^2 in a 24 well plate, and incubated for 24 hours. Triplicate wells were then assigned to the groups as indicated in Figure 5-13, and DEX (50 μM) and DOX (250 nM) were added to appropriate wells for 48 hours before analysis by flow cytometry.

The aims of this experiment were 1) to ensure that 50 μM DEX was non-toxic in HL-1 cells, and 2) to verify whether DEX protected against DOX cytotoxicity in HL-1 cells. Results (Figure 5-13) suggested that 50 μM DEX was toxic to HL-1 cells with a lower survival rate of 46% compared to the 84% survival rate in untreated cells ($p < 0.0001$). Although 50 μM DEX significantly improved cell survival rate in cells treated with 250 nM DOX (58 ± 1% vs. 38 ± 1% in the DOX only group; $p < 0.001$), the protective benefit of DEX in DOX treated cells appeared to be limited by the threshold for the toxic effects of DEX itself.

The initial experiment demonstrated that the DEX concentration needed to be optimized. Furthermore, it was unclear whether the cell death noted in the DEX-only group was caused by DEX itself or the DMSO solvent, which is known to be toxic to cell culture, including the HL-1 cell line. Previous study using DMSO-dissolved DEX in HL-1 cells limited the DMSO concentration in media to 0.1% [337]. In contrast, the experiment shown in Figure 5-13 had 0.25% DMSO for the 50 μM DEX groups. Thus, future DEX groups were tested using DMSO as a vehicle control to differentiate the toxic effects of DEX and DMSO.

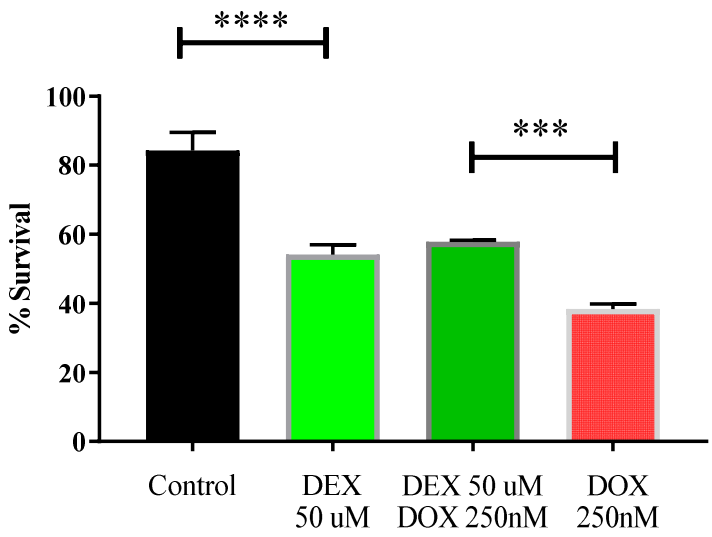


Figure 5-13: DEX protection in cells treated with 48-hour DOX treatment

DEX at 50 µM protects against DOX cytotoxicity in HL-1 cells, however, this concentration itself is toxic to HL-1 cells. Results were analysed with one-way ANOVA with Bonferroni's post-hoc test. n = 3 per group (*** = $p < 0.001$; **** = $p < 0.0001$)

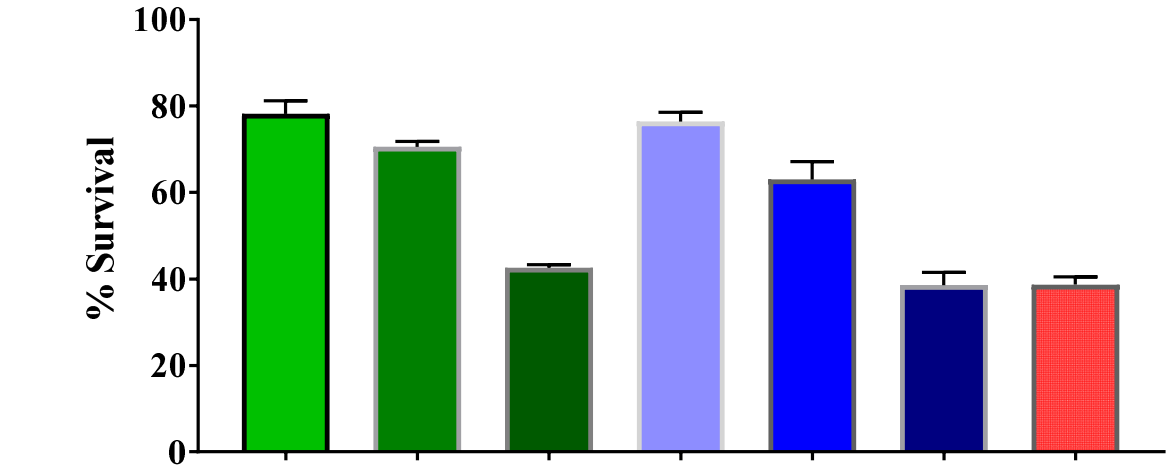
The literature did not suggest that DEX could be toxic to HL-1 cells. One study suggested that when DEX is co-incubated with DOX in HL-1 cells, DEX had an additive cytotoxic effect on DOX-induced cell death [358], though whether DEX treatment alone caused HL-1 cell cytotoxicity was not reported. To determine the maximum sub-lethal concentration, various DEX concentrations (1, 10, and 50 µM) were evaluated. Furthermore, in clinical practice, DEX in prevention and treatment of DOX-induced cardiotoxicity generally involved pre-treatment in patients with DEX before DOX administration [359], hence the protective potential of pre-treatment in HL-1 cells prior to DOX incubation were also assessed. To clarify between different treatment options, "pre-treatment", as subsequently mentioned, refers to addition of the tested positive control (*e.g.* DEX,) in the media used to seed the cells for 24 hours. However, when this media is replaced with DOX-infused media (after the 24-hour seeding step), the tested

positive control was no longer included for the 48 hour DOX-incubation period. In contrast, "co-treatment", as subsequently used, refers to addition of the tested positive control only with the DOX-infused media (for 48 hours), and not during the initial 24-hour seeding step.

Therefore, a subsequent experiment was undertaken to maximize the DEX dosage that HL-1 cells could tolerate without significant cytotoxicity. It was found (data not shown) that the maximum tolerated DEX dosages were 1 μM for 48 hours ("co-treatment" option) and 50 μM for 3 hours ("pre-treatment" option). Experiments (data not shown) also demonstrated that the cytotoxicity noted in Figure 5-13 was entirely attributed to DEX, and that the DMSO concentrations utilized were not cytotoxic.

An experiment was then conducted to determine whether the optimized DEX treatment strategies could protect against DOX cytotoxicity. Cells were seeded in plates as previously described, and the experimental groups are detailed in Figure 5-14.

The survival rates were 39% in the 3-hour pre-treatment group (50 μM DEX + 250 nM DOX) and 43% in the 24-hour co-treatment group (1 μM DEX + 250 nM DOX). Neither of these survival rates were significantly different from the DOX-only treated group, which exhibited 39% cell viability ($p>0.05$). Therefore, the results suggested that sub-lethal DEX dosages did not protect HL-1 cells against DOX toxicity. Further attempts were made to optimize DEX conditions (*e.g.* 72-hour incubation periods), but no results supported the hypothesis that DEX protected against the DOX dosage (250 nM for 48 hours) that had been optimized for HL-1 cells in the current experiment.



DMSO	0.5 µL	0.5 µL	0.5 µL	2.5 µL	2.5 µL	2.5 µL	-
DEX Strategy	-	Co-treatment	Co-treatment	-	Pre-treatment	Pre-treatment	-
DEX Concentration	-	1 µM	1 µM	-	50 µM	50 µM	-
DOX (250 nM)	-	-	+	-	-	+	+

Figure 5-14: Optimized DEX conditions do not protect against DOX toxicity in HL-1 cells

The effects of pre-treatment and co-treatment with DEX on survival in HL-1 cells treated with DOX. For the "co-treatment" group, 1 µM DEX was incubated with 250 nM DOX for 48 hours before analysis by flow cytometry. For the "pre-treatment" group, HL-1 cells were incubated with 50 µM DEX, 21 hours after seeding. After a 3-hour incubation period, DEX media was removed from wells, and new media containing 250 nM DOX was added to the wells for 48 hours before analysis by flow cytometry. Results were analysed with one-way ANOVA with Bonferroni's post-hoc test, with no significant difference in survival rate between the three DOX-treated groups. n = 3 wells per group.

5.3.2.3.3 Metformin and Visnagin do not protect against DOX induced cytotoxicity

The literature suggested that 1-5 mM metformin protected against DOX-induced cytotoxicity [344,346]. Thus, these concentrations were tested in the current experiment. There was no need to test a vehicle, as metformin was soluble in water. As shown in Figure 5-15, metformin failed to protect against DOX-induced cardiotoxicity in any of the conditions tested (1-5 mM metformin for 48-hour co-incubation with 250 nM DOX).

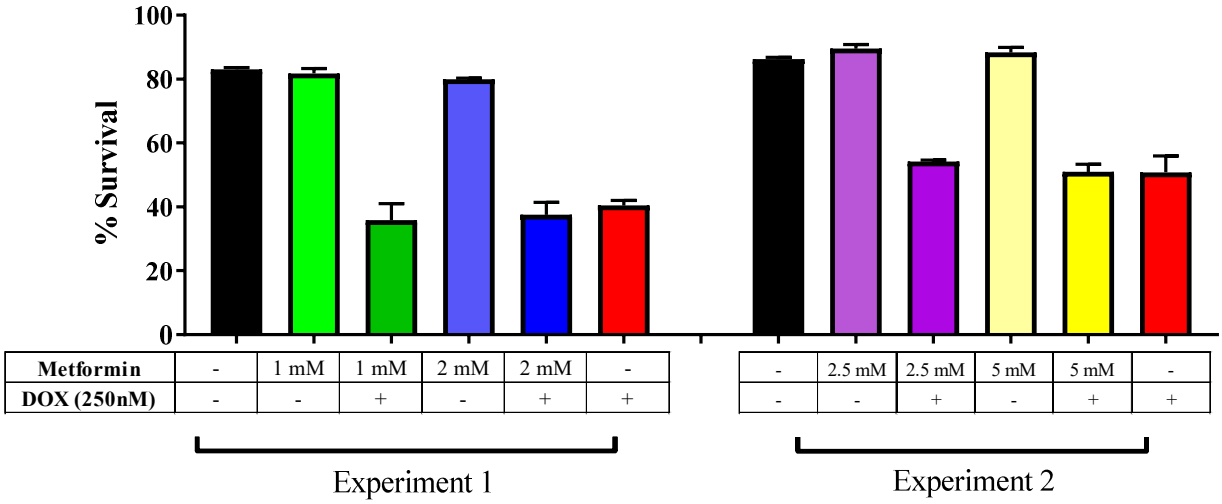


Figure 5-15: Metformin does not protect against DOX cytotoxicity in HL-1 cells

Various treatment strategies showed that metformin does not protect against DOX cytotoxicity in HL-1 cells. Results were analysed with one-way ANOVA with Bonferroni's post-hoc test for Metformin/DOX group against DOX-only treated cells. n = 3 wells per group

Visnagen was tested at concentrations (25 µM and 50 µM) similar to those used in the previous experiment demonstrating its protective effect against DOX [348], with the established DOX treatment strategy (250 nM DOX for 48 hours) and testing protocol. 51% of the cells survived in the DOX-only group; 48-hour co-treatment of Visnagen with DOX demonstrated 54% and

53% survival, respectively (Figure 5-16), which were not significantly different from the DOX-only group ($p > 0.05$). Additional experiments (data not shown) were conducted with both metformin and Visnagin involving pre-incubation, co-incubation, or both, though no incubation strategies that produced a beneficial effect could be identified.

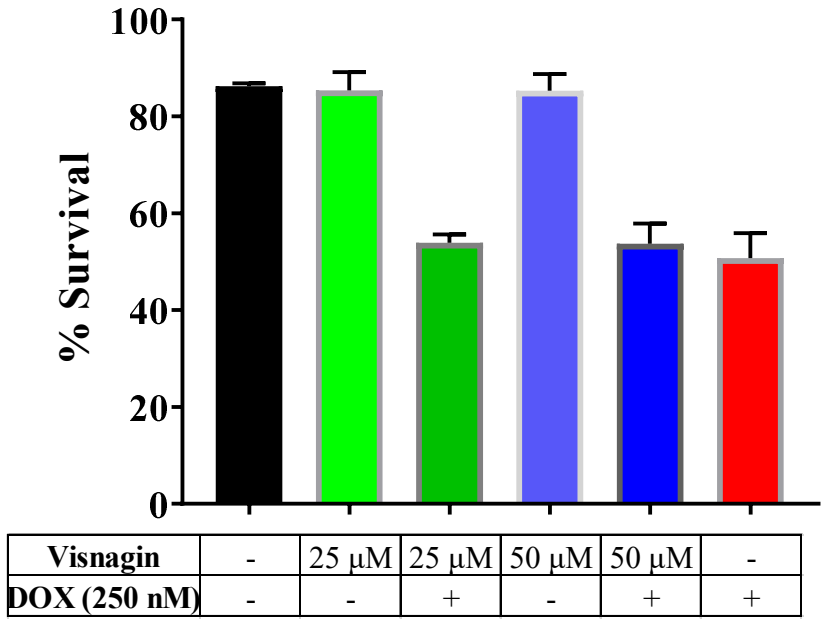


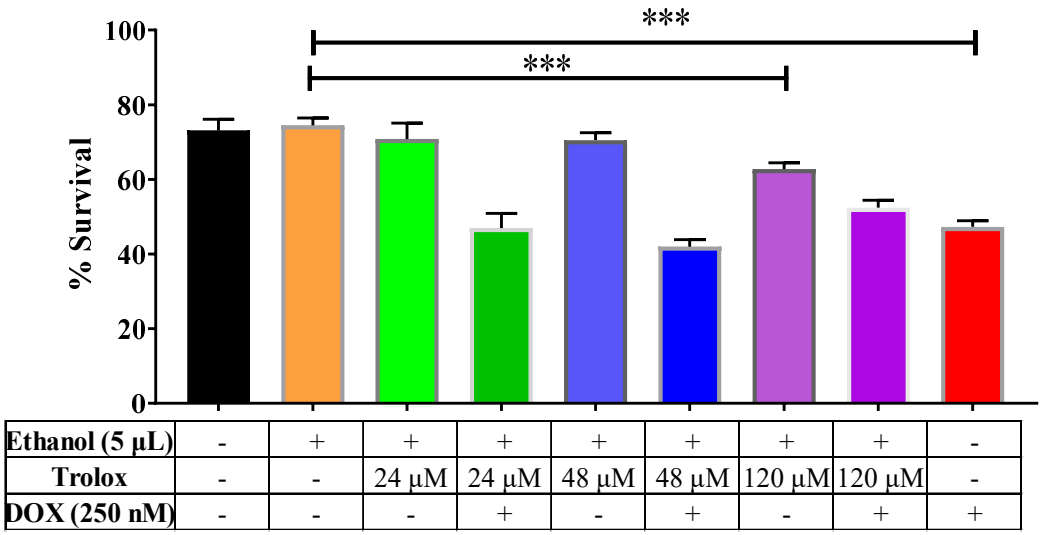
Figure 5-16: Visnagin does not protect against DOX cytotoxicity in HL-1 cells

Various treatment strategies with Visnagin failed to show protection against DOX cytotoxicity. Results were analysed with one-way ANOVA with Bonferroni's post-hoc test for Visnagin-treated group against DOX-only treated cells. n = 3 wells per group

5.3.2.3.4 Trolox protects against DOX induced cytotoxicity

Two pilot experiments were conducted to identify the effective concentrations and treatment durations for Trolox protection against DOX. Our lab had utilized 24 μM Trolox in previous HL-1 cell experiments, which was used as the baseline in the current experiment. In the first experiment, cells were seeded at 0.5 x 10^5 cells/cm^2, and 24 hours later, Trolox at 24, 48, or 120 μM were added to the cells, which were co-incubated with or without 250 nM DOX in triplicate wells. Triplicate wells were treated with medium containing 0.5% ethanol as a vehicle control for Trolox. The cells were then incubated with treatments for 48 hours before analysis by flow cytometry, and the results were shown in Figure 5-17.

The data suggested that Trolox at 24 μM and 48 μM were not toxic to HL-1 cells (75%, 73%, and 70% cell survival for control, 24 μM and 48 μM Trolox groups, respectively; $p > 0.05$). However, Trolox at 120 μM appeared to represent a dose limit with 63% survival ($p < 0.001$, compared to control). The survival rate in the ethanol vehicle (75%) was not significantly different from the survival rate in the untreated control (70%; $p > 0.05$). The survival rates of cells treated with DOX and Trolox were 44%, 42%, and 52% for the 24 μM, 48 μM, and 120 μM Trolox groups, respectively, which were not significantly different from the 47% survival rate in DOX treated cells ($p > 0.05$). Thus, the tested concentrations of Trolox did not protect against DOX cytotoxicity in HL-1 cells.



Ethanol (5 µL)	-	+	+	+	+	+	+	+	-
Trolox	-	-	24 µM	24 µM	48 µM	48 µM	120 µM	120 µM	-
DOX (250 nM)	-	-	-	+	-	+	-	+	+

Figure 5-17: Optimization of Trolox concentrations in HL-1 cells with 48 hour treatment

HL-1 cells were treated with 24, 48, or 120 µM Trolox in the presence or absence of 250 nM DOX for 48 hours. Trolox at tested concentrations did not protect HL-1 cells from DOX-induced cytotoxicity; however, 120 µM Trolox was found to be toxic to HL-1 cells. Results were analysed with one-way ANOVA with Bonferroni's post-hoc test (*** = $p < 0.0001$). n = 3 wells per group.

A second experiment was conducted to test whether prolonged Trolox treatment (simultaneous pre-treatment and co-treatment) would improve outcomes. Cells were co-incubated with 24 or 48 µM Trolox for 24 hours prior to DOX treatment ("pre-treatment"). After a 24-hour pre-treatment, fresh media with 24 or 48 µM Trolox and with/without DOX was added to the cell culture for additional 48-hour incubation (total 72 hour Trolox treatment). Cells were then trypsinized and analysed by flow cytometry.

As shown in Figure 5-18, Trolox increased cell survival rates with the prolonged incubation period. 72-hour incubation with Trolox at 48 µM improved cell survival in cells treated with DOX to 79%, compared to 64% in DOX-only cells ($p < 0.001$). Thus, Trolox at 48 µM served as a positive control for subsequent experiments using the experimental protocol described above.

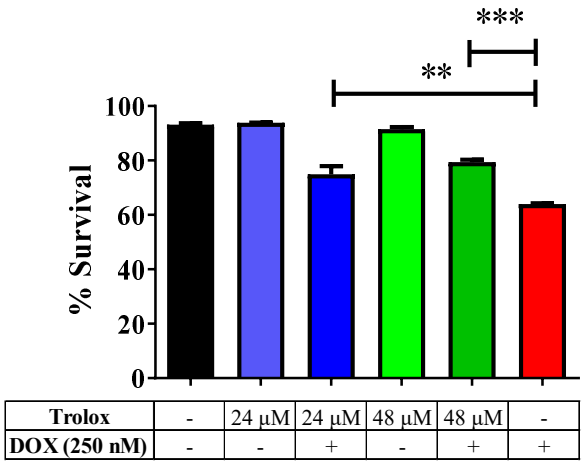


Figure 5-18: 72-hour Trolox treatment protects against DOX-induced cytotoxicity in HL-1 cells

HL-1 cells were pre-treated with 24, or 48 µM Trolox for 24 hours. Following the 24 hours pre-treatment, HL-1 cells were then treated with 250 nM DOX with/without 24 or 48 µM Trolox for an additional 48 hours. Trolox produced significantly higher cell survival. Significance was calculated with One-Way ANOVA with Bonferroni's post-hoc test (** $p < 0.01$; *** $p < 0.001$). n = 3 wells per group.

5.3.2.4 Confirmation of transient transfection in HL-1 cells with CK overexpression vectors

After incubation conditions had been optimized and a positive control had been identified, the next step was to confirm that CK-overexpression vectors could be successfully transfected into HL-1 cells. Our group had previously optimized a transient transfection protocol for HL-1 cells using Fugene HD 6 (Promega, UK); protocol details can be found in Section 2.5. Briefly, cells were seeded for 24 hours and subsequently incubated with CK overexpression vectors in transfection media for an additional 24 hours. Cells were then collected and tested for transfection success and efficiency.

Four experimental groups were used to confirm successful transfection. The sham transfected group was incubated in transfection media, but with no vector. The pcDNA 3.1(-) group was

transfected with the empty pcDNA 3.1 vector cassette, which was the cassette used for the CK-OE transgenes. The CK-Mt OE group was transfected with the CK-Mt overexpression vector that was utilized in subsequent experiments. The results of the HL-1 section of this study were published, thus the vector maps can be found in [176]. Finally, the CK-Mt + GFP group was transfected with two vectors, containing both the CK-Mt overexpression vector, as well as the GFP vector. The purpose of this group was to have visual confirmation that the transfection protocol was successful through observation of GFP fluorescence in cells by epifluorescence microscopy. The CK-Mt OE and GFP vector maps are depicted in Figure 5-19.

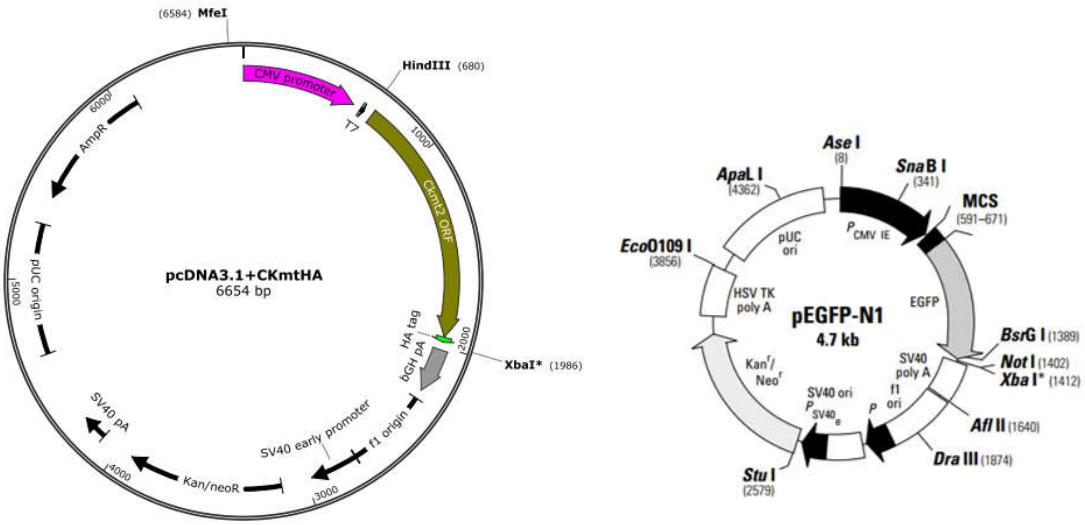


Figure 5-19: CK-Mt OE vector and GFP vector maps

CK-Mt OE vector presents CMV promoter region, and CK-Mt open reading frame. GFP vector map was obtained from manufacturer's documentation (Clontech).

Cells transfected with the CK-Mt OE and GFP vectors allowed visualization of successful transfection via confocal microscopy, as shown in Figure 5-20. In addition, RNA was isolated from transfected cells and transfection was verified by qRT-PCR analysis (Section 2.6). The primers used for qRT-PCR are shown in Table 5-1 and were designed by Dr Philip Ostrowski. Transgene mRNA was quantified as a ratio of reference gene Polr2A. The results, shown in Figure 5-21, suggest successful transfection in both the CK-Mt group as well as the CK-Mt + GFP group.

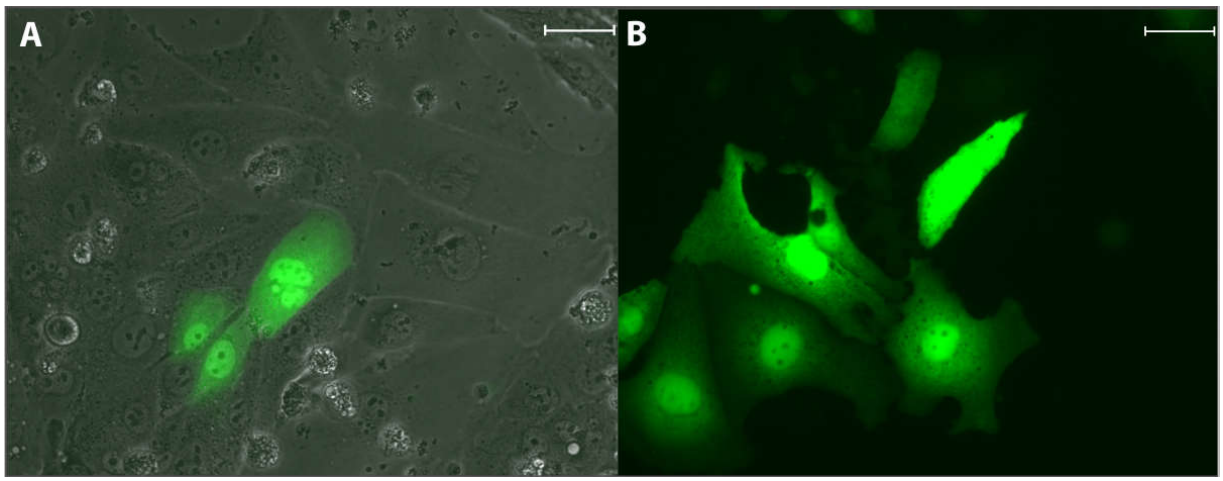


Figure 5-20: Confirmation of transfection technique in HL-1 cells

Confirmation of transfection of the GFP vector in HL-1 cells. (A) Brightfield and confocal images of transfected cells merged, demonstrating GFP vector protein expression. (B) Confocal image of a cluster of transfected cells. Scale bars 50 μm.

Table 5-1: Primers for CK transfection experiments in HL-1 cells

Transgenes	Primer names	Primer sequences
CK-Mt	Ckmt2_ex9-10_F	5' – TCGGCAGATCAGAGGTTGAG-3'
	Ckmt2_ex9-10_R	5' –ACTTCCTGCCAAACTGAGGCA -3'
Polr2A Control mRNA	Polr2a_F cDNA	5'- TGTGCAGGAAACATGACCGA -3'
	Polr2a_R cDNA	5'- GAAGCAGACACAGCGCAAAA -3'

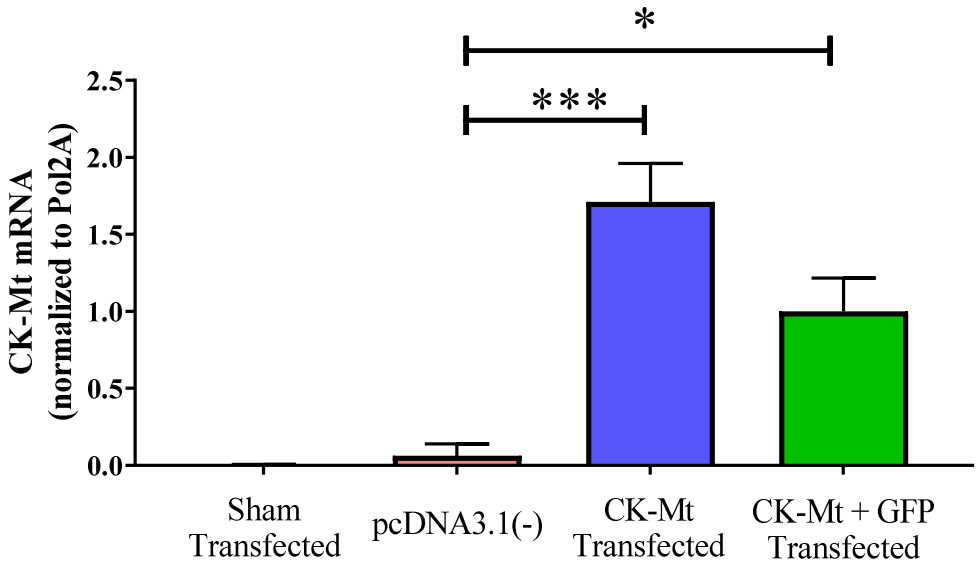


Figure 5-21: CK mRNA expression in transfected HL-1 Cells

CK-Mt mRNA in transiently transfected HL-1 cells was verified by qRT-PCR. Results were analysed by one-way ANOVA with Bonferroni's post-hoc test (* = $p < 0.05$; *** = $p < 0.001$). $n = 3$ wells per group.

5.3.2.5 Transfection and verification of transfected cells

5.3.2.5.1 Transgenic Vectors for CK

Transgenic vectors utilized in this experiment were previously generated and verified by Dr Philip Ostrowski. *Mus Musculus* cDNA of each isoenzyme (CK-Mt, CK-B, CK-M) was inserted into a pcDNA3.1 vector (Invitrogen, UK), along with a HA tag for protein detection purposes. The pcDNA3.1 vector contained a cytomegalovirus promoter-enhancer (P_{CMV}), which drives constitutive expression of the inserted transgene in mammalian cells. Previously, vectors were amplified in competent *E. Coli*, and plasmid DNA was extracted using Maxiprep kits (QIAGEN). The extracted plasmid DNA was subsequently verified by restriction enzyme digest, and verified vector was then used in transient transfection in HL-1 experiments. Previous attempts to generate a stably transfected HL-1 cells using these vectors had not succeeded despite optimizations, hence transient transfection was used for transgene expression in the current experiment.

5.3.2.5.2 HL-1 cell transfection and verification

The CK activity of transfected HL-1 cells was measured by the CK activity assay, as described in Section 2.3.3. Triplicate wells of HL-1 cells were seeded and transfected with all three CK transgenes using the Fugene HD 6 transfection system as detailed in Section 2.5.1. After transfection, cells were trypsinized and prepared for the CK activity assay. The results as shown in Figure 5-22 demonstrated that transfected cells had an isoform-specific increase in CK activity. Compared to pcDNA3.1(-) transfected cells, CK-Mt activity increased 88% in CK-Mt transfected cells and CK-MM activity increased 77% in CK-M transfected cells. In CK-B transfected cells, CK-MB activity increased 74% and CK-BB activity increased 3-fold

compared to that of pcDNA3.1(-) transfected cells. Total CK activity was significantly increased in CK-M OE cells by 33% compared to CK activity in pcDNA3.1(-) transfected cells ($p < 0.01$). CK-Mt and CK-B transfected cells exhibited 8% and 18% higher total CK activity, which were not significant compared to pcDNA3.1(-). These results demonstrated successful transgene expression as well as an appropriate isoenzyme-specific increase in CK activity. Our group had previously confirmed CK-Mt localization in mitochondria by co-localization with mitochondria marker COXIV using immunocytochemistry, as seen in [176], hence it was not repeated in the current study.

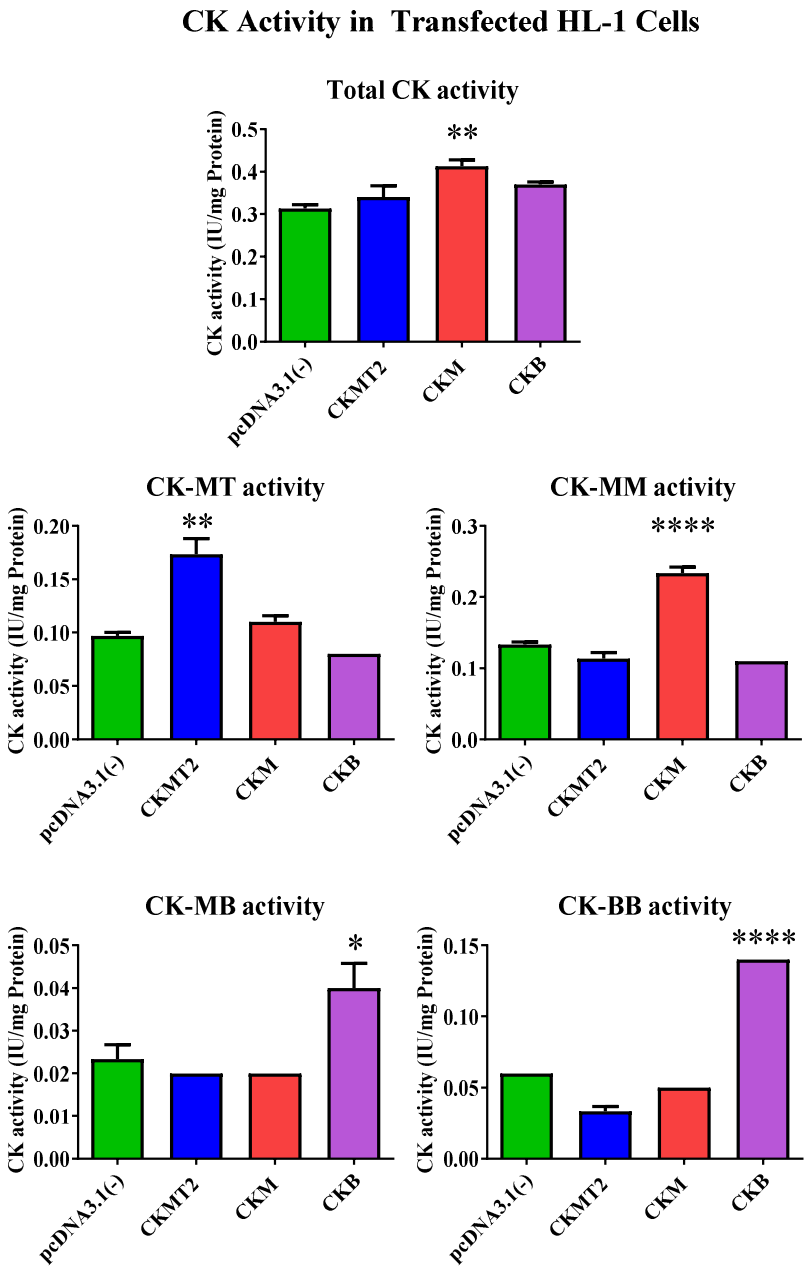


Figure 5-22: Increased total CK and CK isoenzyme activity in CK-transfected HL-1 cells

CK isoenzyme activity at 48 hours after transfection of pcDNA3.1(-), or pcDNA3.1(-)-CK vectors. Each bar in the x-axis for each graph represents a different transfected group (*e.g.* Green bars = pcDNA3.1(-) transfected cells), and Y-axis represents CK activity. SAS isoenzyme electrophoresis was used to determine CK subunit specific enzyme activity. n=3 assays per group. One-way ANOVA with Bonferroni's post-hoc test; compared to pcDNA3.1(-) transfected cells (*= p <0.05, **= p <0.01, ***= p <0.001, ****= p < 0.0001).

5.3.2.6 Evaluation of protective effects of CK overexpression on DOX cytotoxicity in transfected HL-1 cells

After optimization of all experimental variables, the final experiment could be conducted to determine whether CK overexpression protected against DOX induced cytotoxicity. The below table (Table 5-2) shows the optimized final protocol used to evaluate the protective function of CK overexpression against DOX cytotoxicity in HL-1 cells. The HL-1 cells used for these experiments were passage #54-57.

Table 5-2: Optimized final protocol for investigation of CK or creatine in protection against DOX cytotoxicity in HL-1 cells transfected with CK

Day 1	Day 2	Day 3	Day 4	Day 5
Cells seeded	Cells transfected	DOX added	Incubation	Flow cytometry analysis
	Trolox Added	Trolox refreshed		
	Creatine Added	Creatine refreshed		

5.3.2.6.1 Creatine loading

Previously, it was demonstrated that CrT overexpression had a protective effect against DOX cytotoxicity only if cells were preloaded with creatine [328]. It is possible that additional creatine substrate was required to maximize the potential protection of CK enzyme overexpression, as it has been suggested that the potential cardioprotective effects of CK enzyme and substrate may be synergistic [289], and therefore should be augmented simultaneously. Thus, a separate experimental group was included for each transgenic vector, in which cells were incubated with 250 μM creatine and DOX, with the purpose of exploring whether simultaneous CK enzyme/substrate augmentation produced greater protection against DOX insult than CK enzyme augmentation alone. Optimization of creatine concentration was not required, as previous experiments in HL-1 cells by our group had demonstrated that 250 μM-10 mM creatine had no difference in protection against H_2O_2 induced toxicity [2], hence

250 μM concentration was chosen, as higher concentrations carried the risk of causing downregulation of the creatine transporter, as discussed in Section 1.7.1.5. Co-transfection with creatine transporter was not necessary as HL-1 cells endogenously express creatine transporter [327].

It should be noted that creatine was not tested without CK overexpression (*i.e.* with EV-transfected cells) for two reasons. First, the effects of creatine itself on DOX-induced cytotoxicity has previously been explored in detail [328]. Second, the goal of creatine loading in the current study was to assess whether substrate supplementation enhanced any protective effect observed with CK enzyme over-expression. For the experiment, on day 2, 250 μM creatine was added to fresh media to three of six DOX-treated samples for each of the three transgenic groups. These samples had their creatine refreshed in new media on day 3.

5.3.2.6.2 Positive control and DOX

Positive control samples were treated with 48 μM Trolox on day 2, and fresh Trolox/media was added on day 3. For all DOX treated samples, 250 nM of DOX was added on day 3, with cell viability assessed by flow cytometry on day 5. Viable cells were defined as cells that stained negative for Annexin V and Thermo Scientific Live/Dead Violet Dye. 10,000 cells were counted for each sample, and triplicate samples were used for each experimental group per run. Cell viability in experimental groups were normalized to the viability of the control group transfected with pcDNA3.1(-), an empty vector (EV). Three separate assays were conducted, each including the three transgenic groups (n = 3).

5.3.2.6.3 Results

In each experiment, cell survival was expressed as a ratio compared to cell survival in the EV control. Transfection with CK-Mt, CK-M, or CK-B vectors had no significant effects on cell survival. Cells transfected with CK-Mt, CK-M, or CK-B demonstrated 95% ± 5%, 94% ± 2%, and 91% ± 6% cell survival rates, respectively, when compared to survival rates in the EV transfected control group. This demonstrates that CK overexpression neither increased nor decreased cell viability. However, CK isoenzyme overexpression did not protect against DOX cytotoxicity. Compared to control, DOX at 250 nM resulted in a survival rate of 67% ± 3%. For DOX-treated cells transfected with CK-Mt, CK-M, or CK-B, the survival rates were 56% ± 9%, 53% ± 19%, 52% ± 18%, respectively. In all three groups, the survival rates were not significantly different from the survival rate in EV transfected cells treated with DOX. Trolox at 48 μM significantly increased cell survival rate in DOX treated cells to 79% ± 4% (p <0.05). Representative flow cytometry results from the experiment are exhibited in Figure 5-23 with overall findings in Figure 5-24.

CK-Mt, CK-M, or CK-B transfected cells that were co-incubated with DOX and creatine exhibited 52% ± 20%, 47% ± 16%, and 45% ± 18% cell survival rate, respectively. Thus, overexpression of the three CK isoenzymes and simultaneous creatine supplementation in HL-1 cells did not protect cells against DOX cytotoxicity.

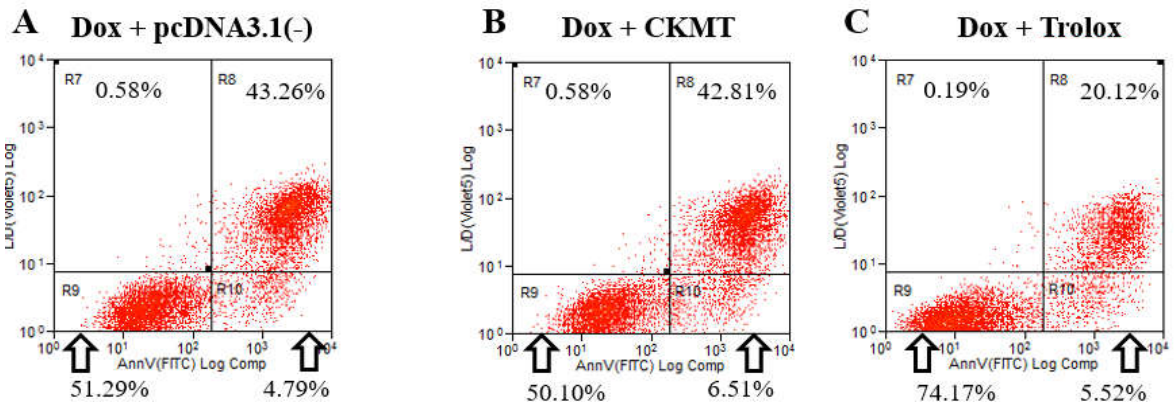
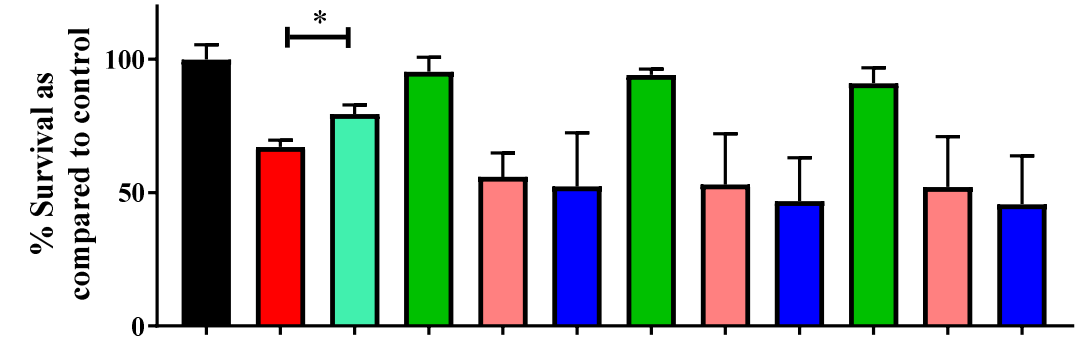


Figure 5-23: Representative flow cytometry results of DOX in CK OE HL-1 cells

(A) DOX effect in pcDNA(-) transfected HL-1 cells. (B) DOX effect in CK-Mt transfected HL-1 cells is not significantly different from (A). (C) Trolox demonstrates significant protection against DOX insult in HL-1 cells and reduces cellular cytotoxicity.



Vector	EV			CK-Mt			CK-M			CK-B		
Trolox	-	-	+	-	-	-	-	-	-	-	-	-
DOX (250 nM)	-	+	+	-	+	+	-	+	+	-	+	+
Creatine	-	-	-	-	-	+	-	-	+	-	-	+

Figure 5-24: Lack of protection of CK-isoenzyme overexpression in HL-1 cells treated with DOX

CK-Mt, CK-M, and CK-B transfected HL-1 cells were treated with 250 nM DOX in the presence or absence of 250 µM creatine. Over expression of CK isoenzymes and increased creatine did not improve cell survival against DOX cytotoxicity as compared to cells transfected with empty vector (EV). Trolox, the positive control, significantly improved cell survival in DOX-treated cells (*= $p < 0.05$). One-Way ANOVA with Bonferroni's post-hoc test; all columns compared to EV. $n = 3$ trials.

5.4 Discussion

5.4.1 HEK293 cells and resistance to DOX

5.4.1.1 Summary of experiments and conclusions

The goal of the experiments in this section was to optimize experimental conditions in HEK293 cells to generate a cell culture model of DOX-mediated cytotoxicity. Flow cytometry experiments with propidium iodide (PI) were conducted to determine DOX concentrations that were lethal to HEK293 cells. Initially, the fluorescence signal from PI appeared to indicate significant cell death after DOX treatment. However, additional experiments demonstrated that the observed fluorescence signal in the flow cytometry results was completely attributed to DOX auto-fluorescence rather PI. This indicates that PI was not entering cells, and that DOX-treated cells were not dead. Further experiments using Annexin V as a fluorescent marker of cell death and apoptosis demonstrated that DOX at concentrations up to 100 μM was minimally toxic to HEK293 cells following 18 hours treatment, which was subsequently confirmed through the Trypan Blue exclusion assay.

Three important conclusions could be made from the results of these experiments. First, DOX has significant auto-fluorescence, which may interfere with results from fluorescence-based assays. Second, the DOX emission spectrum occurs at a very similar wavelength to PI, hence PI is not an appropriate flow cytometry marker for DOX-mediated cytotoxicity experiments. Ideally, other dyes such as Annexin V-FITC and Violet Live/Dead should be utilized. If a dye with an overlapping emission spectrum to DOX is necessary, then DOX concentrations should be less than 500 nM, when auto-fluorescence is negligible. Previous studies that used significantly higher concentrations of DOX (up to 100 μM) and PI staining, without

consideration of the interference of DOX auto-fluorescence [90-92], should be interpreted with caution. Third, DOX at up to 100 μM was not toxic to HEK293 cells under tested conditions.

5.4.1.2 DOX cytotoxicity in HEK293 cells

The results from current experiments are in contrast with a previously published study that has shown DOX is cytotoxic to HEK293 when evaluated through flow cytometry [332]. Wang *et al.* reported that treatment with 5 μM DOX for 48 hours produced 70% cell death in HEK293 cells, as evaluated using PI in flow cytometry [332]. This conclusion was based on a shift in the PI fluorescence curve similar to what was observed in the current experiments. However, the evidence presented in the current study regarding fluorescent interference suggests it is possible that the cell viability rates identified in the study were confounded by auto-fluorescence from intracellular doxorubicin.

Ichikawa *et al.* [308] demonstrated that DOX at 10 μM failed to cause HEK293 cell deaths after 16-hour treatment, which supported the current finding. Utilizing three different cell viability markers (DAPI, Annexin V, and Trypan Blue), Ichikawa *et al.* conclusively demonstrated that 10 μM DOX had no cytotoxic effect on HEK293 cells following 16 hours treatment. Combined with the results of the current study, it appears that DOX at concentrations of 1-100 μM is non-toxic to HEK293 cells with treatment durations of up to 18 hours.

However, it has been reported that HEK293 cells treated with DOX at 2 μM for 48 hours was toxic when cell viability was evaluated by staining with a combination dye followed by use of a cell counting kit [360]. Similarly, it was found DOX at 1 μM for 72 hours caused 40% cell death as evaluated through trypan blue exclusion staining, with apoptosis being confirmed through protein assays for cleaved caspase 3 [361]. Therefore, treatment durations and methods

used in analysis of cell viability may play an important role in evaluation of DOX-mediated cytotoxicity in HEK293 cells.

5.4.2 CK overexpression does not protect against DOX cardiotoxicity in HL-1 cells

5.4.2.1 Summary of findings and conclusions

An *in vitro* model was developed using HL-1 cells to investigate the effect of CK overexpression on DOX cardiotoxicity. First, DOX incubation conditions were optimized, and Trolox was then identified as a positive control against DOX cytotoxicity. Second, HL-1 cells were transiently transfected with CK vectors, and the transfection was verified by visualization of a co-transfected GFP vector and by increased cellular total and isoenzyme-specific CK activity confirmed through the CK activity assay. Finally, DOX was administered to CK-OE cells to evaluate whether CK overexpression protected against DOX-induced cardiotoxicity. CK-overexpression did not improve cell viability in HL-1 cells exposed to 250 nM DOX for 48 hours. Increasing creatine availability to the transfected cells also did not significantly affect survival from DOX insult.

It should be noted that HL-1 cells have some significant differences in CK system function compared to cardiomyocytes. Various studies have demonstrated that CK activity in HL-1 cells is 15-30 fold lower than activity levels in primary rat cardiomyocytes [202,203]. The CK system may be less important in HL-1 cells due to the reliance of the cell line on glycolytic pathways and relatively lower levels of mitochondrial proteins including CK-Mt [203]. It has

also been reported that CK isoform proportions are different in HL-1 cells, with higher CK-B mRNA and lower CK-M mRNA as compared to cardiomyocytes [203]. Therefore, it may be possible that CK overexpression may have produced a protective effect in primary cardiomyocytes, in which CK system function appears to be more prominent than in HL-1 cells.

Overall, the current results are in contrast to previous studies that suggest CK system augmentation can protect against DOX-induced cardiotoxicity [192,328]. The discrepancy between the current study and the published literature may also be explained by the existing proposed mechanisms underlying DOX-induced cardiotoxicity. The literature suggests three main mechanisms by which DOX may cause cardiotoxicity: 1) DOX impairment of myocardial bioenergetics, 2) DOX-induced ROS synthesis, and 3) DOX cytotoxicity through DNA intercalation and inhibition of DNA replication machinery. The results of the current study are examined in the context of each proposed mechanism.

5.4.2.2 DOX cardiotoxicity and impaired bioenergetics

While several mechanisms for DOX induced cardiotoxicity have been suggested, the mechanism most relevant to the CK system is the impaired bioenergetics hypothesis [297]. This hypothesis suggests that impairment of myocardial metabolism, including the CK system, plays a major causative role in DOX-induced cardiotoxicity. This hypothesis is supported by several studies that demonstrate a decline in the CK system occurs early in the pathogenesis of DOX-induced cardiotoxicity, and that the CK system deterioration precedes outright cell death and functional impairment [192,327,328].

Two reasons may explain why there was a lack of protection in the current study despite elevation of CK activity. One possibility is that the level of CK overexpression was insufficient. Gupta *et al.* utilized an *in vivo* CK-M OE model that resulted in ~70% increased total CK activity [190], whereas CK-M transfected cells in the current study only had a 31% increase in total CK activity. CK-Mt and CK-B transfected cells in the current study exhibited 8% and 18% higher total CK activity, which were not significantly different from the pcDNA 3.1(-) transfected control. This could be a crucial reason for the discrepancy between the study results - our model may not have sufficiently elevated CK to compensate for the impaired bioenergetics in DOX-induced cardiotoxicity. Further study may demonstrate whether a stronger promoter or an alternative transfection technique could produce a protective effect.

The second reason concerns the different DOX treatment protocols used in the studies. It is difficult to compare the current *in vitro* treatment (250 nM DOX for 48 hours) to the *in vivo* model treatment from Gupta *et al.*, which involved weekly DOX injections for a total dosage of 25 mg/kg over five weeks [192]. The current protocol caused ~40% cell death, whereas the *in vivo* study noted only mild myofibrillar loss at the end of the protocol, suggesting that the current protocol may have been too severe to see a protective effect of CK overexpression.

The current treatment is also significantly more severe (~40% cell death) than the protocol used by Darrabie *et al.* in HL-1 cells (10-15% cell death) [327]. The DOX treatment strategy used by Darrabie *et al*. represents a model of mild DOX toxicity in which CK system augmentation was protective, whereas CK system augmentation has less of an effect in the current model of comparatively severe cytotoxicity.

5.4.2.3 DOX cardiotoxicity and ROS

Trolox, an antioxidant and the positive control for this assay, significantly reduced DOX-induced cytotoxicity in HL-1 cells, which suggests that ROS-mediated cytotoxicity is particularly relevant in the current *in vitro* model.

Creatine has been reported to have an antioxidant effect [328,362,363] and creatine supplementation produced a beneficial effect during elevated oxidative stress in myoblasts [11], and rats undergoing cerebral ischemia [364]. Indeed, Santacruz *et al.* have reported that creatine supplementation at 5 mM protected against DOX-induced cytotoxicity in both HL-1 cells and rat neonatal cardiomyocytes via its antioxidant function [328].

However, in the current study, 250 μM creatine supplementation failed to protect HL-1 cells from DOX-induced cytotoxicity. While this argues against the results of Santacruz *et al.*, the fact that creatine does not protect against DOX or ROS is not without precedence. Our group had previously reported that ~75% increased intracellular creatine and complete creatine deficiency in the intact heart did not alter cardiac response to DOX insult, nor against H_2O_2 challenge [329]. Additionally, experiments by our group showed that 250 μM – 5 mM creatine supplementation did not protect against H_2O_2 insult in HL-1 cells [2]. Taken together, these results suggest that creatine-induced protection against ROS damage may be dependent on experimental conditions. For instance, Santacruz *et al.* challenged HL-1 cells with 1.5 μM DOX for 24 hours, whereas the current study utilized 250 nM DOX for 48 hours, hence the DOX incubation strategy may have affected results [328]. Alternatively, it is possible that that the 250 μM creatine supplementation in the current assay was insufficient compared to the 5 mM creatine utilized in Santacruz *et al.* [328]. The 250 μM had been selected as excessive creatine loading was found to reduce intracellular transport of creatine through negative

regulation of the number of active creatine transporters on the cell surface [2,135]. It should be noted that intracellular creatine was not measured in the current assay, hence the magnitude of intracellular creatine elevation remains unclear. Ultimately, it is possible that higher creatine concentrations may have resulted in a protective effect; however, this was not pursued as the focus of the current experiments was to test the effects of CK augmentation rather than creatine augmentation.

Although one study reported that CK-Mt can reduce mitochondrial ROS production [255], there is little evidence that CK exerts a direct antioxidant effect. Given that Trolox protected against DOX-induced cardiotoxicity in the current experiment, this suggests that in the current *in vitro* model, ROS plays an important role in DOX-induced cardiotoxicity, hence CK supplementation may not have protected due to its limited antioxidant effect.

5.4.2.4 DOX cardiotoxicity and DNA intercalation

The final major mechanism involved in DOX-induced cardiotoxicity is DNA intercalation and inhibition of DNA replication machinery [291]. This could explain why CK-M was found to be protective *in vivo*, but not in the current *in vitro* model. DNA damage and interference of DNA replication may be especially important *in vitro* with the proliferating HL-1 cells in the current experiment, whereas it is probably less critical to G_0-arrested cardiomyocytes *in vivo* [176]. Therefore, should this mechanism be a substantial cause of the cell death in HL-1 cell culture treated with DOX, it could explain why CK overexpression failed to protect in the current experimental system.

In summary, there is currently no consensus regarding the specific mechanism of DOX-induced cardiotoxicity in the *in vitro* setting. Impaired bioenergetics, ROS damage, and DNA damage may all play a causative role in disease pathogenesis. The results of this study indicate that moderate CK overexpression in the *in vitro* setting does not protect against DOX-induced cardiac cytotoxicity.

5.5 Future work

While the results of this study were negative, different results may have been obtained in a more physiologically relevant model. For instance, a critical limitation of the current study is that the choice of HL-1 cells as opposed to primary cardiomyocytes. Cardiomyocytes could be isolated from the CK-Mt and CK-M OE mice lines (currently possessed by our group) for further investigation without the need for transfection, however these were unavailable at the time that this study was commenced.

In addition to *in vitro* studies, *in vivo* studies could also be conducted on CK-Mt OE mice to explore whether there are any protective benefits on *in vivo* DOX cardiotoxicity. Conventional parameters could be explored (*e.g*. *in vivo* cardiac function, survival rates), and should significant differences be observed, additional metrics could be studied through hyperpolarized ^{13}C MRS. Professor Damian Tyler's group has investigated DOX cardiotoxicity *in vivo* in rats by following hyperpolarized ^{13}C pyruvate through cellular metabolism, and found significant metabolic changes (Professor Tyler, *personal communication*). For instance, the ^{13}C-pyruvate study reported that DOX treatment decreased glucose-derived acetyl-CoA incorporation into acetyl carnitine by approximately 35%. In comparison, CK-Mt OE mice were found to have

40% increased acetyl carnitine production as compared to wild-type controls, as seen in Section 3.4.1. Thus, should a cardio-protective effect be seen *in vivo* with CK-Mt OE mice, further study with ^{13}C MRS could clarify the underlying mechanistic basis for protection.

6 Development of *in vitro* tools for investigation of CK transcriptional regulators

6.1 Introduction

This chapter details experiments conducted to develop an *in vitro* model system for exploring transcriptional control of CK. Specifically, HEK293 cells were used to develop two stably transfected cell lines containing the luciferase reporter gene under control of the CK-M and CK-Mt promoters. These cell lines were then used to screen potential CK transcriptional regulators, which would alter luciferase and endogenous CK mRNA expression through their action on the CK promoter region. This reporter system was validated and tested on an initial screen of compounds to assess their effect on CK-M and CK-Mt transcriptional activity. This introduction will cover the rationale for developing and validating a system for investigating CK transcriptional regulators, the background of the luciferase assay, and the known gene regulation of CK-M and CK-Mt.

6.1.1 The necessity for tools to explore CK transcriptional regulation

The literature suggests that loss of CK may have a causative role in cardiac dysfunction, and that CK augmentation can have therapeutic benefit. These studies have been detailed at length in previous chapters, and involve varied conditions such as I/R injury, heart failure, and DOX-induced cardiotoxicity. Therefore, CK transcriptional regulators could potentially represent a class of effective treatment options for a wide range of cardiac diseases. However, there is limited understanding of CK transcriptional regulation (summarized in Sections 6.1.4 and

6.1.5), and to our knowledge, there are no published screening tools designed specifically for investigation of CK transcriptional regulators. Therefore, the experiments in this chapter were conducted to develop *in vitro* models that could be utilized to identify potential modulators of CK transcription through the luciferase assay.

6.1.2 The firefly luciferase reporter system

Firefly luciferase was first cloned by de Wet *et al.* in 1988 [365], tested as a reporter system in eukaryotic cells two years later [366], and has since been utilized with mammalian cells [367]. High-throughput luciferase screening assays have been established to screen drug-like compounds for transcriptional control of G-protein coupled receptors [368] and steroid receptors [369]. The luciferase reporter system [370] employed in the current study utilizes the firefly (*Photinus Pyralis*) luciferase enzyme as the reporter gene. The luciferase reporter system provides several key advantages. First, as a chemiluminescent assay, the luciferase system has significantly lower optic background when compared to systems utilizing fluorescence proteins (*e.g.* GFP), since there is no need to introduce photons [371]. This enhanced sensitivity is crucial as it reduces the cell populations and resources required to sustain screening. Second, the luciferase system requires less sophisticated laboratory equipment when compared to other reporter gene systems. For instance, the bacterial chloramphenicol acetyltransferase reporter system [372] requires both radiolabeled chloramphenicol and thin layer chromatography, whereas the luciferase system only requires a plate reader [372]. Third, the species of luciferase (firefly) used in the current study was important because the firefly luciferase reaction has the highest quantum yield of known bioluminescent reactions, providing the strongest possible

signal intensity [373]. Fourth, as the reporter gene is of insect origin, there is no risk of interference due to protein/gene interactions in mammalian cell lines such as HEK293. This is not necessarily the case for other reporter molecules such as human growth hormone [372]. Finally, the luciferase assay system utilized in the current study has the advantage of a sustained luciferase signal, thus decreasing variability between samples in a screening assay [370].

6.1.3 Principle of luciferase assay

The luciferase reporter system utilizes the firefly (*Photinus Pyralis*) luciferase enzyme, which is a 62 kDa monomer protein that catalyses the reaction shown in Figure 6-1 [373].

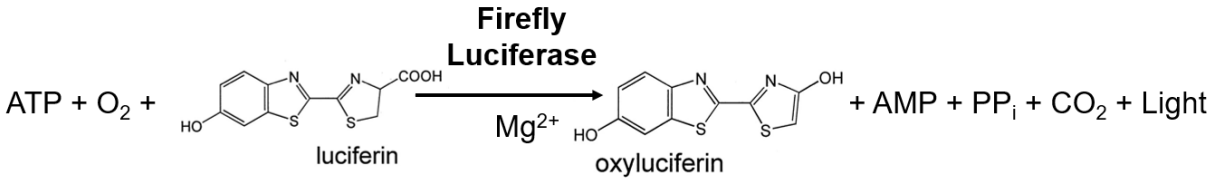


Figure 6-1: Firefly luciferase reaction

In the reaction, beetle luciferin, Mg^{2+}, and ATP are added to a solution of cell lysate containing firefly luciferase protein. The firefly luciferase enzyme, in the presence of Mg^{2+}, converts beetle luciferin to oxyluciferin, consuming ATP and generating light. Figure adapted from manufacturer's documentation [370].

Firefly luciferase catalyses the formation of oxyluciferin and a photon, which is emitted at a wavelength of 562 nm [373]. The intensity of light produced can then be measured by a luminometer. To avoid interference from insufficient substrates on measured luciferase enzyme, ATP and luciferin must be added in abundance, so that the enzyme is the limiting

component in the reaction. Thus, the enzyme activity measured in the reaction is dependent on the quantity of luciferase protein produced as a result of transcription of the reporter gene.

6.1.4 Promoter structure and regulation of CK genes

The CK promoter regions present in the vectors were designed to include all putative response elements upstream of the first exon. The compounds tested in the luciferase assay were selected due to their ability to regulate known CK transcription factors, such as MyoD and myogenin.

6.1.4.1 CK-M

The transcriptional activation of CK-M depends on many elements, largely localized on upstream enhancer region and the basal promoter region (Figure 6-2). There are two enhancer boxes ("E-boxes") in the enhancer region, and an additional E-box in the basal promoter [374]. E-boxes bind myogenic DNA binding proteins, such as MyoD, [374-376], MuRF-4 (muscle-ring-finger 4), myogenin, and MEF-2 (myosin enhancement factor 2) [377]. Alternating activation patterns of the three E-boxes are responsible for different CK-M expression levels in various tissues [378]. There is also an AT-rich site in the enhancer, which is responsible for binding to MEF-2 and MHox [374]. The AT-rich region is responsible for increasing CK-M expression in skeletal muscle, where CK-M is found at concentrations five-fold higher than that in cardiac muscle [379]. Finally, there is a 5-nucleotide response element, known as a "CArG element" (short for $CC(A/T)_6GG$), which binds serum response factor (SRF) and muscle actin protein factor (MAP-F) [380,381]. This region may be responsible for gene expression in cardiomyocytes [377,381,382], though this is not a universal finding [374,382,383].

In cultured cardiomyocytes, knockout of this element resulted in a 20-fold decline in CK-M expression, but this result could not be recapitulated in transgenic mice [381]. In summary, CK-M expression is regulated by multiple proteins and at least five response elements, which allows differential expression in fast-twitch skeletal muscle, slow-twitch skeletal muscle, and cardiac muscle as summarized in Figure 6-2 and Table 6-1 below.

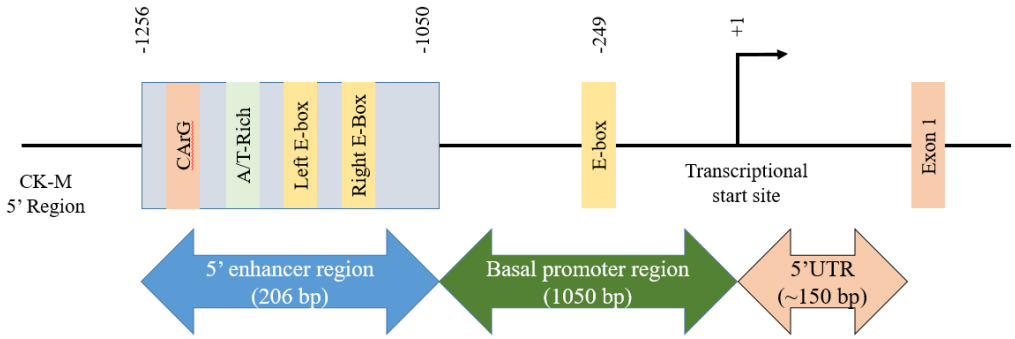


Figure 6-2: Schematic illustration of CK-M promoter region

Illustrates key enhancer/promoter regions, including Left/Right/Promoter E-boxes, AT-rich region, and CArG binding sites. UTR = untranslated region. Adapted from [374].

Table 6-1: CK-M promoter binding elements*

Muscle Region	E-Boxes	Other binding sites	Known binding Elements
Fast twitch skeletal muscle	Promoter E-Box only	AT-rich region MPEX†	MyoD, Myogenin, MuRF-4, MHox, MEF-2
Slow twitch skeletal muscle	Promoter E-Box Left (downregulates)	AT-rich region MPEX†	MyoD, Myogenin, MuRF-4, MHox, MEF-2
Cardiac muscle	Promoter E-Box only	CArG†	MHox, MEF-2, MEF-2C, SRF†, MAPF†
Cell culture – skeletal myocytes	Left, Right	AT-rich region MPEX†	MyoD, Myogenin, MuRF-4, MHox, MEF-2
Cell culture – rat cardiomyocytes	Left	CArG†	SRF†, MAPF†

† = inconclusive

* Information presented in table is derived from: E Boxes [377], CArG and AT-rich region [374], Myogenin, MuRF-4 and MyoD [377], MPEX [384], MHox [385], SRF and MAPF [386]

6.1.4.2 CK-Mt

The CK-sMt gene has 11 exons and many upstream enhancers. Two response element domains can be found in the promoter region [387]. The first domain is a group of five E-boxes and the second domain consists of three E-box, 4 GATT motifs, and a MEF-2 binding site [387,388], as illustrated in Figure 6-3. The function of the first domain is currently unknown, but the second domain may specify gene expression for cardiac muscle. Several CK-M regulators (*e.g.* MEF-1/2 and MyoD) also control CK-sMt expression [387]. The CK-sMt promoter region contains cAMP response elements [388], and *in vitro* supplementation of norepinephrine may increase CK-sMt mRNA expression [55], though this is disputed [389]. Ultimately, far more is known about CK-M transcriptional regulation than CK-sMt regulation.

There are differences in terms of gene regulation between CK-uMt and CK-sMt due to the tissue-specific expression patterns. CK-uMT has hormone-sensitive response elements that respond to oestrogen and glucocorticoids [390], likely because placenta and uterus have substantial CK-uMt expression [391]. For instance, estradiol significantly increased the expression of CK-uMt mRNA in uterine horn and placentas of pregnant rats [391]. Thus far, hormone-sensitive response elements have not been discovered for CK-sMt. Since CK-uMt concordantly expresses with CK-B, they may share gene regulation mechanisms [55].

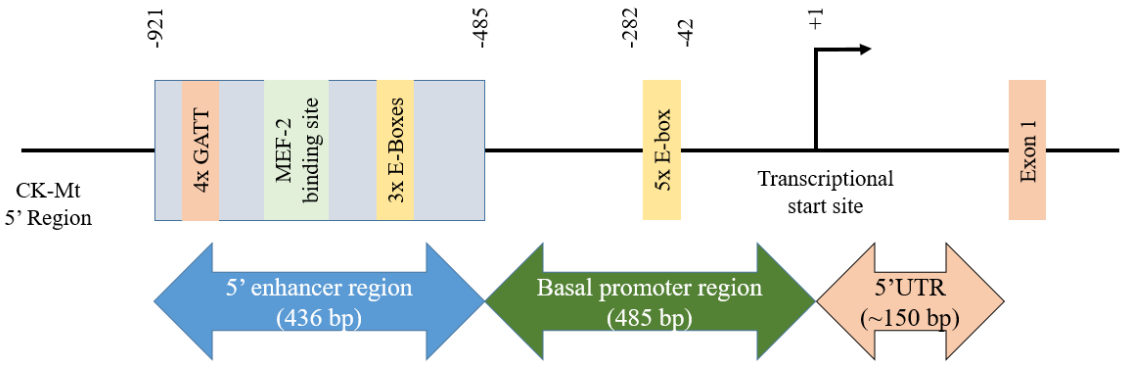


Figure 6-3: Schematic illustration of CK-Mt promoter region

Illustrates key enhancer/promoter regions, including various E-boxes, GATT binding domains, and MEF-2 binding site. UTR = untranslated region. Data was derived from [387].

6.1.5 Putative CK transcriptional regulators

Studies have reported that several hormones and pharmacological agents, such as β-estradiol, raloxifene, LYS294002, insulin, isoproterenol, and norepinephrine could be used to alter CK transcription and activity. β-estradiol and raloxifene are oestrogen receptor agonists. It has been reported that β-estradiol stimulates CK activity in rat LV [392], though the specific CK isoenzyme stimulated was not assessed. Oestrogen is a known regulator of CK-B and CK-uMt, both of which have oestrogen receptor response elements (see Chapter 1) in their promoter regions. Oestrogen agonists have been shown to increase CK activity in rat bone and uterus, which express CK-B and CK-uMt [392,393]. It remains unclear whether oestrogen receptor agonists affect CK-M and CK-sMt gene regulation.

Phosphatidylinositol 3-kinase (PI3K) is involved in various functions, from regulation of cell cycle [394] to control of muscle-specific transcriptional regulators such as MyoD and myogenin [395,396]. LYS294002, a PI3K inhibitor, decreased CK-M gene transcription in 10T1/2 mesodermal stem cells [397], and in C2C12 myoblasts as assessed by luciferase assay [396].

In both cases, the most likely mechanism of action for LYS294002 was its inhibition of the PI3K pathway, which propagated down-regulation of MyoD and myogenin expression [396,397]. As MyoD and myogenin are both implicated in CK-M and CK-Mt transcription (see Section 6.1.4), there was considerable rationale to investigate whether LYS294002 could down-regulate CK-M and CK-Mt transcription. While insulin regulates both muscle differentiation and proliferation, it specifically exerts its effects on differentiation through the PI3K pathway [396,398]. Insulin is a known activator of the PI3K pathway [396], and has been shown to attenuate the decline in cardiac CK-M and CK-Mt mRNA, as well as CK-M and total CK activity, observed in diabetes [399,400].

Isoproterenol and norepinephrine are β-adrenergic agonists, though norepinephrine also functions as an α-adrenergic agonist. Our group has previously demonstrated that isoproterenol administration causes an 18% decline in CK-M mRNA in rat heart [389], though no effect was observed on CK-Mt mRNA. This was an unexpected result, as β-agonists increase intracellular cAMP and cAMP response elements have been found on the CK-Mt promoter, but not the CK-M promoter [55,388]. Therefore, this merited further research to determine whether such a finding could be replicated.

In conclusion, there was some circumstantial evidence that each of the four compounds (β-estradiol, LYS294002, insulin, and isoproterenol) could function as CK transcriptional regulators. Hence in the current experiment, these compounds were evaluated for their effect on CK-M and CK-Mt transcription.

6.2 Experimental aims

The goals of the experiments described in this chapter are threefold: 1) develop and validate HEK293 cell lines that stably express luciferase reporter gene; 2) optimize the luciferase assay for the established cell lines; and 3) screen potential CK transcriptional regulators using the luciferase assay.

6.3 Methods

6.3.1 Luciferase vector structure and reporter system

The pGL4 empty vector served as a control for transfection [370]. The CK-M-Luc and CK-Mt-Luc vectors were previously created using SnapGene (v. 4.1), and the vectors were commercially produced by gene synthesis, cloned, and verified through restriction digest and direct sequencing by GeneWiz [401]. Each CK-Luc vector contained the appropriate human CK-M or CK-Mt promoter region, which was used to drive expression of the firefly luciferase mRNA in the pGL4.20[luc2/Puro] firefly luciferase reporter gene [370]. This generated a chimeric gene that allows the transcription factors for the target promoter to control luciferase expression. A puromycin resistance gene in the vectors was used to select successfully transfected cells. Vector maps are shown in Figure 6-4.

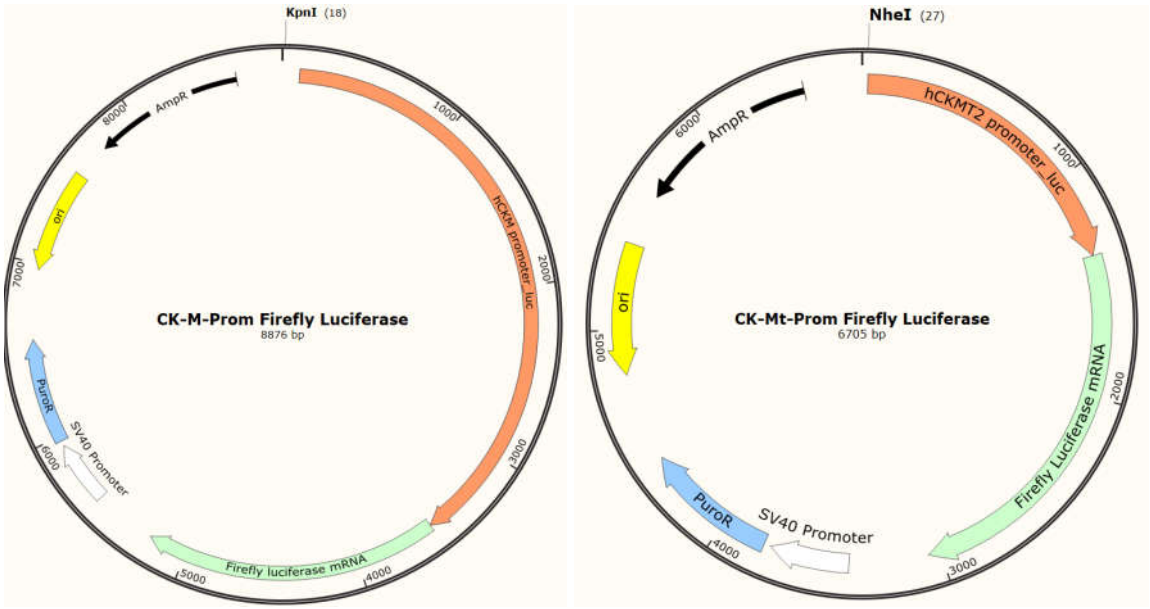


Figure 6-4: Vector maps of luciferase reporter system

The empty vector (pGL4.20), and CK-M-Luc and CK-Mt-Luc plasmids are presented, with major features labelled. The *KpnI* restriction site was used to linearize the CK-M-Luc plasmid, whereas the *NheI* site was used to linearize the pGL4 and CK-Mt-Luc plasmids. pGL4 vector map is adapted from manufacturer's documentation [370], with puromycin resistance gene and Firefly luciferase (luc2) included in the vector.

6.3.2 Optimization of puromycin concentration

An optimization experiment was conducted to identify the proper puromycin concentration to use for later selection of stably transfected HEK293 cells. General information regarding HEK293 was previously described in Section 2.4. For this experiment, HEK293 (passage # 65) cells were plated at 2 x 10^5 cells/cm^2 in a 24 well plate and incubated with various concentrations of puromycin (0 ng/mL – 10 µg/mL) (Sigma), with media changed daily for five days. After five days, cells were trypsinized, washed with PBS, and stained with propidium iodide, and analysed by flow cytometry (flow cytometry details are described in Section 2.7).

6.3.3 RNA extraction and qRT-PCR verification of mRNA expression

The RNA extraction and qRT-PCR methodology are described in Section 2.6. Three sets of primers (Table 6-2) were used in the luciferase transfection experiments to confirm the expressions of target genes through qRT-PCR. The luciferase region primers were utilized to detect expression of luciferase mRNA in transiently and stably transfected HEK293 cells, thus validating the presence of the CK-Luc construct in the transfected cells. The CK mRNA primers were utilized to verify compounds identified through the luciferase assay, specifically to quantify effect on CK-mRNA transcription. Each sample was assessed with either the luciferase mRNA primers or the CK-M/CK-Mt mRNA primers, in addition to Polr2A mRNA primers. This qRT-PCR method and the primers in Table 6-2 were used for all subsequent mRNA analysis in this chapter.

Table 6-2: Primers for luciferase transfection experiments

Luciferase mRNA Region	**Primer names**	**Primer sequences**
	CKMT2 luc For	5'-TTCTAAAAGCTTGGCAATCC-3'
	CKMT2 luc Rev	5'-CTGCTCGCCGGCGGTCCCGT-3'
	CKM luc For	5'-GTACTGAAGCTTGGCAATCC-3'
	CKM luc Rev	5'-CATGGCTTTGTGCAGCTGC-3'
CK mRNA Region	**Primer names**	**Primer sequences**
	CKMT2 mRNA For	5'-CCTCCAAGCGCAGACTAC-3'
	CKMT2 mRNA Rev	5'-CGTTGGGTGTCACCTTGT-3'
	CKM mRNA For	5'-GACAACCCAGGTCACCCC-3'
	CKM mRNA Rev	5'-AGATGATGGGGTCAAAGAG-3'
Polr2A mRNA Region	**Primer names**	**Primer sequences**
	Polr2a_F cDNA	5'- TGTGCAGGAAACATGACCGA -3'
	Polr2a_R cDNA	5'- GAAGCAGACACAGCGCAAAA -3'

6.3.4 Luciferase assay protocol

6.3.4.1 Standard Luciferase assay protocol

The luciferase assay was conducted using the Promega Luciferase Assay System (Promega, UK), as per manufacturer's instructions [370]. Incubation and treatment conditions were varied for each luciferase assay, and are described in the sub-chapter headings specific to each experiment. Described here are the methods that apply to all luciferase assays conducted throughout various experiments. After incubation and treatment with tested compounds, the cell culture media was aspirated, and the cells were washed with 100 µL PBS. Following PBS removal, 30 µL of 1x Luciferase Lysis Buffer [370] was added to wells. The plate was then placed on a plate shaker for 20-minute at RT to lyse cells. The plate was then briefly spun down, and 10 µL of lysate was transferred from each well to a new well in a white opaque-bottom 96-well plate (Greiner Bio-One Inc) for luciferase luminescence measurement. The plate was placed into an PolarStar plate reader (BMG Labtech), and 100 µL of luciferase working reagent containing luciferin, ATP, and Mg^{2+} [370] was automatically injected into each well immediately prior to the luminescence reading. Luminescence data was processed with Mars v. 3.00 software (BMG Labtech), with further analysis conducted in Microsoft Excel and Graphpad Prism (v. 5 and v. 7). All luciferase experiments were conducted with the standard Luciferase assay system unless otherwise specified (*i.e.* see below).

6.3.4.2 Steady-Glo Luciferase and Resazurin Assay

After initial experiments utilizing the Luciferase Assay System above, additional experiments were conducted utilizing the Steady-Glo Luciferase System (Promega), which utilizes the same luciferase reaction but produces a luminescence signal that is far more stable, with a half-life

of over five hours. The Steady-Glo system offers two main advantages [402]. First, it reduces luminescence signal variability and improves the consistency of high-throughput screening. Second, it reduces the steps required for the assay, as media can be left in wells and washing is not required, which greatly increases the number of compounds that can feasibly be tested. Taken together, this new luciferase system, which was optimized by our group recently, allowed experiments to be performed in a high-throughput fashion, which would allow much more rapid compound screening.

The resazurin assay is a colourimetric assay that is utilized to assess cell proliferation, with the advantage of being applicable to high throughput systems [402]. Resazurin is a weakly fluorescent dye that is reduced in the mitochondria of viable cells, most commonly by NAD(P)H dehydrogenase, to resorufin, which is intensely fluorescent. The rate of resazurin production is therefore proportional to the number of viable cells. Our group had previously optimized resazurin for the luciferase assay, in which it was confirmed that resazurin was an accurate measure of cell proliferation. The resazurin assay could be performed prior to the luciferase assay in the same plate of cells, therefore reducing the variability of the results.

The protocol for the combined Steady-Glo luciferase/resazurin assay is as follows. Cells were plated at 2 x 10^4 cells/well in 96 well plates, with 100 μL of media containing treatments as described in Section 6.3.8 and 6.3.9. 47 hours after seeding, cells were treated with 3 μg/mL resazurin in PBS solution. Cells were then incubated for an additional hour at 37°C, before resazurin fluorescence was measured by a BMG Omega-Star plate reader, using a 550 nm excitation wavelength, and a 590 nm emission wavelength. Subsequently, cells were then incubated with 100 μL/well of Steady-Glo Luciferase assay solution (Promega) for 5 minutes

at RT to lyse cells, before luminescence was measured using the plate reader. Luciferase results were normalized to resazurin values, and the normalized results were reported.

It should be noted that the cell seeding/treatment strategy was modified for the Steady-Glo Luciferase assay as compared to the standard luciferase assay, to be more amendable towards high throughput screening. High throughput screens often have compounds already injected into plates, with cells added afterwards – hence the cells attach and proliferate in the presence of compounds. Therefore, the 24-hour seeding step in the original protocol was eliminated, and cells were directly seeded into media containing test compounds, with the luciferase/resazurin assay being conducted 48 hours after seeding.

6.3.5 Validation of CK-Luc constructs in transiently transfected cells

6.3.5.1 Verification of transfection efficiency and luciferase mRNA expression

A pilot run was conducted with a cohort of transiently transfected cells to evaluate transfection viability of the CK-Luc constructs presented in Section 6.3.1 and to quantify transfection efficiency.

HEK293 cells were seeded at a density of 3.5 x 10^4 cells/cm^2 with 100 µL DMEM, in a 96-well plate. (All experiments in this chapter conducted in 96 well plates used 100 µL DMEM medium per well.) Cells (n = 2-4 wells per group) were transfected with empty pGL4 vector, CK-Mt-Luc, CK-M-Luc, or creatine-transporter-luciferase (CrT-Luc) vectors. CrT-Luc transfected cells served as a positive control, since the vector had been stably transfected into HEK293, and the resulting cell line has been previously validated by our group. Additional triplicate wells were also included for each of the groups above, containing the vector + GFP for

fluorescence microscopy to estimate transfection efficiency. The protocol for transfection (with Fugene HD transfection agent) was described in detail in Section 2.5, and the vectors utilized were described in Section 6.3.3.

All transfected cells were cultured in 1 μg puromycin/mL DMEM, as optimized from the kill curve. 24 hours after transfection, the groups containing the GFP vector were trypsinized and re-suspended in media. A 20 μL aliquot of re-suspended cells (approximately 500 - 1,000 cells) was injected into the cell counting chamber of Nexcelom Cellometer and GFP positive cells was counted as a measure of transfection efficiency.

Forty eight hours after transfection, the remaining cell cultures (not transfected with GFP) were subject to qRT-PCR analysis of the luciferase region as described in Section 6.3.3.

6.3.5.2 Verification of luciferase expression

To test the viability of the luciferase assay and transgenic luciferase activity, cells were seeded and transfected as described in Section 6.3.5.1. Forty eight hours after transfection, cells were prepared for the luciferase assay as detailed in Section 0.

6.3.6 Generation of stably transfected CK-Luc cell lines

After validation of the CK-Mt-Luc and CK-M-Luc constructs in transiently transfected HEK293 cells, experiments were undertaken to generate HEK293 cells stably transfected with the CK-Luc constructs.

6.3.6.1 Vector linearization

The circular vectors needed to be linearized prior to stable genome integration since a circular plasmid would only stably integrate in the rare event of a spontaneous breakage. Thus, the vectors were linearized by restriction digest. The *KpnI* and *NheI* restriction enzymes were used to linearize the CK-M-Luc and the CK-Mt-Luc vectors, respectively. *NheI* was also used to digest the pGL4 empty vector. Duplicate samples containing 2 µg of transgene DNA were used in digestion mixtures presented in Table 6-3, which were prepared on ice.

Table 6-3: Digestion solutions for vector linearization

CK-M	CK-Mt and pGL4
1.2 µL (2 µg) DNA	0.7 µL (2 µg) DNA
5 µL 10x "CutSmart" NEBuffer	5 µL 10x "2.1" NEBuffer
2 µL *KpnI* Enzyme	2 µL *NheI* Enzyme
Made up to 50 µL with ddH_2O	Made up to 50 µL with ddH_2O

For restriction digest, samples were incubated for 40 minutes at 37°C in a water bath according to manufacturer's protocol (NEB CutSmart). The *KpnI* enzyme of CK-M-Luc mixtures was then inactivated at 60°C in the water bath for 20 minutes. The *NheI* enzyme was inactivated upon being returned to RT. A 0.5 µL aliquot of the restriction digest product was mixed with

loading buffer and then loaded into a 1% agarose gel supplemented with ethidium bromide. The products were then separated by gel electrophoresis at 100 volts for 90 minutes.

After confirmation of digest, the linearized vectors were then precipitated from the digestion product. 50 µL Tris-EDTA buffer (10 mM Tris HCl, 1 mM EDTA, pH 8), 200 µL phenol/chloroform/isoamyl alcohol (25:24:1 dilution), and 50 µL ddH_2O were added to the digestion products, which were then centrifuged at 16,000 rpm for 5 minutes at RT to separate the aqueous and lipid phases. The aqueous phases were then extracted, and diluted 1:3 with 100% ethanol and 10:1 with 3 M sodium acetate. The mixtures were precipitated at -20°C for 30 minutes, then centrifuged at 16,000 rpm for 15 minutes at 4°C. The supernatants were discarded, and the pellets were air-dried for 15 minutes at RT to evaporate all residual ethanol. Subsequently, the pellets were re-suspended in 20 µL ddH_2O, then assessed for DNA concentration and purity through spectrophotometry by Nano-Drop.

6.3.6.2 Stable transfection

The stable transfection utilized the same Fugene HD based protocol as used for transient transfection (detailed in Section 2.5.2) [370]. Cells were seeded at 2 x 10^4 cells/cm^2 in a 96 well plate, and subject to transfection with linearized vector 24 hours after seeding. Six wells were transfected with each of the 3 linearized transgenic vectors (pGL4, CK-M-Luc, CK-Mt-Luc), for 18 wells in total. After transfection, cells were cultured for 24 hours in media with (3 wells) or without (3 wells) 1 µg/ml puromycin, with the puromycin-free wells acting as a control. Thereafter, puromycin and puromycin-free media was changed daily, until seven days

after transfection by which time individual puromycin-resistant colonies could be observed by microscopy in the CK-Mt-Luc and CK-M-Luc transfected wells.

Individual puromycin-resistant colonies were selected from the CK-Luc transfected wells, trypsinized, and seeded in 24-well plates for further growth in 1 mL DMEM medium with 1 µg/ml puromycin. Media was changed daily until cells were fully confluent, after which cells were then passaged and seeded in 6-well plates, and then 25 cm^2 and 75 cm^2 flasks to generate the CK-M-Luc and CK-Mt-Luc cell lines. All subsequent experiments utilized media with 1 µg puromycin/mL DMEM to ensure continuous expression of the integrated vector.

6.3.6.3 qRT-PCR analysis of luciferase mRNA

After the CK-M-Luc and CK-Mt-Luc had been successfully transfected in HEK293 cells, total RNA of stably transfected cells was then extracted for qRT-PCR using the one step protocol as described in Section 2.6. qRT-PCR for the luciferase mRNA region was then conducted to assess transfection success.

6.3.6.4 Luciferase assay

The luciferase assay was conducted for both cell lines to confirm whether the levels of transgenic luciferase expression were sufficient for experimental purposes. Cells were plated in triplicate wells at 2 x 10^4 cells/per well, in a 96 well plate. Untransfected HEK293 cells served as a negative control, and CrT-Luc stably transfected cells were used as a positive control. Forty-eight hours after plating, cells were washed with PBS and lysed before being analysed via the luciferase assay as described in Section 0.

6.3.7 Luciferase screening of putative CK transcriptional regulators

6.3.7.1 Strategy for compound identification.

Since the validated CK-Mt-Luc and CK-M-Luc cell lines could be used for the luciferase assay based on the findings described in Section 6.1.5, the next step was to test putative CK transcriptional regulators. Four compounds (β-estradiol, isoproterenol, insulin, and LYS294002) were selected for evaluation in both cell lines based on the rationale discussed in Section 6.1.5.

It should be noted that there are no conclusively confirmed CK transcriptional regulators that could be utilized as a transcriptional positive/negative control in the current assay, hence one of the putative transcriptional regulators could also serve as a transcriptional control for the luciferase assay if it was verified to regulate CK transcription.

To address the lack of a positive control for the luciferase assay, OXO2393 (kindly donated by Oxford Department of Chemistry) was utilized as a non-transcriptional positive control for luciferase assay. OXO2393 acted as a false positive for the assay by stabilizing luciferase protein, thus substantially increasing the luminescence signal. Our group had previously validated and utilized OXO2393 as a false positive control (luciferase stabilizer) in the luciferase assay.

With OXO2393 as a false positive control and untransfected HEK293 cells as a negative control for the luciferase assay, the assay could be used to test several compounds identified in the literature as potential CK transcriptional regulators.

6.3.7.2 Screening of optimal incubation conditions by luciferase assay

Appropriate concentrations for each compound (β-estradiol, isoproterenol, insulin, and LYS294002) were identified based on literature search, and these concentrations served as references to create a serial dilution for each compound. The tested concentrations and solvents for each compound are presented in Table 6-4. There were two HEK293 control groups in the experiment: cells incubated in DMEM media ("Untreated"), and cells incubated in DMEM media with 0.3% DMSO ("DMSO"). Compounds were compared to the "untreated" or the "DMSO" control as shown in Table 6-4, based on the solvent used to dissolve the compound.

Table 6-4: Concentrations and solvents for candidate CK transcriptional regulators

Compound	Range of concentrations	Source for concentrations	Solvent	Compared to Control
β-estradiol	1 nM - 1 mM	[403,404]	ddH_2O	Untreated
Isoproterenol	1 μM - 1 mM	[405,406]	ddH_2O	Untreated
Insulin	0.5 - 500 μg/mL	[396]	ddH_2O	Untreated
LYS294002	1 – 100 μM	[395,407]	DMSO	DMSO

Cells were seeded in 96 well plates at 2 x 10^4 cells/cm^2, with three wells for each control, and four wells for each experimental group. Twenty four hours after seeding, cells were treated with each compound at the range of concentrations described above, for 24 hours before the luciferase assay as described in Section 0.

Subsequently, the experiment was repeated with 48 hour incubation time to allow more time for compound uptake and transcriptional activation. The compound concentrations used for the 48 hour experiment were identical to that of the 24 hour experiment.

6.3.7.3 Evaluation of CK mRNA by qRT-PCR

The luciferase assay allowed identification of the treatment concentrations/timeframe that produced the greatest potential change in CK transcription, as presented in Sections 6.4.4.1 and 6.4.4.3. The effects of these treatment strategies on CK transcription were evaluated through qRT-PCR with CK mRNA primers.

Cells were treated for 48 hours with 0.5 μg/mL – 500 μg/mL insulin, 10 and 100 μM isoproterenol, or 1 and 5 μM LYS294002, which were the optimal incubation strategies identified through the luciferase assay for generating a potential change in CK transcription. After treatment, cells were lysed and RNA was extracted for qRT-PCR as described in Section 0.

6.3.7.4 Assessment of putative control compounds with Steady-Glo Luciferase/Resazurin assay

The treatment strategies described in Section 6.3.7.3 were subsequently re-assessed utilizing the Steady-Glo Luciferase System/Resazurin assay, as described in Section 6.3.4.2. The results of this assay were verified utilizing qRT-PCR to measure changes in CK transcription, as described in Section 6.3.3.

6.3.8 Luciferase screening of compounds for CK-M-Luc cell line

After the luciferase assay was optimized and validated, compounds were screened on the CK-M-Luc cell line to identify their ability to regulate CK-M transcription. Tested compounds were supplied by TOCRIS (Biotechne, MN, USA), and were either known transcriptional regulators (*e.g.* rosiglitazone, aldosterone), or were suspected to affect CK activity (*e.g.* glucocorticoid receptor modulators). A full list of compounds can be found in Section 6.4.5. In summary, the screen was enriched for nuclear receptor agonist and antagonists, with four major classes of receptor modulators tested: sex hormone (androgen/oestrogen/progesterone) receptor modulators (16 compounds), glucocorticoid receptor modulators (6 compounds), peroxisome proliferator-activated receptor (PPARs) modulators (19 compounds), and retinoid/retinoic acid receptor (RAR/RXR) modulators (14 compounds). Seven compounds belonged to miscellaneous classes. The author was blind to compound names and classes while conducting the luciferase assay. The order of compounds tested was randomized prior to screening.

For the luciferase assay, cells were plated at 2 x 10^4 cells/cm^2 in 96 well plates, with 4 wells per compound. All of the test compounds were dissolved in DMSO, and 1 µL of each compound was further diluted 1:3 in DMSO and mixed in each well with 97 µL of 1 µg/mL puromycin DMEM to make a 100 µM concentration solution in 0.3% DMSO. Therefore, results from the compounds were compared to results from CK-M-Luc cells similarly incubated in 0.3% DMSO medium. OXO2393 was utilized as a false positive control. Twenty-four hours after seeding, cells were treated with tested compounds for 48 hours, after which cells were prepared for luciferase assay.

After initial screening utilizing the standard luciferase assay, the positive hits were subsequently re-assessed utilizing the Steady-Glo Luciferase System/Resazurin assay, as described in Section 6.3.4.2. The results of this assay were verified utilizing qRT-PCR to measure changes in CK-M mRNA, as described in Section 6.3.3.

6.3.9 Luciferase screening of compounds for CK-Mt-Luc cell line

The Steady-Glo Luciferase System/Resazurin assay, as described in Section 6.3.4.2, was utilized to screen the 62 compound plate detailed in Section 6.3.8, for the CK-Mt-Luc cell line. An initial screen was conducted with one well per compound in a 96 well plate, which yielded seven positive hits. These positive hits were confirmed through a repeat assay with larger sample sizes. The results were then confirmed with qRT-PCR, as described in Section 6.3.3, to measure changes in CK-Mt mRNA.

6.4 Results

6.4.1 Puromycin kill curve

The optimal concentration of puromycin for stable selection with HEK293 cells was determined to be 1 µg/mL, which was the lowest concentration that showed no viable colonies (Figure 6-5).

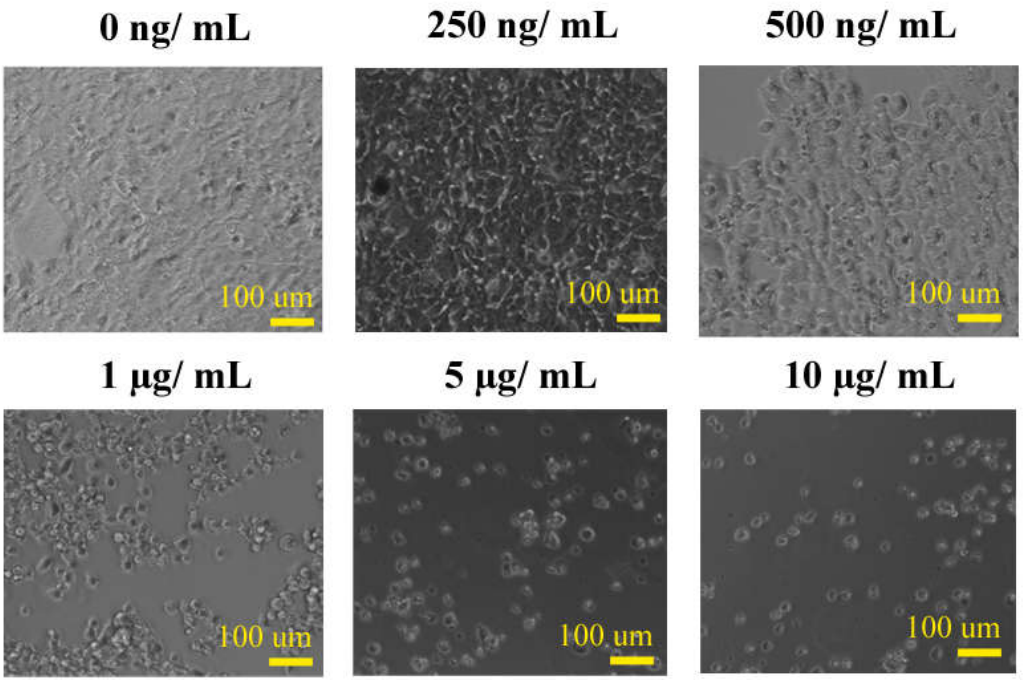


Figure 6-5: Puromycin causes dose-dependent death HEK293 cells.

Representative phase-contrast microscopy images of HEK293 cells cultured with a range of puromycin concentrations as indicated. Cell viability decreased significantly at 1 µg/ml. After microscopic observation, the death rates were quantified by flow cytometry, which showed that 1 µg/mL puromycin was lethal to approximately 80% of the HEK293 cells (Figure 6-6). Thus, it was confirmed that the lowest concentration required for the stable selection process was 1 µg/ml.

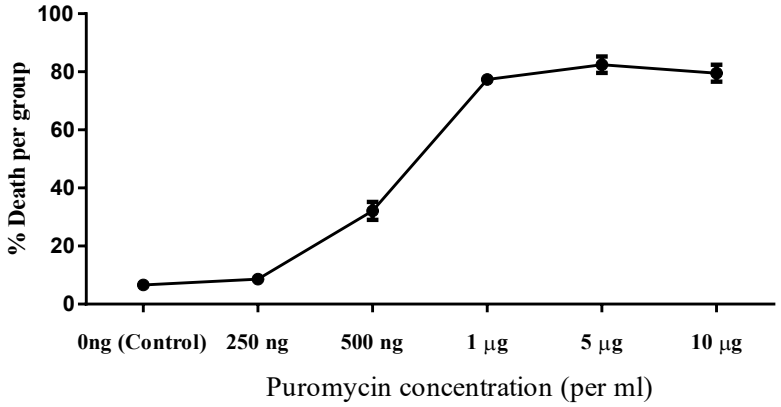


Figure 6-6: Puromycin kill curve as assessed by flow cytometry

Flow cytometry results demonstrating 1 μg puromycin is the lowest concentration that results in minimal viable colonies. Cell viability was assessed with PI. n = 2 wells per group.

6.4.2 CK-Luc constructs in transiently transfected cells

6.4.2.1 Transfection efficiency and luciferase mRNA expression

Transient transfection efficiency, as determined by proportion of GFP positive cells of total cells counted by the cell counter, was 20-25% for each group (data not shown).

Results of qRT-PCR, as shown in Figure 6-7, demonstrated that HEK293 cells were successfully transfected with the transgenic vectors, as the luciferase mRNA region of transgenes was clearly detectable in transfected cells. In contrast, there was no expression of the transgene in untransfected HEK293 cells and cells transfected with pGL4 empty vector (Figure 6-7).

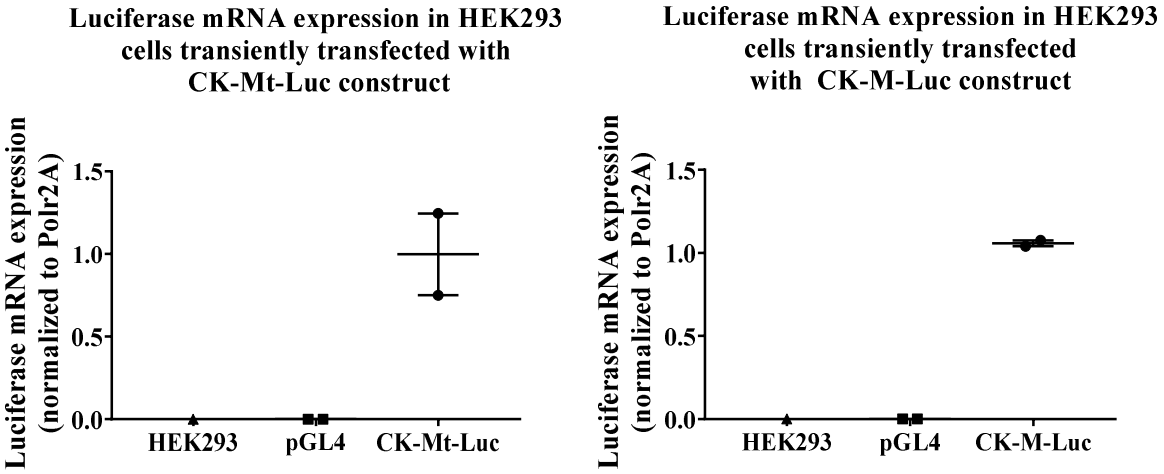


Figure 6-7: Expression of luciferase mRNA in transiently transfected HEK293 cells by qRT-PCR.

The expression of the CK-M and CK-Mt luciferase mRNA region was analysed by qRT-PCR in the CK-M-Luc and CK-Mt-Luc transfected cells, respectively. Luciferase mRNA expression levels were normalized to the expression of the reference gene Polr2A. Results demonstrate detection of CK-Luc construct in the transfected cells. n = 1-2 wells per group.

6.4.2.2 Transiently transfected cells express luciferase

As shown below in Figure 6-8, the luciferase assay results from the transfected cells suggest that both the CK-Mt-Luc and the CK-M-Luc vectors were successfully transfected. The transgenic cells expressed significant quantities of the luciferase enzyme, comparable to that of cells transfected with CrT-Luc, which were previously generated and validated in our laboratory.

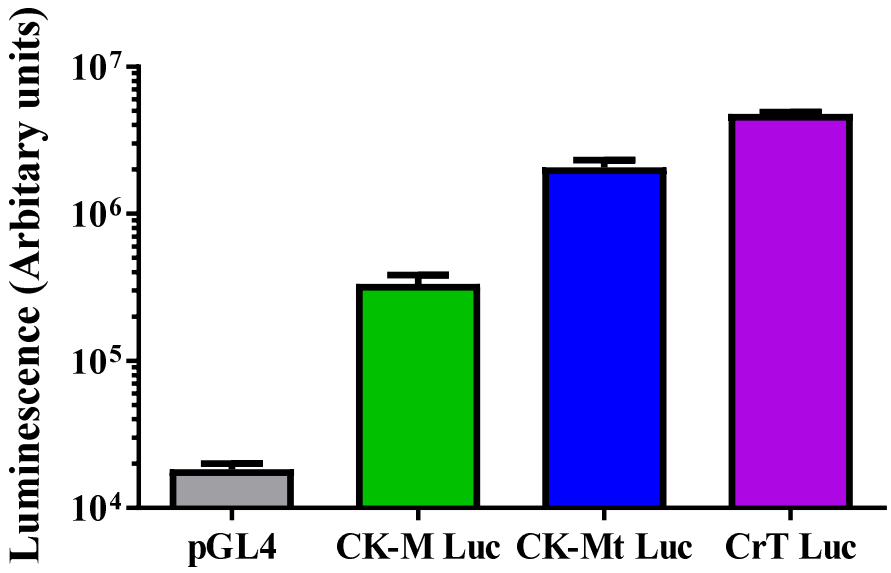


Figure 6-8: Luciferase assay results from HEK293 cells transiently transfected with CK-Mt-Luc or CK-M-Luc

Luminescence (arbitrary units) of HEK293 cells transfected with pGL4 empty vector, CK-Mt-Luc, CK-M-Luc, and CrT-Luc, which functioned as a positive control. $n = 3$ wells per group. Y-axis is logarithmic scale.

6.4.3 Characterization of stably transfected CK-Luc cell lines

6.4.3.1 Linearized vector by restriction digest

The circular vectors were linearized by appropriate restriction enzymes and the linearized vectors were separated by gel electrophoresis as presented in Figure 6-9 below.

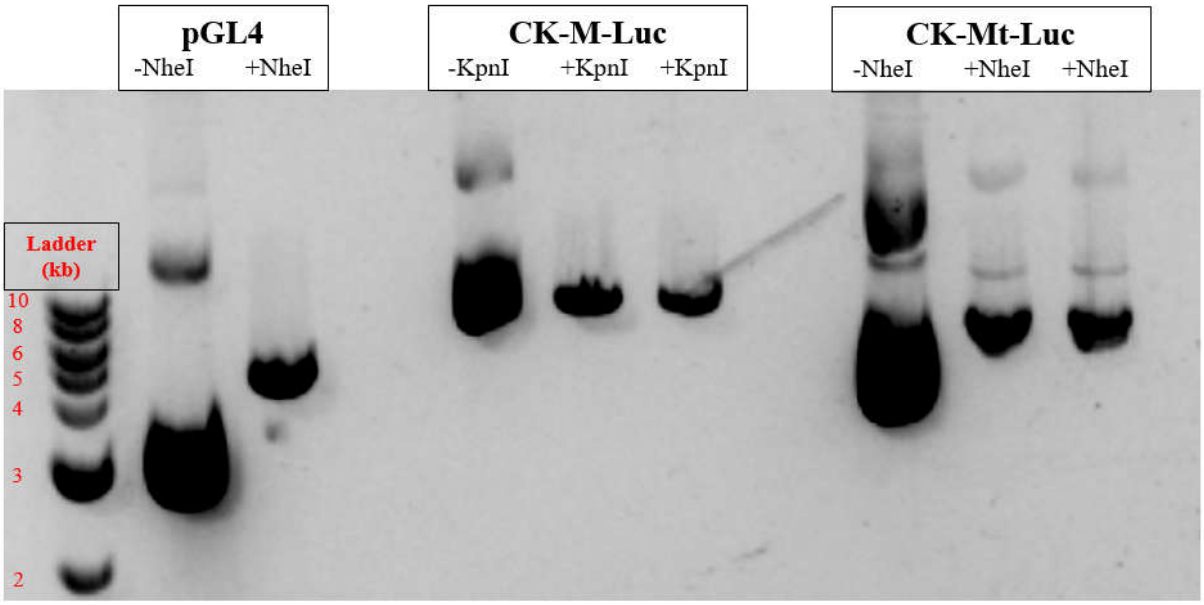


Figure 6-9: Restriction digest of CK-Luc vectors

Gel electrophoresis showed circular vectors, and linearized vectors after restriction digest with appropriate enzymes. Note that the undigested vector for each sample shows two bands due to the circular structure.

6.4.3.2 Identification and selection of stably transfected colonies

After cells were stably transfected with the appropriate linearized vectors and challenged with puromycin, individual puromycin-resistant colonies of CK-Mt-Luc and CK-M-Luc could be identified under microscopy, as shown in Figure 6-10. Unfortunately, there were no surviving colonies in the pGL4 group despite the presence of the puromycin resistance gene and two attempts to generate a stable cell line.

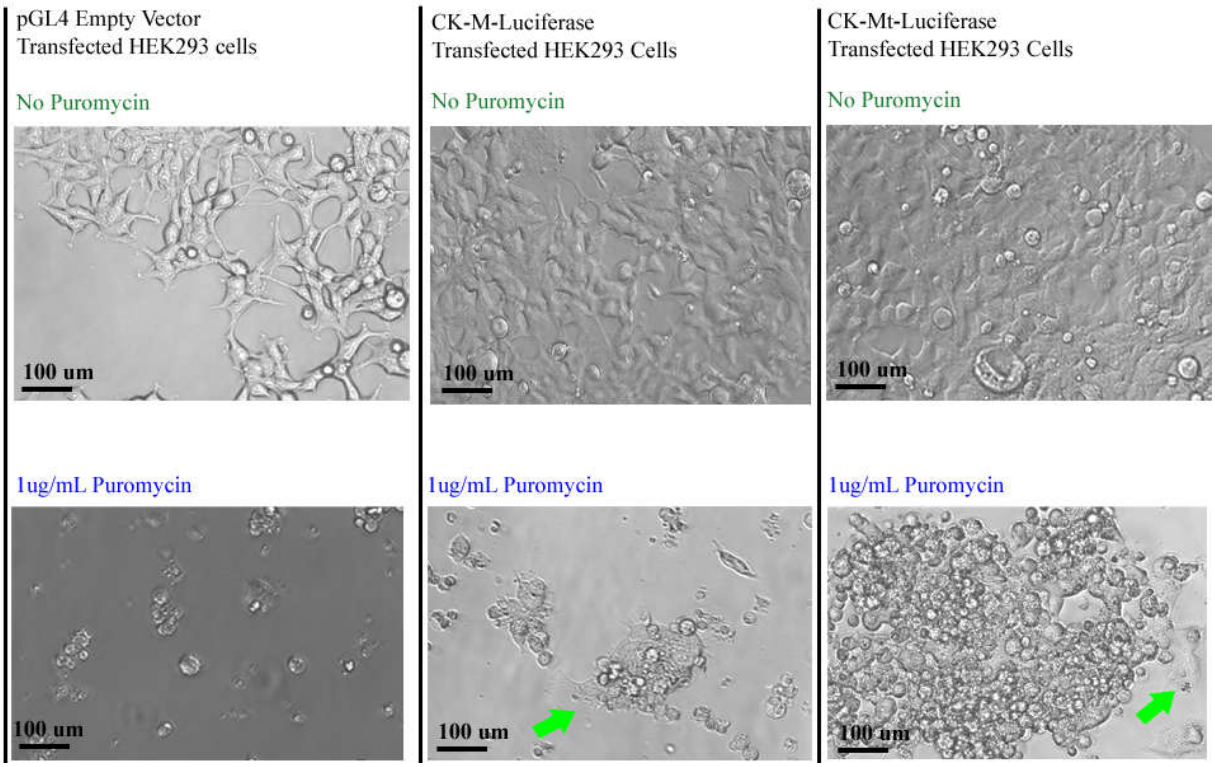


Figure 6-10: Puromycin selection of CK-M-Luc or CK-Mt-Luc plasmid transfected HEK293 cells

HEK293 cells in DMEM media (top panels) demonstrated proliferation, whereas HEK293 cells in 1 µg puromycin/mL DMEM media showed significant cell death (bottom panels). pGL4 transfected cells in 1 µg puromycin/mL DMEM media did not show surviving colonies, whereas puromycin-resistant cells survived in the CK-M-Luc and CK-Mt-Luc transfected wells (bottom middle and right) as green arrows indicated. Bar scale: 100 µm

6.4.3.3 Detection of luciferase mRNA through qRT-PCR

qRT-PCR analysis of the stably transfected cells revealed expression of the luciferase mRNA regions, as presented in Figure 6-11. These findings confirmed successful vector integration in both CK-Luc cell lines.

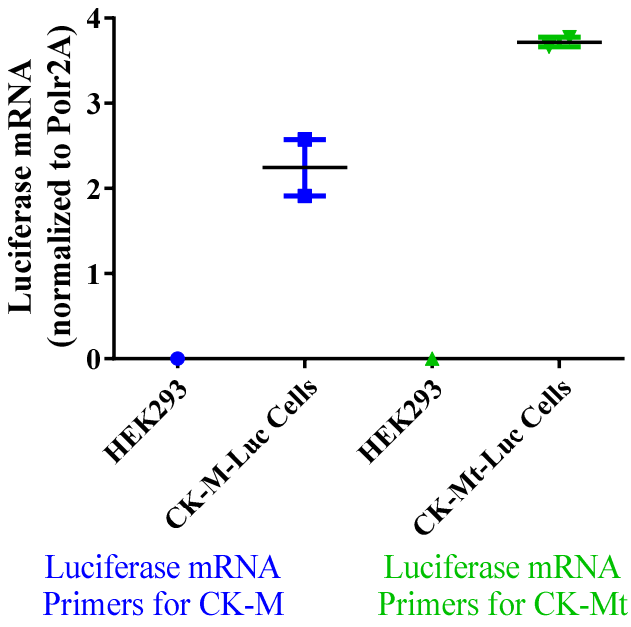


Figure 6-11: Confirmation of luciferase mRNA expression in stably transfected HEK293 cells

qRT-PCR analysis for the CK-M-Luc and CK-Mt-Luc cell lines indicated successful stable integration of the full transgene, as luciferase mRNA expression were detected in each transgenic line. Transgene expression was normalized to Polr2A reference gene. n = 1-2 wells per group.

6.4.3.4 Stably transfected cells expressed luciferase

Luciferase luminescence values for both stably transfected cell lines were within an order of magnitude of CrT-Luc control, with CK-Mt-Luc cells exhibiting a similar level of luminescence (Figure 6-12). These results demonstrated that the stably transfected cell lines had robust luciferase protein expression and activity.

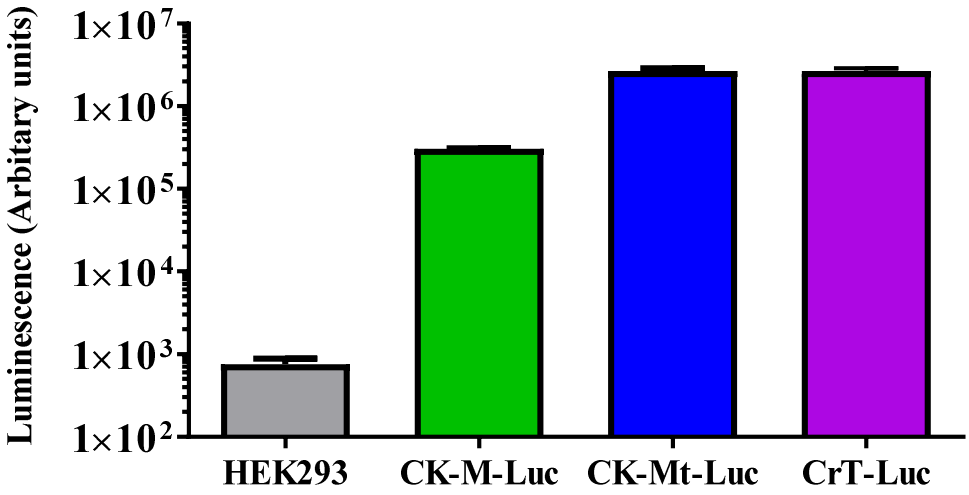


Figure 6-12: Luciferase assay results for stably transfected CK-Luc cells

Luminescence was measured for untransfected HEK293 cells, and HEK293 cells stably transfected with CK-Mt-Luc, CK-M-Luc, and CrT-Luc, which acted as a positive control. Y-axis is logarithmic scale. n = 3 wells per group.

6.4.4 Evaluation of putative CK transcriptional regulators

6.4.4.1 Effects on luciferase activity in CK-M-Luc cell line by luciferase assay

The luciferase assay results for the CK-M-Luc cell line are described below. Following 24 hours of treatment (Figure 6-13A), β-estradiol and insulin at tested concentrations appeared to have no effect on luciferase activity. Isoproterenol at concentrations of 1-100 μM did not alter luciferase activity, but appeared to result in cell death at 1 mM, as observed through microscopy.

As shown in Figure 6-13B, β-estradiol treatment did not appear to cause any significant alterations in luciferase activity at 48 hours, recapitulating findings seen at 24 hours. Isoproterenol appeared to produce a dose-dependent decline in luciferase activity (which was not seen at 24 hours), although it still appeared to be cytotoxic at 1 mM. The effects of insulin on luciferase activity were more pronounced following 48-hour treatment. Insulin treatment induced approximately a 30% increase in luciferase activity at 48 hours at all four concentrations ($p < 0.001$), though it was unclear whether this was a dose-dependent effect.

The results of LYS294002 treatment are presented in Figure 6-14. With 24-hour treatment, LYS294002 at 100 μM significantly decreased luciferase activity, though this may have been related to cytotoxicity, which was evident under microscopy (data not shown). There was no significant effect at other incubation concentrations. With 48-hour incubation, LYS294002 induced a dose-dependent decline in luciferase activity. However, this was again complicated by its potentially cytotoxic effects, as there appeared to be substantial cell death in wells treated with 10 μM and 100 μM LYS294002.

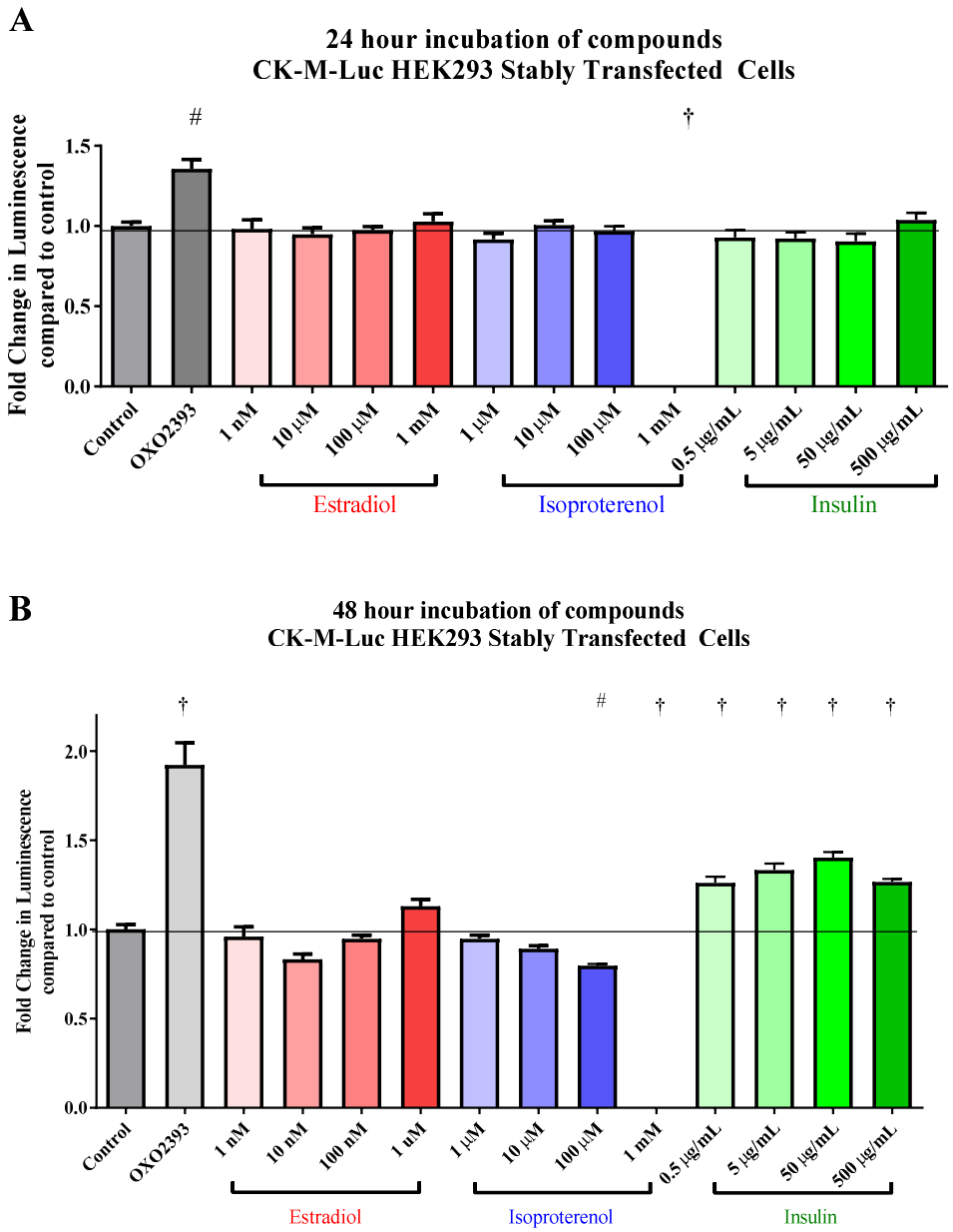


Figure 6-13: Effect of putative transcriptional regulators on luciferase activity of CK-M-Luc cells

(A): Luciferase values of CK-M-Luc cells incubated for 24 hours with various agents, compared to values from control (CK-M-Luc stably transfected HEK293 cells in normal DMEM). (B): Same experiment as (A), but with 48-hour incubation. Y axis: luminescence value in tested sample/respective control value (fold change compared to control). Data was analysed by one-way ANOVA with Bonferroni's post hoc test. # = $p < 0.001$; † = $p < 0.0001$. $n = 4$ trials (16 wells) for each incubation time.

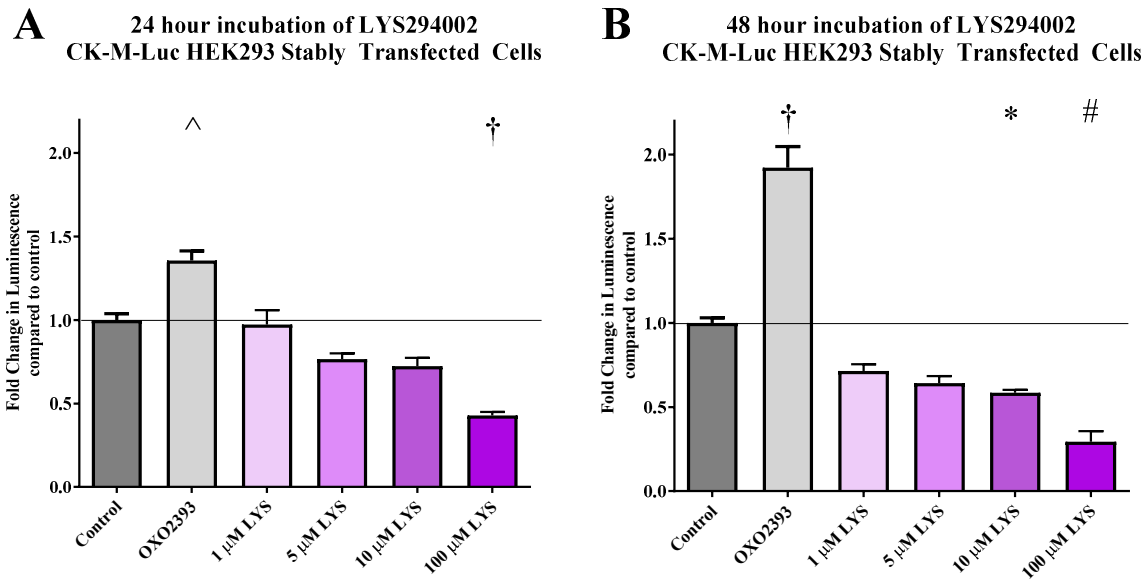


Figure 6-14: Effect of LYS294002 on luciferase activity of CK-M-Luc cells

(A): Luciferase values of CK-M-Luc cells incubated for 24 hours with LYS294002, compared to values from control (0.3% DMSO in DMEM). (B): Same experiment as (A), but with 48-hour incubation. Y axis: luminescence value in tested sample/respective control value (fold change compared to controls). Data was analysed by one-way ANOVA with Bonferroni's post hoc test. * = $p < 0.05$; ^ = $p < 0.01$; # = $p < 0.001$; † = $p < 0.0001$. $n = 4$ trials (16 wells) for each incubation time.

6.4.4.2 Changes in CK-M mRNA transcription as assessed by qRT-PCR

Luciferase assay results indicated that insulin, isoproterenol, and LYS294002 could potentially modulate CK transcription. Thus, qRT-PCR was conducted to investigate whether these compounds affected CK-M transcription.

qRT-PCR results (Figure 6-15) showed that insulin treatment appeared to produce a trend towards increased CK-M mRNA levels. CK-M transcription after isoproterenol treatment did not appear to change, whereas there appeared to be a trend towards decreased CK-M transcription with LYS294002 treatment.

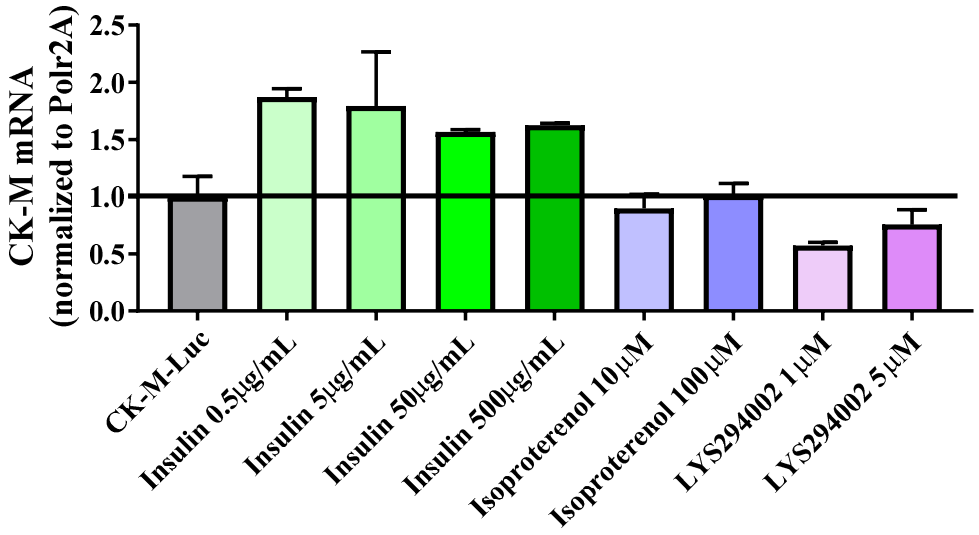


Figure 6-15: Effects of putative transcriptional regulators on CK-M mRNA as analysed through qRT-PCR in CK-M-Luc cells

CK-M-Luc stably transfected HEK293 cells were incubated with compounds for 48 hours before qRT-PCR analysis. Results are expressed as a ratio of CK-M mRNA level normalized to Polr2A mRNA level, and then to CK-M mRNA expression of CK-M-Luc cells. n = 2 wells for each group.

6.4.4.3 Effects on luciferase activity in CK-Mt-Luc cell line by luciferase assay

As shown in Figure 6-16A, at 24 hour of incubation, β-estradiol, isoproterenol, and insulin did not appear to significantly affect luciferase activity, with the exception that 1 mM isoproterenol appeared toxic to cells and almost no luciferase activity was detected. Figure 6-16B exhibits the results at 48 hours of treatment. β-estradiol again did not affect luciferase activity. Isoproterenol appeared to cause a dose-dependent inhibition on luciferase activity, although under microscopy, it was visibly cytotoxic at 1mM. Insulin at 5 μg/mL – 500 μg/mL appeared to produce approximately 30% higher luciferase activity.

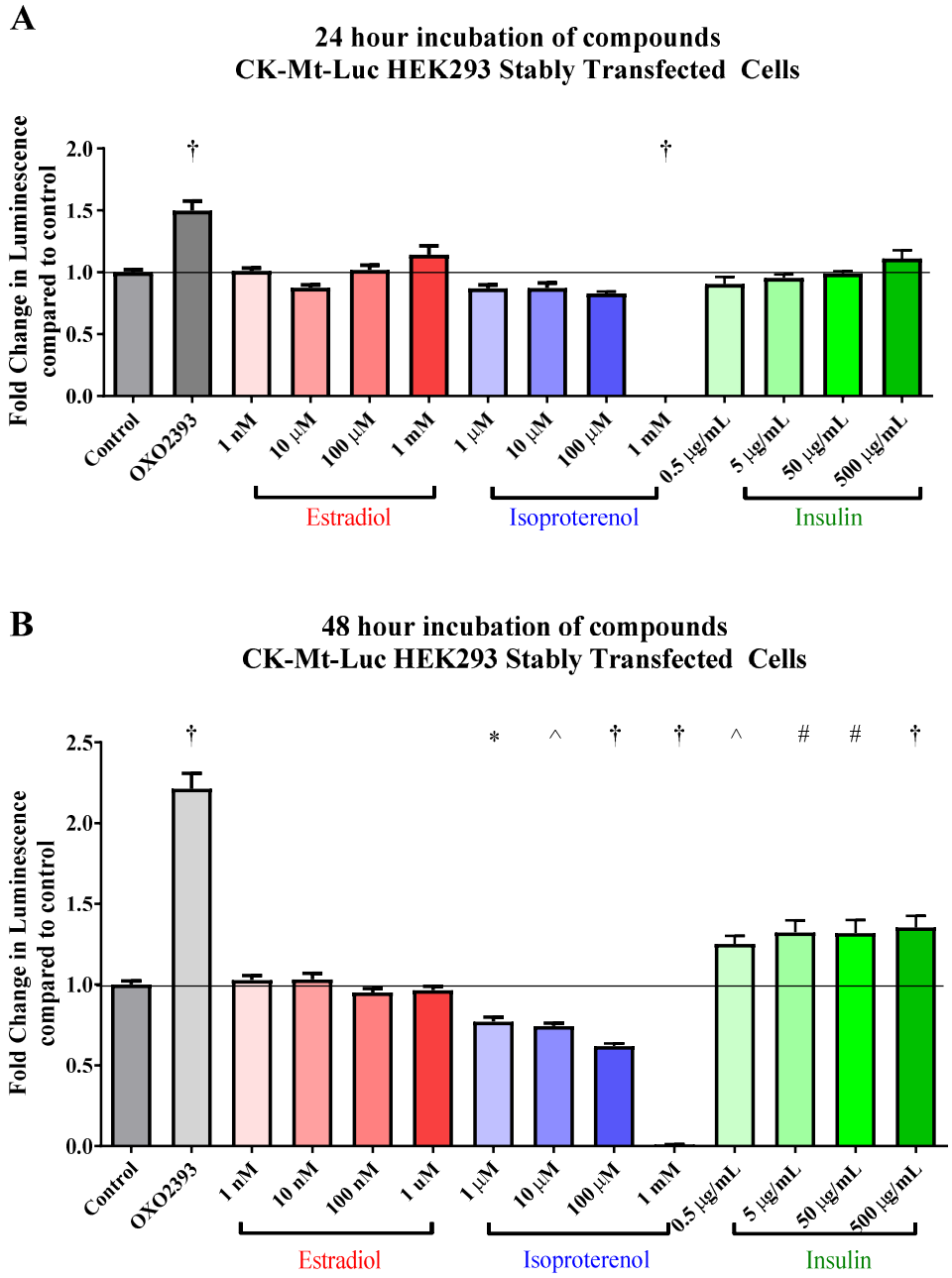


Figure 6-16: Effect of putative transcriptional regulators on luciferase activity of CK-Mt-Luc cells

(A): Luciferase values of CK-Mt-Luc cells incubated for 24 hours with various agents, compared to values from control (CK-Mt-Luc stably transfected HEK293 cells in normal DMEM). (B): Same experiment as (A), but with 48-hour incubation. Y axis: luminescence value in tested sample/respective control value (fold change compared to controls). Data was analysed by one-way ANOVA with Bonferroni's post hoc test. * = $p < 0.05$, ^ = $p < 0.01$; # = $p < 0.001$, † = $p < 0.0001$. (A) $n = 1$ trial (4 wells); (B) $n = 4$ trials (16 wells)

At both 24 and 48 hours, LYS294002 treatment reduced luciferase activity, and this was dose-dependent at 48 hours (Figure 6-17). However, this was complicated by the fact that there appeared to be cytotoxicity under microscopy in the 10 µM and 100 µM treatment group at both time periods.

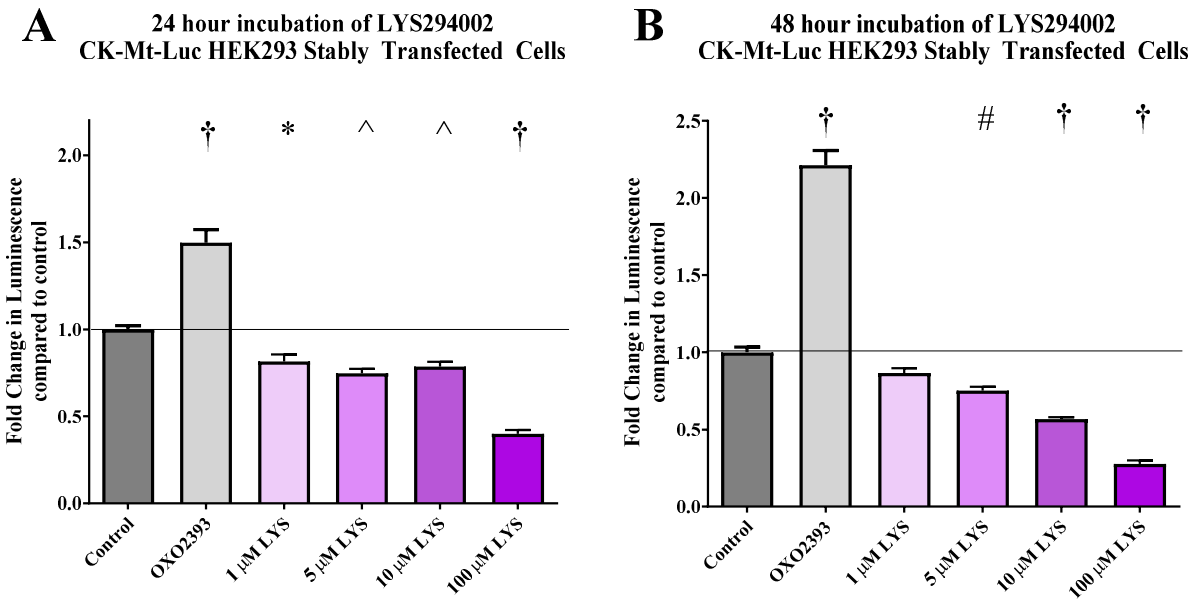


Figure 6-17: Effect of LYS294002 on luciferase activity of CK-Mt-Luc cells

(A): Luciferase values of CK-Mt-Luc cells incubated for 24 hours with LYS294002, compared to values from control (0.3% DMSO in DMEM). (B): Same experiment as (A), but with 48-hour incubation. Y axis: luminescence value in tested sample/respective control value (fold change compared to controls). Data was analysed by one-way ANOVA with Bonferroni's post hoc test. * = $p < 0.05$; ^ = $p < 0.01$; # = $p < 0.001$; † = $p < 0.0001$. $n = 4$ trials (16 wells) for each incubation time.

6.4.4.4 Changes in CK-Mt mRNA transcription as assessed by qRT-PCR

Similar as CK-M, qRT-PCR was conducted to investigate whether compounds that altered luciferase activity in the luciferase assay caused changes in CK-Mt mRNA expression.

qRT-PCR results (Figure 6-18) showed that insulin at 0.5 μg/mL trended towards increased CK-Mt mRNA levels. Isoproterenol did not appear to exert any effect on CK-Mt transcription, whereas LYS294002 appeared to cause a trend towards decreased CK-Mt expression.

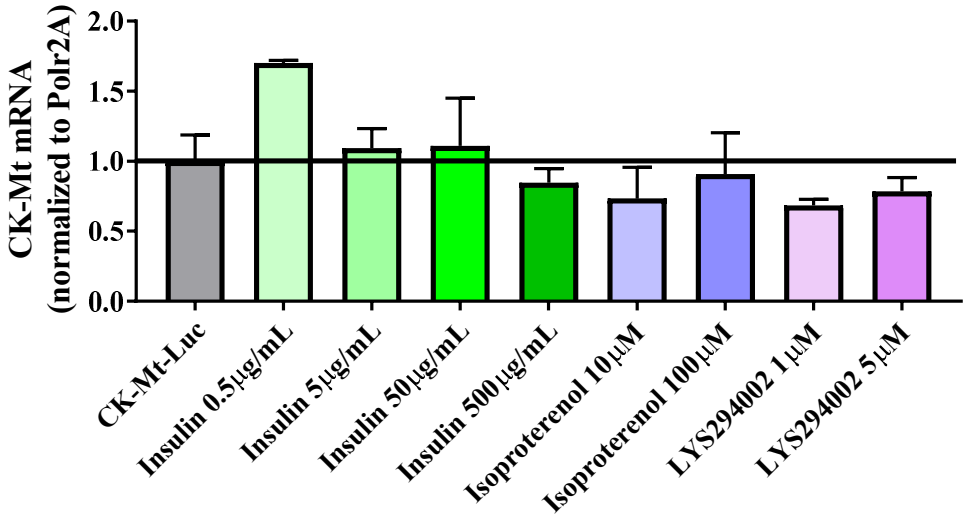


Figure 6-18: Effects of putative transcriptional regulators on CK-Mt mRNA as analysed through qRT-PCR in CK-Mt-Luc cells

CK-Mt-Luc stably transfected HEK293 cells were incubated with the compounds for 48 hours before qRT-PCR analysis. Results are expressed as a ratio of CK-Mt mRNA level normalized to Polr2A mRNA level, and then to CK-Mt mRNA expression of CK-Mt-Luc cells. $n = 2$ wells for each group.

6.4.5 Screening of compounds for the CK-M-Luc and CK-Mt-Luc cell lines with the luciferase assay

Compound screening occurred in the following order. First, an initial screen of 62 compounds was conducted using the standard Luciferase Assay System (Promega), with the CK-M-Luc cell line. Subsequently, CK-M-Luc and CK-Mt-Luc cell lines were both tested using the Steady-Glo Luciferase Assay System (Promega), which was more appropriate for high-throughput screening. Simultaneously, the resazurin assay was conducted to assess cell proliferation. The results of the Steady-Glo Luciferase/resazurin assay were then verified by qRT-PCR for CK-M and CK-Mt mRNA.

6.4.5.1 Initial screening results using standard luciferase assay

Additional compound screening was conducted for CK-M-Luc, though only at one concentration (100 μM) and at one time-period (48 hours) per compound. Sixty two compounds were screened and positive results are shown in Figure 6-19. A summary of the results from all compounds tested is given in Table 6-5.

There are no consensus guidelines for what defines a positive hit using the luciferase assay. For the current assay it was arbitrarily decided to set positive hits at >3 SD of the DMSO control (>25.4% increase in relative luminescence) to minimize the risk of false positives and to select compounds with a robust response. Twelve of the 62 compounds showed increased luciferase activity based on this criterion, with five compounds demonstrating at least a two-fold increase in luminescence signal.

Of the 12 compounds that were positive hits, six were glucocorticoid receptor agonists (dexamethasone, hydrocortisone, fluticasone propionate, methylprednisolone, budesonide, and GSK 9027). The other compounds with positive hits included three RAR/RXR agonists (EC23, AC261066 and SR11237), an oestrogen receptor agonist (WAY 200070), a PPAR agonist (pioglitazone HCl), and a thyroid receptor agonist (GC1). The glucocorticoid receptor agonists appeared to produce the most robust increase in luciferase activity, with on average 2.2-fold higher activity than that of DMSO-treated CK-M-Luc cells.

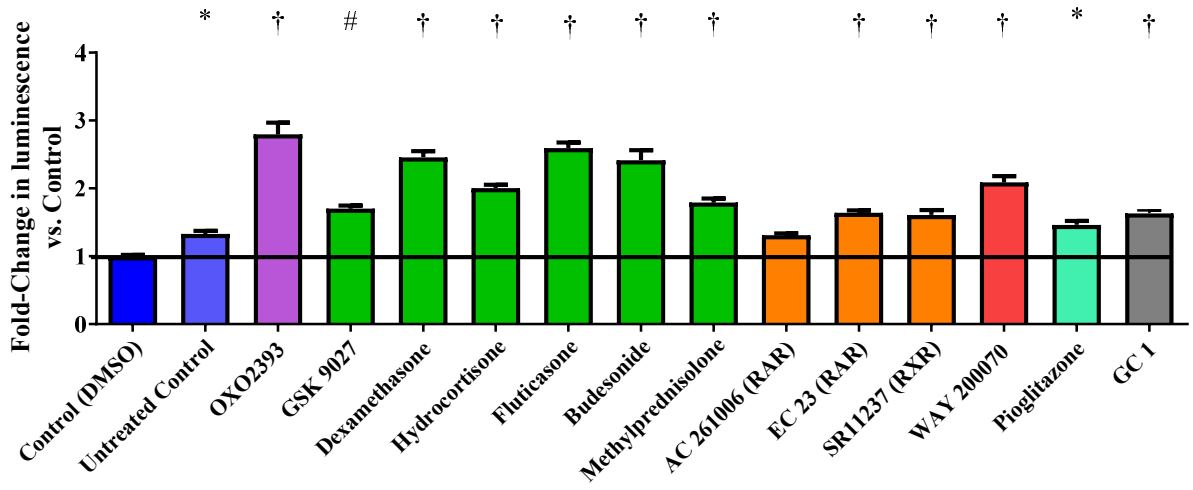


Figure 6-19: Positive hits from luciferase screening for CK-M-Luc cell line

The figure includes the results from compounds that increased luciferase activity by at least 30% as compared to DMSO-treated HEK293 control cells, which were considered positive hit. OXO2393 was utilized as a non-transcriptional positive control. All compounds were tested at 100 µM. Green bars: Glucocorticoid receptor agonists; Orange bars: RAR/RXR agonists; Red bar: Oestrogen Receptor β agonist; Teal bar: PPAR-γ agonist; Grey bar: Thyroid receptor agonist. Results were analysed by one-way ANOVA with Bonferroni's post-hoc test (* = $p < 0.05$; # = $p < 0.001$; † = $p < 0.0001$). n = 1-4 trials (4-16 wells) per group.

Table 6-5: All results of luciferase screening for the CK-M-Luc cell line

Compound	n	Average*	SD**
DMSO Control	15	1.0	0.08
Glucocorticoid receptor modulators			
Budesonide	4	2.41	0.3
Dexamethasone	4	2.46	0.18
Fluticasone	12	2.7	0.32
GSK 9027	4	1.7	0.09
Hydrocortisone	12	2.01	0.17
Methylprednisolone	4	1.79	0.11
Sex hormone receptor modulators			
AC 186	4	1.15	0.04
Bazedoxifene	4	0.8	0.06
Bicalutamide	4	0.76	0.05
DY131	4	0.71	0.07
FERb 033	4	1.24	0.09
Flutamide	4	0.96	0.05
ICI 182,780	4	0.54	0.02
Meclizine HCl	4	0.61	0.05
Mifepristone	4	0.35	0.02
PHTPP	4	1.02	0.09
PPT	4	0.33	0.01
Raloxifene HCl	4	0.88	0.02
Tamoxifen citrate	4	0.52	0.03
WAY 200070	4	2.09	0.19
Y 134	4	0.64	0.05
ZK 164015	4	0.19	0.01
Other compounds			
GW 3965 HCl	4	0.48	0.09
Fexaramine	4	0.58	0.04
T 0901317	4	1	0.1
Spironolactone	4	1.14	0.12
SID 7969543	4	0.96	0.06
GC 1	16	1.51	0.2
ML 179	4	0.83	0.06

PPAR receptor modulators			
Compound	**n**	**Average***	**SD****
CP 775146	4	0.69	0.08
DG 172 HCl	4	0.98	0.07
Edaglitazone	4	0.93	0.04
Fenofibrate	4	0.87	0.05
GSK 0660	4	0.77	0.05
GSK 3787	4	0.87	0.12
GW 0742	4	1.23	0.09
GW 6471	8	0.2	0.1
GW 7647	4	0.93	0.1
L-165,041	4	0.88	0.12
nTZDpa	4	0.84	0.03
Pioglitazone HCl	4	1.46	0.11
Rosiglitazone	4	1.09	0.09
S26948	4	0.75	0.02
SR 1664	4	0.53	0.03
T 0070907	4	1.2	0.07
Tesaglitazar	4	1.03	0.1
Troglitazone	4	0.73	0.31
WY 14643	4	0.81	0.07
RAR/RXR receptor modulators			
AC 261066	12	1.31	0.09
AC 55649	4	1.07	0.04
Adapalene	4	0.25	0.02
AM 580	4	1.05	0.1
CD 437	4	0.08	0.01
Ch 55	4	0.64	0.06
EC 23	12	1.57	0.12
ER 50891	4	0.75	0.03
LE 135	4	0.62	0.03
MM 11253	4	0.68	0.12
PA 452	4	0.37	0.01
SR 1078	4	0.13	0.02
SR 11237	12	1.68	0.2
SR 2211	4	0.55	0.02

*: Fold-change in luciferase activity produced by compound, as compared to DMSO-treated CK-M-Luc cells.

**: Standard deviation n: Number of wells for compound (1 trial = 4 wells); Green = Considered positive hit; Pink = clear cytotoxicity under microscopy. All samples were tested at 100 µM.

6.4.5.2 Steady-Glo Luciferase, Resazurin, and qRT-PCR Results for CK-M-Luc cell line

The Steady-Glo Luciferase assay/Resazurin protocol was applied to the control compounds and positive hits previously identified in Section 6.3.7.1 and Table 6-5. The results are shown in Figure 6-20. All of the positive screening hits from the standard Luciferase assay were confirmed with the Steady-Glo luciferase/resazurin assay. All of the positive hits showed increased luciferase signal after normalizing for cell proliferation through the resazurin assay, indicating that their effect was independent of cell proliferation. LYS294002 did not show a significant decrease in resazurin-normalized luciferase signal; both the luminescence signal as well as the resazurin signal declined at the same rate, suggesting that the decrease in luminescence was due to reduced cell proliferation rather than reduced CK-M promoter activation. Likewise, there was no significant difference between CK-M-Luc cells treated with insulin and isoproterenol, as compared to control Figure 6-20, indicating the changes in luminescence could be attributed to effects on cell proliferation. 100 μM isoproterenol treatment produced a notable but not statistically significant reduction in resazurin-normalized luminescence, however, the treatment also substantially reduced cell proliferation, with 28% reduced resazurin signal as compared to untreated HEK293 cells.

The results of the assays were then verified through qRT-PCR conducted on a separate plate of cells with the same treatments, as presented in Figure 6-21 below. Four of the six tested glucocorticoid agonists (Fluticasone propionate, GSK9027, Dexamethasone, and Budesonide) were found to significantly increase CK-M mRNA at least two-fold (Budesonide; $p = 0.05$). None of the three RAR/RXR agonists tested caused a significant increase in CK-M mRNA. WAY200070, pioglitazone, and GC1 all significantly increased CK-M mRNA expression. Insulin, isoproterenol, and LYS294002 did not significantly alter CK-M mRNA expression.

The insulin/isoproterenol and LYS294002 results could not be combined with the data presented in Figure 6-15 due to the different incubation conditions (48 hour seeding/treatment time below, in contrast, 24 hour seeding + 48 hour treatment time in Figure 6-15).

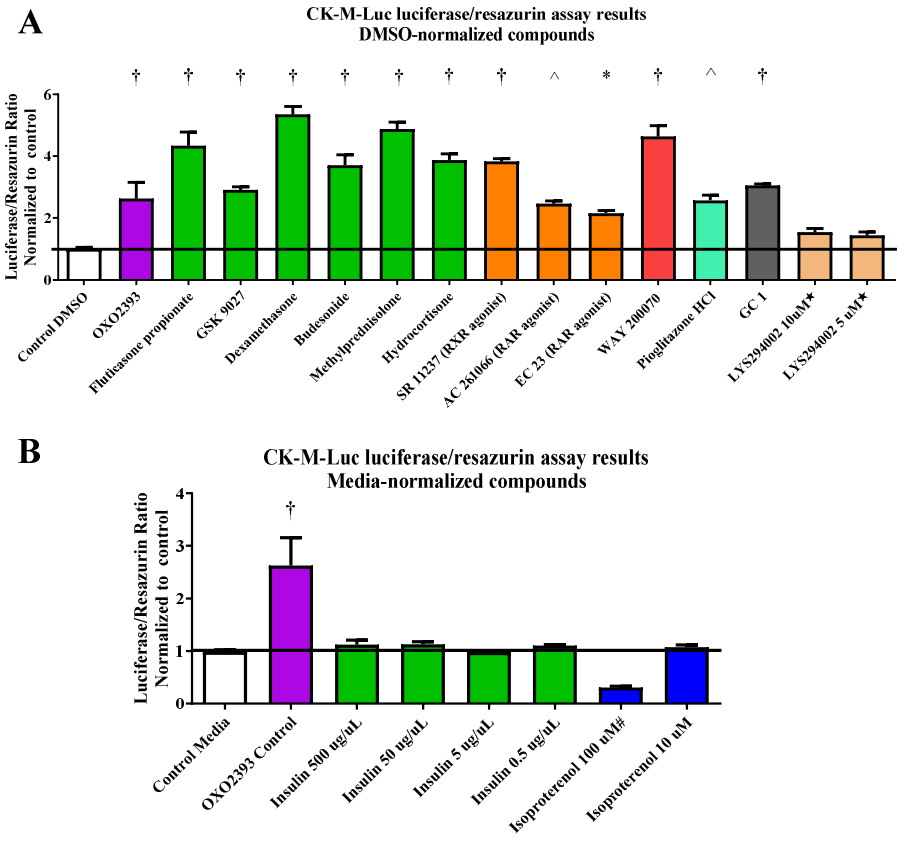


Figure 6-20: Steady-Glo Luciferase and Resazurin results for CK-M-Luc cell line

(A) Demonstrates the luciferase/resazurin results of CK-M-Luc cells incubated with treatments in 0.3% DMSO. Luminescence results are normalized to resazurin assay results, and expressed as a ratio of cells treated with only 0.3% DMSO. All compounds except LYS 294002 were tested at 100 µM. Green bars: Glucocorticoid receptor agonists; Orange bars: RAR/RXR agonists; Red bar: Oestrogen Receptor β agonist; Teal bar: PPAR-γ agonist; Grey bar: Thyroid receptor agonist. (B) Demonstrates the luciferase/resazurin results of CK-M-Luc cells incubated with treatments in media. OXO2393 was utilized as a non-transcriptional positive control. Results were analysed by one-way ANOVA with Bonferroni's post-hoc test (* = $p < 0.05$; ^ = $p < 0.01$; † = $p < 0.0001$, compared to control.). ★: Cells treated with LYS294002 had > 50% reduced cell count, as measured by the resazurin assay. #: cells treated with isoproterenol 100 µM demonstrated 28% reduced cell count, as measured by the resazurin assay. n = 3-4 wells per group.

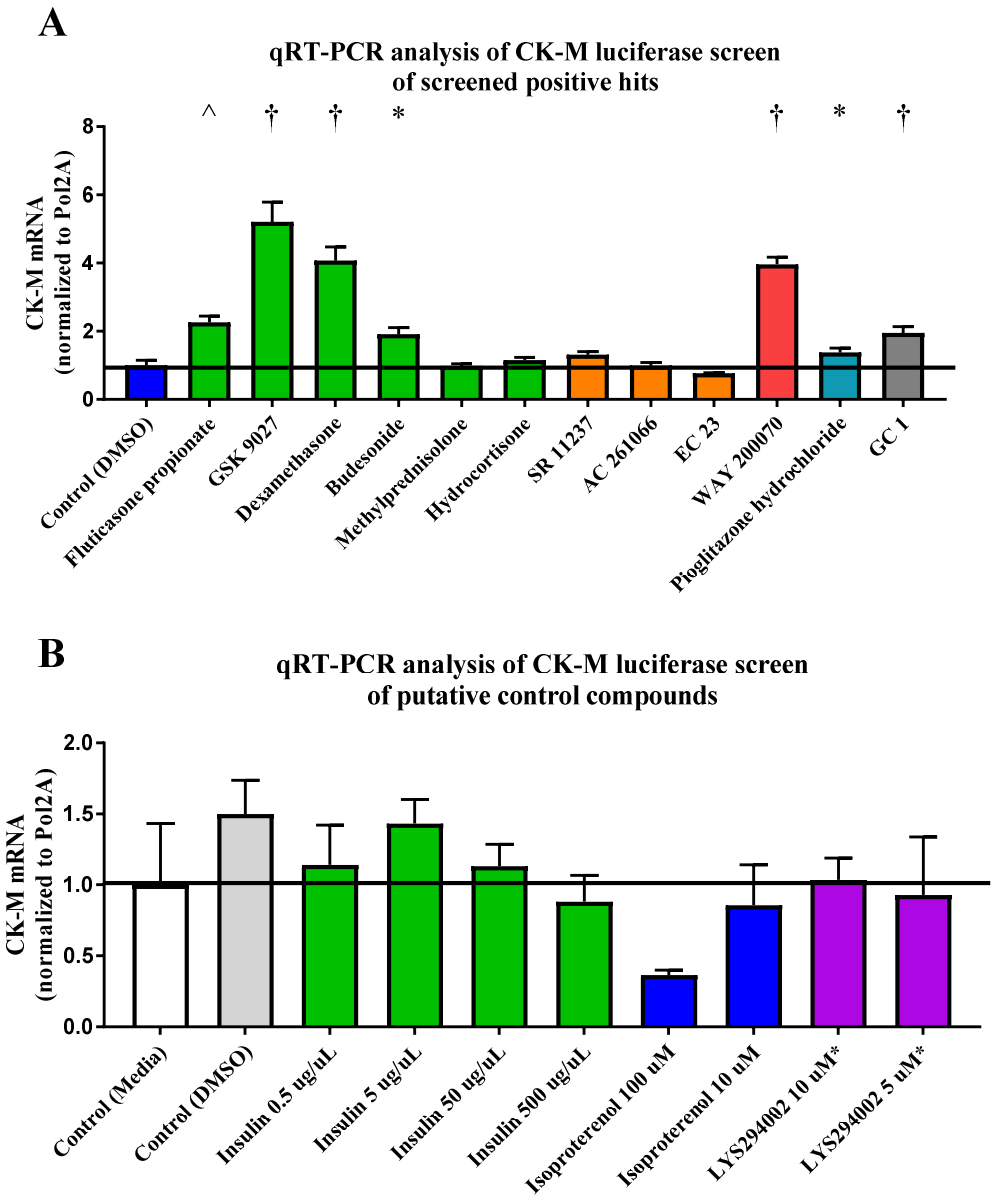


Figure 6-21: Effects of treatments on CK-M mRNA analysed through qRT-PCR

CK-M mRNA in CK-M-Luc transfected cells subjected to treatments as described in Section 6.4.4.1 was measured through qRT-PCR analysis. Results are expressed as a ratio of CK-M mRNA level normalized to Polr2A mRNA level. Results were analysed by one-way ANOVA with Bonferroni's post-hoc test (* = $p < 0.05$; ^ = $p < 0.01$; † = $p < 0.0001$, compared to control). n = 3 wells per group.

6.4.5.3 Steady-Glo Luciferase, Resazurin, and qRT-PCR Results for CK-Mt-Luc cell line

Given that the new Steady-Glo Luciferase/Resazurin assay was successful in the CK-M-Luc cell line, the procedure was used to screen the 62 compounds described in Table 6-5 for the CK-Mt-Luc cell line. An initial screen of one well per sample identified seven compounds considered positive hits (luciferase signal was > 3 SD higher than that of control, when normalized to resazurin (Data not shown). These seven compounds were then re-tested with 4 wells per sample, and the results are shown in Figure 6-22A. The increased luciferase signal was recapitulated in all groups (albeit not significantly in T0070907), indicating that the single-well approach can likely be utilized in the future for high throughput screening. There were no class of compounds that consistently increased luciferase signal in the CK-Mt-Luc cells, though three RAR/RXR agonists showed an increased signal. Subsequently, a second plate of cells using the same treatment and sample size (n = 4 wells per sample) was used to assess CK-Mt mRNA expression by qRT-PCR, and the results are shown in Figure 6-22B. Only T0070907, a PPAR-γ agonist, showed a statistically significant increase in CK-Mt mRNA, but as this increase was less than 2-fold, its biological significance remains to be determined. The other compounds did not produce a significant increase in CK-Mt mRNA. It appears that AM580 actually significantly reduced CK-Mt mRNA by one-fold.

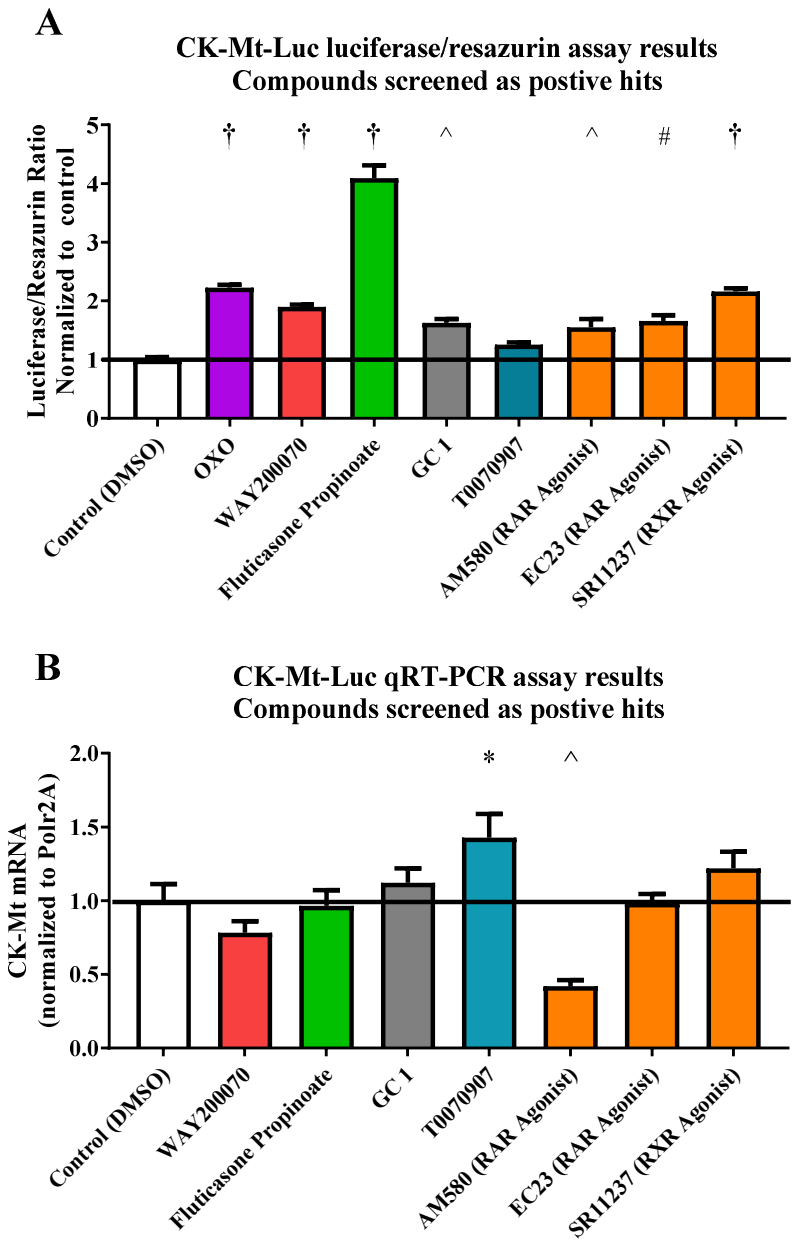


Figure 6-22: Steady-Glo Luciferase, Resazurin, and qRT-PCR screening results for CK-Mt-Luc cell line

Demonstrates the luciferase/resazurin results of CK-Mt-Luc cells incubated with treatments in 0.3% DMSO. Results were analysed by one-way ANOVA with Bonferroni's post-hoc test (* = $p < 0.05$; ^ = $p < 0.01$; $p < 0.001$; † = $p < 0.0001$, compared to control). n = 4 wells per group.

6.5 Discussion

In this experiment, an *in vitro* model system in HEK293 cells was developed and validated for investigation of CK transcriptional regulation. This model was subsequently used to assess whether potential CK transcriptional regulators had an effect on CK mRNA expression through the luciferase assay and qRT-PCR. In total, 66 compounds have been screened with the standard luciferase assay. Subsequently positive hits were further investigated utilizing the Steady-Glo/resazurin assay, as well as qRT-PCR.

6.5.1 Validation of CK-luciferase constructs

GFP co-transfection experiments found that the transient transfection efficiency was approximately 25%. Although the transfection methodology appeared viable, the transfection efficiency was lower than expected. This was suspected to be due to the excessively high seeding cell density, as visual examination of the wells prior to trypsinization revealed that the cells were over-confluent at 24 hours. As a result, the cell seeding density was reduced from 3.5×10^4 cells/cm^2 to 2×10^4 cells/cm^2 for subsequent experiments. Luciferase assay results confirmed that both of the transiently transfected CK-Luc cell lines expressed sufficient luciferase for signal measurement by the plate reader. The signal strength for both CK transfected groups, especially CK-M-Luc, was somewhat weaker than expected compared to CrT-Luc transfected cells. This may be explained by the fact that the CK-M-Luc vector was large at approximately 8.8 kb, and was therefore more difficult to transfect. Nevertheless, compared to the pGL4 transfected cells, the signals from both CK-M-Luc and CK-Mt-Luc transgenes were sufficiently robust to measure luciferase luminescence. Furthermore, both CK-

Luc cell lines expressed luciferase mRNA, as measured by qRT-PCR analysis, demonstrating that the elevation in luciferase activity resulted from transgene promoter activity.

HEK293 cells stably transfected with CK-M-Luc and CK-Mt-Luc also had sufficient luciferase expression for the luciferase assay, and luciferase mRNA expression was verified through qRT-PCR. Thus, HEK293 cells stably transfected with CK-luciferase constructs were validated as an *in vitro* model for screening compounds for their ability to regulate CK-M and CK-Mt transcription.

6.5.2 Effects of putative CK transcriptional regulators on CK-M and CK-Mt transcription

The literature suggested several compounds that may be implicated in regulation of the CK-M or CK-Mt promoter activity, of which four (β-estradiol, isoproterenol, insulin, and LYS294002) were tested. The results from these studies should be interpreted with caution due to limitations, as discussed in Sections 6.5.4 and 6.6.

The luciferase assay was utilized to screen various incubation concentrations and timeframes for these four compounds to identify the treatment strategies that resulted in the greatest potential effect on CK transcription, as reflected by the most significant changes in luminescence. The optimal incubation strategies were then tested with qRT-PCR with primers for CK mRNA to validate whether they affected CK transcription. Any confirmed modulators of CK transcription would have been used as a transcriptional control in subsequent luciferase screens.

For both cell lines, the standard luciferase assay showed that various concentrations of insulin, isoproterenol, and LYS294002 at 48 hours may affect CK transcription, as there were alterations in luciferase activity without any visual signs of cytotoxicity at some tested concentrations.

Insulin significantly increased luciferase activity in both CK-M-Luc and CK-Mt-Luc cell lines, indicating that insulin may enhance CK-M and CK-Mt transcription. Further investigation was carried out in the CK-M-Luc cell line utilizing the Steady-Glo Luciferase/Resazurin assay, which was not done for the CK-Mt-Luc cell line due to insufficient cell numbers at the time of writing.

The results from the Steady-Glo Luciferase/Resazurin assay in CK-M-Luc cells strongly suggests that the increased luciferase signal was entirely due to cell proliferation. The results of resazurin assay demonstrated that insulin increased cell proliferation approximately 30%, and there was no increase in luciferase signal when normalized to its resazurin result. This result is supported by the literature (it is well known that insulin has cell proliferation effects [396]), as well as by two different qRT-PCR experiments that failed to detect a significant increase in CK-M mRNA in any of the insulin treated groups. Thus, current study indicated that insulin cannot be selected as a transcriptional positive control in screening assay since it had no effect on CK-M transcription, a finding that likely holds true for the CK-Mt-Luc cell line as well (though this could not be formally assessed), given that both are HEK293 cells.

LYS294002 at ≥ 5 μM and isoproterenol at ≥ 10 μM significantly decreased luciferase activity in both CK-M-Luc and CK-Mt-Luc cell lines. However, 10 μM and 100 μM LYS 294002, as well as 1 mM isoproterenol appeared cytotoxic under microscopy. Based on these findings, the moderate treatment strategies for both compounds (1 μM and 5 μM LYS294002 and 10 μM

and 100 μM isoproterenol for 48 hours) were assessed for effects on CK mRNA by qRT-PCR. The qRT-PCR results did not reveal any substantial changes in either cell line, which indicates that the decline in luciferase activity may have been due to cytotoxicity. Therefore, further investigation was conducted utilizing the Steady-Glo Luciferase/Resazurin assay in the CK-M cell line, which demonstrated that both LYS294002 and isoproterenol were substantially cytotoxic. After correction for resazurin-measured cell toxicity, the luciferase signal was not significantly different from control, indicating that neither compound exerted a significant effect on CK-M transcription. This was subsequently verified by additional qRT-PCR for CK-M mRNA. These findings are in agreement with the literature - isoproterenol has been shown to be cytotoxic at high concentrations (100 μM) in muscle cell culture [408], and LYS294002 is a PI3K inhibitor, which is a class of compounds known to prevent cell proliferation [409]. Hence, neither compound was suitable as a transcriptional control for the luciferase screening assay. Again, while results were not explicitly assessed in the CK-Mt-Luc cell line due to technical difficulties, it is likely that LYS294002 and isoproterenol exert similar cytotoxic effects in the CK-Mt-Luc cell line.

For both the CK-M-Luc and the CK-Mt-Luc cell lines, β-estradiol at ≥ 1 nM had no significant impact on luciferase activity. This suggests that β-estradiol likely did not affect CK transcription, hence further investigation with qRT-PCR was not pursued. This would be in agreement with the literature, which does not suggest that the CK-M and CK-Mt promoters contained gonadocorticoid response elements.

6.5.3 Results from compound screen

6.5.3.1 CK-M-Luc results

Of the compounds tested during the luciferase screening of CK-M-Luc cells with the standard luciferase assay, glucocorticoid receptor agonists produced the most profound increase in luciferase activity, with all six tested compounds increasing luciferase activity by at least 70%. These results were subsequently confirmed utilizing the Steady-Glo Luciferase/resazurin assay, and verified through qRT-PCR, which showed that four of the six tested compounds (Dexamethasone, fluticasone, GSK9027, and budesonide) significantly increased CK-M mRNA expression. This finding would be consistent with existing data. The most relevant was a study that reported antenatal administration of dexamethasone increased CK-M and CK-Mt mRNA transcription and protein expression in rat heart [410], with other studies reporting that glucocorticoids increase CK activity in C2C12 myoblast cells [411,412]. Overall, it appears that glucocorticoids can regulate CK transcription because they promote differentiation of muscle cells and maturation of the heart at birth [411,412]. The pathway by which glucocorticoids regulate CK has yet to be definitively identified. Since glucocorticoids are known to activate myogenin and MyoD, this could be a potential mechanism [411].

The other classes of drugs that demonstrated increases in luciferase activity were RAR/RXR modulators and thyroid hormone agonists. The RAR/RXR luciferase results were not as consistent as those of glucocorticoid receptor modulators. Of 14 compounds tested, only three RAR/RXR agonists showed significantly increased luminescence. Subsequent qRT-PCR experiments demonstrated that none of the three compounds significantly increased CK-M mRNA, suggesting that the class does not affect CK-M transcription. Only one thyroid receptor

agonist (GC1) was tested, which showed 50% elevated luciferase activity, and was subsequently confirmed through qRT-PCR analysis to increase CK-M mRNA. Hypothyroidism has been suggested to decrease total CK activity [413], thus more compounds of this class should be assessed.

The remaining compound classes did not appear to consistently affect luciferase activity. CK transcription may be controlled by PPAR, which are highly active in heart [414]. However, of 19 compounds tested (which cover PPAR-α, -β, -γ, -δ classes), only pioglitazone increased luciferase activity 45% and CK-m RNA levels. Likewise, of 16 sex hormone compounds tested, only the compound WAY200070, a selective β-oestrogen receptor agonist, produced an increase in luciferase activity and CK-M mRNA. These results are in agreement with the earlier findings from β-estradiol that oestrogen likely only regulates CK-B and CK-uMt, but not CK-M and CK-Mt.

6.5.3.2 CK-Mt results

Of the 62 compounds screened for the CK-Mt-Luc cell line, seven were initially identified, of which six were later recapitulated with a larger sample size. However, of these compounds only T0070907, a PPAR-γ agonist, produced statistically significantly higher CK-Mt mRNA expression as assessed by qRT-PCR, though this finding is of questionable biological significance as CK-Mt mRNA/luciferase signal increased <50%. It is reasonable that far more CK-M transcriptional regulators were identified, as compared to CK-Mt transcriptional regulators – as described in Section 6.1.4, the CK-M promoter region has far more binding sites, and is much better understood as compared to the CK-Mt promoter region.

6.5.4 Limitations of the luciferase assay

The initial screening of 66 compounds resulted in 12 positive hits, which represents a promising preliminary finding. However, there are several limitations of the luciferase assay that must be considered when interpreting these results. The high rate of positive results is likely in part because the tested compounds were selected due to their known role as transcriptional regulators, and in many cases, their apparent relationship to the CK system [410]. However, there are also several other reasons that could cause false positives, such as effects of cell proliferation and stabilization of luciferase. Similarly, there are several confounding factors that may produce negative results. As each of these situations requires additional experiments to clarify, they are discussed in details in the Future Work section below.

6.6 Future Work

The next steps for the current experiments can be classified in three areas: 1) Test compounds that would allow better understanding of CK developmental regulation, 2) counter-screening and improvements on the existing luciferase assay, and 3) translating findings to more physiologically relevant model systems.

Currently, the most promising results are in regards to glucocorticoids and thyroid-receptor agonists, hence more compounds of these classes should be assessed. Glucorticoid receptor antagonists have been identified [410], hence an inhibitory effect on CK-M transcription should be evaluated with these compounds.

As discussed earlier, positive hits found through the luciferase assay require additional counter-screening studies to conclusively demonstrate that they are the result of increased mRNA and not from other causes. The current results have been verified for their effect on CK mRNA through qRT-PCR. There is also the possibility that tested compounds may be luciferase stabilizing compounds, which would produce false positives. For instance, the phenol resveratrol, which has been intensively investigated as a pharmacological compound, stabilizes luciferase (similar to OXO2393) and increases luminescence without affecting gene transcription [415]. To exclude this confounding factor, compounds should also be tested on a luciferase cell line in which luciferase mRNA is driven by a constitutive promoter. If the compound increases the luminescence in this cell line, it would indicate that the compound may stabilize luciferase, rather than directly altering promoter activity. Alternatively, a cell line could be generated that expressed a separate reporter line, such as CK promoter with β-Lactamase or GFP, which could be used in conjunction with the current luciferase assay to identify compounds that directly act on the luciferase protein [416].

Likewise, negative results cannot be discounted, as currently, only one concentration and timepoint were tested for most of the compounds. Additionally, it is possible that the negative results were because HEK293 cells do not express the necessary cellular machinery required to respond to chemical stimulus, such as absence of receptors and signalling pathways. This was not an issue for the putative CK transcriptional regulators currently tested, as the insulin receptor [417,418], IGF-1 receptor [418], PI3K protein [419,420], β adrenergic receptor [421], and oestrogen receptor [422] are all endogenously expressed by HEK293 cells. HEK293 cells also appear to express the receptors and intracellular pathways required for the compounds

currently tested through the screening phase of the experiment [423,424], though this will become an increasingly important consideration as more classes of compounds are investigated.

Additional experiments would need to be conducted to confirm high-throughput screening results from the optimized luciferase assay. First, positive hits would need to be checked for a dose-dependent effect. Second, increased CK protein (through western blot) and CK activity (through CK assay) would be required to confirm that there is an actual effect on CK function. Third, confirmed positive compounds could then be tested in the HL-1 cell line to examine whether the results can translate into a cardiac cell line.

7 Summary and future directions

CK system augmentation represents one avenue of investigation in the field of metabolic therapies for heart failure and other cardiac conditions. Currently, besides the CK system, there is substantial interest in modulation of cardiac metabolism in cardiac pathophysiologies, particularly the substrate metabolism balance between FA and carbohydrates. For instance, evidence from animal studies suggests that upregulating glucose oxidation and downregulating FAO during pressure overload heart failure attenuated LV dysfunction and improved outcomes in mice [99,425]. Similarly, oxfenicine, a compound that downregulates FAO (hence indirectly increasing glucose oxidation), was associated with reduced LV dilation in a canine model of heart failure [426]. Glucose oxidation has been hypothesized to be beneficial in heart failure as it is more oxygen-efficient than FAO. However, FAO remains essential during heart failure. For instance, excessive inhibition of FAO resulted in impaired cardiac function in heart failure patients, even with compensatory increases in glucose oxidation [427]. Thus, it is possible that FAO may remain critical as it makes use of available FA substrates and helps reduce the risk of mitochondrial lipotoxicity. Ultimately, it appears that the best solution to treat heart failure would be to restore the physiological metabolic capacities of the heart. Specifically, therapies will need to augment the ability of the heart to maintain substrate flexibility and the ability to utilize both carbohydrates and FA.

Clinical trials are currently under way to translate findings from animal studies to heart failure patients. For instance, mitochondrial fatty acid uptake inhibitors, such as the carnitine palmitoyl transferase (CPT) blockers etomoxir and perhexiline, have been investigated with promising outcomes for patients, including improved ejection fraction and peak myocardial function,

though etomoxir produces hepatotoxicity and perhexiline has a narrow therapeutic window [428]. Dichloroacetate, which increases PDH activity, did not significantly improve cardiac function [428]. Therefore, it remains unclear which findings in animal studies can be recapitulated in heart failure patients.

However, CK augmentation represents an alternative avenue of investigation to the current focus on substrate modulation in heart failure. Evidence suggests that there may be a narrow therapeutic window for metabolic alterations during heart failure [99], which is similar to how CK system augmentation also needs to be moderated to avoid significant side effects [2,209]. In both cases, substantial research is required to determine whether a safe and therapeutic approach can be developed for heart failure patients.

A. Appendices

A.1. PCR Protocol

Genotyping PCR

Reaction Mixture

Component	Stock Conc.	Final Conc.	Volume (µl)
F primer	10 µM	0.5 µM	1
R primer	10 µM	0.5 µM	1
DNA			5
Immolase polymerase	10 U/µL	1 U/µL	0.2
Immolase buffer	10 x	1 x	2
MgCl2	50 mM	3 mM	1.2
dNTP	25 mM	0.2 mM	1.6
H2O			7.44
Total			**20**

Cycling Conditions

Step	Temperature (ºC)	Time	Cycles
Activation	95	10 minutes	1
Denaturation	95	30 seconds	30
Annealing	70-55 (-0.5/cycle)	30 seconds	30
Extension	72	30 seconds	30
Final extension	72	10 minutes	1

A.2. qRT-PCR Protocol

qRT-PCR for mRNA

Reaction Mixture

Component	Stock Conc.	Final Conc.	Volume (µl)
SYBR RT Master Mix	2 x	1 x	5
iScript RT	10 x	1 x	0.2
RNA	1 ng/µL	0.2 ng/µL	2
Forward primer	50 µM	0.625 µM	0.06
Reverse primer	50 µM	0.625 µM	0.06
H2O	50 x	3 x	2.68
Total			**10**

Cycling Conditions

Step	Temperature (ºC)	Time	Cycles
Reverse transcription	50	10 minutes	1
Activation	95	5 minutes	1
Denaturation	95	10 seconds	40
Annealing/extension	58	30 seconds	40
Read SYBR	58	-	40
Denaturation	95	10 seconds	1
Melt curve	65-90 (+0.5/cycle)	5 seconds	1

A.3 Primers

Experiment	Name	Notes	Sequence (5'-3')	Length (bp)
All experiments	Polr2a_F	qPCR reference/internal standard	TGTGCAGGAAACATGACCGA	20
All experiments	Polr2a_R	qPCR reference/internal standard	GAAGCAGACACAGCGCAAAA	22
Genotyping	Rosa26_F	Control / WT allele for CK-Mt	ATACCTTTCTGGGAGTTCTCTGCTGC	27
Genotyping	Rosa26_R	Control / WT allele for CK-Mt	GGAGCGGGAGAAATGGATATG	22
Genotyping	HA_R	R primer for all Tg-specific PCRs	TGCGTAATCTGGAACATCGT	20
Genotyping/Dox	Ckmt2_ex9-10_F	Amplifies Tg and WT sequence	TCGGCAGATCAGAGGTTGAG	20
Dox	Ckmt2_ex9-10_R		ACTTCCTGCCAAACTGAGGCA	21
Luciferase	CKMT2 mRNA For		CCTCCAAGCGCAGACTAC	18
Luciferase	CKMT2 mRNA Rev		CGTTGGGTGTCACCTTGT	18
Luciferase	CKM mRNA For		GACAACCCAGGTCACCCC	18
Luciferase	CKM mRNA Rev		AGATGATGGGGTCAAAGAG	19

A.4 Solutions

Antibiotics
The following concentrations were used:
Penicillin 100U/ml
Streptomycin 100µg/ml
Puromycin 1µg/ml

Ear-notch lysis buffer
100 mM EDTA
50 mM Tris-HCl
1% SDS
200 mM NaCl
pH 8

T0.1E solution
10 mM Tris HCl
0.1 mM EDTA
pH 8

TBE solution
89 mM Tris borate, pH 8.3
2 mM EDTA

RIPA western blot extraction buffer
5 mL RIPA lysis buffer consisting of:
- 1.0% v/v IGEPAL® CA-630
- 0.5% w/v Sodium deoxycholate
- 0.1% w/v SDS
- 50 mM Tris
- pH 8

1 mM DTT
1 x Protease inhibitor cocktail (Roche, Germany)

Tris-HEPES running buffer (Pierce 28368)
0.1 M Tris
0.1 M HEPES
0.87% w/v SDS
pH 8

SDS transfer buffer
39 mM Glycine
48 mM Tris-base
0.0375%w/v SDS
20% v/v Methanol

References

1. Ingwall, J. S., & Shen, W. The Chemistry of ATP in the Failing Heart The Fundamentals. *Heart Failure Reviews,* **4**, 221-228 (1999).
2. Lygate, C. A.*, et al.* Moderate elevation of intracellular creatine by targeting the creatine transporter protects mice from acute myocardial infarction. *Cardiovascular Research,* **96**, 466-475 (2012).
3. Bose, S.*, et al.* Metabolic network control of oxidative phosphorylation multiple roles of inorganic phosphate. *J Biol Chem,* **278**, 39155-39165 (2003).
4. Langen, P., & Hucho, F. Karl Lohmann and the discovery of ATP. *Angew Chem Int Ed Engl,* **47**, 1824-1827 (2008).
5. Snow, R. J., & Murphy, R. M. Creatine and the creatine transporter: A review. *Molecular and Cellular Biochemistry,* **224**, 169-181
6. Braissant, O.*, et al.* Creatine synthesis and transport during rat embryogenesis: Spatiotemporal expression of AGAT, GAMT and CT1. *BMC Developmental Biology,* **5**, 9 (2005).
7. Wyss, M., & Kaddurah-Daouk, R. Creatine and creatinine metabolism. *Physiol Rev,* **80**, 1107-1213 (2000).
8. Zervou, S., Whittington, H. J., Russell, A. J., & Lygate, C. A. Augmentation of Creatine in the Heart. *Mini Rev Med Chem,* **16**, 19-28 (2016).
9. Neubauer , S. The Failing Heart — An Engine Out of Fuel. *New England Journal of Medicine,* **356**, 1140-1151 (2007).
10. Boehm, E.*, et al.* Creatine transporter activity and content in the rat heart supplemented by and depleted of creatine. *Am J Physiol Endocrinol Metab,* **284**, E399-406 (2003).
11. Horn, M.*, et al.* Chronic high-dose creatine feeding does not attenuate left ventricular remodeling in rat hearts post-myocardial infarction. *Cardiovascular Research,* **43**, 117-124 (1999).
12. Hoberman, H. D., Sims, E. A., & Peters, J. H. Creatine and creatinine metabolism in the normal male adult studied with the aid of isotopic nitrogen. *J Biol Chem,* **172**, 45-58 (1948).
13. Lygate, C., & Neubauer, S. The Myocardial Creatine Kinase System in the Normal, Ischaemic and Failing Heart. 155-168 (2014).
14. Yoshizaki, K., Watari, H., & Radda, G. K. Role of phosphocreatine in energy transport in skeletal muscle of bullfrog studied by 31P-NMR. *Biochim Biophys Acta,* **1051**, 144-150 (1990).
15. Weiss, R. G., Gerstenblith, G., & Bottomley, P. A. ATP flux through creatine kinase in the normal, stressed, and failing human heart. *Proceedings of the National Academy of Sciences,* **102**, 808-813 (2005).
16. Muhlebach, S. M.*, et al.* Sequence homology and structure predictions of the creatine kinase isoenzymes. *Mol Cell Biochem,* **133-134**, 245-262 (1994).
17. Wallimann, T.*, et al.* Intracellular compartmentation, structure and function of creatine kinase isoenzymes in tissues with high and fluctuating energy demands: the 'phosphocreatine circuit' for cellular energy homeostasis. *Biochem J,* **281 (Pt 1)**, 21-40 (1992).
18. Lygate, C. A.*, et al.* The creatine kinase energy transport system in the failing mouse heart. *J Mol Cell Cardiol,* **42**, 1129-1136 (2007).

19. Veksler, V. I.*, et al.* Muscle creatine kinase-deficient mice. II. Cardiac and skeletal muscles exhibit tissue-specific adaptation of the mitochondrial function. *J Biol Chem,* **270**, 19921-19929 (1995).
20. Stallings, R. L.*, et al.* Human creatine kinase genes on chromosomes 15 and 19, and proximity of the gene for the muscle form to the genes for apolipoprotein C2 and excision repair. *American Journal of Human Genetics,* **43**, 144-151 (1988).
21. Trask, R. V., & Billadello, J. J. Tissue-specific distribution and developmental regulation of M and B creatine kinase mRNAs. *Biochimica et Biophysica Acta (BBA) - Gene Structure and Expression,* **1049**, 182-188 (1990).
22. Fischer, A.*, et al.* Changes in creatine transporter function during cardiac maturation in the rat. *BMC Developmental Biology,* **10**, 70 (2010).
23. Chamberlain, J. S., Jaynes, J. B., & Hauschka, S. D. Regulation of creatine kinase induction in differentiating mouse myoblasts. *Molecular and Cellular Biology,* **5**, 484-492 (1985).
24. Perriard, J. C. Developmental regulation of creatine kinase isoenzymes in myogenic cell cultures from chicken. Levels of mRNA for creatine kinase subunits M and B. *J Biol Chem,* **254**, 7036-7041 (1979).
25. Rao, J. K., Bujacz, G., & Wlodawer, A. Crystal structure of rabbit muscle creatine kinase. *FEBS Lett,* **439**, 133-137 (1998).
26. McLeish, M. J., & Kenyon, G. L. Relating structure to mechanism in creatine kinase. *Crit Rev Biochem Mol Biol,* **40**, 1-20 (2005).
27. Wegmann, G., Zanolla, E., Eppenberger, H. M., & Wallimann, T. In situ compartmentation of creatine kinase in intact sarcomeric muscle: the acto-myosin overlap zone as a molecular sieve. *J Muscle Res Cell Motil,* **13**, 420-435 (1992).
28. Boehm, E.*, et al.* Glycolysis Supports Calcium Uptake by the Sarcoplasmic Reticulum in Skinned Ventricular Fibres of Mice Deficient in Mitochondrial and Cytosolic Creatine Kinase. *J Mol Cell Cardiol,* **32**, 891-902 (2000).
29. Stolz, M., & Wallimann, T. Myofibrillar interaction of cytosolic creatine kinase (CK) isoenzymes: allocation of N-terminal binding epitope in MM-CK and BB-CK. *J Cell Sci,* **111 (Pt 9)**, 1207-1216 (1998).
30. Turner, D. C., Wallimann, T., & Eppenberger, H. M. A Protein That Binds Specifically to the M-Line of Skeletal Muscle Is Identified as the Muscle Form of Creatine Kinase. *Proceedings of the National Academy of Sciences,* **70**, 702-705 (1973).
31. Schlattner, U., Tokarska-Schlattner, M., & Wallimann, T. Mitochondrial creatine kinase in human health and disease. *Biochimica et Biophysica Acta (BBA) - Molecular Basis of Disease,* **1762**, 164-180 (2006).
32. Kraft, T.*, et al.* Coupling of creatine kinase to glycolytic enzymes at the sarcomeric I-band of skeletal muscle: a biochemical study in situ. *J Muscle Res Cell Motil,* **21**, 691-703 (2000).
33. Rossi, A. M.*, et al.* Muscle-type MM creatine kinase is specifically bound to sarcoplasmic reticulum and can support Ca2+ uptake and regulate local ATP/ADP ratios. *J Biol Chem,* **265**, 5258-5266 (1990).
34. de Groof, A. J.*, et al.* The creatine kinase system is essential for optimal refill of the sarcoplasmic reticulum Ca2+ store in skeletal muscle. *J Biol Chem,* **277**, 5275-5284 (2002).

35. Spindler, M.*, et al.* Creatine kinase-deficient hearts exhibit increased susceptibility to ischemia-reperfusion injury and impaired calcium homeostasis. *Am J Physiol Heart Circ Physiol,* **287**, H1039-1045 (2004).
36. Korge, P., Byrd, S. K., & Campbell, K. B. Functional coupling between sarcoplasmic-reticulum-bound creatine kinase and Ca2+-ATPase. *European Journal of Biochemistry,* **213**, 973-980 (1993).
37. Steeghs, K.*, et al.* Altered Ca2+ Responses in Muscles with Combined Mitochondrial and Cytosolic Creatine Kinase Deficiencies. *Cell,* **89**, 93-103 (1997).
38. Crawford, R. M.*, et al.* Creatine kinase is physically associated with the cardiac ATP-sensitive K+ channel in vivo. *Faseb j,* **16**, 102-104 (2002).
39. Zhu, Z.*, et al.* Sarcolemmal ATP-sensitive potassium channels modulate skeletal muscle function under low-intensity workloads. *The Journal of General Physiology,* **143**, 119-134 (2014).
40. Blum, H., Balschi, J. A., & Johnson, R. G., Jr. Coupled in vivo activity of creatine phosphokinase and the membrane-bound (Na+,K+)-ATPase in the resting and stimulated electric organ of the electric fish Narcine brasiliensis. *J Biol Chem,* **266**, 10254-10259 (1991).
41. Zhao, T. J., Yan, Y. B., Liu, Y., & Zhou, H. M. The generation of the oxidized form of creatine kinase is a negative regulation on muscle creatine kinase. *J Biol Chem,* **282**, 12022-12029 (2007).
42. Lin, G., Liu, Y., & MacLeod, K. M. Regulation of muscle creatine kinase by phosphorylation in normal and diabetic hearts. *Cell Mol Life Sci,* **66**, 135-144 (2009).
43. Ponticos, M.*, et al.* Dual regulation of the AMP-activated protein kinase provides a novel mechanism for the control of creatine kinase in skeletal muscle. *The EMBO Journal,* **17**, 1688-1699 (1998).
44. Ingwall, J. S. Is creatine kinase a target for AMP-activated protein kinase in the heart? *J Mol Cell Cardiol,* **34**, 1111-1120 (2002).
45. Tsuchiya, Y.*, et al.* Protein CoAlation: a redox-regulated protein modification by coenzyme A in mammalian cells. *Biochemical Journal,* **474**, 2489-2508 (2017).
46. Hendriks, D.*, et al.* Identification of the carboxypeptidase responsible for the post-synthetic modification of creatine kinase in human serum. *Clin Chim Acta,* **172**, 253-260 (1988).
47. Zaninotto, M., Altinier, S., Lachin, M., & Plebani, M. Carboxypeptidase N and creatine kinase-MB isoforms in acute myocardial infarction. *Eur J Clin Chem Clin Biochem,* **35**, 291-295 (1997).
48. Kanemitsu, F., & Okigaki, T. Characterization of human creatine kinase BB and MB isoforms by means of isoelectric focusing. *Clin Chim Acta,* **231**, 1-9 (1994).
49. Clark, J. R., & Cunningham, L. The acetylation of creatine phosphokinase with p-nitrophenyl acetate. *Biochemistry,* **4**, 2637-2643 (1965).
50. Maggio, E., & Kenyon, G. L. Properties of a CH3-blocked creatine kinase with altered catalytic activity. Kinetic consequences of the presence of the blocking group. *J Biol Chem,* **252**, 1202-1207 (1977).
51. Wolosker, H., Panizzutti, R., & Engelender, S. Inhibition of creatine kinase by S-nitrosoglutathione. *FEBS Lett,* **392**, 274-276 (1996).
52. NCBI. (2015). CKMT2 creatine kinase, mitochondrial 2 [Homo sapiens (human)].
53. NCBI. (2015). Ckmt1 creatine kinase, mitochondrial 1, ubiquitous

54. Thomure, M. F., Gast, M. J., Srivastava, N., & Payne, R. M. Regulation of creatine kinase isoenzymes in human placenta during early, mid-, and late gestation. *J Soc Gynecol Investig,* **3**, 322-327 (1996).
55. Payne, R. M., & Strauss, A. W. Expression of the mitochondrial creatine kinase genes. *Mol Cell Biochem,* **133-134**, 235-243 (1994).
56. Haas, R. C., & Strauss, A. W. Separate nuclear genes encode sarcomere-specific and ubiquitous human mitochondrial creatine kinase isoenzymes. *J Biol Chem,* **265**, 6921-6927 (1990).
57. Hall, N., & DeLuca, M. Developmental changes in creatine phosphokinase isoenzymes in neonatal mouse hearts. *Biochem Biophys Res Commun,* **66**, 988-994 (1975).
58. Schnyder, T., Rojo, M., Furter, R., & Wallimann, T. The structure of mitochondrial creatine kinase and its membrane binding properties. *Molecular and Cellular Biochemistry,* **133**, 115-123 (1994).
59. Schlattner, U., & Wallimann, T. Octamers of mitochondrial creatine kinase isoenzymes differ in stability and membrane binding. *J Biol Chem,* **275**, 17314-17320 (2000).
60. Maniti, O.*, et al.* Mitochondrial Creatine Kinase Binding to Phospholipid Monolayers Induces Cardiolipin Segregation. *Biophysical Journal,* **96**, 2428-2438 (2009).
61. Biermans, W., Bakker, A., & Jacob, W. Contact sites between inner and outer mitochondrial membrane: A dynamic microcompartment for creatine kinase activity. *Biochimica et Biophysica Acta (BBA) - Bioenergetics,* **1018**, 225-228 (1990).
62. Müller, M., Moser, R., Cheneval, D., & Carafoli, E. Cardiolipin is the membrane receptor for mitochondrial creatine phosphokinase. **Vol. 260**, 3839-3843 (1985).
63. Saks, V.*, et al.* Structure–function relationships in feedback regulation of energy fluxes in vivo in health and disease: Mitochondrial Interactosome. *Biochimica et Biophysica Acta (BBA) - Bioenergetics,* **1797**, 678-697 (2010).
64. Dolder, M.*, et al.* Inhibition of the mitochondrial permeability transition by creatine kinase substrates. Requirement for microcompartmentation. *J Biol Chem,* **278**, 17760-17766 (2003).
65. Vial, C. Creatine Kinase. (2006).
66. Halestrap, A. Biochemistry: A pore way to die. *Nature,* **434**, 578-579 (2005).
67. Kim, J.-S., He, L., & Lemasters, J. J. Mitochondrial permeability transition: a common pathway to necrosis and apoptosis. *Biochem Biophys Res Commun,* **304**, 463-470 (2003).
68. Tsujimoto, Y., & Shimizu, S. Role of the mitochondrial membrane permeability transition in cell death. *Apoptosis,* **12**, 835-840 (2007).
69. Kwon, S.*, et al.* ASB9 interacts with ubiquitous mitochondrial creatine kinase and inhibits mitochondrial function. *BMC Biology,* **8**, 1-22 (2010).
70. Fei, X.*, et al.* Crystal structure of Human ASB9-2 and substrate-recognition of CKB. *Protein J,* **31**, 275-284 (2012).
71. Bürklen, T. S.*, et al.* The Creatine Kinase/Creatine Connection to Alzheimer's Disease: CK Inactivation, APP-CK Complexes, and Focal Creatine Deposits. *Journal of Biomedicine and Biotechnology*35936 (2006).

72. Schmid, H., *et al.* Macroenzyme creatine kinase (CK) type 2 in HIV-infected patients is significantly associated with TDF and consists of ubiquitous mitochondrial CK. *Antivir Ther,* **11**, 1071-1080 (2006).
73. Kaldis, P., & Wallimann, T. Functional differences between dimeric and octameric mitochondrial creatine kinase. *Biochemical Journal,* **308**, 623-627 (1995).
74. Wendt, S., Schlattner, U., & Wallimann, T. Differential effects of peroxynitrite on human mitochondrial creatine kinase isoenzymes. Inactivation, octamer destabilization, and identification of involved residues. *J Biol Chem,* **278**, 1125-1130 (2003).
75. Schlegel, J., *et al.* Native mitochondrial creatine kinase forms octameric structures. I. Isolation of two interconvertible mitochondrial creatine kinase forms, dimeric and octameric mitochondrial creatine kinase: characterization, localization, and structure-function relationships. *J Biol Chem,* **263**, 16942-16953 (1988).
76. Stachowiak, O., Dolder, M., Wallimann, T., & Richter, C. Mitochondrial creatine kinase is a prime target of peroxynitrite-induced modification and inactivation. *J Biol Chem,* **273**, 16694-16699 (1998).
77. Koufen, P., *et al.* Free radical-induced inactivation of creatine kinase: influence on the octameric and dimeric states of the mitochondrial enzyme (Mib-CK). *Biochemical Journal,* **344**, 413-417 (1999).
78. Konorev, E. A., Hogg, N., & Kalyanaraman, B. Rapid and irreversible inhibition of creatine kinase by peroxynitrite. *FEBS Lett,* **427**, 171-174 (1998).
79. Sun, J., Steenbergen, C., & Murphy, E. S-Nitrosylation: NO-Related Redox Signaling to Protect Against Oxidative Stress. *Antioxid Redox Signal,* **8**, 1693-1705 (2006).
80. Weekes, J., *et al.* Hyperubiquitination of proteins in dilated cardiomyopathy. *Proteomics.,* **3**, 208-216 (2003).
81. Dzeja, P. P., *et al.* Rearrangement of energetic and substrate utilization networks compensate for chronic myocardial creatine kinase deficiency. *The Journal of Physiology,* **589**, 5193-5211 (2011).
82. Nahrendorf, M., *et al.* Creatine kinase knockout mice show left ventricular hypertrophy and dilatation, but unaltered remodeling post-myocardial infarction. *Cardiovascular Research,* **65**, 419-427 (2005).
83. Rosenberg, U. B., *et al.* Molecular cloning and expression during myogenesis of sequences coding for M-creatine kinase. *Proceedings of the National Academy of Sciences,* **79**, 6589-6592 (1982).
84. Shen, W., *et al.* Expression of creatine kinase isoenzyme genes during postnatal development of rat brain cerebellum: evidence for transcriptional regulation. *Biochem J,* **367**, 369-380 (2002).
85. Ritchie, M. E. Characterization of human B creatine kinase gene regulation in the heart in vitro and in vivo. *J Biol Chem,* **271**, 25485-25491 (1996).
86. Simionescu-Bankston, A., *et al.* Creatine kinase B is necessary to limit myoblast fusion during myogenesis. *Am J Physiol Cell Physiol,* **308**, C919-931 (2015).
87. Eder, M., *et al.* Crystal structure of brain-type creatine kinase at 1.41 A resolution. *Protein Sci,* **8**, 2258-2269 (1999).
88. Khan, M. A. Effect of calcium on creatine kinase activity of cerebellum. *Histochemistry,* **48**, 29-32 (1976).

89. Schlattner, U.*, et al.* Cellular compartmentation of energy metabolism: creatine kinase microcompartments and recruitment of B-type creatine kinase to specific subcellular sites. *Amino Acids,* **48**, 1751-1774 (2016).
90. Manos, P., Bryan, G. K., & Edmond, J. Creatine Kinase Activity in Postnatal Rat Brain Development and in Cultured Neurons, Astrocytes, and Oligodendrocytes. *Journal of Neurochemistry,* **56**, 2101-2107 (1991).
91. David, S., Shoemaker, M., & Haley, B. E. Abnormal properties of creatine kinase in Alzheimer's disease brain: correlation of reduced enzyme activity and active site photolabeling with aberrant cytosol-membrane partitioning. *Brain Res Mol Brain Res,* **54**, 276-287 (1998).
92. Kim, J.*, et al.* Reduced creatine kinase as a central and peripheral biomarker in Huntington's disease. *Biochim Biophys Acta,* **1802**, 673-681 (2010).
93. Jost, C. R.*, et al.* Creatine kinase B-driven energy transfer in the brain is important for habituation and spatial learning behaviour, mossy fibre field size and determination of seizure susceptibility. *Eur J Neurosci,* **15**, 1692-1706 (2002).
94. Streijger, F.*, et al.* Mice lacking the UbCKmit isoform of creatine kinase reveal slower spatial learning acquisition, diminished exploration and habituation, and reduced acoustic startle reflex responses. *Mol Cell Biochem,* **256-257**, 305-318 (2004).
95. Li, C.*, et al.* Hydrogen peroxide targets the cysteine at the active site and irreversibly inactivates creatine kinase. *International Journal of Biological Macromolecules,* **49**, 910-916 (2011).
96. Aksenov, M., Aksenova, M., Butterfield, D. A., & Markesbery, W. R. Oxidative modification of creatine kinase BB in Alzheimer's disease brain. *J Neurochem,* **74**, 2520-2527 (2000).
97. Quest, A. F.*, et al.* Phosphorylation of chicken brain-type creatine kinase affects a physiologically important kinetic parameter and gives rise to protein microheterogeneity in vivo. *FEBS Lett,* **269**, 457-464 (1990).
98. Ramírez Ríos, S.*, et al.* Regulation of brain-type creatine kinase by AMP-activated protein kinase: Interaction, phosphorylation and ER localization. *Biochimica et Biophysica Acta (BBA) - Bioenergetics,* **1837**, 1271-1283 (2014).
99. Kolwicz, S. C., & Tian, R. Fuel Metabolism Plasticity in Pathological Cardiac Hypertrophy and Failure. *Cardiac Energy Metabolism in Health and Disease*, 169-182 (2014).
100. Glatz, J. F., & Luiken, J. J. Control of myocardial fatty acid uptake. *Cardiac Energy Metabolism in Health and Disease*, 49-67 (2014).
101. Ceddia, R. B., & Sweeney, G. Creatine supplementation increases glucose oxidation and AMPK phosphorylation and reduces lactate production in L6 rat skeletal muscle cells. *The Journal of Physiology,* **555**, 409-421 (2004).
102. Sharma, V., & McNeill, J. H. Adrenergic Control of Cardiac Fatty Acid Oxidation in Diabetes. *Cardiac Energy Metabolism in Health and Disease*, 131-153 (2014).
103. Taegtmeyer, H. A Primer on Carbohydrate Metabolism in the Heart. *Cardiac Energy Metabolism in Health and Disease*, 3-14 (2014).
104. Stanley, W. C. Myocardial lactate metabolism during exercise. *Med Sci Sports Exerc,* **23**, 920-924 (1991).
105. Hue, L., & Taegtmeyer, H. The Randle cycle revisited: a new head for an old hat. *Am J Physiol Endocrinol Metab,* **297**, E578-E591 (2009).

106. Randle, P. J., Garland, P. B., Hales, C. N., & Newsholme, E. A. The glucose fatty-acid cycle. Its role in insulin sensitivity and the metabolic disturbances of diabetes mellitus. *Lancet,* **1**, 785-789 (1963).
107. Byrne, N. J., Sung, M. M., & Dyck, J. R. The Role of AMPK in the Control of Cardiac Hypertrophy. *Cardiac Energy Metabolism in Health and Disease*, 199-220 (2014).
108. Tran, K., Loiselle, D. S., & Crampin, E. J. Regulation of cardiac cellular bioenergetics: mechanisms and consequences. *Physiological Reports,* **3**, e12464 (2015).
109. Aasum, E. Relationship Between Substrate Metabolism and Cardiac Efficiency. *Cardiac Energy Metabolism in Health and Disease*, 103-114 (2014).
110. Sata, M.*, et al.* Coupling between myosin ATPase cycle and creatinine kinase cycle facilitates cardiac actomyosin sliding in vitro. A clue to mechanical dysfunction during myocardial ischemia. *Circulation,* **93**, 310-317 (1996).
111. Savabi, F. Interaction of creatine kinase and adenylate kinase systems in muscle cells. *Cellular Bioenergetics: Role of Coupled Creatine Kinases*, 145-152 (1994).
112. Janssen, E., Terzic, A., Wieringa, B., & Dzeja, P. P. Impaired intracellular energetic communication in muscles from creatine kinase and adenylate kinase (M-CK/AK1) double knock-out mice. *J Biol Chem,* **278**, 30441-30449 (2003).
113. Feldman, A. M., Cheksis-Feiner, E., Hamad, E., & Chan, T. Adenosine Receptor Subtypes and the Heart Failure Phenotype: Translating Lessons from Mice to Man. *Transactions of the American Clinical and Climatological Association,* **122**, 198-214 (2011).
114. Abraham, M. R.*, et al.* Coupling of cell energetics with membrane metabolic sensing. Integrative signaling through creatine kinase phosphotransfer disrupted by M-CK gene knock-out. *J Biol Chem,* **277**, 24427-24434 (2002).
115. Dzeja, P. P., & Terzic, A. Phosphotransfer networks and cellular energetics. *Journal of Experimental Biology,* **206**, 2039-2047 (2003).
116. Ventura-Clapier, R., Garnier, A., & Veksler, V. Energy metabolism in heart failure. *The Journal of Physiology,* **555**, 1-13 (2004).
117. Tian, R., Nascimben, L., Kaddurah-Daouk, R., & Ingwall, J. S. Depletion of energy reserve via the creatine kinase reaction during the evolution of heart failure in cardiomyopathic hamsters. *J Mol Cell Cardiol,* **28**, 755-765 (1996).
118. Ye, Y.*, et al.* High-energy phosphate metabolism and creatine kinase in failing hearts: a new porcine model. *Circulation,* **103**, 1570-1576 (2001).
119. Allard, M. F.*, et al.* Contribution of oxidative metabolism and glycolysis to ATP production in hypertrophied hearts. *Am J Physiol,* **267**, H742-750 (1994).
120. Depre, C.*, et al.* Unloaded heart in vivo replicates fetal gene expression of cardiac hypertrophy. *Nat Med,* **4**, 1269-1275 (1998).
121. Razeghi, P.*, et al.* Metabolic Gene Expression in Fetal and Failing Human Heart. *Circulation,* **104**, 2923-2931 (2001).
122. Schaper, J.*, et al.* Impairment of the myocardial ultrastructure and changes of the cytoskeleton in dilated cardiomyopathy. *Circulation,* **83**, 504-514 (1991).
123. Casademont, J., & Miro, O. Electron transport chain defects in heart failure. *Heart Fail Rev,* **7**, 131-139 (2002).

124. Murray, A. J., *et al.* Increased mitochondrial uncoupling proteins, respiratory uncoupling and decreased efficiency in the chronically infarcted rat heart. *J Mol Cell Cardiol,* **44**, 694-700 (2008).
125. Saavedra, W. F., *et al.* Imbalance Between Xanthine Oxidase and Nitric Oxide Synthase Signaling Pathways Underlies Mechanoenergetic Uncoupling in the Failing Heart. *Circulation,* **90**, 297-304 (2002).
126. Dzeja, P. P., Redfield, M. M., Burnett, J. C., & Terzic, A. Failing energetics in failing hearts. *Curr Cardiol Rep,* **2**, 212-217 (2000).
127. Faller, K. M., *et al.* Impaired cardiac contractile function in arginine: glycine amidinotransferase knockout mice devoid of creatine is rescued by homoarginine but not creatine. *Cardiovascular Research*cvx242 (2017).
128. Shen, W., *et al.* The fall in creatine levels and creatine kinase isozyme changes in the failing heart are reversible: Complex post-transcriptional regulation of the components of the CK system. *J Mol Cell Cardiol,* **39**, 537-544 (2005).
129. Liao, R., *et al.* Decreased energy reserve in an animal model of dilated cardiomyopathy. Relationship to contractile performance. *Circulation,* **78**, 893-902 (1996).
130. Nascimben, L., *et al.* Creatine Kinase System in Failing and Nonfailing Human Myocardium. *Circulation,* **94**, 1894-1901 (1996).
131. Bottomley, P. A., *et al.* Metabolic Rates of ATP Transfer Through Creatine Kinase (CK Flux) Predict Clinical Heart Failure Events and Death. *Science translational medicine,* **5**, 215re213-215re213 (2013).
132. Lygate, C. A., & Neubauer, S. Metabolic flux as a predictor of heart failure prognosis. *Circulation,* **114**, 1228-1230 (2014).
133. Neubauer, S., *et al.* Myocardial phosphocreatine-to-ATP ratio is a predictor of mortality in patients with dilated cardiomyopathy. *Circulation,* **96**, 2190-2196 (1997).
134. Neubauer, S., *et al.* Downregulation of the Na+-Creatine Cotransporter in Failing Human Myocardium and in Experimental Heart Failure. *Circulation,* **100**, 1847-1850 (1999).
135. Phillips, D., *et al.* Mice Over-Expressing the Myocardial Creatine Transporter Develop Progressive Heart Failure and Show Decreased Glycolytic Capacity. *J Mol Cell Cardiol,* **48**, 582-590 (2010).
136. Shen, W., *et al.* Progressive Loss of Myocardial ATP Due to a Loss of Total Purines During the Development of Heart Failure in Dogs. *A Compensatory Role for the Parallel Loss of Creatine,* **100**, 2113-2118 (1999).
137. Yagi, K., & Mase, R. Coupled reaction of creatine kinase and myosin A-adenosine triphosphatase. *J Biol Chem,* **237**, 397-403 (1962).
138. Haagensen, L., Jensen, D. H., & Gesser, H. Dependence of myosin-ATPase on structure bound creatine kinase in cardiac myofibrils from rainbow trout and freshwater turtle. *Comp Biochem Physiol A Mol Integr Physiol,* **150**, 404-409 (2008).
139. Fitch, C. D., & Shields, R. P. Creatine Metabolism in Skeletal Muscle: I. Creatine movement across muscle membranes. *J Biol Chem,* **241**, 3611-3614 (1966).
140. Wyss, M., & Wallimann, T. Creatine metabolism and the consequences of creatine depletion in muscle. *Mol Cell Biochem,* **133-134**, 51-66 (1994).

141. Oudman, I., Clark, J. F., & Brewster, L. M. The Effect of the Creatine Analogue Beta-guanidinopropionic Acid on Energy Metabolism: A Systematic Review. *PLOS ONE,* **8**, e52879 (2013).
142. Mekhfi, H.*, et al.* Myocardial adaptation to creatine deficiency in rats fed with beta-guanidinopropionic acid, a creatine analogue. *Am J Physiol,* **258**, H1151-1158 (1991).
143. Horn, M.*, et al.* Chronic Phosphocreatine Depletion by the Creatine Analogue β-Guanidinopropionate Is Associated With Increased Mortality and Loss of ATP in Rats After Myocardial Infarction. *Circulation,* **104**, 1844-1849 (2001).
144. Lorentzon, M.*, et al.* In vivo effects of myocardial creatine depletion on left ventricular function, morphology, and energy metabolism--consequences in acute myocardial infarction. *J Card Fail,* **13**, 230-237 (2007).
145. van Deursen, J.*, et al.* Effects of the creatine analogue beta-guanidinopropionic acid on skeletal muscles of mice deficient in muscle creatine kinase. *Biochim Biophys Acta,* **1185**, 327-335 (1994).
146. Shoubridge, E. A.*, et al.* Creatine kinase kinetics, ATP turnover, and cardiac performance in hearts depleted of creatine with the substrate analogue β-guanidinopropionic acid. *Biochimica et Biophysica Acta (BBA) - Molecular Cell Research,* **847**, 25-32 (1985).
147. Boehm, E. A., Radda, G. K., Tomlin, H., & Clark, J. F. The utilisation of creatine and its analogues by cytosolic and mitochondrial creatine kinase. *Biochim Biophys Acta,* **1274**, 119-128 (1996).
148. Schmidt, A.*, et al.* Severely altered guanidino compound levels, disturbed body weight homeostasis and impaired fertility in a mouse model of guanidinoacetate N-methyltransferase (GAMT) deficiency. *Hum Mol Genet,* **13**, 905-921 (2004).
149. ten Hove, M.*, et al.* Reduced inotropic reserve and increased susceptibility to cardiac ischemia/reperfusion injury in phosphocreatine-deficient guanidinoacetate-N-methyltransferase-knockout mice. *Circulation,* **111**, 2477-2485 (2005).
150. Schneider, J. E.*, et al.* Cardiac structure and function during ageing in energetically compromised Guanidinoacetate N-methyltransferase (GAMT)-knockout mice - a one year longitudinal MRI study. *J Cardiovasc Magn Reson,* **10**, 9 (2008).
151. Lygate, C. A.*, et al.* Living without creatine: unchanged exercise capacity and response to chronic myocardial infarction in creatine-deficient mice. *Circulation,* **112**, 945-955 (2013).
152. Branovets, J.*, et al.* Unchanged mitochondrial organization and compartmentation of high-energy phosphates in creatine-deficient GAMT-/- mouse hearts. *Am J Physiol Heart Circ Physiol,* **305**, H506-520 (2013).
153. Kan, H. E., Renema, W. K., Isbrandt, D., & Heerschap, A. Phosphorylated guanidinoacetate partly compensates for the lack of phosphocreatine in skeletal muscle of mice lacking guanidinoacetate methyltransferase. *J Physiol,* **560**, 219-229 (2004).
154. Choe, C. U.*, et al.* L-arginine:glycine amidinotransferase deficiency protects from metabolic syndrome. *Hum Mol Genet,* **22**, 110-123 (2013).
155. Nabuurs, C. I.*, et al.* Disturbed energy metabolism and muscular dystrophy caused by pure creatine deficiency are reversible by creatine intake. *J Physiol,* **591**, 571-592 (2013).

156. Faller, K. M. E., *et al.* Impaired cardiac contractile function in arginine:glycine amidinotransferase knockout mice devoid of creatine is rescued by homoarginine but not creatine. *Cardiovascular Research,* **114**, 417-430 (2018).
157. Lygate, C. A., *et al.* Chronic Creatine-deficiency is not the Underlying Cause of Cardiac Dysfunction in Mice Lacking the Creatine Biosynthetic Enzyme Arginine:glycine Amidinotransferase. *Circulation,* **128**, A10723-A10723 (2013).
158. Whittington, H., *et al.* Loss of homoarginine is responsible for cardiac dysfunction in creatine-deficient arginine:glycine amidinotransferase (AGAT) knockout mice. *Heart,* **100**, A11-A11 (2014).
159. Kakoki, M., Kim, H. S., Arendshorst, W. J., & Mattson, D. L. L-Arginine uptake affects nitric oxide production and blood flow in the renal medulla. *Am J Physiol Regul Integr Comp Physiol,* **287**, R1478-1485 (2004).
160. Marz, W., *et al.* Homoarginine, cardiovascular risk, and mortality. *Circulation,* **122**, 967-975 (2010).
161. Choe, C. U., *et al.* Homoarginine levels are regulated by L-arginine:glycine amidinotransferase and affect stroke outcome: results from human and murine studies. *Circulation,* **128**, 1451-1461 (2013).
162. Skelton, M. R., *et al.* Creatine Transporter (CrT; Slc6a8) Knockout Mice as a Model of Human CrT Deficiency. *PLOS ONE,* **6**, e16187 (2011).
163. Russell, A. P., *et al.* Creatine transporter (SLC6A8) knockout mice display an increased capacity for in vitro creatine biosynthesis in skeletal muscle. *Front Physiol,* **5**, 314 (2014).
164. Wallis, J., *et al.* Supranormal myocardial creatine and phosphocreatine concentrations lead to cardiac hypertrophy and heart failure: insights from creatine transporter-overexpressing transgenic mice. *Circulation,* **112**, 3131-3139 (2005).
165. Liu, J., *et al.* Mitochondrial ATPase and high-energy phosphates in failing hearts. *Am J Physiol Heart Circ Physiol,* **281**, H1319-1326 (2001).
166. Tian, R., Nascimben, L., Ingwall, J. S., & Lorell, B. H. Failure to maintain a low ADP concentration impairs diastolic function in hypertrophied rat hearts. *Circulation,* **96**, 1313-1319 (1997).
167. Glyn-Jones, S., *et al.* Transcriptomic analysis of the cardiac left ventricle in a rodent model of diabetic cardiomyopathy: molecular snapshot of a severe myocardial disease. *Physiological Genomics,* **28**, 284-293 (2007).
168. Keller, A., *et al.* Differential expression of alpha- and beta-enolase genes during rat heart development and hypertrophy. *Am J Physiol Heart Circ Physiol,* **269**, H1843-H1851 (1995).
169. Saeedi, R., *et al.* Gender and post-ischemic recovery of hypertrophied rat hearts. *BMC Cardiovascular Disorders,* **6**, 8 (2006).
170. Ong, S. B., Samangouei, P., Kalkhoran, S. B., & Hausenloy, D. J. The mitochondrial permeability transition pore and its role in myocardial ischemia reperfusion injury. *J Mol Cell Cardiol,* **78**, 23-34 (2015).
171. Whittington, H. J., *et al.* Protective Effect of Creatine Elevation against Ischaemia Reperfusion Injury Is Retained in the Presence of Co-Morbidities and during Cardioplegia. *PLOS ONE,* **11**, (2016).
172. Fossel, E. T., & Hoefeler, H. Complete inhibition of creatine kinase in isolated perfused rat hearts. *Am J Physiol,* **252**, E124-129 (1987).

173. Boyer, P. D. Preface. *The Enzymes,* **Vol. Volume 7**, xv-xvi (1972).
174. Williamson, J. R. Glycolytic control mechanisms. 3. Effects of iodoacetamide and fluoroacetate on glucose metabolism in the perfused rat heart. *J Biol Chem,* **242**, 4476-4485 (1967).
175. Wallimann, T., Schlosser, T., & Eppenberger, H. M. Function of M-line-bound creatine kinase as intramyofibrillar ATP regenerator at the receiving end of the phosphorylcreatine shuttle in muscle. *J Biol Chem,* **259**, 5238-5246 (1984).
176. Zervou, S.*, et al.* Increasing creatine kinase activity protects against hypoxia / reoxygenation injury but not against anthracycline toxicity in vitro. *PLOS ONE,* **12**, e0182994 (2017).
177. Ventura-Clapier, R.*, et al.* Muscle creatine kinase-deficient mice. I. Alterations in myofibrillar function. *J Biol Chem,* **270**, 19914-19920 (1995).
178. van Deursen, J.*, et al.* Skeletal muscles of mice deficient in muscle creatine kinase lack burst activity. *Cell,* **74**, 621-631 (1993).
179. Saupe, K. W., Spindler, M., Tian, R., & Ingwall, J. S. Impaired cardiac energetics in mice lacking muscle-specific isoenzymes of creatine kinase. *Circulation,* **82**, 898-907 (1998).
180. Spindler, M.*, et al.* Mitochondrial creatine kinase is critically necessary for normal myocardial high-energy phosphate metabolism. *Am J Physiol Heart Circ Physiol,* **283**, H680-687 (2002).
181. Kass, D. A., Hare, J. M., & Georgakopoulos, D. Murine cardiac function: a cautionary tail. *Circulation,* **82**, 519-522 (1998).
182. Nahrendorf, M.*, et al.* Multimodal functional cardiac MRI in creatine kinase-deficient mice reveals subtle abnormalities in myocardial perfusion and mechanics. *Am J Physiol Heart Circ Physiol,* **290**, H2516-2521 (2006).
183. Kaasik, A.*, et al.* Energetic crosstalk between organelles: architectural integration of energy production and utilization. *Circulation,* **89**, 153-159 (2001).
184. Nahrendorf, M.*, et al.* Creatine kinase knockout mice show left ventricular hypertrophy and dilatation, but unaltered remodeling post-myocardial infarction. *Cardiovascular Research,* **65**, 419-427 (2005).
185. Deschepper, C. F., Olson, J. L., Otis, M., & Gallo-Payet, N. Characterization of blood pressure and morphological traits in cardiovascular-related organs in 13 different inbred mouse strains. *Journal of Applied Physiology,* **97**, 369-376 (2004).
186. Lygate, C. A.*, et al.* Cardiac phenotype of mitochondrial creatine kinase knockout mice is modified on a pure C57BL/6 genetic background. *J Mol Cell Cardiol,* **46**, 93-99 (2009).
187. Lygate, C. A.*, et al.* Chronic creatine kinase deficiency eventually leads to congestive heart failure, but severity is dependent on genetic background, gender and age. *Basic Res Cardiol,* **107**, 276 (2012).
188. Boehm, E.*, et al.* Maintained coupling of oxidative phosphorylation to creatine kinase activity in sarcomeric mitochondrial creatine kinase-deficient mice. *J Mol Cell Cardiol,* **30**, 901-912 (1998).
189. Steeghs, K.*, et al.* Use of gene targeting for compromising energy homeostasis in neuro-muscular tissues: The role of sarcomeric mitochondrial creatine kinase. *Journal of Neuroscience Methods,* **71**, 29-41 (1997).

190. Gupta, A.*, et al.* Creatine kinase-mediated improvement of function in failing mouse hearts provides causal evidence the failing heart is energy starved. *J Clin Invest,* **122**, 291-302 (2012).
191. Akki, A.*, et al.* Creatine kinase overexpression improves ATP kinetics and contractile function in postischemic myocardium. *Am J Physiol Heart Circ Physiol,* **303**, H844-852 (2012).
192. Gupta, A.*, et al.* Creatine kinase-overexpression improves myocardial energetics, contractile dysfunction and survival in murine doxorubicin cardiotoxicity. *PLOS ONE,* **8**, e74675 (2013).
193. Oliver, I. T. A spectrophotometric method for the determination of creatine phosphokinase and myokinase. *Biochem J,* **61**, 116-122 (1955).
194. Rosalki, S. B. An improved procedure for serum creatine phosphokinase determination. *J Lab Clin Med,* **69**, 696-705 (1967).
195. Szasz, G., Waldenstrom, J., & Gruber, W. Creatine kinase in serum: 6. Inhibition by endogenous polyvalent cations, and effect of chelators on the activity and stability of some assay components. *Clin Chem,* **25**, 446-452 (1979).
196. Basson, C. T., Grace, A. M., & Roberts, R. Enzyme kinetics of a highly purified mitochondrial creatine kinase in comparison with cytosolic forms. *Mol Cell Biochem,* **67**, 151-159 (1985).
197. Wiegand, G., & Remington, S. J. Citrate synthase: structure, control, and mechanism. *Annu Rev Biophys Biophys Chem,* **15**, 97-117 (1986).
198. Park, S. Y.*, et al.* Cardiac, skeletal, and smooth muscle mitochondrial respiration: are all mitochondria created equal? *Am J Physiol Heart Circ Physiol,* **307**, H346-352 (2014).
199. Thomas, P., & Smart, T. G. HEK293 cell line: a vehicle for the expression of recombinant proteins. *J Pharmacol Toxicol Methods,* **51**, 187-200 (2005).
200. Claycomb, W. C.*, et al.* HL-1 cells: a cardiac muscle cell line that contracts and retains phenotypic characteristics of the adult cardiomyocyte. *Proceedings of the National Academy of Sciences,* **95**, 2979-2984 (1998).
201. Pelloux, S.*, et al.* Non-beating HL-1 cells for confocal microscopy: application to mitochondrial functions during cardiac preconditioning. *Prog Biophys Mol Biol,* **90**, 270-298 (2006).
202. Monge, C.*, et al.* Comparative analysis of the bioenergetics of adult cardiomyocytes and nonbeating HL-1 cells: respiratory chain activities, glycolytic enzyme profiles, and metabolic fluxes. *Can J Physiol Pharmacol,* **87**, 318-326 (2009).
203. Eimre, M.*, et al.* Distinct organization of energy metabolism in HL-1 cardiac cell line and cardiomyocytes. *Biochimica et Biophysica Acta (BBA) - Bioenergetics,* **1777**, 514-524 (2008).
204. Winer, J., Jung, C. K., Shackel, I., & Williams, P. M. Development and validation of real-time quantitative reverse transcriptase-polymerase chain reaction for monitoring gene expression in cardiac myocytes in vitro. *Anal Biochem,* **270**, 41-49 (1999).
205. Livak, K. J., & Schmittgen, T. D. Analysis of relative gene expression data using real-time quantitative PCR and the 2(-Delta Delta C(T)) Method. *Methods,* **25**, 402-408 (2001).
206. Bustin, S. A.*, et al.* The MIQE guidelines: minimum information for publication of quantitative real-time PCR experiments. *Clin Chem,* **55**, 611-622 (2009).

207. Eppenberger-Eberhardt, M.*, et al.* Adult rat cardiomyocytes cultured in creatine-deficient medium display large mitochondria with paracrystalline inclusions, enriched for creatine kinase. *J Cell Biol,* **113**, 289-302 (1991).
208. O'Gorman, E.*, et al.* Mitochondrial intermembrane inclusion bodies: the common denominator between human mitochondrial myopathies and creatine depletion, due to impairment of cellular energetics. *Mol Cell Biochem,* **174**, 283-289 (1997).
209. Miller, K., Sharer, K., Suhan, J., & Koretsky, A. P. Expression of functional mitochondrial creatine kinase in liver of transgenic mice. *Am J Physiol,* **272**, C1193-1202 (1997).
210. Kanzaki, Y.*, et al.* Giant Mitochondria in the Myocardium of a Patient With Mitochondrial Cardiomyopathy. *Transmission and 3-Dimensional Scanning Electron Microscopy,* **121**, 831-832 (2010).
211. Stadhouders, A. M.*, et al.* Mitochondrial creatine kinase: a major constituent of pathological inclusions seen in mitochondrial myopathies. *Proceedings of the National Academy of Sciences,* **91**, 5089-5093 (1994).
212. Whittington, H. J.*, et al.* Over-expression of mitochondrial creatine kinase in the murine heart improves functional recovery and protects against injury following ischaemia–reperfusion. *Cardiovascular Research*cvy054-cvy054 (2018).
213. Crompton, M., Ellinger, H., & Costi, A. Inhibition by cyclosporin A of a Ca2+-dependent pore in heart mitochondria activated by inorganic phosphate and oxidative stress. *Biochemical Journal,* **255**, 357-360 (1988).
214. Tanveer, A.*, et al.* Involvement of cyclophilin D in the activation of a mitochondrial pore by Ca2+ and oxidant stress. *Eur J Biochem,* **238**, 166-172 (1996).
215. Halestrap, A. P., & Pasdois, P. The role of the mitochondrial permeability transition pore in heart disease. *Biochim Biophys Acta,* **1787**, 1402-1415 (2009).
216. Bernardi, P., & Di Lisa, F. The mitochondrial permeability transition pore: Molecular nature and role as a target in cardioprotection. *J Mol Cell Cardiol,* **78**, 100-106 (2015).
217. Malekova, L.*, et al.* Bongkrekic acid and atractyloside inhibits chloride channels from mitochondrial membranes of rat heart. *Biochimica et Biophysica Acta (BBA) - Bioenergetics,* **1767**, 31-44 (2007).
218. Elrod, J. W., & Molkentin, J. D. Physiologic functions of cyclophilin D and the mitochondrial permeability transition pore. *Circ J,* **77**, 1111-1122 (2013).
219. Szabo, I., & Zoratti, M. The mitochondrial permeability transition pore may comprise VDAC molecules. I. Binary structure and voltage dependence of the pore. *FEBS Lett,* **330**, 201-205 (1993).
220. Shimizu, S.*, et al.* Essential Role of Voltage-Dependent Anion Channel in Various Forms of Apoptosis in Mammalian Cells. *J Cell Biol,* **152**, 237-250 (2001).
221. Baines, C. P.*, et al.* Voltage-dependent anion channels are dispensable for mitochondrial-dependent cell death. *Nat Cell Biol,* **9**, 550-555 (2007).
222. Kokoszka, J. E.*, et al.* The ADP/ATP translocator is not essential for the mitochondrial permeability transition pore. *Nature,* **427**, 461-465 (2004).
223. Basso, E.*, et al.* Properties of the permeability transition pore in mitochondria devoid of Cyclophilin D. *J Biol Chem,* **280**, 18558-18561 (2005).
224. O'Gorman, E., Beutner, G., Wallimann, T., & Brdiczka, D. Differential effects of creatine depletion on the regulation of enzyme activities and on creatine-stimulated

mitochondrial respiration in skeletal muscle, heart, and brain. *Biochim Biophys Acta,* **1276**, 161-170 (1996).
225. Lenz, H.*, et al.* Inhibition of cytosolic and mitochondrial creatine kinase by siRNA in HaCaT- and HeLaS3-cells affects cell viability and mitochondrial morphology. *Molecular and Cellular Biochemistry,* **306**, 153-162 (2007).
226. Giorgio, V.*, et al.* Dimers of mitochondrial ATP synthase form the permeability transition pore. *Proceedings of the National Academy of Sciences,* **110**, 5887-5892 (2013).
227. Bonora, M.*, et al.* Role of the c subunit of the F0 ATP synthase in mitochondrial permeability transition. *Cell Cycle,* **12**, 674-683 (2013).
228. Karch, J., & Molkentin, J. D. Identifying the components of the elusive mitochondrial permeability transition pore. *Proceedings of the National Academy of Sciences,* **111**, 10396-10397 (2014).
229. Denton, R. M. Regulation of mitochondrial dehydrogenases by calcium ions. *Biochimica et Biophysica Acta (BBA) - Bioenergetics,* **1787**, 1309-1316 (2009).
230. Hunter, D. R., & Haworth, R. A. The Ca2+-induced membrane transition in mitochondria. I. The protective mechanisms. *Arch Biochem Biophys,* **195**, 453-459 (1979).
231. Haworth, R. A., & Hunter, D. R. The Ca2+-induced membrane transition in mitochondria. II. Nature of the Ca2+ trigger site. *Arch Biochem Biophys,* **195**, 460-467 (1979).
232. Karamanlidis, G.*, et al.* Mitochondrial complex I deficiency increases protein acetylation and accelerates heart failure. *Cell Metab,* **18**, 239-250 (2013).
233. Halestrap, A. P. What is the mitochondrial permeability transition pore? *J Mol Cell Cardiol,* **46**, 821-831 (2009).
234. Bernardi, P., & Petronilli, V. The permeability transition pore as a mitochondrial calcium release channel: a critical appraisal. *J Bioenerg Biomembr,* **28**, 131-138 (1996).
235. Ong, S. G.*, et al.* HIF-1 reduces ischaemia-reperfusion injury in the heart by targeting the mitochondrial permeability transition pore. *Cardiovascular Research,* **104**, 24-36 (2014).
236. Mewton, N.*, et al.* Effect of cyclosporine on left ventricular remodeling after reperfused myocardial infarction. *J Am Coll Cardiol,* **55**, 1200-1205 (2010).
237. Piot , C.*, et al.* Effect of Cyclosporine on Reperfusion Injury in Acute Myocardial Infarction. *New England Journal of Medicine,* **359**, 473-481 (2008).
238. Cung, T. T.*, et al.* Cyclosporine before PCI in Patients with Acute Myocardial Infarction. *New England Journal of Medicine,* **373**, 1021-1031 (2015).
239. Ottani, F.*, et al.* Cyclosporine A in Reperfused Myocardial Infarction: The Multicenter, Controlled, Open-Label CYCLE Trial. *J Am Coll Cardiol,* **67**, 365-374 (2016).
240. Sharov, V. G.*, et al.* Cyclosporine A attenuates mitochondrial permeability transition and improves mitochondrial respiratory function in cardiomyocytes isolated from dogs with heart failure. *J Mol Cell Cardiol,* **42**, 150-158 (2007).
241. Zervou, S.*, et al.* Proteomic and metabolomic changes driven by elevating myocardial creatine suggest novel metabolic feedback mechanisms. *Amino Acids,* **48**, 1969-1981 (2016).

242. Tokarska-Schlattner, M.*, et al.* Reduced creatine-stimulated respiration in doxorubicin challenged mitochondria: Particular sensitivity of the heart. *Biochimica et Biophysica Acta (BBA) - Bioenergetics,* **1767**, 1276-1284 (2007).
243. Walsh, B.*, et al.* The role of phosphorylcreatine and creatine in the regulation of mitochondrial respiration in human skeletal muscle. *The Journal of Physiology,* **537**, 971-978 (2001).
244. Brand, Martin D., & Nicholls, David G. Assessing mitochondrial dysfunction in cells. *Biochemical Journal,* **435**, 297-312 (2011).
245. Di Lisa, F.*, et al.* Opening of the Mitochondrial Permeability Transition Pore Causes Depletion of Mitochondrial and Cytosolic NAD+and Is a Causative Event in the Death of Myocytes in Postischemic Reperfusion of the Heart. *J Biol Chem,* **276**, 2571-2575 (2001).
246. Hall, A. R.*, et al.* Hearts deficient in both Mfn1 and Mfn2 are protected against acute myocardial infarction. *Cell Death Dis,* **7**, e2238 (2016).
247. Hafner, A. V.*, et al.* Regulation of the mPTP by SIRT3-mediated deacetylation of CypD at lysine 166 suppresses age-related cardiac hypertrophy. *Aging,* **2**, 914-923 (2010).
248. Hall, A. R.*, et al.* The adult murine heart is protected against ischemia-reperfusion injury in the absence of both mitofusin (mfn) proteins. *Heart,* **100**, A22-A23 (2014).
249. Lam, C. K.*, et al.* HAX-1 regulates cyclophilin-D levels and mitochondria permeability transition pore in the heart. *Proceedings of the National Academy of Sciences,* **112**, E6466-E6475 (2015).
250. Lanza, I. R., & Nair, K. S. Functional Assessment of Isolated Mitochondria In Vitro. *Methods in enzymology,* **457**, 349-372 (2009).
251. Halestrap, A. P., Clarke, S. J., & Javadov, S. A. Mitochondrial permeability transition pore opening during myocardial reperfusion—a target for cardioprotection. *Cardiovascular Research,* **61**, 372-385 (2004).
252. Longnus, S. L.*, et al.* Regulation of myocardial fatty acid oxidation by substrate supply. *Am J Physiol Heart Circ Physiol,* **281**, H1561-H1567 (2001).
253. Emwas, A.-H. The Strengths and Weaknesses of NMR Spectroscopy and Mass Spectrometry with Particular Focus on Metabolomics Research. **Vol. 1277**, 161-193 (2015).
254. Dunn, W. B.*, et al.* Systems level studies of mammalian metabolomes: the roles of mass spectrometry and nuclear magnetic resonance spectroscopy. *Chem Soc Rev,* **40**, 387-426 (2011).
255. Meyer, L. E.*, et al.* Mitochondrial creatine kinase activity prevents reactive oxygen species generation: antioxidant role of mitochondrial kinase-dependent ADP re-cycling activity. *J Biol Chem,* **281**, 37361-37371 (2006).
256. Sokolova, N.*, et al.* ADP Protects Cardiac Mitochondria under Severe Oxidative Stress. *PLOS ONE,* **8**, e83214 (2013).
257. Rojo, M.*, et al.* Interaction of mitochondrial creatine kinase with model membranes A monolayer study. *FEBS Lett,* **281**, 123-129 (1991).
258. Speer, O.*, et al.* Octameric mitochondrial creatine kinase induces and stabilizes contact sites between the inner and outer membrane. *Biochemical Journal,* **385**, 445-450 (2005).

259. Halestrap, A. P., & Richardson, A. P. The mitochondrial permeability transition: a current perspective on its identity and role in ischaemia/reperfusion injury. *J Mol Cell Cardiol,* **78**, 129-141 (2015).
260. Pasdois, P., Parker, J. E., & Halestrap, A. P. Extent of Mitochondrial Hexokinase II Dissociation During Ischemia Correlates With Mitochondrial Cytochrome c Release, Reactive Oxygen Species Production, and Infarct Size on Reperfusion. *Journal of the American Heart Association: Cardiovascular and Cerebrovascular Disease,* **2**, e005645 (2013).
261. Hamman, B. L.*, et al.* Inhibition of the creatine kinase reaction decreases the contractile reserve of isolated rat hearts. *Am J Physiol,* **269**, H1030-1036 (1995).
262. Starkov, A. A. Measurement of Mitochondrial ROS Production. *Methods in Molecular Biology,* **648**, 245-255 (2010).
263. Griffiths, E. J., & Halestrap, A. P. Mitochondrial non-specific pores remain closed during cardiac ischaemia, but open upon reperfusion. *Biochemical Journal,* **307**, 93-98 (1995).
264. Ayoub, I. M., Radhakrishnan, J., & Gazmuri, R. J. In vivo opening of the mitochondrial permeability transition pore in a rat model of ventricular fibrillation and closed-chest resuscitation. *American Journal of Translational Research,* **9**, 3345-3359 (2017).
265. Ferdinandy, P.*, et al.* Interaction of Risk Factors, Comorbidities, and Comedications with Ischemia/Reperfusion Injury and Cardioprotection by Preconditioning, Postconditioning, and Remote Conditioning. *Pharmacological Reviews,* **66**, 1142-1174 (2014).
266. Yancy, C. W.*, et al.* 2013 ACCF/AHA Guideline for the Management of Heart Failure. *A Report of the American College of Cardiology Foundation,* **128**, e240-e327 (2013).
267. UCL. (2010). *National Heart Failure Audit Report for the audit period ending March 2010*.
268. Savarese, G., & Lund, L. H. Global Public Health Burden of Heart Failure. *Cardiac Failure Review,* **3**, 7-11 (2017).
269. Cowie, M. R. The heart failure epidemic: a UK perspective. *Echo Research and Practice,* **4**, R15-R20 (2017).
270. Chen-Scarabelli, C.*, et al.* Dilemmas in end-stage heart failure. *Journal of Geriatric Cardiology : JGC,* **12**, 57-65 (2015).
271. Brown, D. A.*, et al.* Mitochondrial function as a therapeutic target in heart failure. *Nature Reviews Cardiology,* **14**, 238 (2016).
272. Ventura-Clapier, R., Garnier, A., Veksler, V., & Joubert, F. Bioenergetics of the failing heart. *Biochimica et Biophysica Acta (BBA) - Molecular Cell Research,* **1813**, 1360-1372 (2011).
273. Horn, M.*, et al.* Chronic phosphocreatine depletion by the creatine analogue beta-guanidinopropionate is associated with increased mortality and loss of ATP in rats after myocardial infarction. *Circulation,* **104**, 1844-1849 (2001).
274. deAlmeida, A. C., van Oort, R. J., & Wehrens, X. H. T. Transverse Aortic Constriction in Mice. *Journal of Visualized Experiments : JoVE*1729 (2010).

275. Rockman, H. A.*, et al.* Segregation of atrial-specific and inducible expression of an atrial natriuretic factor transgene in an in vivo murine model of cardiac hypertrophy. *Proceedings of the National Academy of Sciences,* **88**, 8277-8281 (1991).
276. Lygate, C. Surgical models of hypertrophy and heart failure: Myocardial infarction and transverse aortic constriction. *Drug Discovery Today: Disease Models,* **3**, 283-290 (2006).
277. Abdurrachim, D.*, et al.* Diabetic db/db mice do not develop heart failure upon pressure overload: a longitudinal in vivo PET, MRI, and MRS study on cardiac metabolic, structural, and functional adaptations. *Cardiovascular Research,* **113**, 1148-1160 (2017).
278. Wandt, B., Bojö, L., Tolagen, K., & Wranne, B. Echocardiographic assessment of ejection fraction in left ventricular hypertrophy. *Heart,* **82**, 192-198 (1999).
279. Maguire, M. L.*, et al.* Compressed sensing to accelerate magnetic resonance spectroscopic imaging: evaluation and application to (23)Na-imaging of mouse hearts. *Journal of Cardiovascular Magnetic Resonance,* **17**, 45 (2015).
280. Flögel, U., Jacoby, C., Gödecke, A., & Schrader, J. In vivo 2D mapping of impaired murine cardiac energetics in NO-induced heart failure. *Magnetic resonance in medicine,* **57**, 50-58 (2007).
281. Teerlink, T., Hennekes, M., Bussemaker, J., & Groeneveld, J. Simultaneous determination of creatine compounds and adenine nucleotides in myocardial tissue by high-performance liquid chromatography. *Anal Biochem,* **214**, 278-283 (1993).
282. Lygate, C. A.*, et al.* Serial high resolution 3D-MRI after aortic banding in mice: band internalization is a source of variability in the hypertrophic response. *Basic Res Cardiol,* **101**, 8-16 (2006).
283. Chinen, D.*, et al.* Left ventricular outflow tract velocity time integral correlates with low cardiac output syndrome in patients with acute decompensated heart failure. *European Heart Journal,* **34**, P4249-P4249 (2013).
284. Mohammed, S. F.*, et al.* Variable phenotype in murine transverse aortic constriction. *Cardiovascular Pathology,* **21**, 188-198
285. Neubauer, S.*, et al.* Impairment of energy metabolism in intact residual myocardium of rat hearts with chronic myocardial infarction. *J Clin Invest,* **95**, 1092-1100 (1995).
286. Spindler, M.*, et al.* Alterations in the myocardial creatine kinase system precede the development of contractile dysfunction in B-adrenergic receptor transgenic mice. *J Mol Cell Cardiol,* **35**, 389-397
287. Gupta, A.*, et al.* Creatine kinase–mediated improvement of function in failing mouse hearts provides causal evidence the failing heart is energy starved. *J Clin Invest,* **122**, 291-302
288. Lygate, C. A. Metabolic arithmetic: do two wrongs make a right? *Cardiovascular Research,* **113**, 1093-1095 (2017).
289. Wu, F., Zhang, J., & Beard, D. A. Experimentally observed phenomena on cardiac energetics in heart failure emerge from simulations of cardiac metabolism. *Proceedings of the National Academy of Sciences,* **106**, 7143-7148 (2009).
290. Arcamone, F.*, et al.* Adriamycin, 14-hydroxydaunomycin, a new antitumor antibiotic from S. peucetius var. caesius. Reprinted from Biotechnology and Bioengineering, Vol. XI, Issue 6, Pages 1101-1110 (1969). *Biotechnol Bioeng,* **67**, 704-713 (2000).

291. Minotti, G.*, et al.* Anthracyclines: molecular advances and pharmacologic developments in antitumor activity and cardiotoxicity. *Pharmacol Rev,* **56**, 185-229 (2004).
292. Machado, V.*, et al.* Carvedilol as a protector against the cardiotoxicity induced by anthracyclines (doxorubicin) **Vol. 27**, 1277-1296 (2008).
293. Gewirtz, D. A. A critical evaluation of the mechanisms of action proposed for the antitumor effects of the anthracycline antibiotics adriamycin and daunorubicin. *Biochem Pharmacol,* **57**, 727-741 (1999).
294. Mitry, M. A., & Edwards, J. G. Doxorubicin induced heart failure: Phenotype and molecular mechanisms. *IJC Heart & Vasculature,* **10**, 17-24 (2016).
295. Lindsey, M. L.*, et al.* The tell-tale heart: molecular and cellular responses to childhood anthracycline exposure. *American Journal of Physiology - Heart and Circulatory Physiology,* **307**, H1379-H1389 (2014).
296. Rabbani, A., Finn, R. M., & Ausio, J. The anthracycline antibiotics: antitumor drugs that alter chromatin structure. *Bioessays,* **27**, 50-56 (2005).
297. Tokarska-Schlattner, M.*, et al.* New insights into doxorubicin-induced cardiotoxicity: the critical role of cellular energetics. *J Mol Cell Cardiol,* **41**, 389-405 (2006).
298. DeAtley, S. M.*, et al.* Adriamycin-induced changes of creatine kinase activity in vivo and in cardiomyocyte culture. *Toxicology,* **134**, 51-62 (1999).
299. Buja, L. M.*, et al.* Cardiac ultrastructural changes induced by daunorubicin therapy. *Cancer,* **32**, 771-788 (1973).
300. Singal, P. K., Dixon, I.M.C, Beamish, R.E, Dhalla, N.S. Mechanisms of Heart Failure. (1995).
301. Singal, P. K., & Pierce, G. N. Adriamycin stimulates low-affinity Ca2+ binding and lipid peroxidation but depresses myocardial function. *Am J Physiol,* **250**, H419-425 (1986).
302. Zhang, S.*, et al.* Identification of the molecular basis of doxorubicin-induced cardiotoxicity. *Nat Med,* **18**, 1639-1642 (2012).
303. Poizat, C., Puri, P. L., Bai, Y., & Kedes, L. Phosphorylation-dependent degradation of p300 by doxorubicin-activated p38 mitogen-activated protein kinase in cardiac cells. *Mol Cell Biol,* **25**, 2673-2687 (2005).
304. Shi, J., Abdelwahid, E., & Wei, L. Apoptosis in Anthracycline Cardiomyopathy. *Current pediatric reviews,* **7**, 329-336 (2011).
305. Zhang, Y.-W., Shi, J., Li, Y.-J., & Wei, L. Cardiomyocyte death in doxorubicin-induced cardiotoxicity. *Archivum immunologiae et therapiae experimentalis,* **57**, 435-445 (2009).
306. Birben, E.*, et al.* Oxidative Stress and Antioxidant Defense. *The World Allergy Organization journal,* **5**, 9-19 (2012).
307. Swain, S. M.*, et al.* Cardioprotection with dexrazoxane for doxorubicin-containing therapy in advanced breast cancer. *J Clin Oncol,* **15**, 1318-1332 (1997).
308. Ichikawa, Y.*, et al.* Cardiotoxicity of doxorubicin is mediated through mitochondrial iron accumulation. *J Clin Invest,* **124**, 617-630 (2014).
309. Davies, K. J., & Doroshow, J. H. Redox cycling of anthracyclines by cardiac mitochondria. I. Anthracycline radical formation by NADH dehydrogenase. *J Biol Chem,* **261**, 3060-3067 (1986).

310. Yen, H. C., *et al.* The protective role of manganese superoxide dismutase against adriamycin-induced acute cardiac toxicity in transgenic mice. *J Clin Invest,* **98**, 1253-1260 (1996).
311. Bianchi, C., Bagnato, A., Paggi, M. G., & Floridi, A. Effect of adriamycin on electron transport in rat heart, liver, and tumor mitochondria. *Experimental and Molecular Pathology,* **46**, 123-135 (1987).
312. Tokarska-Schlattner, M., Wallimann, T., & Schlattner, U. Multiple Interference of Anthracyclines with Mitochondrial Creatine Kinases: Preferential Damage of the Cardiac Isoenzyme and Its Implications for Drug Cardiotoxicity. **Vol. 61**, 516-523 (2002).
313. Yen, H.-C., *et al.* Manganese Superoxide Dismutase Protects Mitochondrial Complex I against Adriamycin-Induced Cardiomyopathy in Transgenic Mice. **Vol. 362**, 59-66 (1999).
314. Sterba, M., *et al.* Oxidative stress, redox signaling, and metal chelation in anthracycline cardiotoxicity and pharmacological cardioprotection. *Antioxid Redox Signal,* **18**, 899-929 (2013).
315. Thomas, C., Carr, A. C., & Winterbourn, C. C. Free radical inactivation of rabbit muscle creatinine kinase: catalysis by physiological and hydrolyzed ICRF-187 (ICRF-198) iron chelates. *Free Radic Res,* **21**, 387-397 (1994).
316. Vyssokikh, M. Y., & Brdiczka, D. The function of complexes between the outer mitochondrial membrane pore (VDAC) and the adenine nucleotide translocase in regulation of energy metabolism and apoptosis. *Acta Biochim Pol,* **50**, 389-404 (2003).
317. Wallace, K. B. Doxorubicin-induced cardiac mitochondrionopathy. *Pharmacol Toxicol,* **93**, 105-115 (2003).
318. de Wolf, F. A. Binding of doxorubicin to cardiolipin as compared to other anionic phospholipids--an evaluation of electrostatic effects. *Biosci Rep,* **11**, 275-284 (1991).
319. Goormaghtigh, E., *et al.* Structure of the adriamycin-cardiolipin complex. Role in mitochondrial toxicity. *Biophys Chem,* **35**, 247-257 (1990).
320. Cheneval, D., & Carafoli, E. Identification and primary structure of the cardiolipin-binding domain of mitochondrial creatine kinase. *Eur J Biochem,* **171**, 1-9 (1988).
321. Tokarska-Schlattner, M., *et al.* Acute toxicity of doxorubicin on isolated perfused heart: response of kinases regulating energy supply. *Am J Physiol Heart Circ Physiol,* **289**, H37-47 (2005).
322. Seraydarian, M. W., Artaza, L., & Goodman, M. F. Adriamycin: Effect on mammalian cardiac cells in culture I. Cell population and energy metabolism. *J Mol Cell Cardiol,* **9**, 375-382 (1977).
323. Vidal, R. F., *et al.* Doxorubicin- and daunorubicin-induced energy deprivation and nucleotide degradation in isolated cardiomyocytes. *Toxicology,* **114**, 1-10 (1996).
324. Cini Neri, G., *et al.* Anthracycline cardiotoxicity: in vivo and in vitro effects on biochemical parameters and heart ultrastructure of the rat. *Oncology,* **48**, 327-333 (1991).
325. Ohhara, H., Kanaide, H., & Nakamura, M. A protective effect of coenzyme Q10 on the adriamycin-induced cardiotoxicity in the isolated perfused rat heart. *J Mol Cell Cardiol,* **13**, 741-752 (1981).

326. Eidenschink, A. B., Schroter, G., Muller-Weihrich, S., & Stern, H. Myocardial high-energy phosphate metabolism is altered after treatment with anthracycline in childhood. *Cardiol Young,* **10**, 610-617 (2000).
327. Darrabie, M. D.*, et al.* Exposing cardiomyocytes to subclinical concentrations of doxorubicin rapidly reduces their creatine transport. *Am J Physiol Heart Circ Physiol,* **303**, H539-548 (2012).
328. Santacruz, L.*, et al.* Creatine supplementation reduces doxorubicin-induced cardiomyocellular injury. *Cardiovasc Toxicol,* **15**, 180-188 (2015).
329. Aksentijević, D.*, et al.* Myocardial Creatine Levels Do Not Influence Response to Acute Oxidative Stress in Isolated Perfused Heart. *PLOS ONE,* **9**, e109021 (2014).
330. Chemicals, C. (Producer). Annexin V FITC Assay Kit.
331. Cheng, A., & Solomon, M. J. Speedy/Ringo C regulates S and G2 phase progression in human cells. *Cell Cycle,* **7**, 3037-3047 (2008).
332. Wang, B., Liu, K., Lin, F. T., & Lin, W. C. A role for 14-3-3 tau in E2F1 stabilization and DNA damage-induced apoptosis. *J Biol Chem,* **279**, 54140-54152 (2004).
333. Ahmadi, M., Madrakian, T., & Afkhami, A. Solid phase extraction of doxorubicin using molecularly imprinted polymer coated magnetite nanospheres prior to its spectrofluorometric determination. *New Journal of Chemistry,* **39**, 163-171 (2015).
334. Scientific, T. F. (Producer). (2015). LIVE/DEAD™ Fixable Violet Dead Cell Stain Kit, for 405 nm excitation.
335. Garcia-Gras, E.*, et al.* Suppression of canonical Wnt/β-catenin signaling by nuclear plakoglobin recapitulates phenotype of arrhythmogenic right ventricular cardiomyopathy. *J Clin Invest,* **116**, 2012-2021 (2006).
336. Ali-Boucetta, H.*, et al.* Multiwalled carbon nanotube-doxorubicin supramolecular complexes for cancer therapeutics. *Chemical Communications*459-461 (2008).
337. Aryal, B., Jeong, J., & Rao, V. A. Doxorubicin-induced carbonylation and degradation of cardiac myosin binding protein C promote cardiotoxicity. *Proceedings of the National Academy of Sciences,* **111**, 2011-2016 (2014).
338. Strigun, A.*, et al.* Doxorubicin Increases Oxidative Metabolism in HL-1 Cardiomyocytes as Shown by 13C Metabolic Flux Analysis. *Toxicological Sciences,* **125**, 595-606 (2012).
339. Dawson, K. M. Studies on the stability and cellular distribution of dioxopiperazines in cultured BHK-21S cells. *Biochem Pharmacol,* **24**, 2249-2253 (1975).
340. Lebrecht, D.*, et al.* Dexrazoxane prevents doxorubicin-induced long-term cardiotoxicity and protects myocardial mitochondria from genetic and functional lesions in rats. *British Journal of Pharmacology,* **151**, 771-778 (2007).
341. Choi, H. S.*, et al.* Dexrazoxane for Preventing Anthracycline Cardiotoxicity in Children with Solid Tumors. *Journal of Korean Medical Science,* **25**, 1336-1342 (2010).
342. Speyer, J. L.*, et al.* ICRF-187 permits longer treatment with doxorubicin in women with breast cancer. *J Clin Oncol,* **10**, 117-127 (1992).
343. El Messaoudi, S., Rongen, G. A., & Riksen, N. P. Metformin therapy in diabetes: the role of cardioprotection. *Curr Atheroscler Rep,* **15**, 314 (2013).
344. Kobashigawa, L. C.*, et al.* Metformin Protects Cardiomyocyte from Doxorubicin Induced Cytotoxicity through an AMP-Activated Protein Kinase Dependent Signaling Pathway: An In Vitro Study. *PLOS ONE,* **9**, e104888 (2014).

345. Asensio-Lopez, M. C., *et al.* Involvement of ferritin heavy chain in the preventive effect of metformin against doxorubicin-induced cardiotoxicity. *Free Radic Biol Med,* **57**, 188-200 (2013).
346. Asensio-Lopez, M. C., *et al.* Metformin protects against doxorubicin-induced cardiotoxicity: involvement of the adiponectin cardiac system. *Free Radic Biol Med,* **51**, 1861-1871 (2011).
347. Haug, K. G., Weber, B., Hochhaus, G., & Butterweck, V. Nonlinear pharmacokinetics of visnagin in rats after intravenous bolus administration. *European Journal of Pharmaceutical Sciences,* **45**, 79-89 (2012).
348. Liu, Y., *et al.* Visnagin protects against doxorubicin-induced cardiomyopathy through modulation of mitochondrial malate dehydrogenase. *Science translational medicine,* **6**, 266ra170-266ra170 (2014).
349. Mimnaugh, E. G., *et al.* The effects of alpha-tocopherol on the toxicity, disposition, and metabolism of adriamycin in mice. *Toxicol Appl Pharmacol,* **49**, 119-126 (1979).
350. Wang, Y. M., *et al.* Effect of vitamin E against adriamycin-induced toxicity in rabbits. *Cancer Res,* **40**, 1022-1027 (1980).
351. Salgo, M. G., Bermúdez, E., Squadrito, G. L., & Pryor, W. A. Peroxynitrite causes DNA damage and oxidation of thiols in rat thymocytes [corrected]. *Arch Biochem Biophys,* **322**, 500-505 (1995).
352. Rezk, B. M., Haenen, G. R. M. M., van der Vijgh, W. J. F., & Bast, A. The extraordinary antioxidant activity of vitamin E phosphate. *Biochimica et Biophysica Acta (BBA) - Molecular and Cell Biology of Lipids,* **1683**, 16-21 (2004).
353. Sedlic, F., *et al.* Differences in Production of Reactive Oxygen Species and Mitochondrial Uncoupling as Events in the Preconditioning Signaling Cascade Between Desflurane and Sevoflurane. *Anesthesia and analgesia,* **109**, 405-411 (2009).
354. Forrest, V. J., *et al.* Oxidative stress-induced apoptosis prevented by trolox. *Free Radical Biology and Medicine,* **16**, 675-684 (1994).
355. Molyneux, C. A., Glyn, M. C., & Ward, B. J. Oxidative stress and cardiac microvascular structure in ischemia and reperfusion: the protective effect of antioxidant vitamins. *Microvasc Res,* **64**, 265-277 (2002).
356. Sagach, V. F., *et al.* The water-soluble vitamin E analogue Trolox protects against ischaemia/reperfusion damage in vitro and ex vivo. A comparison with vitamin E. *Pharmacol Res,* **45**, 435-439 (2002).
357. Vassilopoulos, A., & Papazafiri, P. Attenuation of oxidative stress in HL-1 cardiomyocytes improves mitochondrial function and stabilizes Hif-1α. *Free Radic Res,* **39**, 1273-1284 (2005).
358. Sweeney, Y., *et al.* Abstracts from the 5th International Conference for Healthcare and Medical Students (ICHAMS): Dublin, Ireland. 19-20 February 2016. *BMC Proceedings,* **10**, 4 (2016).
359. Langer, S. W. Dexrazoxane for the treatment of chemotherapy-related side effects. *Cancer Management and Research,* **6**, 357-363 (2014).
360. Cho, S.-Y., *et al.* Doxorubicin Induces the Persistent Activation of Intracellular Transglutaminase 2 That Protects from Cell Death. *Molecules and Cells,* **33**, 235-241 (2012).

361. Calcagno, A. M.*, et al.* Single-step doxorubicin-selected cancer cells overexpress the ABCG2 drug transporter through epigenetic changes. *British Journal of Cancer,* **98**, 1515-1524 (2008).
362. Sestili, P.*, et al.* Creatine as an antioxidant. *Amino Acids,* **40**, 1385-1396 (2011).
363. Sestili, P.*, et al.* Creatine supplementation affords cytoprotection in oxidatively injured cultured mammalian cells via direct antioxidant activity. *Free Radical Biology and Medicine,* **40**, 837-849 (2006).
364. Prass, K.*, et al.* Improved reperfusion and neuroprotection by creatine in a mouse model of stroke. *Journal of Cerebral Blood Flow & Metabolism,* **27**, 452-459 (2007).
365. de Wet, J. R., Wood, K. V., Helinski, D. R., & DeLuca, M. Cloning of firefly luciferase cDNA and the expression of active luciferase in Escherichia coli. *Proceedings of the National Academy of Sciences,* **82**, 7870-7873 (1985).
366. de Wet, J. R.*, et al.* Firefly luciferase gene: structure and expression in mammalian cells. *Molecular and Cellular Biology,* **7**, 725-737 (1987).
367. Lohcharoenkal, W.*, et al.* Luciferase reporter cells as a platform to detect SMAD-dependent collagen production. *Journal of bioscience and bioengineering,* **118**, 732-735 (2014).
368. Cheng, Z.*, et al.* Luciferase Reporter Assay System for Deciphering GPCR Pathways. *Current Chemical Genomics,* **4**, 84-91 (2010).
369. Sedlak, D., Paguio, A., & Bartunek, P. Two panels of steroid receptor luciferase reporter cell lines for compound profiling. *Comb Chem High Throughput Screen,* **14**, 248-266 (2011).
370. Promega. Luciferase Assay System Complete Protocol. (2015).
371. Fan, F., & Wood, K. V. Bioluminescent assays for high-throughput screening. *Assay Drug Dev Technol,* **5**, 127-136 (2007).
372. Alam, J., & Cook, J. L. Reporter genes: application to the study of mammalian gene transcription. *Anal Biochem,* **188**, 245-254 (1990).
373. Gould, S. J., & Subramani, S. Firefly luciferase as a tool in molecular and cell biology. *Anal Biochem,* **175**, 5-13 (1988).
374. Donoviel, D. B.*, et al.* Analysis of muscle creatine kinase gene regulatory elements in skeletal and cardiac muscles of transgenic mice. *Molecular and Cellular Biology,* **16**, 1649-1658 (1996).
375. Olson, E. N. Regulation of muscle transcription by the MyoD family. The heart of the matter. *Circulation,* **72**, 1-6 (1993).
376. Weintraub, H. The MyoD family and myogenesis: redundancy, networks, and thresholds. *Cell,* **75**, 1241-1244 (1993).
377. Cserjesi, P., & Olson, E. N. Myogenin induces the myocyte-specific enhancer binding factor MEF-2 independently of other muscle-specific gene products. *Mol Cell Biol,* **11**, 4854-4862 (1991).
378. Shield, M. A., Haugen, H. S., Clegg, C. H., & Hauschka, S. D. E-box sites and a proximal regulatory region of the muscle creatine kinase gene differentially regulate expression in diverse skeletal muscles and cardiac muscle of transgenic mice. *Molecular and Cellular Biology,* **16**, 5058-5068 (1996).
379. Muscle Enzymes. *Dermatomyositis: Advances in Recognition, Understanding and Management*, 205-209 (2009).

380. Amacher, S. L., Buskin, J. N., & Hauschka, S. D. Multiple regulatory elements contribute differentially to muscle creatine kinase enhancer activity in skeletal and cardiac muscle. *Mol Cell Biol,* **13**, 2753-2764 (1993).
381. Buskin, J. N., & Hauschka, S. D. Identification of a myocyte nuclear factor that binds to the muscle-specific enhancer of the mouse muscle creatine kinase gene. *Mol Cell Biol,* **9**, 2627-2640 (1989).
382. Miwa, T., & Kedes, L. Duplicated CArG box domains have positive and mutually dependent regulatory roles in expression of the human alpha-cardiac actin gene. *Mol Cell Biol,* **7**, 2803-2813 (1987).
383. Lee, T. C., Chow, K. L., Fang, P., & Schwartz, R. J. Activation of skeletal alpha-actin gene transcription: the cooperative formation of serum response factor-binding complexes over positive cis-acting promoter serum response elements displaces a negative-acting nuclear factor enriched in replicating myoblasts and nonmyogenic cells. *Mol Cell Biol,* **11**, 5090-5100 (1991).
384. Himeda, C. L., Ranish, J. A., & Hauschka, S. D. Quantitative proteomic identification of MAZ as a transcriptional regulator of muscle-specific genes in skeletal and cardiac myocytes. *Mol Cell Biol,* **28**, 6521-6535 (2008).
385. Cserjesi, P.*, et al.* MHox: a mesodermally restricted homeodomain protein that binds an essential site in the muscle creatine kinase enhancer. *Development,* **115**, 1087-1101 (1992).
386. Himeda, C. L.*, et al.* KLF3 Regulates Muscle-Specific Gene Expression and Synergizes with Serum Response Factor on KLF Binding Sites. *Molecular and Cellular Biology,* **30**, 3430-3443 (2010).
387. Qin, W., Khuchua, Z., Klein, S. C., & Strauss, A. W. Elements regulating cardiomyocyte expression of the human sarcomeric mitochondrial creatine kinase gene in transgenic mice. *J Biol Chem,* **272**, 25210-25216 (1997).
388. Klein, S. C.*, et al.* Regulatory element analysis and structural characterization of the human sarcomeric mitochondrial creatine kinase gene. *J Biol Chem,* **266**, 18058-18065 (1991).
389. Hammerschmidt, S.*, et al.* Acute changes of myocardial creatine kinase gene expression under β-adrenergic stimulation. *Biochimica et Biophysica Acta (BBA) - Molecular Basis of Disease,* **1502**, 471-480 (2000).
390. Steeghs, K.*, et al.* Mouse ubiquitous mitochondrial creatine kinase: gene organization and consequences from inactivation in mouse embryonic stem cells. *DNA Cell Biol,* **14**, 539-553 (1995).
391. Payne, R. M.*, et al.* Creatine kinase isoenzymes are highly regulated during pregnancy in rat uterus and placenta. *Am J Physiol,* **265**, E624-635 (1993).
392. Somjen, D., Shen, M., Stern, N., & Mirsky, N. Diabetes modulates differentially creatine kinase-specific activity responsiveness to estradiol-17β and to raloxifene in rat organs. *Journal of Cellular Biochemistry,* **99**, 133-139 (2006).
393. Somjen, D., & Yoles, I. DT56a (Tofupill®/Femarelle™) selectively stimulates creatine kinase specific activity in skeletal tissues of rats but not in the uterus. *The Journal of Steroid Biochemistry and Molecular Biology,* **86**, 93-98 (2003).
394. Lee, C. M.*, et al.* Phosphatidylinositol 3-Kinase Inhibition by LY294002 Radiosensitizes Human Cervical Cancer Cell Lines. *Clinical Cancer Research,* **12**, 250-256 (2006).

395. Tamir, Y., & Bengal, E. Phosphoinositide 3-Kinase Induces the Transcriptional Activity of MEF2 Proteins during Muscle Differentiation. *J Biol Chem,* **275**, 34424-34432 (2000).
396. Sumitani, S.*, et al.* Akt1 and Akt2 Differently Regulate Muscle Creatine Kinase and Myogenin Gene Transcription in Insulin-Induced Differentiation of C2C12 Myoblasts. *Endocrinology,* **143**, 820-828 (2002).
397. Lee, N.*, et al.* Creatine inhibits adipogenesis by downregulating insulin-induced activation of the phosphatidylinositol 3-kinase signaling pathway. *Stem Cells Dev,* **24**, 983-994 (2015).
398. Coolican, S. A.*, et al.* The Mitogenic and Myogenic Actions of Insulin-like Growth Factors Utilize Distinct Signaling Pathways. *J Biol Chem,* **272**, 6653-6662 (1997).
399. Mitani, S.*, et al.* Insulin alters cardiac muscle creatine kinase activity. *Heart and Vessels,* **15**, 23-29 (2000).
400. Popovich, B. K., Sayen, M. R., & Dillmann, W. H. Insulin responsiveness of CK-M and CK-B mRNA in the diabetic rat heart. *American Journal of Physiology-Endocrinology and Metabolism,* **261**, E377-E381 (1991).
401. Yoshioka, J.*, et al.* Targeted deletion of thioredoxin-interacting protein regulates cardiac dysfunction in response to pressure overload. *Circulation,* **101**, 1328-1338 (2007).
402. Didiot, M. C.*, et al.* Multiplexed reporter gene assays: monitoring the cell viability and the compound kinetics on luciferase activity. *J Biomol Screen,* **16**, 786-793 (2011).
403. Musso, R., Maggi, A., & Eva, C. 17β-Estradiol Stimulates Mouse Neuropeptide Y-Y1 Receptor Gene Transcription by Binding to Estrogen Receptor Alpha in Neuroblastoma Cells. *Neuroendocrinology,* **72**, 360-367 (2000).
404. Paterni, I., Granchi, C., Katzenellenbogen, J. A., & Minutolo, F. Estrogen Receptors Alpha (ERα) and Beta (ERβ): Subtype-Selective Ligands and Clinical Potential. *Steroids,* **0**, 13-29 (2014).
405. Cunha, F. M.*, et al.* Intracellular Peptides as Natural Regulators of Cell Signaling. *J Biol Chem,* **283**, 24448-24459 (2008).
406. Bittinger, M. A.*, et al.* Activation of cAMP response element-mediated gene expression by regulated nuclear transport of TORC proteins. *Curr Biol,* **14**, 2156-2161 (2004).
407. Bae, S.*, et al.* Akt is negatively regulated by the MULAN E3 ligase. *Cell Res,* **22**, 873-885 (2012).
408. Branco, A. F.*, et al.* Isoproterenol cytotoxicity is dependent on the differentiation state of the cardiomyoblast H9c2 cell line. *Cardiovasc Toxicol,* **11**, 191-203 (2011).
409. Ciraolo, E., Morello, F., & Hirsch, E. Present and future of PI3K pathway inhibition in cancer: perspectives and limitations. *Curr Med Chem,* **18**, 2674-2685 (2011).
410. Mizuno, M.*, et al.* Antenatal glucocorticoid therapy accelerates ATP production with creatine kinase increase in the growth-enhanced fetal rat heart. *Circ J,* **74**, 171-180 (2010).
411. Montano, M. M., & Lim, R. W. Glucocorticoid effects on the skeletal muscle differentiation program: analysis of clonal proliferation, morphological differentiation and the expression of muscle-specific and regulatory genes. *Endocr Res,* **23**, 37-57 (1997).

412. Yoshiko, Y., Hirao, K., & Maeda, N. Dexamethasone regulates the actions of endogenous insulin-like growth factor-II during myogenic differentiation. *Life Sci,* **63**, 77-85 (1998).
413. Seppet, E. K., & Saks, V. A. Thyroid hormones and the creatine kinase system in cardiac cells. *Mol Cell Biochem,* **133-134**, 299-309 (1994).
414. Lee, W.-S., & Kim, J. Peroxisome Proliferator-Activated Receptors and the Heart: Lessons from the Past and Future Directions. *PPAR Research,* **2015**, 18 (2015).
415. Bakhtiarova, A.*, et al.* Resveratrol inhibits firefly luciferase. *Biochem Biophys Res Commun,* **351**, 481-484 (2006).
416. Thorne, N.*, et al.* Firefly luciferase in chemical biology: a compendium of inhibitors, mechanistic evaluation of chemotypes, and suggested use as a reporter. *Chem Biol,* **19**, 1060-1072 (2012).
417. Wharton, J., Meshulamy, T., Vallega, G., & Pilch, P. Dissociation of Insulin Receptor Expression and Signaling from Caveolin-1 Expression. *J Biol Chem,* **280**, 13483-13486 (2005).
418. Lavan, B. E.*, et al.* A Novel 160-kDa Phosphotyrosine Protein in Insulin-treated Embryonic Kidney Cells Is a New Member of the Insulin Receptor Substrate Family. *J Biol Chem,* **272**, 21403-21407 (1997).
419. Kim, D.*, et al.* A Small Molecule Inhibits Akt through Direct Binding to Akt and Preventing Akt Membrane Translocation. *J Biol Chem,* **285**, 8383-8394 (2010).
420. Alonso, N.*, et al.* PI3K pathway is involved in ERK signaling cascade activation by histamine H2R agonist in HEK293T cells. *Biochim Biophys Acta,* **1860**, 1998-2007 (2016).
421. Schmitt, J. M., & Stork, P. J. S. β2-Adrenergic Receptor Activates Extracellular Signal-regulated Kinases (ERKs) via the Small G Protein Rap1 and the Serine/Threonine Kinase B-Raf. *J Biol Chem,* **275**, 25342-25350 (2000).
422. Uhlen, M.*, et al.* A human protein atlas for normal and cancer tissues based on antibody proteomics. *Mol Cell Proteomics,* **4**, 1920-1932 (2005).
423. Uhlen, M.*, et al.* Proteomics. Tissue-based map of the human proteome. *Science,* **347**, 1260419 (2015).
424. Uhlen, M.*, et al.* Towards a knowledge-based Human Protein Atlas. *Nat Biotechnol,* **28**, 1248-1250 (2010).
425. Liao, R.*, et al.* Cardiac-specific overexpression of GLUT1 prevents the development of heart failure attributable to pressure overload in mice. *Circulation,* **106**, 2125-2131 (2002).
426. Lionetti, V.*, et al.* Carnitine palmitoyl transferase-I inhibition prevents ventricular remodeling and delays decompensation in pacing-induced heart failure. *Cardiovasc Res,* **66**, 454-461 (2005).
427. Augustus, A. S.*, et al.* Loss of Lipoprotein Lipase-derived Fatty Acids Leads to Increased Cardiac Glucose Metabolism and Heart Dysfunction. *J Biol Chem,* **281**, 8716-8723 (2006).
428. Heggermont, W. A., Papageorgiou, A. P., Heymans, S., & van Bilsen, M. Metabolic support for the heart: complementary therapy for heart failure? *European Journal of Heart Failure,* **18**, 1420-1429 (2016).